ALFRED-WEGENER-INSTITUT
HELMHOLTZ-ZENTRUM FÜR POLAR- UND MEERESFORSCHUNG

706
2017

Berichte
zur Polar- und Meeresforschung

Reports on Polar and Marine Research

The Expedition PS101 of the Research Vessel POLARSTERN to the Arctic Ocean in 2016

Edited by
Antje Boetius and Autun Purser
with contributions of the participants

HELMHOLTZ GEMEINSCHAFT

Die Berichte zur Polar- und Meeresforschung werden vom Alfred-Wegener-Institut, Helmholtz-Zentrum für Polar- und Meeresforschung (AWI) in Bremerhaven, Deutschland, in Fortsetzung der vormaligen Berichte zur Polarforschung herausgegeben. Sie erscheinen in unregelmäßiger Abfolge.

Die Berichte zur Polar- und Meeresforschung enthalten Darstellungen und Ergebnisse der vom AWI selbst oder mit seiner Unterstützung durchgeführten Forschungsarbeiten in den Polargebieten und in den Meeren.

Die Publikationen umfassen Expeditionsberichte der vom AWI betriebenen Schiffe, Flugzeuge und Stationen, Forschungsergebnisse (inkl. Dissertationen) des Instituts und des Archivs für deutsche Polarforschung, sowie Abstracts und Proceedings von nationalen und internationalen Tagungen und Workshops des AWI.

Die Beiträge geben nicht notwendigerweise die Auffassung des AWI wider.

Herausgeber
Dr. Horst Bornemann

Redaktionelle Bearbeitung und Layout
Birgit Reimann

Alfred-Wegener-Institut
Helmholtz-Zentrum für Polar- und Meeresforschung
Am Handelshafen 12
27570 Bremerhaven
Germany

www.awi.de
www.reports.awi.de

Der Erstautor bzw. herausgebende Autor eines Bandes der Berichte zur Polar- und Meeresforschung versichert, dass er über alle Rechte am Werk verfügt und überträgt sämtliche Rechte auch im Namen seiner Koautoren an das AWI. Ein einfaches Nutzungsrecht verbleibt, wenn nicht anders angegeben, beim Autor (bei den Autoren). Das AWI beansprucht die Publikation der eingereichten Manuskripte über sein Repositorium ePIC (electronic Publication Information Center, s. Innenseite am Rückdeckel) mit optionalem print-on-demand.

The Reports on Polar and Marine Research are issued by the Alfred Wegener Institute, Helmholtz Centre for Polar and Marine Research (AWI) in Bremerhaven, Germany, succeeding the former Reports on Polar Research. They are published at irregular intervals.

The Reports on Polar and Marine Research contain presentations and results of research activities in polar regions and in the seas either carried out by the AWI or with its support.

Publications comprise expedition reports of the ships, aircrafts, and stations operated by the AWI, research results (incl. dissertations) of the Institute and the Archiv für deutsche Polarforschung, as well as abstracts and proceedings of national and international conferences and workshops of the AWI.

The papers contained in the Reports do not necessarily reflect the opinion of the AWI.

Editor
Dr. Horst Bornemann

Editorial editing and layout
Birgit Reimann

Alfred-Wegener-Institut
Helmholtz-Zentrum für Polar- und Meeresforschung
Am Handelshafen 12
27570 Bremerhaven
Germany

www.awi.de
www.reports.awi.de

The first or editing author of an issue of Reports on Polar and Marine Research ensures that he possesses all rights of the opus, and transfers all rights to the AWI, inlcuding those associated with the co-authors. The non-exclusive right of use (einfaches Nutzungsrecht) remains with the author unless stated otherwise. The AWI reserves the right to publish the submitted articles in its repository ePIC (electronic Publication Information Center, see inside page of verso) with the option to "print-on-demand".

Titel: Wissenschaftler nutzen die Ski-doos der Polarstern, um ihr Equipment von der Eiskante aus dem dicken Eis einer Eisstation zu bergen und zurück zur Polarstern zu bringen (Foto: Laura Wischnewski, AWI).

Cover: Scientists taking ski-doos from the Polarstern and ice edge to retrieve equipment from an ice station, frozen into the thick, multiyear ice (Photo: Laura Wischnewski, AWI).

The Expedition PS101 of the Research Vessel POLARSTERN to the Arctic Ocean in 2016

Edited by

Antje Boetius and Autun Purser

with contributions of the participants

Please cite or link this publication using the identifiers
hdl:10013/epic.50642 or http://hdl.handle.net/10013/epic.50642 and
doi:10.2312/BzPM_0706_2017 or http://doi.org/10.2312/BzPM_0706_2017

ISSN 1866-3192

PS101

9 September 2016 - 23 October 2016

Tromsø – Bremerhaven

Chief scientist
Antje Boetius

Scientific coordinator
Rainer Knust

Contents

1. ÜBERBLICK UND FAHRTVERLAUF

Antje Boetius AWI

Zusammenfassung

Die Expedition PS101 „KARASIK“ war vor allem der Untersuchung von geologischen, geochemischen und biologischen Prozessen an Seebergen und Hydrothermalquellen des Gakkelrückens gewidmet. Ziele des Infrastrukturprogramms FRAM „Frontiers in Arctic Marine Montitoring“ waren zudem, mit neuen Technologien den Zustand und die Änderung des Meereissystems des Eurasischen Beckens zu untersuchen. Zu unseren vorrangigen Arbeitsgebieten bei 87°N und 60°E gehörten der große Karasik Seeberg, sowie ein hydrothermaler Seeberg im Trog des Gakkelrückens, die 2001 während der gemeinsamen AMORE Expedition mit zwei Eisbrechern, der *Polarstern* und der *Healy* entdeckt wurden. Unser Arbeitsprogramm zielte darauf ab, die Morphologie, Geophysik, Biogeochemie, Petrologie, Mikrobiologie und die faunale Zusammensetzung des Gakkelrückens und seiner Seeberge zu untersuchen. Die Forschung trägt weiterhin zum Programm „Geosphären-Biosphären Interaktion“ des Exzellenzcluster MARUM an der Universität Bremen bei, wie auch zum Helmholtz Programm ROBEX und zum NASA Programm „PSTAR - Planetary Science and Technology Through Analog Research Program“. Zur Weiterentwicklung mariner Robotik für Untereisforschung wurden erstmals der neue Tiefsee-Hybridroboter der Woods Hole Oceanographic Institution (WHOI, USA), das ROV BEAST und das OFOS-Sonar des Infrastruktur Programms FRAM eingesetzt. Wir waren ein Team von 46 Wissenschaftlern und Technikern aus fünf verschiedenen Ländern und vom 09.09.-23.10.2016 gemeinsam im Nansenbecken der zentralen Arktis unterwegs.

Abb. 1.1: Polarstern im Eis (Quelle: S. Dreutter, AWI)

Fig. 1.1: Polarstern in the ice (Source: S. Dreutter, AWI)

Fahrtverlauf

Am 09.09.2016 mittags liefen wir aus Tromsø aus. Das Forschungsprogramm begann mit dem Aussetzen ozeanographischer Bojen in norwegischen Gewässern bei Spitzbergen. Eine erste Teststation am 11.09.2016 verlief erfolgreich mit dem Einsatz des Zooplankton-Rekorders LOKI und des OFOS „Ocean Floor Observation System“. Die Test-Bilder nordöstlich von Spitzbergen zeigten ungestörten, stark belebten Meeresboden in 250 m Wassertiefe. Den Eisrand nördlich von Spitzbergen erreichten wir bei 81.5°N um Mitternacht des 11. September. Die Forschungsarbeiten begannen mit einem engmaschigen En-Route-Programm von ozeanographischen Messungen am 30°-Ost Transekt, bis wir am 13.09. das tiefe Nansen Becken erreichten. Die Ergebnisse zeigen eine Fortsetzung der Erwärmung des Tiefenwassers, das im Rahmen von Langzeitmessungen der AWI-Ozeanographie untersucht wird. Bei der Anfahrt in unser zentrales Arbeitsgebiet bei 87°N und 60°E kamen wir für diese Jahreszeit und Eisbedeckung mit Durchschnittsgeschwindigkeiten von ca. 6 Knoten im Eis schnell voran. Dabei begegneten wir immer wieder großen, kaum überfrorenen Wasserlöchern zwischen den ohnehin dünnen Eisschollen (Abb. 1.1). Eine wichtige Erneuerung an Bord für die verbesserte Eisnavigation ist das frisch installierte Meereis-Geoinformationssystem (kurz ICEGIS), das uns eine Vielfalt von Informationen auf interaktiven Karten darstellt und das wir ausgiebig testeten. Zum System gehören hoch aufgelöste Radarbilder vom Schiff, Satelliten-Daten zur Eiskonzentration und Eisschollenverteilung, Vorhersagen von Eisdrift und Wind sowie die Meeresbodenkarten. In der Nacht vom 14.-15.09. erreichten wir die Position des ersten zu bergenden FRAM Observatoriums bei 85°N und begannen die Arbeiten mit einer weiteren tiefen CTD-Wasserschöpfer-Station. Im Rahmen des Infrastrukturprogramms FRAM konnte hier in 2015 ein mit physikalisch-pelagobenthischen Sensoren und Probennehmern ausgestattetes Observatorium verankert werden, das wir erfolgreich am Morgen des 15.09. bergen konnten. Es folgte eine erste längere Eisstation, mit parallelen Planktonfängen bis in die Tiefsee und eine benthische Beprobung mit Multicorer und Kastengreifer. Die ersten Einsätze des neuen Untereis-ROV BEAST (Abb. 1.2) bestätigten, dass die Unterseite der Eisschollen über den Sommer 2016 stark abgeschmolzen war.

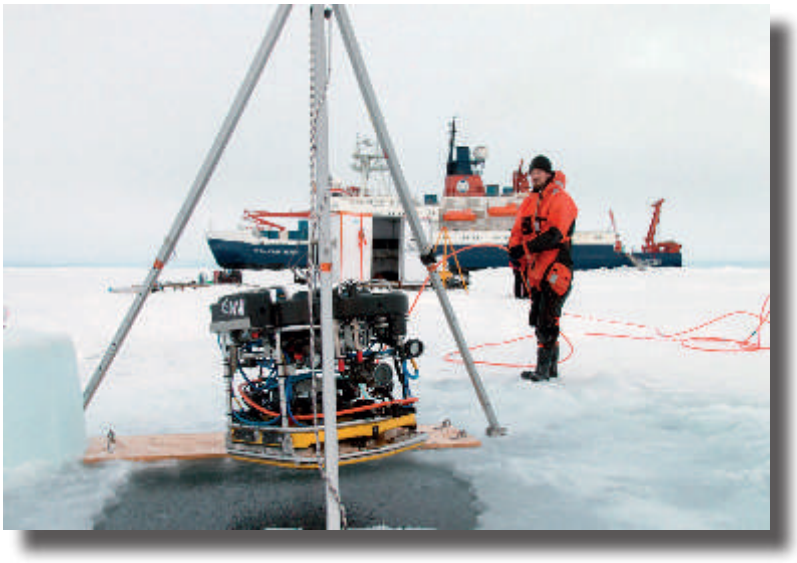

Abb. 1.2: ROV BEAST Einsatz für die Meereisphysik (Quelle: M. Nicolaus AWI)

Fig. 1.2: ROV BEAST used for sea ice physics (Source: M. Nicolaus AWI)

Weiter ging es zum Hauptarbeitsgebiet um den Karasik Seeberg des Gakkel Rückens (Abb. 1.3). Zwei Transekte mit der 5 m langen Temperaturlanze zur Messung von Wärmeflüssen im Meeresboden (16. und 17.9.) zeigen noch Hintergrundwerte im Becken. Am Fuße des Seeberges wurden erste Anzeichen für eine Fluidzirkulation im Meeresboden detektiert. Am 18.9. konnten wir den Gipfel des Karasik Seeberges erreichen und begannen die Untersuchungen mit CTD

Profilen und einem ersten Tauchgang des OFOS (Abb. 1.3) zum Gipfel, wo wir schon 2011 mit dem Kastengreifer große Schwämme in Wassertiefen von 650 m fanden.

Die ersten Bilder bestätigten die Vermutung, dass der Karasik Seeberg von einem riesigen Schwammriff bedeckt ist. Um die Bathymetrie des Seeberges zu vervollständigen, führten wir zudem einige Hydrosweep- und Parasoundtransekte zur Vorbereitung der Beprobung durch. Am 19.9. folgten parallel zu einer längeren Eisstation mit Einsätzen des ROV BEAST eine Serie der LOKI (Lightframe On-sight Keyspecies Investigation) Planktonkamera und des Multinetzes für das Plankton, sowie dem Multicorer und Kastengreifer zur Beprobung des Benthos, um die besondere Fauna der Wassersäule und des Meeresbodens des Karasik Seeberges zu untersuchen. An allen biologischen Stationen führten wir aufeinander abgestimmte Messungen des Eises, der Wassersäule und des Meeresboden durch, um die Ökologie und Biogeochemie der Seeberge systematisch zu untersuchen. In der Nacht auf den 20.9. fanden weitere Messungen mit der Temperaturlanze an den Flanken des Karasik Berges statt.

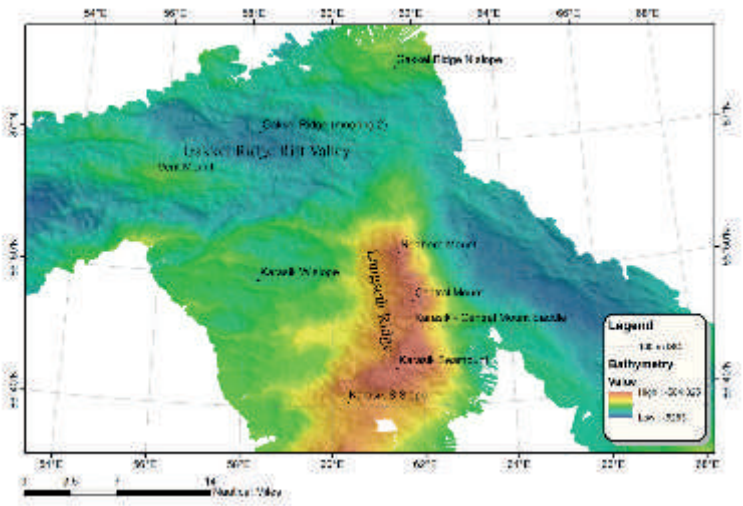

Abb. 1.3: Die Seeberge des Gakkelrückens bei 60°E (Quelle: AWI Bathymetrie und FIELAX)

Fig. 1.3: Seamounts of Gakkel Ridge around 87°N and 60 ° E (Source: AWI Bathymetry and FIELAX)

Die Bathymetrie der Region um den Karasik Seeberges bis ins Tal des Gakkelrückens gibt Aufschluss über die Ausdehnung und Morphologie der Seeberge. Als Teil des quer zum Gakkelrücken liegenden Langseth Rückens - einschließlich des Karasik Seeberges mit dem flachsten Gipfel von unter 600 m - konnten wir noch vier weitere Gipfel vermessen sowie einen einzelnen kleineren Seeberg im Trog des Gakkelrückens. Am Gipfel des Karasik Seeberges fand der erste Testtauchgang des H-ROV NUI (013) statt (Abb. 1.5). „Nereid Under Ice“ (NUI) ist eine Entwicklung des „Deep Submergence Laboratory“ am Ozeanographischen Institut in Woods Hole (WHOI, USA), das in Zusammenarbeit mit der John Hopkins Universität in den Vereinigten Staaten entwickelt wurde und dessen Einsatz auf unserer *Polarstern*-Expedition von der NASA unterstützt war. Nach einer schwierigen Bergung des AUVs aus dem Eis wurde die Vermessung des Langseth Rücken bis in den Graben des Gakkelrückens fortgesetzt. Am 21.9. konnten wir bei günstigen Eisbedingungen die nördliche Verankerung des FRAM Observatoriums bergen. Eine längere Eisstation schloss sich mit einer Vielzahl von Arbeiten auf dem Eis und parallel vom Schiff in der Tiefsee für Wassersäulen- und Plankton-Beprobungen an. Der Meeresboden der nördlichen Flanke des Gakkelrückens erwies sich dabei als zu felsig für benthische Beprobungen, da er von großen Brocken Kissenbasalt dominiert war.

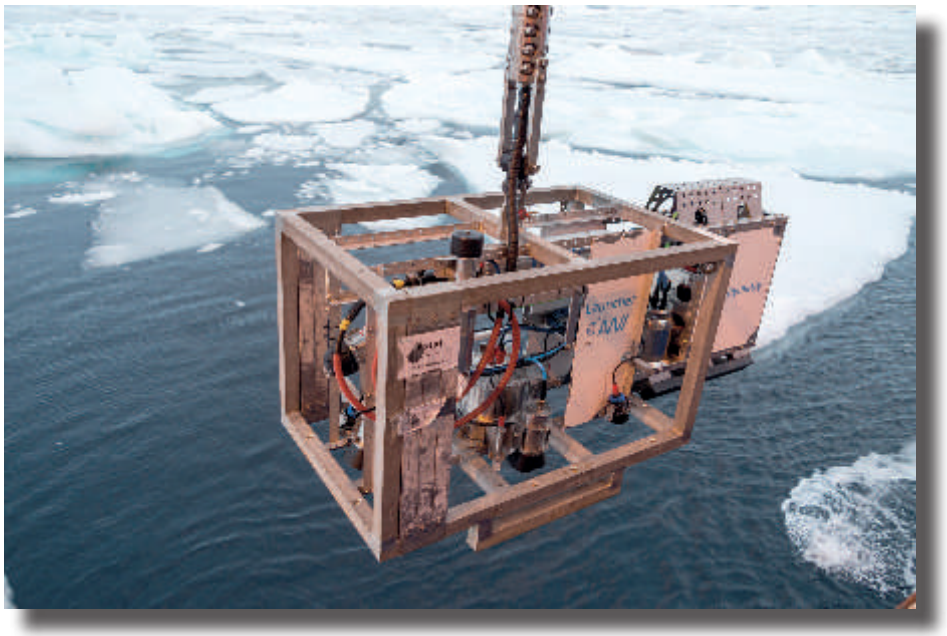

Abb. 1.4: Das OFOS – Ocean Floor Observation System samt Sonar ist mit einer HD Photo- und Videokamera, einem Posidonia-Transponder sowie Sonarsystemen bestückt (Quelle: S. Dreutter, AWI)

Fig. 1.4: The new OFOS - Ocean Floor Observation System is equipped with HD photo and video cameras, a Posidonia transponder, altimeter and sonar systems (Photo: S. Dreutter, AWI)

Nach der Rückkehr zum Langseth Rücken am 21.-22.9. beprobten wir den mittleren Seeberg, der ähnlich wie der Karasik Seeberg von Schwämmen überwuchert war. Am 22.09. wurde ein Transponderfeld für kommende NUI Tauchgänge gesetzt. Nach weiteren CTD/ Wasserschöpfer-Arbeiten und bathymetrischen Vermessungen vom 22.-23.09. konnte am 23.09. der erste erfolgreiche AUV Tauchgang von NUI für die hochauflösende Kartierung eines Teils des Gipfels des Karasik Seeberges durchgeführt werden. Ein langes CTD Tow-Yo bestätigte die Ergebnisse vorheriger kürzerer Profile, dass direkt am Langseth Rücken kein aktiver Hydrothermalismus vorzufinden ist. Tow-Yo bedeutet, dass die CTD im Bereich von bis zu 4.000 m über dem Meeresboden wiederholt gehievt und gefiert wird, um die Ausdehnung einer möglichen hydrothermalen Fahne zu verfolgen. Diese Strategie setzten wir auch am tiefen Seeberg im Trog des Gakkelrückens ein, wo schon in 2001 und 2015 hydrothermale Fahnen detektiert wurden. Vom 23.-26.09. konnten wir mit CTD und OFOS Profilen sowie einer Beprobung mit dem TV MUC den Ursprung der hydothermalen Fahne auf die nordwestliche Flanke des 8 km langen, tiefen Seeberges im Tal des Gakkelrückens einengen. Aufgrund der sich verschlechternden Wetter und Eisbedingungen entschieden wir uns je nach Bedeckung durch größere Eisschollen für das wechselweise Beproben beider Arbeitsgebiete.

Am 26.-27.09. folgte eine längere Eisstation mit paralleler benthischer und geologischer Beprobung der tiefen westlichen Flanke des Langseth Rückens. Nach Rückkehr zum Karasik Seeberg fand tagsüber der NUI AUV Tauchgang 14 statt, der eine erste hochauflösende Karte des Karasik Gipfels erbrachte. In der Nacht setzten wir die benthologische Beprobung des Langseth Rückens fort, um dann am 28.09. zum hydrothermalen Seeberg zurückzukehren. Weitere OFOS und CTD To Yows sowie die Beprobung mit dem TV MUC und Multinetz ergaben ein kohärentes Bild der Fluidaustritte und der assoziierten Gemeinschaften am nordwestlichen Hang bei Tiefen um 3.100 m, während die stärksten Signale der Ventfahne bei 2.600-2.900 m zu finden waren.

Am 30.09. kehrten wir zum Karasik Seeberg zurück, um ein Wetterfenster für einen weiteren NUI Tauchgang (15) als AUV zu nutzen. Eine zweite hochauflösende Karte des Gipfels wie auch ein Fotomosaik mit Markierung möglicher Fluidaustritte wurden erzielt. Danach folgte ein langer OFOS Tauchgang über den Sattel zwischen Karasik und dem mittleren Seeberg. Am 01.10. folgte eine weitere Eisstation mit Wasserschöpfer und Plankton Proben am nördlichen Seeberg. Danach führten wir mit dem Schiff für 24 h einen großen ADCP / Hydrosweep Transekt über den gesamten Langseth Rücken und Gakkeltrog aus, um die Strömungsprofile um den Karasik Seamount, einschließlich weiterer CTD-Wasserschöpfer Profile aufzunehmen. Am 03.10. kehrten wir zum Vent Mount zurück, um weitere Proben der Gase der hydrothermalen Fahne zu gewinnen. Bis zum 05.10. konnten wir mehrere Einsätze mit *in-situ* Pumpen zur Untersuchung der Vent-Plume abschließen. Dazu fanden Beprobungen des Plankton statt sowie ein weiterer OFOS Tauchgang, wie auch ein Dredge-Hol am nordwestlichen Hang in über 3.000 m Wassertiefe. Die nächsten Stationen war ein längerer Temperaturlanzen-Transekt über den Sattel des Karasik Seeberges, sowie weitere benthische Beprobungen. Auch setzten wir einen weiteren Transponder für NUI aus. Die Dredge-Hols von den Flanken des Langseth Rückens erbrachten interessante Gesteinsproben. Ein kurzes Wetterfenster am 06.10. konnten wir nutzen, um einen ersten Testtauchgang des NUI als ROV durchzuführen. Leider musste dieser wegen eines technischen Fehlers frühzeitig abgebrochen werden. Wir führten bei extrem schwierigen Eisbedingungen und geringer Sicht und Schneetreiben ein weiteres Dredge-Hol am Nordhang des Langseth Rückens durch und schlossen die Beprobung des nördlichen Gipfels mit TV MUC und Kastengreifer ab. Am 07.10. folgte der letzte Dredge-Hol am Langseth Rücken. Bei schwierigen Wetterverhältnissen bedingt durch starke Winde und schlechte Sicht sowie zunehmende Dunkelheit konnten weitere Stationen für das Aussetzen von Eisbojen und die Gewinnung von Eiskernen nur mit dem Mummy Chair in unmittelbarer Nähe des Schiffes durchgeführt werden. Vom 7-8. 10. wurde die Beprobung des Sattels zwischen mittlerem Seeberg und dem Karasik abgeschlossen, bevor am 08.10. ein weiteres Wetterfenster einen sehr erfolgreichen NUI Tauchgang im ROV Modus, mit einer Vielzahl wertvoller biologischer Beobachtungen und Proben erlaubte.

Abb. 1.5: Das Nereid Under Ice (NUI) des Woods Hole Oceanographic Institute (WHOI USA) ist mit einem haarfeinen Glasfaserkabel mit dem Schiff verbunden und überträgt hochauflösende Bilder sowie Multibeam Daten und Sensoren Messungen vom Meeresboden bis zu 1000 m unter dem Eis.

Fig. 1.5: The Nereid Under Ice (NUI) of the Woods Hole Oceanographic Institute (WHOI USA) is connected to the ship with a fiber-optic cable and transmits high-resolution images as well as multibeam data and sensor measurements from the seabed up to 1000 m below the ice.

Vom 08.-09.10. wurde die südliche Flanke des Karasik Seeberges beprobt mit einer Reihe von Plankton und Benthos-Geräten. Damit waren die Arbeiten am Langseth Rücken abgeschlossen. Die Transponder wurden wegen sehr ungünstiger Eis und Wetterbedingungen aufgegeben und der Transit zum Vent Mount angetreten.

Vom 09.10.-11.10. lag der Fokus der Arbeiten auf der Kartierung der Fluidaustritte und der aufsteigenden Ventfahne mittels OFOS und der CTD-Rosette im Wechsel. Es gelang, viele kleinere Sulfidschlote und Fluidaustritte zu dokumentieren, und den Ursprung der großen Fahne auf ein Feld von 50x100 m einzuengen. Die T-Sensoren an vielen Geräten zeigten dabei starke Ausschläge. Wir konnten jedoch nicht die Quelle der Ventfahne direkt am Meeresboden aufspüren. Kurzfristig konnte auch mit den Helikoptern geflogen werden, um die verbleibenden Bojen auszubringen. Am Nachmittag des 11.10. mussten wir Richtung Spitzbergen aufbrechen, mit dem Plan, die Geräte einer große FRAM – Eisbojen-Station abzubergen. Am 13.-14.10. wurde ein kurzer X-CTD Transekt im Nansen Becken gefahren. In der Nacht des 14.10. gelang es, dank günstiger Wetterbedingungen den Großteil der Eisbojen von einer großen Scholle aus mehrjährigen Meereis abzubergen. Am 15.10. setzten wir den Weg durchs Eis fort, konnten aber die Durchschnittsgeschwindigkeit von ca. 5 Knoten auch auf dem Weg Richtung Spitzbergen halten. Die Forschungsarbeiten der Reise PS101 wurden mit einem OFOS Tauchgang am Eisrand nördlich von Spitzbergen in Tauchtiefen abgeschlossen, die mit denen am Karasik Seeberg vergleichbar sind. Dabei wurden in Tiefen von 300 m dichte Filtrierergemeinschaften und Korallenfelder vorgefunden; Spuren von Schleppnetzen sahen wir nicht. Als letzte Station der Reise wurde für die AWI Biogeochemie westlich von Spitzbergen am Rande des Yermak Plateaus ein Multicorer genommen. Hier waren viele Trawlspuren bis in Tiefen von 850 m zu verzeichnen.

Der Transit zurück nach Bremerhaven dauerte bis zum frühen Morgen des 23. Oktober. Die En-Route Messungen hydrologischer Parameter der Wasseroberfläche wurden am 22.10. um 10:00 beendet. *Polarstern* legte am 23.10. 8:00 an der Pier der Lloyd Werft an. Die Expedition war ein voller Erfolg. Wir bedanken uns im Namen aller Fahrtteilnehmer bei Kapitän Schwarze und der Besatzung der *Polarstern* für die hervorragende Unterstützung bei den Arbeiten auf See und die freundliche Zusammenarbeit während der Expedition KARASIK (PS101).

Abb. 1.6: Gruppenfoto der Expedition Karasik (PS101) (Quelle: J. Pliet)

Fig. 1.6: Group photo of the Expedition Karasik (PS101) (Source: J. Pliet)

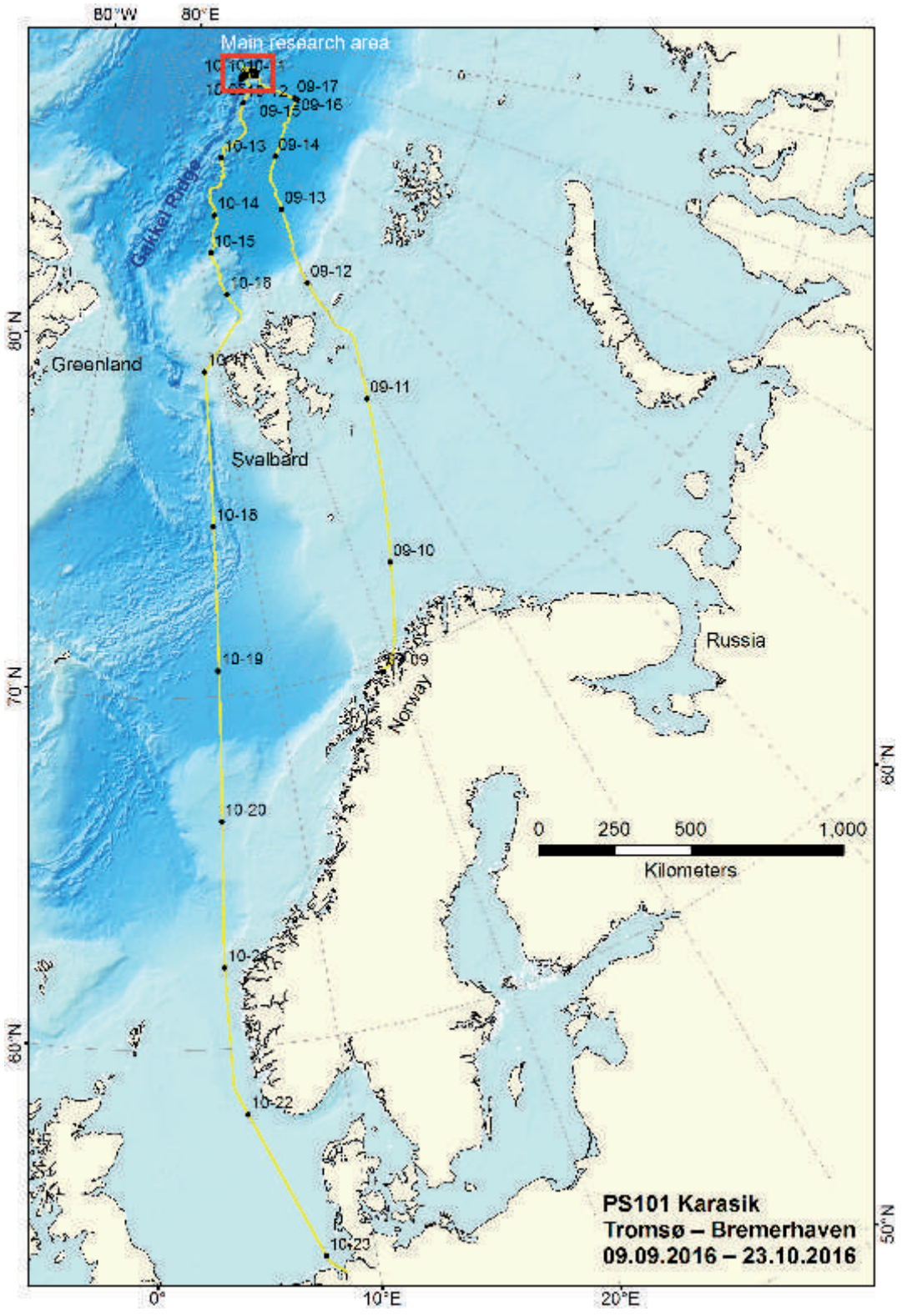

Abb. 1.7: Fahrtroute der Expedition Karasik (PS101) mit dem Hauptuntersuchungsgebiet (Quelle: FIELAX)

Fig. 1.7: Route of the expedition Karasik (PS101) with main research area (Source: FIELAX)

SUMMARY AND ITINERARY

The expedition PS101 "KARASIK" was mainly dedicated to the investigation of geological, geochemical and biological processes associated with the seamounts and hydrothermal vents of Gakkel Ridge. The expedition also contributed to the aim of the FRAM "Frontiers in Arctic Marine Monitoring" infrastructure programme, to innovate technologies for monitoring Arctic change, especially in the Eurasian Basin. Our main working area was in the region of 87° N and 60° E, an area which included the large Karasik Seamount as well as a hydrothermally active mount within Gakkel Ridge. Both structures were discovered in 2001 during the joint AMORE expedition with two icebreakers, the *Polarstern* and the *Healy*. Our research programme was designed to investigate the morphology, geophysics, biogeochemistry, petrology, microbiology and the faunal composition of the seamounts and vents at Gakkel Ridge. This work contributes to the programme "Geosphere-Biosphere Interaction" of the Cluster of Excellence MARUM at the University of Bremen, as well as to the Helmholtz Program ROBEX and NASA Program "PSTAR - Planetary Science and Technology Through Analog Research Program". For furthering the use of marine robotics in extreme environment studies, we used the new deep-sea hybrid robot from the Woods Hole Oceanographic Institution (WHOI, USA), the ROV BEAST and the OFOS-Sonar of the FRAM infrastructure programme for the first time. We were a team of 46 scientists and technicians from five different countries and worked together in the Nansen basin of the Central Arctic from 09.09.-23.10.2016.

Expedition narrative

On 9 September at noon we left the port of Tromsø. The research programme began with the deployment of oceanographic buoys in Norwegian waters near Spitsbergen. A first test station on 11 September was successfully completed with the use of the zooplankton recorder LOKI and the OFOS "Ocean Floor Observation System". The seafloor Northeast of Spitsbergen imaged with the OFOS system and found to be an undisturbed and densely populated at 250 m depth. The ice edge at 81.5° N was reached at midnight on the 11 September. We started a series of oceanographic measurements on the 30° East transect until we reached the deep Nansen basin on the 13 September. Reaching depths of >4,000m we completed a CTD-Rosette water-sampling station. First results from this transect show a continuation of deep water warming, which is investigated in the framework of long-term observations of the AWI-Oceanography group. Considering the season and ice cover, we made swift progress towards our main working area at 87°N and 60° E, with average speeds of about 6 knots through the thin ice. We repeatedly encountered large, barely frozen water leads between the thinned ice floes (Fig. 1.1). An important technology tested on board for improved ice-navigation was the newly installed sea-ice geoinformation system (ICEGIS), which provided us with a variety of interactive maps. These included high-resolution radar images from the ship, satellite data for ice concentration and ice floe distribution, predictions of ice drift and wind, as well as seabed bathymetric maps. In the night of 14 to 15 September we reached the position of the first FRAM observatory at 85°N. As part of the FRAM infrastructure programme, this mooring was equipped with physical-pelagobenthic sensors and deployed in 2015. After more than a year of measurements, it was successfully retrieved in the morning of the 15 September. In parallel to a sea ice station, water sampling and plankton catches as well as a series of seafloor samplings with multicorer and box corer completed the station. The first deployment of the

new Underice ROV BEAST (Fig. 1.2) showed that the underside of the ice floes was strongly melted during the summer of 2016.

We continued towards Karasik Seamount (Fig. 1.3) and completed two transects with the 5 m long temperature lance for the measurement of heat fluxes whilst we were underway, on the 16 and 17 September. First, only background values were retrieved, but at the foot of seamount, signs of fluid advection into the sea floor were detected. On the 18 September we reached the summit of the Karasik Seamount and started the investigations with CTD profiles and a first dive of the OFOS (Fig. 1.4). In 2011 large sponges were sampled by boxcoring at the summit at a depth of 650 m. The first pictures by OFOS confirmed that the Karasik Seamount is covered by dense sponge communities, forming reef-like structures. In order to complete the bathymetry map of the Karasik and to prepare for detailed sampling, we also carried out Hydrosweep and Parasound transects. On 19 September a series of the LOKI (Lightframe On-sight Keyspecies Investigation) plankton camera and the multinet for plankton sampling hauls followed, as well as multicorer and boxcore hauls for the sampling of the benthos. This series of instruments formed our standard set of sampling for biology, often in parallel to carrying out longer ice stations, in order to investigate the special fauna of under ice, within the water column and close to the sea floor, around the seamounts of the Gakkel Ridge. In the night of the 20 September further measurements followed with the temperature lance on the flanks of the Langseth Ridge.

The now improved bathymetry of the region around the Karasik Seamount and the rift valley of Gakkel Ridge revealed the extent and morphology of the seamounts (Fig. 1.3). We were able to map four seamounts north and south of the Karasik Seamount, as well as one deep mount in the trough of Gakkel Ridge, where hydrothermal activity was previously detected. The first full test dive in AUV mode of the hybrid robot NUI (dive 013) took place above Karasik Seamount. "Nereid Under Ice" (NUI) is a development of the "Deep Submergence Laboratory" of the Woods Hole Oceanographic Institute (WHOI, USA), developed in collaboration with John Hopkins University and supported by NASA (Fig. 1.5). After a difficult recovery of the AUV from under the ice, the survey of the Langseth Ridge was continued across the Gakkel Ridge. Between the 20 and 21 September good ice-conditions allowed the fast recovery of the second FRAM observatory. Again, we carried out an ice station, together with a deep-sea CTD cast and plankton sampling in the vicinity of the observatory site. The first TV MUC showed that the seafloor of the northern flank of Gakkel Ridge was too rocky for benthic sampling, as it was predominantly formed by large pillow basalts still exposed at the seafloor surface.

After returning to the Langseth Ridge on 21– 22 September, we sampled the central seamount, which like Karasik Seamount was also densely covered by sponges. In increasingly difficult weather and ice conditions, we decided to move back and forth between the mounts of Langseth Ridge and the Gakkel Rift valley to carry out work in whichever was most clear of thick ice at a particular time. Approximately 25 nautical miles separated the two research sites.

On 22 Sepember a transponder field was set up for upcoming NUI dives. A long CTD –Tow-Yo profile confirmed the results of previous shorter profiles, that no signs of active hydrothermalism are associated with the Langseth Ridge. “Tow-Yo” means that the CTD is repeatedly hoisted between midwater and seafloor depths, in order to detect hydrothermal signatures. We also used this strategy on the deep mount in the Gakkel Ridge rift valley, where hydrothermal plumes were reported from cruises in 2001 and 2015. After the first reconnaissance surveys with the CTD and OFOS between 23 and 26 September we could trace the origin of the hydothermal plume to the north-western flank of the 8 km long mount. First samples were retrieved with water samplers and TV MUC.

On the 26 – 27 September we carried out a longer ice station with parallel benthic and geological sampling of the deep western flank of the Langseth Ridge. After returning to the

Karasik Seamount, the first scientific NUI AUV dive (014) provided a high-resolution map of the Karasik summit. At night, we continued the benthological sampling of the Langseth Ridge. On 28 September we returned to the hydrothermal mount for a series of OFOS and CTD Tow-Yos, plus TV MUC and multinet sampling. This allowed a first coherent picture of the fluid flow sources and their associated communities to be drawn up. On 30 September we returned again to Karasik Seamount, to use a good weather window for another NUI dive (15) in AUV mode, for a second high-resolution map of the summit along with a photomosaic and a survey of chemical signatures in the bottom water to be carried out. This was followed by a long OFOS dive over the saddle between Karasik and the Central Seamount on the 1 October, and a sea ice station with parallel sampling of water plankton to be conduceted at the Northern Seamount. Next we carried out a long ship-based ADCP & Hydrosweep survey across the entire Langseth Ridge and Gakkel Ridge for 24 hours, to record the geostrophic flow.

On the 3 October we returned to the hydrothermally active mount, to obtain further water samples of the hydrothermal plume. Until the 5 October we were able to complete several deployments of *in-situ* pumps into the vent plume, as well as sampling of the plankton and carrying out another OFOS dive. The dredge sampling programme started with a haul across the northwest slope of the vent mount. Upon returning to Langseth Ridge, we completed a temperature lance transect at the saddle between Karasik seamount and the central mount, as well as further benthic sampling. We also deployed another transponder for the upcoming NUI dive. The next dredge hauls brought interesting rock samples from the flank of Langseth Ridge. A short window of good weather on 6 October was used to carry out an initial test dive of the NUI in ROV mode. Unfortunately the dive had to be canceled early because of a technical problem. The next dredge haul at the northern slope of the Langseth Ridge was carried out under extremely difficult ice conditions and poor visibility due to heavy snow. We followed up with the sampling of the northern peak with the TV MUC and the box corer. On the 7 October we completed the last dredge haul on Langseth Ridge. Under increasingly difficult weather conditions, further ice buoys were deployed, and ice cores sampled only during short ice stations next to the ship set up via the mummy chair. From the 7 - 8 October the benthic and planktonic sampling of the saddle between the central seamount and the Karasik was completed. On the 8 October weather was good enough for a further very successful ROV NUI dive, that brought back high resolution observations of benthic life and also important biological samples.

From 8 – 9 October we deployed instruments at the southern flank of Karasik seamount for plankton and benthos sampling. With the collection of this sample set, the work at Langseth Ridge was completed. The NUI transponders had to be abandoned because of very unfavorable ice and weather conditions prohibited their recovery.

From the 9 -11 September we returned to the vent mount. The focus was on the high resolution mapping, probing and photography of the source of the significant hydrothermal vent plume, with OFOS and the CTD rosette. A short improvement of the weather allowed for several ice stations by helicopter to be conducted in parallel, in order to deploy the remaining sea ice buoys. We ended our work at the vent mount with many images and samples from the main field of fluid sources characterized by small chimneys and leakage from the seafloor, but were not able to detect the large source of the persistent plume, which prevailed at depths of 2,600-2,900 m above the chimney field at 3,100 m.

In the afternoon of the 11 October we had to end the work at Gakkel Ridge to return to Svalbard. We planned to retrieve equipment from the large FRAM buoy station deployed in 2015, which had drifted to the north of Svalbard. On the 13 and 14 October another short X-CTD transect was completed in the Nansen Basin. We progressed with an average speed of about 4-5 knots through the ice. In the night of the 14 October we found the large multiyear ice floe with the

FRAM buoy station, and succeeded in retrieving the bulk of the ice buoys thanks to favorable weather conditions. On 15 October we continued the transit to Svalbard. The last stations of the expedition PS101 included an OFOS dive at the ice margin north of Spitsbergen, to compare the benthic community at the comparatively steep seafloor found there with those imaged at the Karasik seamount. We detected a dense and colorful community of filter feeders including many coral species at the ice margin at depths of 300-200 m, and did not see any traces of benthic trawl fishing. For the AWI biogeochemistry group, a multicorer was taken west of Svalbard at the margin of the Yermak plateau, the last stationary science station of the trip. We noted again abundant filter feeders, but saw abundant signs of bottom trawling down to 850 m water depth.

Further underway measurements of ocean surface hydrology were carried out until the 10 am on 22 October. The transit back to Bremerhaven ended in the early morning of October 23. At 8:00 pm, *Polarstern* moored at the pier of the Lloyd shipyard. The expedition was a great success. On behalf of all the participants we would like to thank the captain and the crew of *Polarstern* for the excellent support with work at sea and the friendly cooperation during the expedition KARASIK (PS101).

2. WEATHER CONDITIONS DURING PS101

Max Miller[1], Juliane Hempelt[1] [1]DWD

On late Friday morning September 09 2016, 11:15 am, *Polarstern* left Tromsø for the campaign PS101. Light and variable winds, 12° C and sunshine were observed.

A high over Eastern Europe built a ridge towards Svalbard and a low was centred over Kara Strait. Therefore easterly winds increased rapidly after leaving the fjords and peaked at Bft 7 on Friday evening. But heading north we went away from the low and winds abated. During the weekend winds alternated between north and east at Bft 4 to 5.

Meanwhile the ridge at Svalbard had melted with a high over Siberia and moved away northeast. From Iceland a strong low approached Fram Strait. On Tuesday (Sep. 13) winds veered south and reached the maximum at Bft 6 on Wednesday. The low moved on towards North Pole with north-westerly winds on Thursday (Sep. 15). A high over Scandinavia spread to Barents Sea and built a ridge towards our area.

A storm (Ex-“Ian”) arrived at Iceland on Saturday (Sep. 17) heading north. Together with the high, now over Kara Sea, it caused increasing southerly winds at Bft 6 to 7. The calm centre of Ex-“Ian” crossed *Polarstern* on Monday (Sep. 19). Afterwards winds veered north and freshened rapidly up to Bft 7 during the night to Tuesday. Over Scandinavia a new high had formed and built a ridge north. Therefore winds abated on Wednesday (Sep. 21).

On Friday (Sep. 23) a low over Alaska started to move towards North Pole. At the same time a high south of the Jamal Peninsula spread north. Therefore pressure gradient over our area increased. Winds alternated between north and west and reached their maximum at Bft 8 with some peaks 9 on Saturday (Sep. 24). Already during the night to Sunday winds calmed down – the low had arrived at North Pole and headed towards Severnaya Zemlya. But halfway the low turned back and reached North Pole on Friday (Sep. 30) again. In the meantime we observed moderate to fresh winds around northwest. Low ceiling with light snowfall and fog patches prevented flight operations as it was so often the case.

A new low between Scotland and Iceland moved north. On Saturday (Oct. 01) it reached North Cape, passed between Svalbard and Franz-Josef-Land and headed northwest afterwards. At its northeast side southerly winds at Bft 5 to 6 transported warmer air masses to our area. On Monday (Oct. 03) temperature rose above the freezing point and snow changed to rain.

The rest of the week was dominated by several lows forming at the north-eastern end of Greenland and moving east. They created steady ups and downs of temperature and winds. At their east side temperature rose near zero and dropped clearly below -10° C at the west side. On Wednesday (Oct. 05) southerly winds peaked at Bft 8. But a weak ridge following on Thursday caused a rare situation of clearing skies and good flight conditions. The next low deepened rapidly to a storm with southerly winds up to Bft 9 on Friday (Oct. 07). After the passage of the centre with almost calm conditions we observed Bft 8 again on Saturday (Oct. 08) – now from north to northwest.

On Sunday (Oct. 09) a small ridge of the high over Scandinavia crossed *Polarstern*. Winds abated, clouds broke and opened a short “flight window” again. But another low approached and caused stormy south-easterly winds on Monday (Oct. 10).

On Tuesday (Oct. 11) *Polarstern* set out for home. The low moved away southeast and winds abated. The high over Scandinavia built a ridge towards a high over Beaufort Sea and we observed only light and variable winds on Thursday (Oct. 13).

During the night to Friday (Oct. 14) a low formed once again at the north-eastern end of Greenland, deepened rapidly to a storm and headed northeast. South-easterly winds increased up to Bft 6 on Friday. After passage of the storms centre winds veered northwest on Saturday evening and accelerated to Bft 8 to 9. On Sunday (Oct. 16) winds abated clearly. But during the night to Monday we felt a local effect while passing the north-western corner of Svalbard. For about one hour southerly winds increased up to Bft 8 forced by the parallel coastline. Afterwards winds abated to Bft 4 to 5 according the pressure gradient.

The high over Scandinavia had moved to Russia and its ridge towards Greenland Sea weakened. But a low heading north along the east coast of Greenland weakened, too. While steaming south we often observed southerly winds around Bft 4 with isolated peaks up to Bft 6. The sea state did not exceed 2 m.

After midweek the ridge of the high over Russia built towards Norway intensified again. Together with a low over Central Europe it caused increasing pressure gradient over northern North Sea. During the night to Saturday (Oct. 22) easterly winds out of the Skagerrak freshened up to Bft 7 to 8 forcing a sea state of 3 to 3.5 m. Approaching the German Bight winds abated gradually.

On Sunday morning, October 23 2016, *Polarstern* reached Bremerhaven at moderate to fresh winds from northeast.

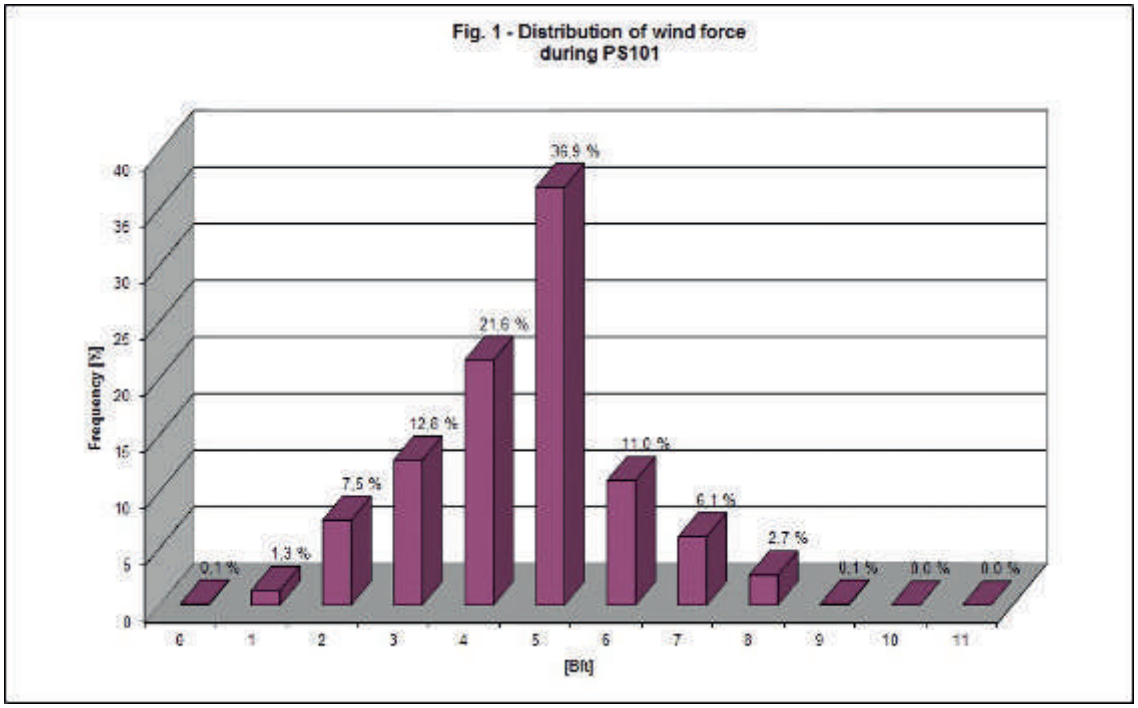

Fig. 2.1: Distribution of wind force

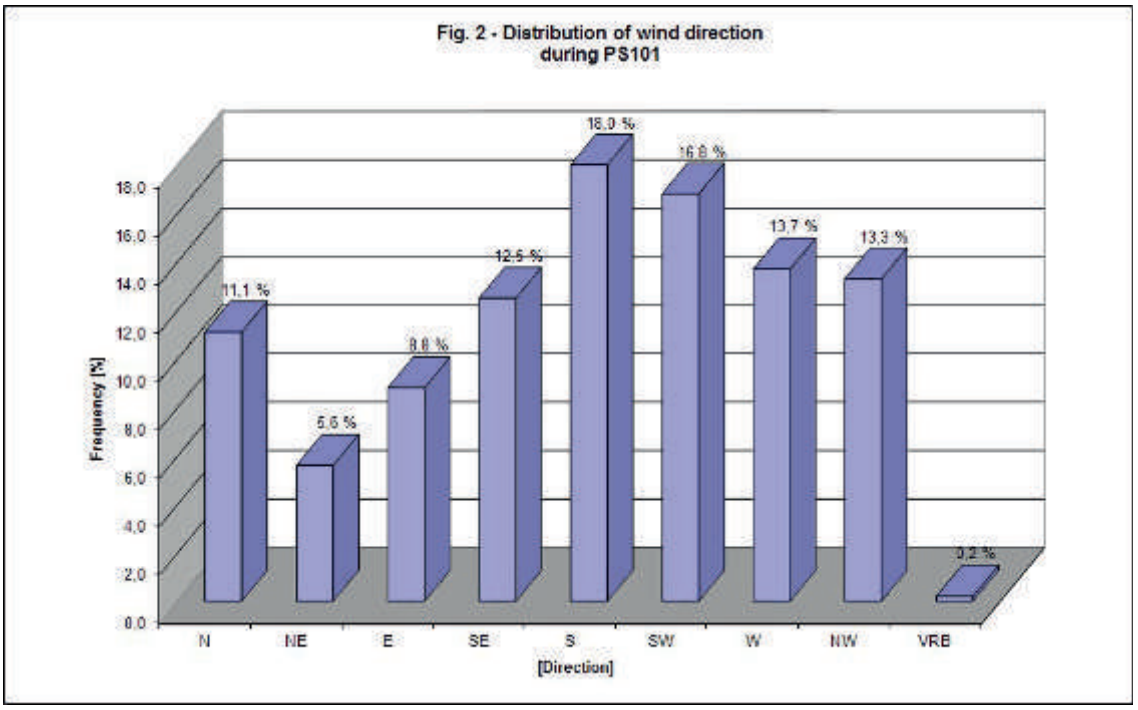

Fig. 2.2: Distribution of wind direction

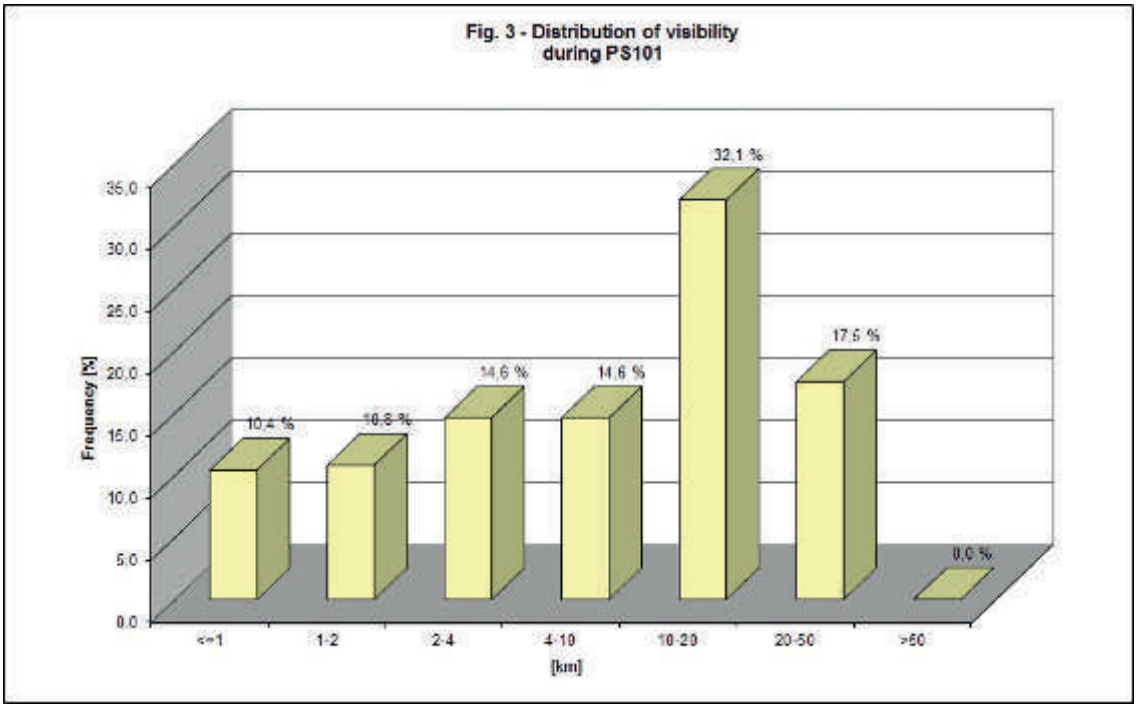

Fig. 2.3: Distribution of visibility

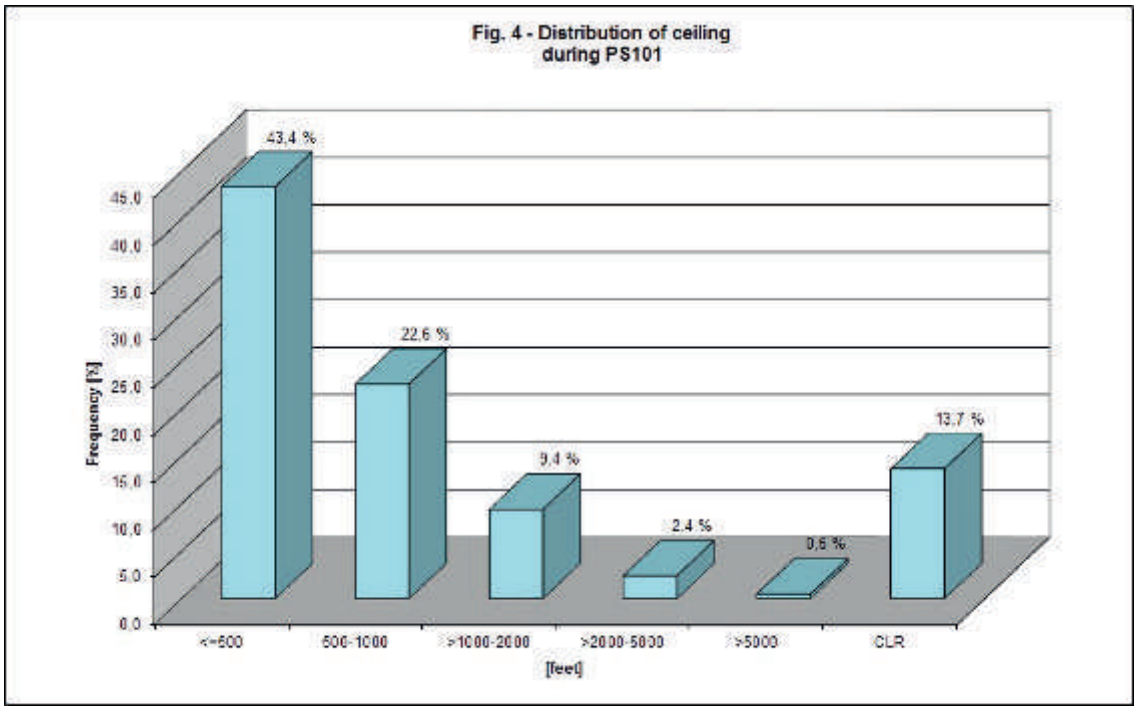

Fig. 2.4: Distribution of cloud coverage

3. BATHYMETRY AND HABITAT MAPPING OF KARASIK SEAMOUNT AND GAKKEL RIDGE

Autun Purser[1], Harald Biebow[2], Antje Boetius[1,3,4], Simon Dreutter[1], Laura Hehemann[1], Sebastian Roessler[5], Frederic Tardeck[5], Boris Dorschel[1] (not on board), Yann Marcon[1,4] (not on board)

[1]AWI
[2]iSITEC
[3]MPI
[4]MARUM
[5]FIELAX

Grant No. AWI_PS101_01

3.1 Bathymetry – Hydrosweep

Frederic Tardeck[1], Sebastian Roessler[1]

[1]FIELAX

Objectives

Most of the worlds' ocean topography has to date not been surveyed with echo sounders. Instead, much of the existing chart data, as used in the IBCAO and GEBCO datasets, is derived from satellite altimetry and gravimetric data. One objective of the PS101 mission was therefore to retrieve a full expedition track of multibeam bathymetry data, to contribute to the existing ocean datasets.

The target research areas were the Karasik Seamount and a vent mount in the Gakkel Ridge Rift Valley, which are located on the Langseth Ridge. The Karasik Seamount is elevated by approximately 2,500 m compared to the surrounding terrain. The peak is 571 m below sea level and is located at 61°26.43'E / 86°42.95'N. This area has been partially surveyed by multibeam echosounders from the joint *Polarstern*/*Healy* expedition, AMORE, in 2001 and by the cruises PS78 (ARK-XXVI/3) and PS80 (ARKXXVII/3). During the PS101 cruise, this existing data was further enhanced by collecting data with a higher resolution multibeam echosounding system.

Sensor description

Polarstern's shipboard deep-sea multibeam echosounder is an *Atlas Hydrosweep DS-3*. Its transducer frequency ranges from 13.6 to 16.4 kHz. Each ping results in a depth profile of 141 preformed hard beams, which are increased by algorithms of up to 345 soft beams. The individual beam width is approximately 2.3°, which gives a beam footprint of around 160 m at the general area depth of 4,000 m. The swath width has been set to 150 % of the water depth throughout the entire mission. Peripheral sensors connected to the multibeam are a GPS *Trimble* receiver for positioning, an internal navigation system and heave sensor system *HYDRINS* (Intertial Navigation System) for retrieving the ship's roll, pitch, heading angles and sound velocity keel probe.

Work at sea

The *Hydrosweep* was in operation 24 hours per day. System parameters were regularly adjusted to the sea and ice conditions. Beam profile and backscatter data was recorded and visualized with *Hypack 2015*. Water column data was not recorded as there were no relevant water column features visible. Vertical sound speed profiles from the CTD or XCTD casts

(kindly provided by the oceanographer's group) were regularly applied. The acquired data was processed on board using *Caris HIPS/SIPS Editor.* The data was manually edited, filtered by applying matrix-based median filters and exported to grids and xyz soundings. Resulting grids were produced at 100 m resolution. These grids were regularly updated as background layers for the real-time mapping tool *GlobalMapper* which was used for navigation and tracking of underwater instruments. In total, 4,366 km² of data in the Nansen Basin and Gakkel Ridge was recorded during the leg.

Preliminary results

The collected bathymetry and sub-bottom data covers a long transect (Fig. 3.1.1) along the Norwegian shelf towards Svalbard, passing the islands Hopen and Kong Karls Land, and entering the Nansen basin by passing the strait between the islands Nordaustlandet and Kvitøya. After recovering an oceanographic mooring, the cruise progressed towards the Karasik Seamount and the adjacent Gakkel Ridge area. During the cruise, several survey transects were performed to fill gaps within the existing bathymetry.

On the journey back to Bremerhaven, Svalbard was passed on the western side over the Yermak Plateau.

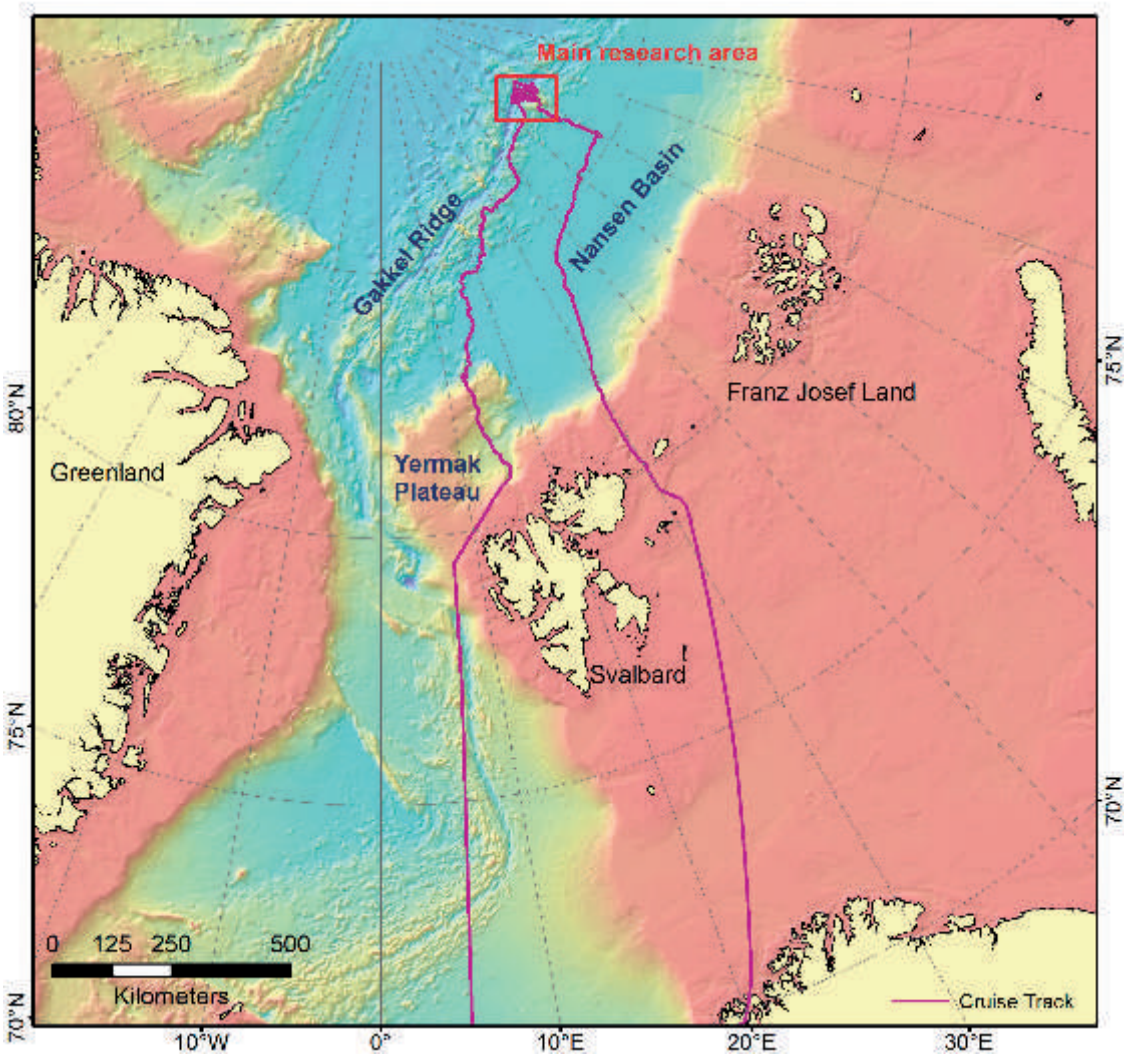

Fig. 3.1.1: Track (purple) of collected Hydrosweep bathymetry and Parasound sub-bottom data collected during this mission; map projection UPS North (WGS84)

The Gakkel Ridge area of the Langseth Ridge was previously charted during the AMORE cruise in 2001 using the former *Hydrosweep DS-2* system of *Polarstern* (59 beams) and a *Seabeam* system of *Healy* (121 beams) (Thiede, 2001). The actual *Hydrosweep DS-3* provides 345 beams which gives a higher spatial resolution and a higher density of measurements. Therefore, all data collected from the same regions further improves the local bathymetry grid (Fig. 3.1.2). Additionally surveys of up to 6 hours each were absolved to fill up gaps of the AMORE bathymetry grid and to reach a reference site outside of that grid.

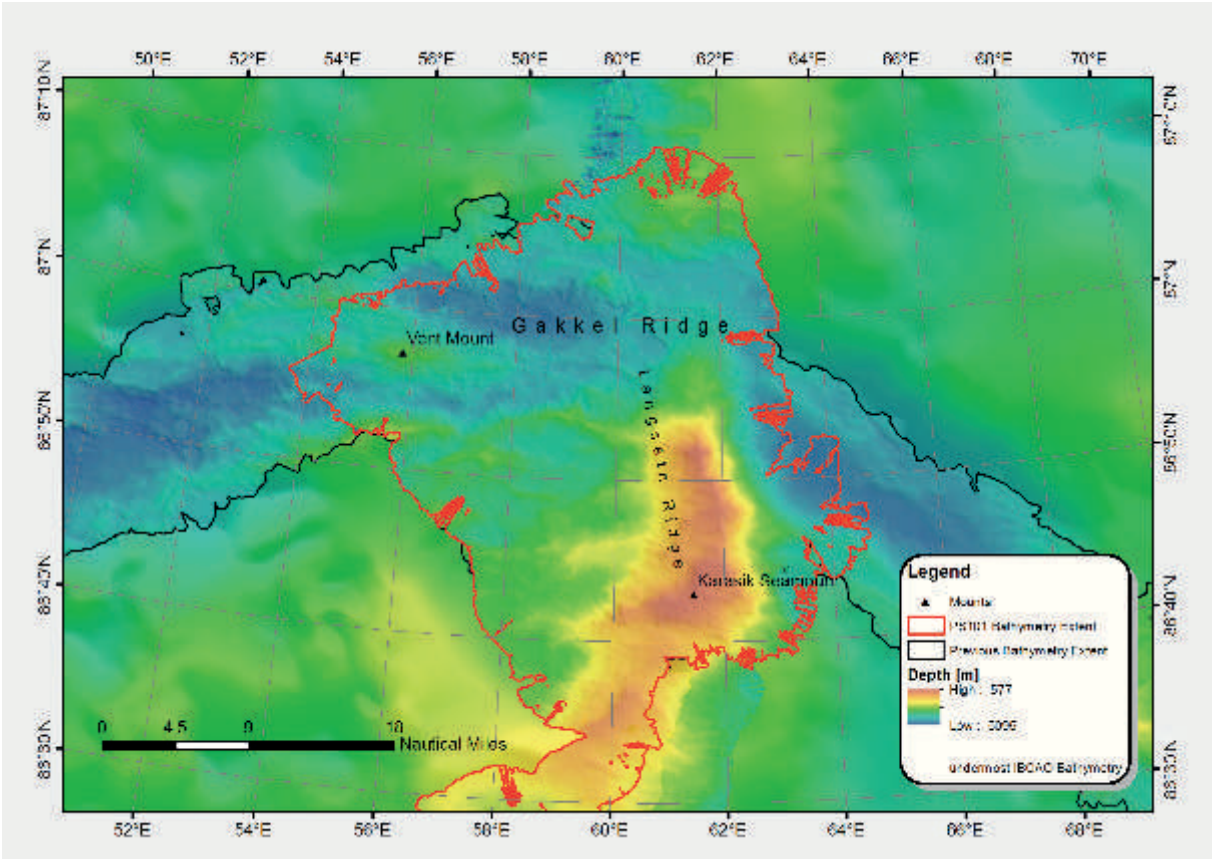

Fig. 3.1.2: Overlaying bathymetry grids from IBCAO charts (the undermost), from AMORE cruise (black outline) and from the current cruise (red outline); map projection UPS North (WGS84)

In transit to the Karasik Seamount a smaller seamount was discovered at 59°21.58'E/ 85°44.52'N (Fig. 3.1.3). The next feature in the IBCAO Bathymetry was 10 km south and had a height difference of over 600 m.

At the main research locations, the Karasik Seamount and vent site, a dense bathymetric dataset was collected during two weeks of station time. Most of the stations were drift stations where the ship drifted slowly between ice floes at a speed of not more than 0.7 kn. This resulted in a dense dataset of very good quality. Nevertheless, the individual beam footprint of 160 m at a depth of 4,000 m physically restricts a higher spatial resolution of bathymetric structures.

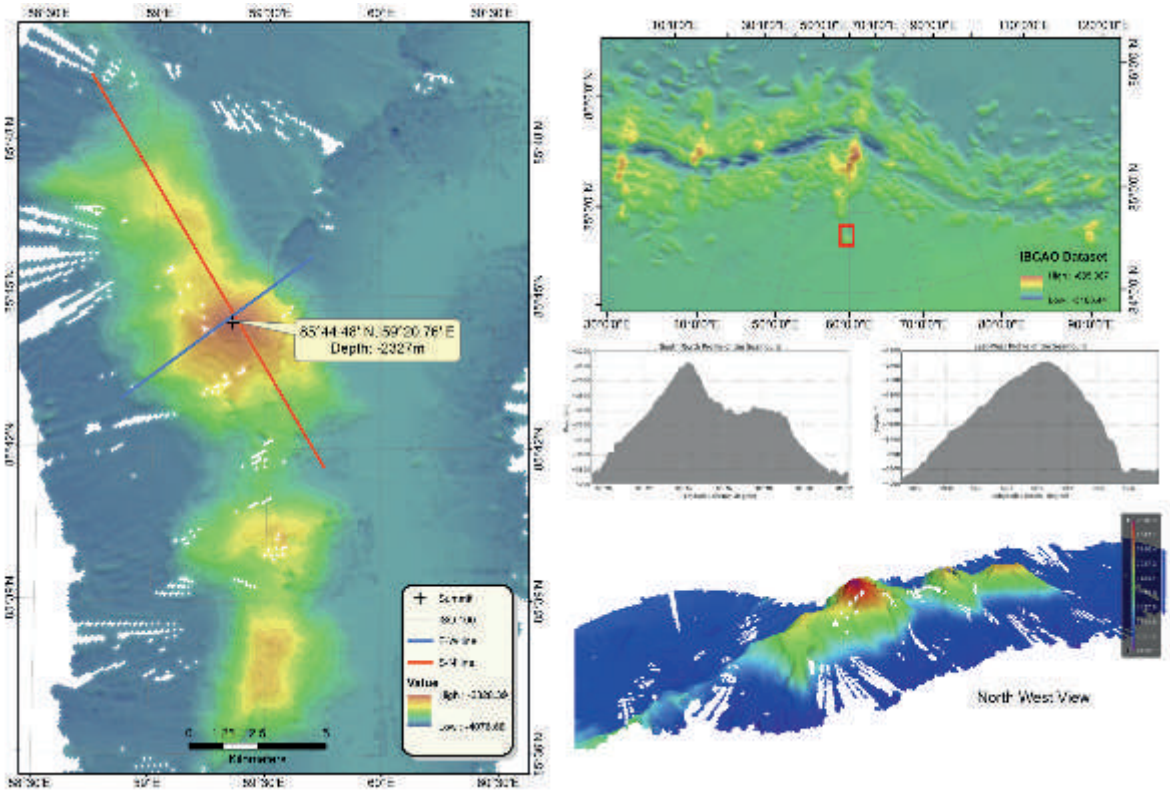

Fig. 3.1.3: Overlaying bathymetry grids from cruise PS80 (ARK-XXVII/3) charts (the undermost), and from the current cruise. Overview map, Depth profiles and a 3D on the right

Data management

Data set has been transferred to the AWI Geophysics / Bathymetry department and made available from the scientific data warehouse PANGAEA. The available data formats are *HSX* (from *Hypack*), *ASD PHF/PHS* (from *Atlas Hydromap Control*) and a grid in *GMT/NetCDF GRD*, *ESRI ASCII Grid* and *XYZ* format, projected in UTM zone 30N (on ellipsoid WGS84) and in LatLon (WGS84). As of January 2017, the following links can be used to access these datasets:

- Corrected Mastertrack in 1-Second-Resolution: https://doi.pangaea.de/10.1594/PANGAEA.869118
- MAPR raw data: https://doi.pangaea.de/10.1594/PANGAEA.869114
- USBL-Data: https://doi.pangaea.de/10.1594/PANGAEA.869118
- SWATH Sonar bathymetry: https://doi.pangaea.de/10.1594/PANGAEA.871047

References

Thiede J (2001) Cruise Report AMORE 2001: Chapter 6 Bathymetry. DOI: 10.2312/BzPM_0421_2002

3.2 Sub-bottom profiling - Parasound

Sebastian Roessler[1], Frederic Tardeck[1] [1]FIELAX

Objectives

The main objective of the sub-bottom profiling echosounder operations with the shipboard Atlas *Parasound DS3* system was the detection of seafloor characteristics and sediment structures along the cruise track, which support geological analyses of the surveyed seamounts. During station work, sub-bottom data helped to increase the success rate of sediment penetrating instruments (e.g. gravity corer, heat flow probe, *cf*. Fig. 3.2.1). The high frequency channel of the echosounder can be further used to detect gas flares in the water column. Such applications have been successfully used with methane gas flares on previous cruises (e.g. PS74 ARK-XXIV/2). During this mission data was collected and analyzed with the aim of identifying reflections of plumes in the water column.

Work at sea

The *Parasound* was in operation 24 hours a day. The echosounder parameters were set to 18.8 kHz, the desired primary high frequency (PHF), and 4 kHz, secondary low frequency (SLF). The pulse length was adjusted between 0.5 to 1.0 ms. The system was not configured to synchronize pinging with the multibeam echosounder *Hydrosweep* in order to receive a higher along-track coverage. Interfering signals from both systems were observable but did not significantly affect the desired data information. During station time and drifting transects with towed instruments, the ship's bow thruster highly disturbed the low frequency signal.

As for the plume-hunt, significant indications for hydro-acoustic anomalies due to plumes, active vents or gas flares were not found. Data files were organized into daily subsets and data of both frequencies plotted as PNG image files.

Preliminary (expected) results

The collected Parasound data covers the same recording track as the *Hydrosweep* multibeam (*cf*. Chapter 3.1). In the main research area of the Langseth Ridge, the general data quality was low due to the steep slopes and cliffs of the ridge system, which resulted in a low reflection of the *Parasound* signals – especially in the secondary low frequency (SLF). Furthermore, during all station and drift station work the bow thrusters of the vessel were enabled, which led to a high noise level disturbing the *Parasound* pulses.

Data management

The data has been transferred to the AWI bathymetry group and will be made available in the scientific data warehouse PANGAEA.

References

Background literature (not cited in text):

Gerchow P (2012) FS *Polarstern* - Geräteakte: Sedimentecholot

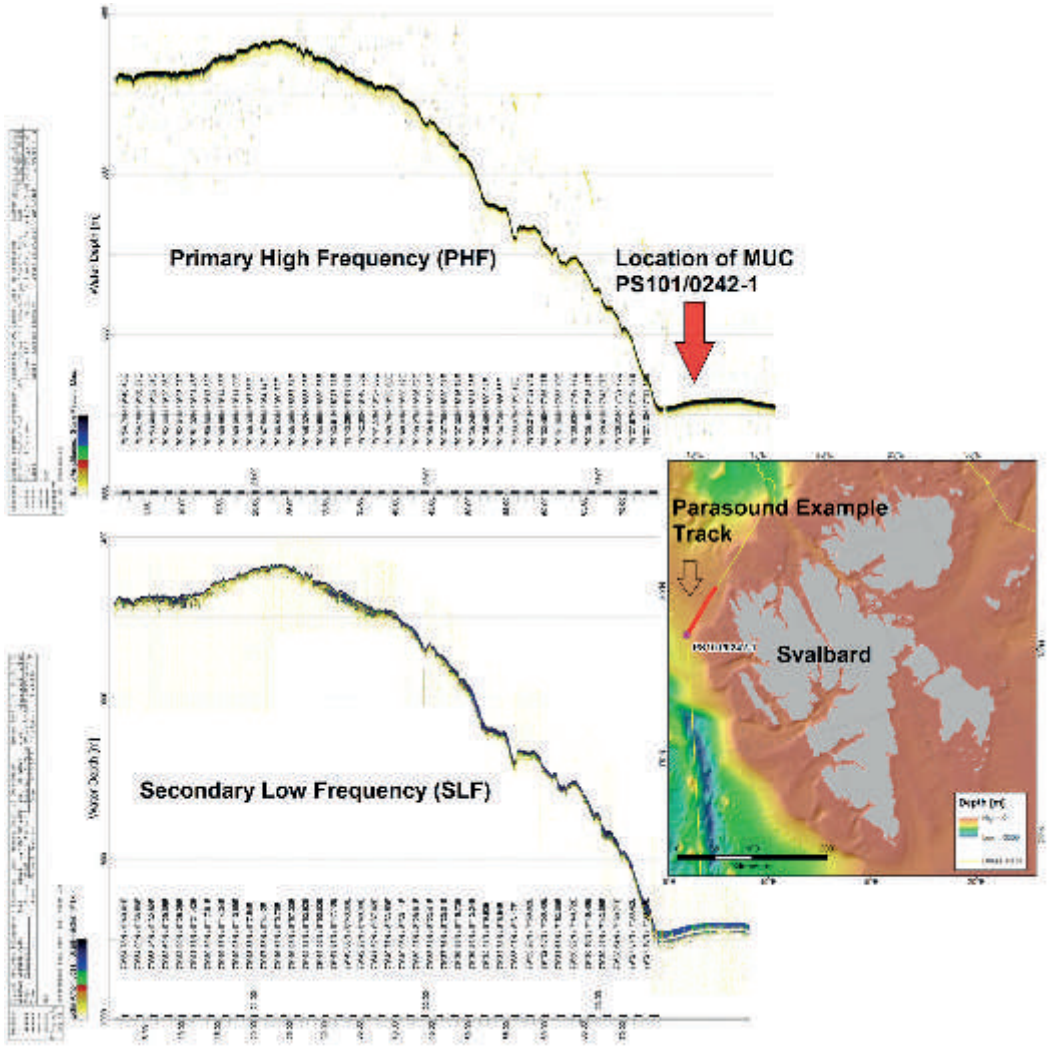

Fig. 3.2.1: The echograms of the primary high frequency (PHF) and the secondary low frequency (SLF) covering a small transect (red line) of the southern Yermak plateau where the TV-MUC PS101/0242-1 was taken.

3.3 Acoustic navigation - Posidonia

Sebastian Roessler[1], Laura Hehemann[2], Frederic Tardeck[1]

[1]FIELAX
[2]AWI

Objectives

The shipboard acoustic navigation system *IXSEA Posidonia* was used to track instruments during station work. The main objectives of the cruise were seafloor observations and hunting plumes, whereby instruments such as CTDs or video sleds were towed slowly using either the engine or sea ice drift. This resulted in an offset between the ships and instruments position of up to 1 km (at 4 km water depth), with towed instruments reacting very slowly to course changes by the ship. If plume signals or interesting locations were found in the CTD or imagery/video data it was necessary to be able to relocate these positions for further sampling. Therefore, every towed instrument and benthic sampling device was equipped with a *Posidonia* transponder beacon.

Sensor description

The *IXSEA Posidonia* is an acoustic underwater positioning system used to determine and track underwater vehicle and instrument positions. The system is composed of two ultra-short baselines (USBL) consisting of four hydrophones and one main transducer. A *Posidonia* transponder beacon has to be mounted on the instrument to be tracked before the launch. Once the gear is lowered into the water, the systems' main transducer transmits an acoustic signal in the shape of a 60°-wide cone at a frequency of 10.5 kHz. The transponder on the instrument receives this signal and replies with a signal of 9.5 kHz. This is being received by the four hydrophones of the vessel with small differences in travel time and phase from which a relative angle and distance to the transponder can be calculated. An absolute geographic transponder position and depth is calculated by applying the ship's current GPS position, the current motion state (roll, pitch and heading) and a sound velocity profile to compensate the refraction of the signal in the water column. The accuracy according to *IXSEA* is 0.3 % (IXSEA 2006) of the water depth which gives a range of ~12 m at the general area depth of 4,000 m. The data is continuously acquired and distributed to the ship's network for data visualization and mapping programs.

Work at sea

The following instruments were equipped with transponders: box corer, CTD/Rosette water sampler, gravity corer, heat flow probe, *in-situ* pump, Lightframe On-sight Keyspecies Investigations (LOKI), mooring, TV-multi corer, Ocean Floor Observation System (OFOS), and Remote Operated Vehicle (ROV).

The antenna was mounted on the ships' hull and was protected during steaming passages and in sea ice with a moveable window. The window was opened once on station and closed during transits. If the ship was actively moving during deployments, the window was shut, but USBL-positions were still received in a lower quality. The connected electronic processing unit used was the *IXBLUE USBL-BOX*. The recurrence interval of the system was set to 8 seconds. Sound velocity profiles were kindly provided by the oceanographer's CTD profiles and regularly updated. Acquired position data were locally logged on a PC as raw NMEA telegram data. Positions of the ship and transponder were displayed in real-time using the mapping software *GlobalMapper* and *PosiView* (Ralf Krocker, AWI). *GlobalMapper* was used to display current positions and tracks from *Posidonia* together with further geographical datasets, such as bathymetry grid layers, station waypoints or points of interest (Fig. 3.3.1). This contributed greatly to the station work by keeping an overview of the instruments' track related to the local bathymetry and observed points. Current bathymetry datasets were kindly provided by the bathymetry group on board.

Data management

All position data were post-processed on board with a filtering and interpolation tool by Yann Marcon (MARUM). The programme filters outliers by applying a speed filter. Afterwards, data were spline-interpolated to create a continuous dataset for a 1-second interval. The data can then be easily referenced by time to other datasets such as photo imagery, MAPR and micro profiler data acquired during a station.

The station positions of the final cruise station list (Appendix A.4) were modified accordingly so that the more accurate USBL positions on the tracked posidonia-equipped instruments were added, instead of the default (ships') position.

The post-processed USBL navigation data for every device are available in the scientific data warehouse *PANGAEA* (https://doi.pangaea.de/10.1594/PANGAEA.869118).

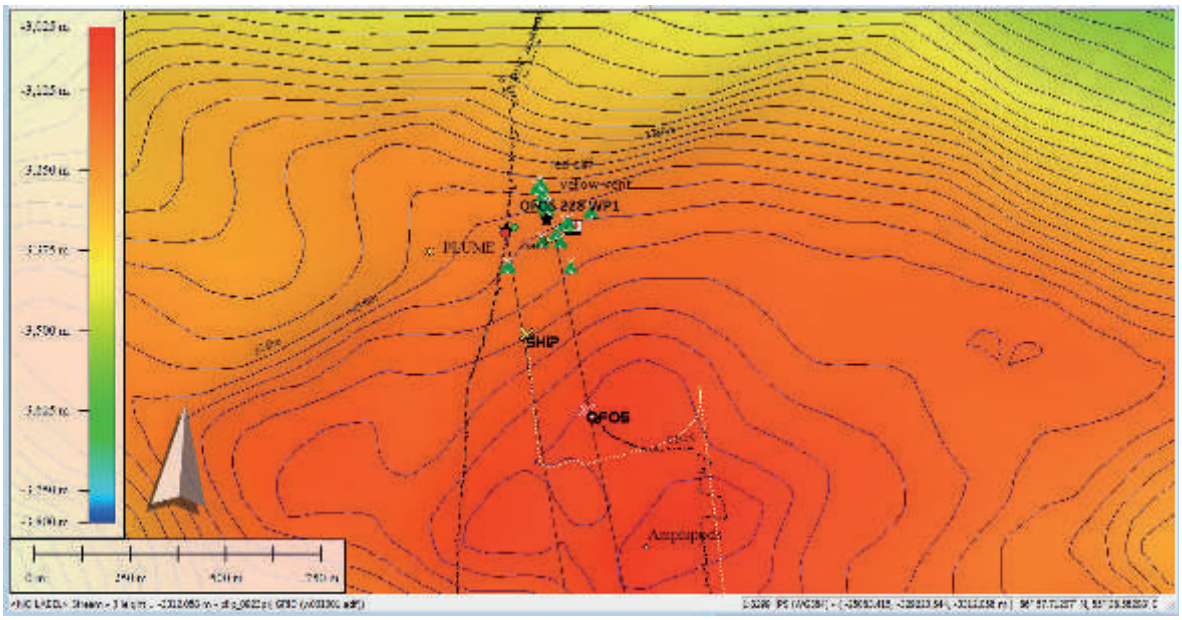

Fig. 3.3.1: A screenshot of the GlobalMapper software used for real- time plotting of an OFOS station PS101/0229-1 showing the ship track (yellow) and the OFOS track (black) together with the bathymetry, points of interest and the track of a previous TV-MUC

References

IXSEA User Manual (2006): Chapter 1.1 System General Description

3.4. Ocean Floor Observation System (OFOS) and TV multicorer habitat mapping

Autun Purser[1], Harald Biebow[2], Antje Boetius[1,3,4], Simon Dreutter[1], Laura Hehemann[1], Sebastian Roessler[5], Frederic Tardeck[5]

[1]AWI
[2]iSiTEC
[3]MPI
[4]MARUM
[5]FIELAX

Objectives

The main objectives of deploying imaging systems such as the Ocean Floor Observatory System (OFOS) and TV Multicorer (Fig. 3.4.1) to a height several meters above the seafloor is to visually determine the geological, sedimentological and biological community structures across the regions surveyed. The community structure on top of the Karasik Seamount, surrounding topographic highs, the Langseth Ridge in general or the Gakkel Ridge Rift Valley were not well known before PS101. For PS101 the OFOS system was augmented with new forward and sidescan sonar systems to acoustically investigate the seafloor features, ideally to allow the extrapolation of communities and relief features of the seafloor observed with the OFOS imaging systems over a larger extent of seafloor. The TV multicorer (TV-MUC), equipped with a video camera, was also used to image regions of the seafloor and to pinpoint locations on the seafloor to be cored directly, for biological and geochemical analysis. By using these systems the overall aim of the seafloor imaging team was to identify any locations of active hydrothermalism and to gauge the composition of seafloor communities.

Work at sea

The OFOS is a towed underwater camera system equipped with both a high-resolution photo-camera (iSiTEC, CANON EOS 5D Mark III) and a high-definition video-camera (iSiTEC, Sony FCB-H11). The cameras are mounted on a steel frame (140L x 92W x 135H cm), together with two strobe lights (iSiTEC UW-Blitz 250, TTL driven), three laser pointers at a distance of 50 cm from each other that were used to estimate the size of seafloor structures, four LED lights, and a USBL positioning system (Posidonia) to track the position of the OFOS during deployments. For PS101 the OFOS was upgraded to additionally mount sidescan and forward looking sonar systems.

The sidescan bathymetry sonar is an interferometric Edgetech 2205 AUV/ROV MPES (Multi Phase Echosounder) with two sidescan frequencies (230 kHz & 540 kHz) for different range and resolution achievements. The transducers additionally hold a bathymetric receive array to calculate bathymetric 2.5D data in the range of the 540 kHz sidescan sonar with around 800 data points per ping.

Fig. 3.4.1: Vehicles for habitat mapping: OFOS (right) and TV MUC (left) (F. Tardek, S. Dreutter)

The forward looking sonar is a BlueView M900 acoustic camera, mounted 5° downward from the horizontal on the front of the OFOS. It creates a 2D swath image of the incoming seabed as can be seen in Fig. 3.4.2.

The aim of equipping the OFOS with the acoustic systems was to increase the survey range of the vehicle: to augment the seafloor photographs with lateral swathes of habitat data provided by the sidescan sonar. While the camera captures an area of approximately 1.2 times the flight height the sidescan sonar ensonifies the surrounding area with ranges of 50 m (high

frequency) and 100 m (low frequency) to both sides of the vehicle. With flight heights between 1.5 -3 m this coverage is frequently disturbed by shadow effects of higher objects like rock formations as well as steep slopes but it still gives a considerably wider field of view than with the camera alone.

The forward looking sonar system was primarily used to aid in obstacle avoidance. This became useful in dives with steep terrain and sudden cliffs as well as bigger rock formations. Additionally, it gives an idea of objects ahead that will be covered by either the camera or the sidescan shortly after being observed in the forward sonar.

Additional sensors, such as the Miniaturized Temperature Loggers (MTL) and the Miniaturized Autonomous Plume Recorders (MAPR, Baker and Milburn, 1997) were systematically mounted on the system's frame to record and monitor various physical and chemical parameters (temperature, pressure, turbidity, redox potential). Those sensors did not provide real-time feedback but their higher robustness over the micro- sensor package ensured that most parameters were recorded. The data collected from these sensors was combined with data collected via CTD for use in narrowing down the search for hydrothermal activity.

The TV-MUC is a video-guided multi-corer system, which is able to sample up to six 50 cm cores. It is equipped with a high-definition video-camera, two strobes, and a USBL positioning system (Posidonia) in order to visualize the sampling area and to precisely select the sampling site and record the sampling.

The OFOS and the TV-MUC were deployed from either the A-frame or the side of *Polarstern* and towed at speeds of less than 1 knot (depending on the drift speed of the ice and whether there was the possibility to steam through one year ice) at heights of 1.5 to 2.5 m above the seafloor.

In total, 15 OFOS and 28 TV-MUC deployments were carried out during the cruise (Tab. 3.4.1). Deployments were made on three mounts of the Langseth Ridge, Vent Mount in the Gakkel Ridge, on the shelf north of Spitsbergen, in the Nansen Basin and East of Spitsbergen on the continental shelf.

Tab. 3.4.1: Locations and details of all OFOS and video and still image TV-MUC deployments made during PS101

Station	Target	Photo #	Length [m]	Mounted Sensors	Comments	Device
PS101/010-1	Test Site	124	1028			OFOS
PS101/068-1	Test Site	160	297			OFOS
PS101/089-1	Karasik Seamount	1044	6041	MAPR		OFOS
PS101/098-1	Central Mount	1	103			TV-MUC
PS101/100-1	Central Mount	550	4220	MTL MAPR		OFOS
PS101/101-1	Karasik Seamount	4	630			TV-MUC
PS101/102-1	Karasik Seamount	9	319			TV-MUC
PS101/103-1	Karasik Seamount	9	252			TV-MUC
PS101/104-1	Karasik Seamount	11	313			TV-MUC
PS101/118-1	Gakkel Ridge Rift Valley	1	691			TV-MUC
PS101/120-1	Northern Mount	763	6101	MAPR		OFOS
PS101/124-1	Karasik Seamount	3	187			TV-MUC

Station	Target	Photo #	Length [m]	Mounted Sensors	Comments	Device
PS101/125-1	Karasik Seamount	2	125	MTL		TV-MUC
PS101/134-1	Vent Mount	260	935	MTL MAPR		OFOS
PS101/135-1	Vent Mount	824	4987	MTL MAPR		OFOS
PS101/140-1	Vent Mount	11	693	MAPR		TV-MUC
PS101/140-1	Karasik S Slope	11	1688	MAPR		TV-MUC
PS101/151-1	Central Mount	12	172			TV-MUC
PS101/152-1	Central Mount	5	253	MTL MAPR		TV-MUC
PS101/153-1	Central Mount	13	139			TV-MUC
PS101/158-1	Vent Mount	1062	7219	MTL MAPR		OFOS
PS101/166-1	Vent Mount	2	1770			TV-MUC
PS101/167-1	Vent Mount	52	1248			TV-MUC
PS101/169-1	Central Mount	805	4816	MTL MAPR		OFOS
PS101/179-1	Vent Mount	524	1853	MTL MAPR		OFOS
PS101/185-1	Vent Mount	356	1396	MTL MAPR		OFOS
PS101/187-1	Vent Mount	96	2066	MTL MAPR		TV-MUC
PS101/194-1	Northern Mount	35	255	MTL MAPR		TV-MUC
PS101/195-1	Northern Mount	37	318	MTL MAPR		TV-MUC
PS101/196-1	Northern Mount	31	393	MTL MAPR		TV-MUC
PS101/205-1	Northern Mount	26	393	MTL MAPR		TV-MUC
PS101/210-1	Central Mount	58	375	MTL MAPR		TV-MUC
PS101/211-1	Central Mount Saddle	120	329	MTL MAPR		TV-MUC
PS101/212-1	Central Mount Saddle	64	824	MTL MAPR		TV-MUC
PS101/218-1	Central Mount Saddle	26	486	MTL MAPR		TV-MUC
PS101/219-1	Karasik S Slope	59	2074	MTL MAPR		TV-MUC
PS101/220-1	Karasik S Slope	74	1176	MTL MAPR		TV-MUC
PS101/225-1	Vent Mount	1223	2883	MTL MAPR		OFOS
PS101/227-1	Vent Mount	92	4469	MTL MAPR		TV-MUC
PS101/229-1	Vent Mount	477	2294	MTL MAPR		OFOS
PS101/232-1	Vent Mount	485	1644	MTL MAPR		OFOS
PS101/241-1	Yermak Plateau	920	2916	MTL		OFOS
PS101/242-1	Yermak Plateau	41	738			TV-MUC

Preliminary (expected) results

Bathymetry

The new sonar systems were very effective for increasing habitat information which could be recovered in real-time by the OFOS system. Full sidescan and forward looking sonar data sets were collected throughout all 15 OFOS dives.

The forward looking sonar, in addition to providing warnings of approaching steep cliffs or rocks, also gave indications on approaching seafloor type. Fig. 3.4.2 shows a typical frame of forward sonar data, with the round mounds of sponges clearly visible, and a lateral crack feature visible at 20 m.

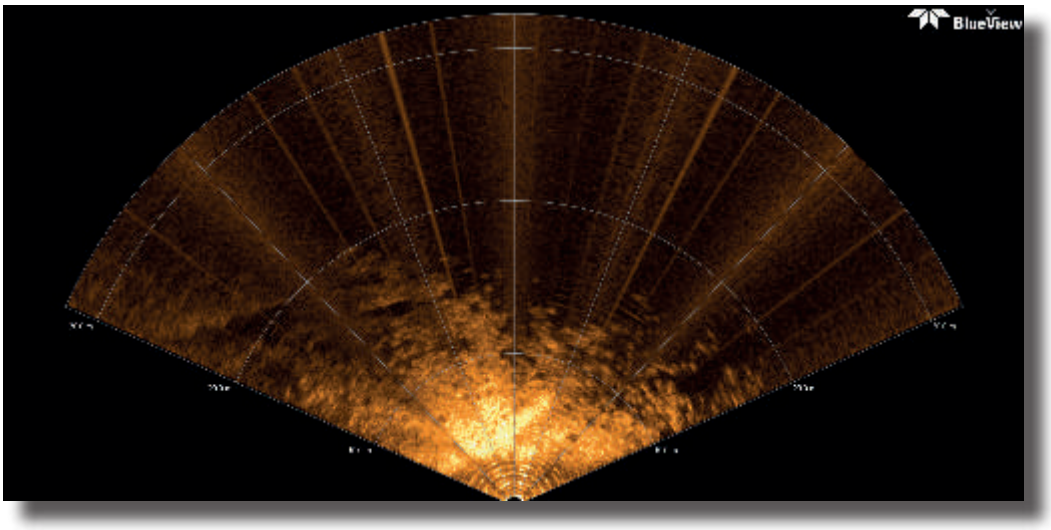

Fig. 3.4.2: Forward looking OFOS sonar framegrab, showing sponges and a crack feature on the Karasik Seamount.

The sidescan sonar was very successful in differentiating habitat types at distances of up to 100 m, to the port and starboard sides of the OFOS. In Fig. 3.4.3 the central track of OFOS can be seen in the bathymetry, with the fields of sponges and crack feature imaged in Fig. 3.4.2 clearly visible.

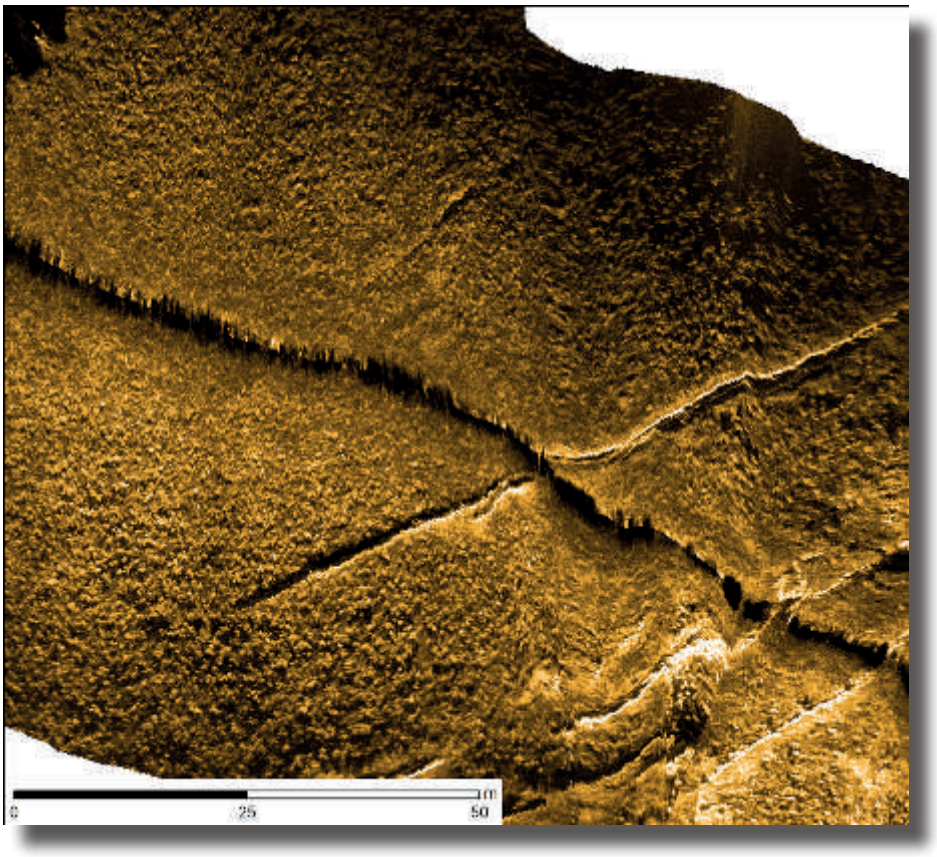

Fig. 3.4.3: Sidescan sonar images collected of numerous small (10 – 50 cm) sponges to the port and starboard sides of OFOS. The long black feature running from top left to bottom right is the path taken by OFOS. This black feature represents the sonar blank region below the system. The SW – NE liner features are deep fissures through the sponge beds into the underlying rocks.

OFOS and TV MUC imagery

The numbers and locations of images collected via the OFOS / TV MUC systems is given in Tab. 3.4.2. Here below a representative image and a short text give a brief overview of each OFOS dive. The video and still images collected via TV MUC covered a far smaller area of seafloor and will not be discussed further here. The main biological features and habitat characteristics will be mentioned below, but for a more detailed description of the biology encountered, please see Chapter 8.

OFOS imagery - Karasik Seamount

A map of all equipment deployed at Karasik Seamount is given in Fig. 3.4.4.

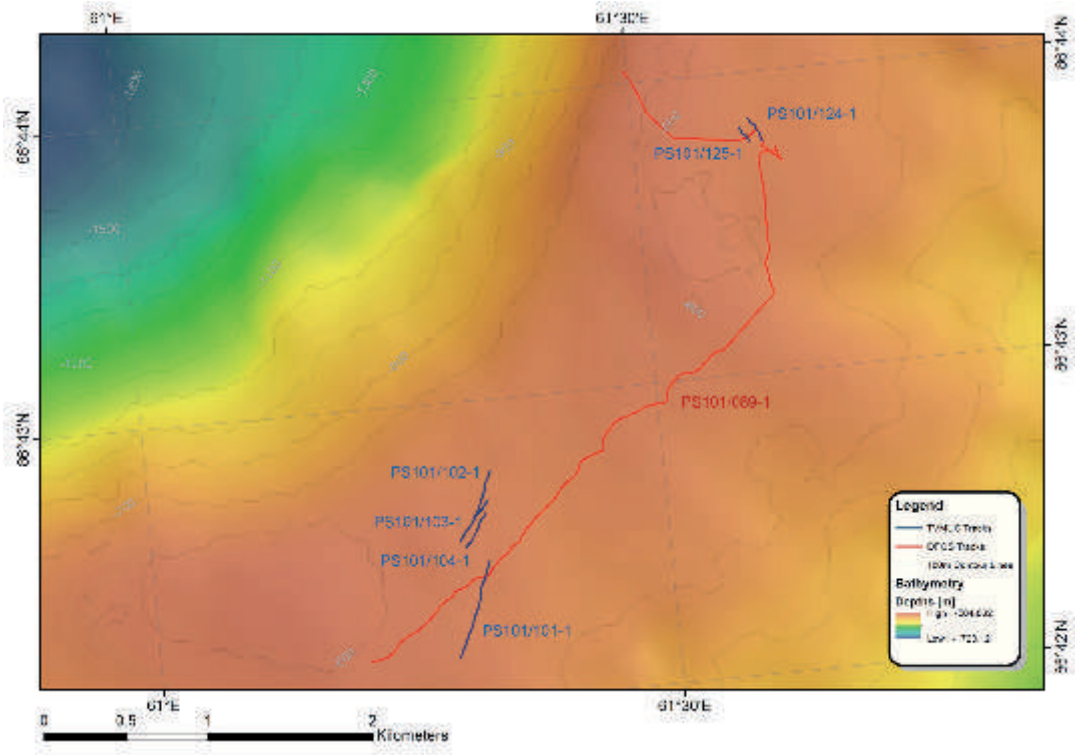

Fig. 3.4.4: Map of OFOS and TV MUC deployments made at Karasik Seamount

OFOS dive PS101/089-01 surveyed Karasik Seamount, following much of the upper crest of the mount from the SW to N. Much of the seamount was summit was covered by sponges and sponge spines (Fig. 3.4.5, *cf.* Chapter 8). Toward the northern section of the mount summit there were several breaks in the sponge cover, where a thick layer of dead tube worm tubes was intermixed with dead mussel, clam and gastropod shells, as well as small pebbles and sand.

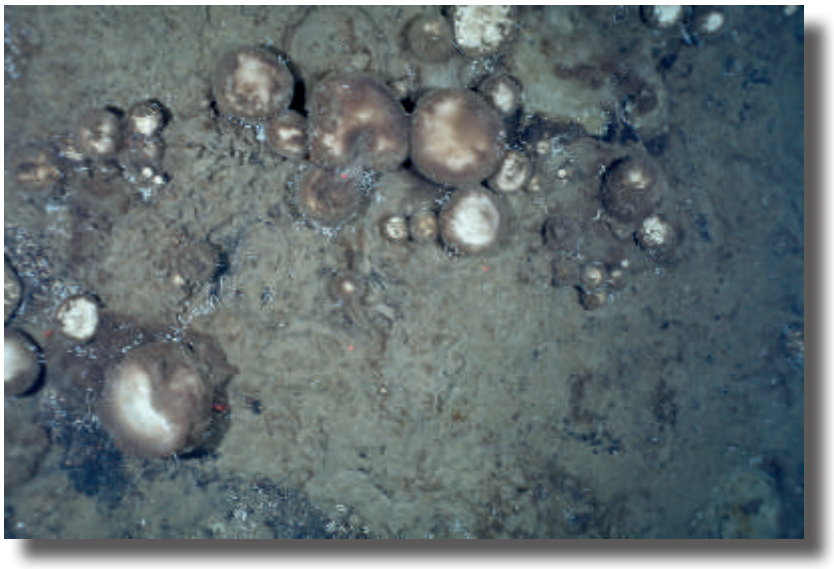

Fig. 3.4.5: A near total seafloor coverage by sponges and sponge spines was imaged throughout much of OFOS dive PS101/089-1.

OFOS imagery – Central Mount and Saddle

The Central Mount of the Langseth Ridge was surveyed by OFOS dives PS101/100-1 and PS101/169-1. Dive PS101/169-01 also surveyed the saddle between Karasik Seamount and the Central Mount (Fig. 3.4.6).

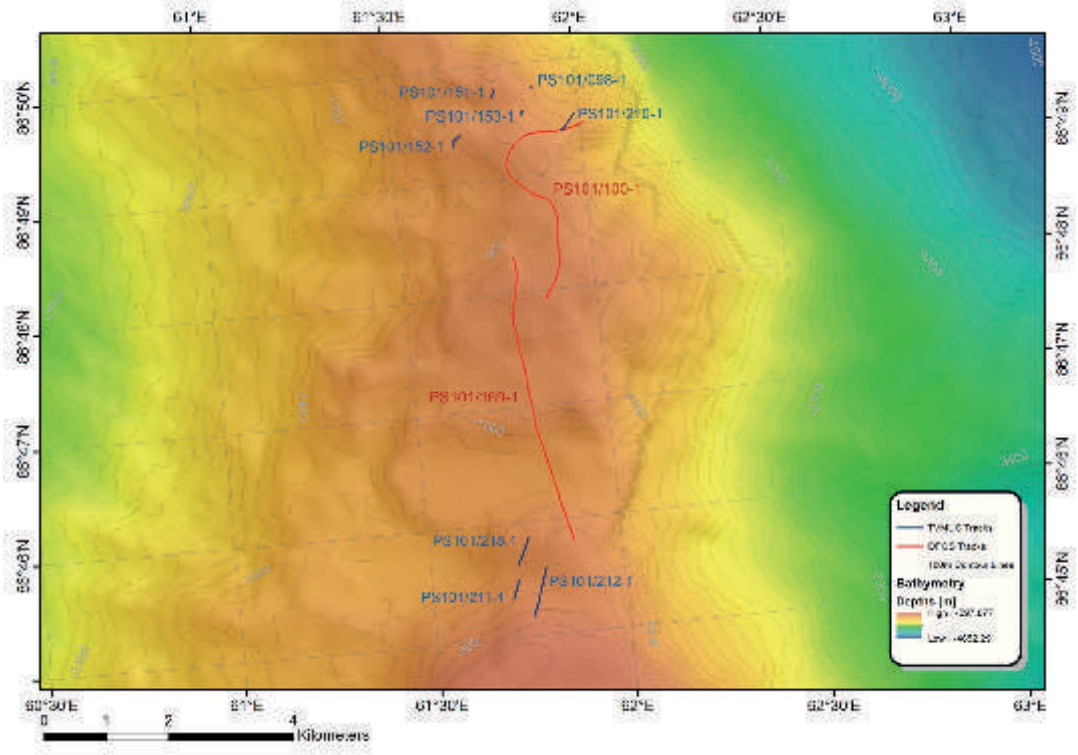

Fig. 3.4.6: OFOS and TV MUC surveys of the Central Mount and Saddle of the Langseth Ridge

With regard to both seafloor relief and seafloor community structure, the sponge community of the Central Mount was reminiscent of the Karasik Seamount, though as shown in Fig. 3.4.7 sponge cover was generally lower, and the abundance of sponge spines between sponges was also lower.

Fig. 3.4.7: Sponges on the Central Mount were at a lower density than was observed at Karasik Seamount. The area surveyed contained larger stretches of seafloor covered with black, dead tubeworms and occasional pebbles and stones, as shown here.

The Saddle between Karasik Seamount and Central Mount was surveyed by OFOS PS101/169-1. The saddle feature was found to be a sand covered, wide ridge running N-S between the two mounts, at a depth of ~1,000 m (Fig. 3.4.8). Numerous small, dark rocks were liberally scattered across the central saddle feature, likely those fallen from the steep cliffs marking the transition from the saddle feature to both the Central Mount and the Karasik Seamount.

Fig. 3.4.8: The Central Saddle between the Karasik and Central Seamounts is a sand covered ridge at approximately 1000 m depth. Sand and broken rock fragments are surrounded by a sandy seafloor. Communities of sponges are focused onto small rocky outcrops.

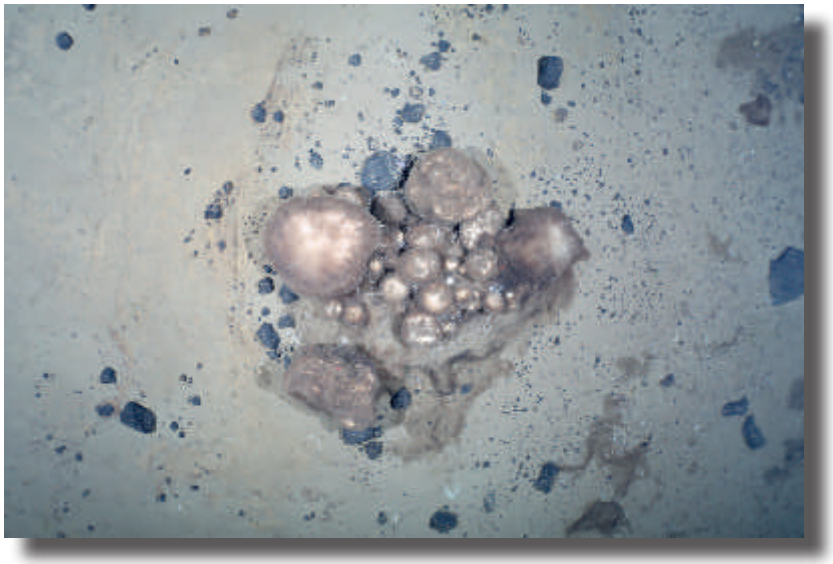

OFOS imagery – Northern Mount

Three TV MUC deployments, and one OFOS dive (PS101/120-1) were carried out at Northern Seamount (Fig. 3.4.9). Dive PS101/120-1 surveyed both the western and eastern flanks of the seamount, as well as imaging the central peak region. An overview of the imaged megafauna is given in Chapter 8.

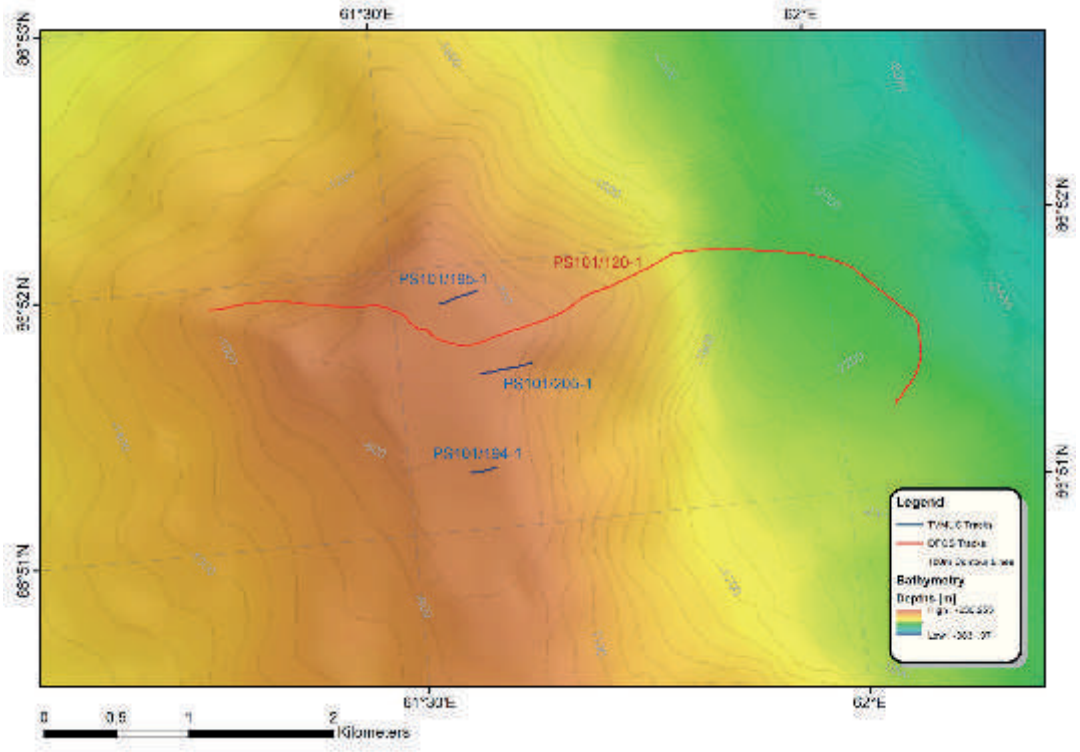

Fig. 3.4.9. TV MUC and OFOS dives carried out at Northern Seamount during PS101

PS101/120-1 surveyed more of the steep flanks of the Langseth Ridge peaks than any of the other dives conducted in the area. Extremely steep facings of rock dropped swiftly from the peak on both the north and east flanks of the seamount (Fig. 3.4.10). Occasional sand covered shelfs were evident on the easterly flank.

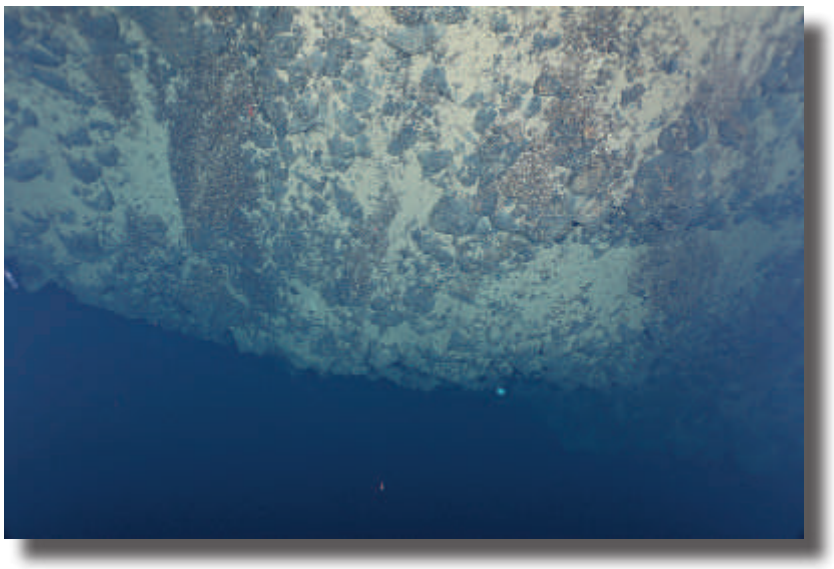

Fig. 3.4.10: Steep eastern flank of the Northern Mount, imaged during OFOS dive PS101/120-1

OFOS imagery – Vent Mount

Vent Mount was the focus of 7 TV MUC and 8 OFOS deployments (Fig. 3.4.11, with these devices commonly equipped with additional sensors to aid in vent location (Tab. 3.4.1).

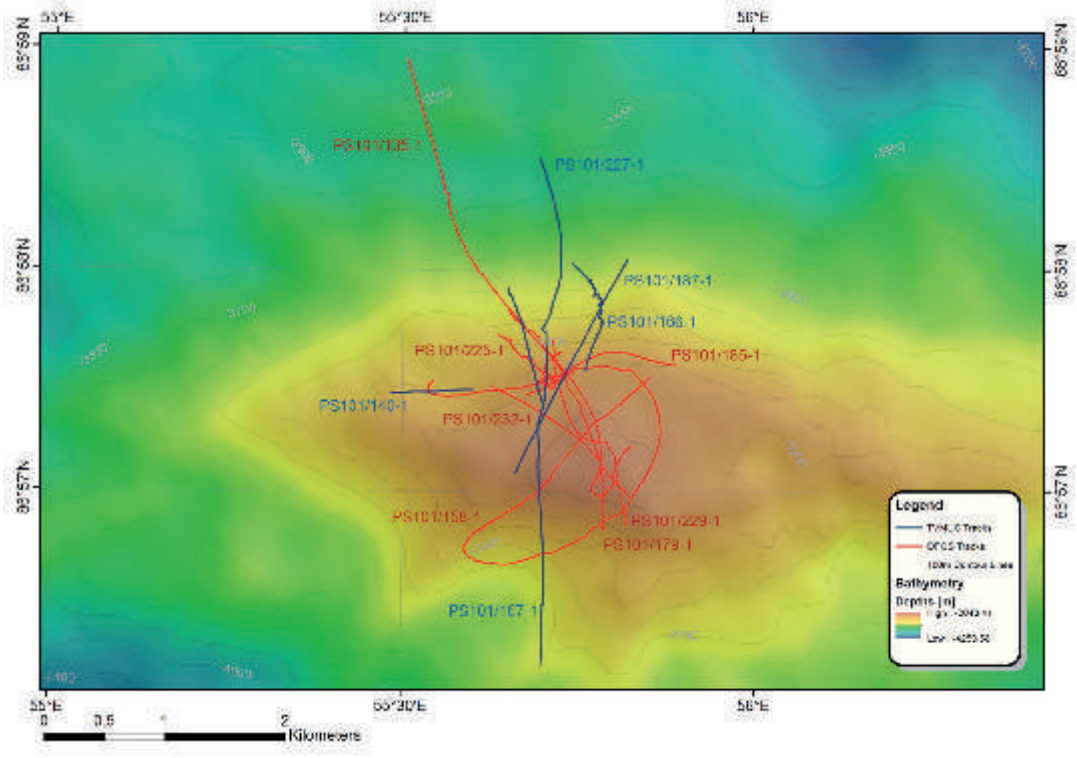

Fig. 3.4.11: TV MUC and OFOS deployments during PS101 at Vent Mount

The vent was found to be particularly active in the northwestern flank region at ~3,200 m depth, with numerous small vents interspersed with precipitate rock fragments. Additionally, there were indications of some activity at the peak of the mount, with several aggregations of amphipods observed with the OFOS cameras.

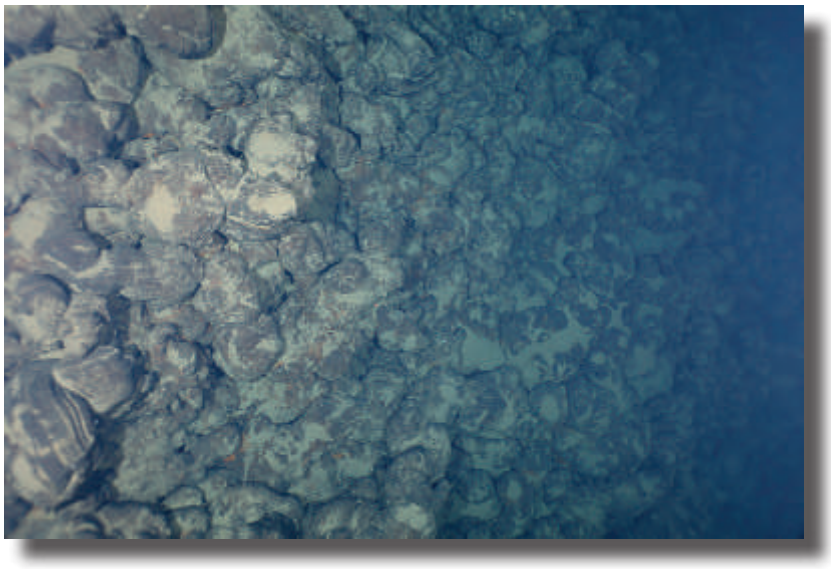

Fig: 3.4.12: Pillow basalts on Vent Mount imaged during OFOS dive PS101/135-1

The bulk of Vent Mount consisted of pillow basalts of various age and in different states of degradation / sediment coverage. Some of the aggregations were very steep, particularly near the central peak region of the mount (OFOS dive PS101/135-1, Fig. 3.4.12).

From ~3,200 m to ~34,00 m terraces of fully sediment-

or precipitate-covered seabed were evident across the north and north westerly flanks of the mount (OFOS dive PS101/185-1, Fig. 3.4.13).

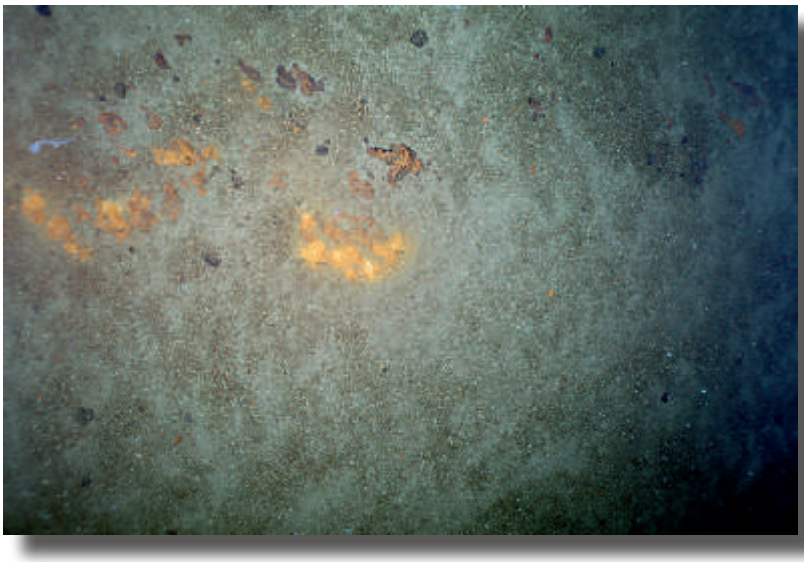

Fig. 3.4.13: Exposed precipitate rocks penetrating out of a sandy gravel matrix. A common seafloor type on the narrow, terrace-like plateaus of the northerly flank of Vent Mount.

At several locations on the north westerly plateau's of Vent Mount the seafloor was a consolidated mix of baked material and precipitates interspersed with small vents (OFOS dive PS101/229-1, Fig. 3.4.14), often associated with local heat anomalies (*cf*. Chapter 5).

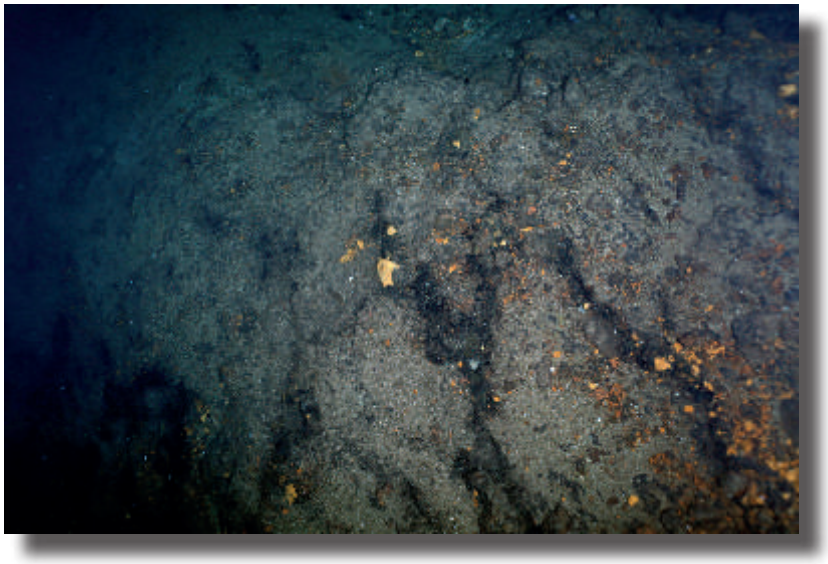

Fig. 3.4.14: Numerous small vents, fissures and precipitates penetrating through a thin gravelly sand, imaged during OFOS dive PS101/225-1.

Data management

All OFOS photographic data are stored in PANGAEA. Video data has been uploaded to the AWI-MARUM Video Library (MARVIDLIB) system for public dissemination and to allow online access to further researchers (http://vidlib.marum.de/).

Track lines of the OFOS and TV MUC surveys, along with links to the associated image galleries and are available from PANGAEA (doi:10.1594/PANGAEA.869118).

3.5 The Langseth Ridge System

Antje Boetius[1], Sebastian Roessler[2], Frederic Tardeck[2]

[1]AWI
[2]FIELAX

Objectives

During the sixteenth meeting of the GEBCO Sub-Committee for Undersea Feature Names (SCUFN), the Langseth Ridge has been defined as an undersea mountain structure, stretching from 87°N 62°E to 85°55'N 57.45'E, a distance of approximately 125 kilometres. The summit of Karasik Seamount has been located on the ridge at 86°43.0'N 61°17.6'E, with the highest elevation of 566 meters below sea level. Additionally, another summit at a depth of only 391 meters has been named Leninskiy Komsomol Seamount, discovered in 1965 during a drift ice station on the Soviet Northern Fleet Hydrographic Expedition (IOC-IHO, 2003).

Since there are still several areas at Langseth Ridge which were not yet mapped in detail, a major task of this cruise was to fill the gaps in the existing bathymetric data in order to get a better understanding of the general geomorphology of this particular area. A proposal has been made to the Committee to name the peaks of the ridge and correct the depths.

Work at Sea and preliminary results

The greater Langseth Ridge

During the transit from the Nansen Basin to the Karasik Seamount area, we encountered several seamounts (some were already known from previous cruises) and collected new topographical information from an extended area. From this data, we assume that the extent of Langseth Ridge (as a "greater" Ridge system) can be prolonged to the south, where the first seamounts occur. Regarding the entire bathymetry of this area, a V-shaped form of the whole ridge system seems possible, providing a hypothesis for further geological analysis. This could indicate that the Langseth Ridge extends on both sides of the Gakkel Ridge (Fig. 3.5.1).

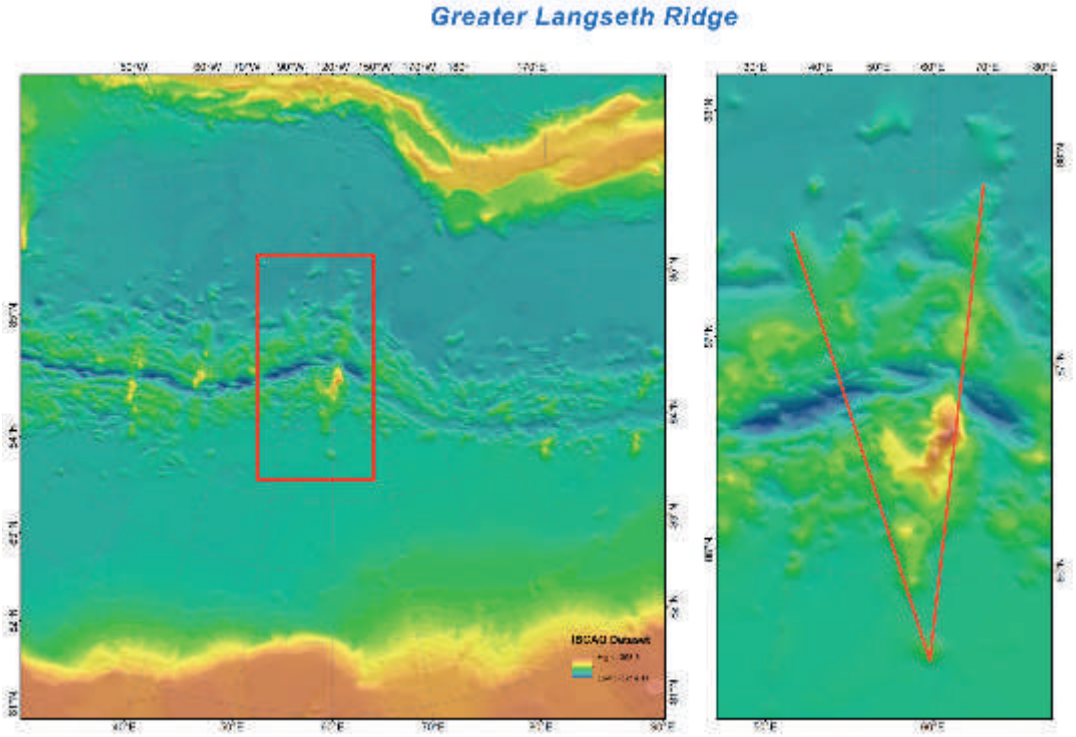

Fig. 3.5.1: Hypothetical extent of the "greater" Langseth Ridge system within the Gakkel Ridge

Summits of the Langseth Ridge

As a result of our multibeam surveys, we were able to identify several summits on the Langseth Ridge. For the Karasik Seamount, we discovered that it consists of three separate summit peaks. The southern peak is that already known as the Karasik Seamount, but the central and northern peaks require names.

Karasik Seamount

The Karasik Seamount remains the highest peak identified in the area, with a maximum elevation reaching to a depth 584.8 meters below sea level. According to our survey, the location of the highest point of the Seamount was found to be 86°42.38'N 61°8.07'E, which is 1.5 kilometers southwest of the proposed summit location. The West-East profile (Fig. 3.5.2) shows the summit at almost 2,500 meters in elevation above the surrounding seafloor.

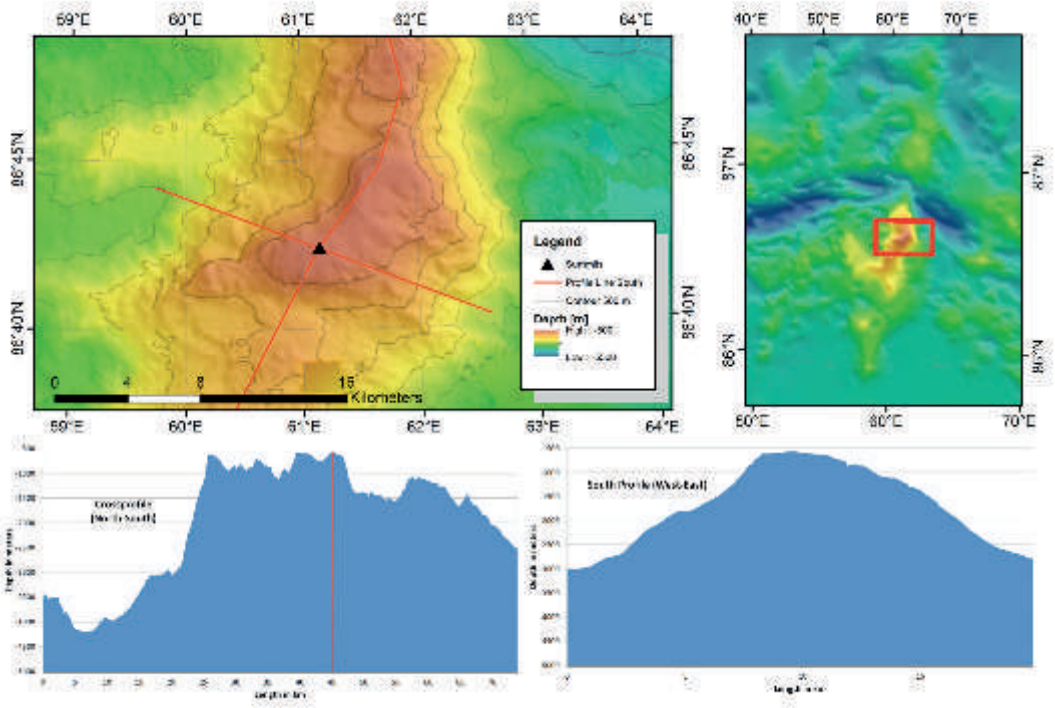

Fig. 3.5.2: Bathymetry of the southern summit of the Langseth Ridge (Karasik Seamount)

Central Mount

The central summit is located at 86°47.83'N 61°54.52'E and reaches a height 721.5 m below sea level. From east to west, the slope increases gradually from a depth of approximately 3,300 m to the highest point, with a steeper slope on the western side. The seafloor then drops to a depth of 4,500 meters below sea level (Fig. 3.5.3).

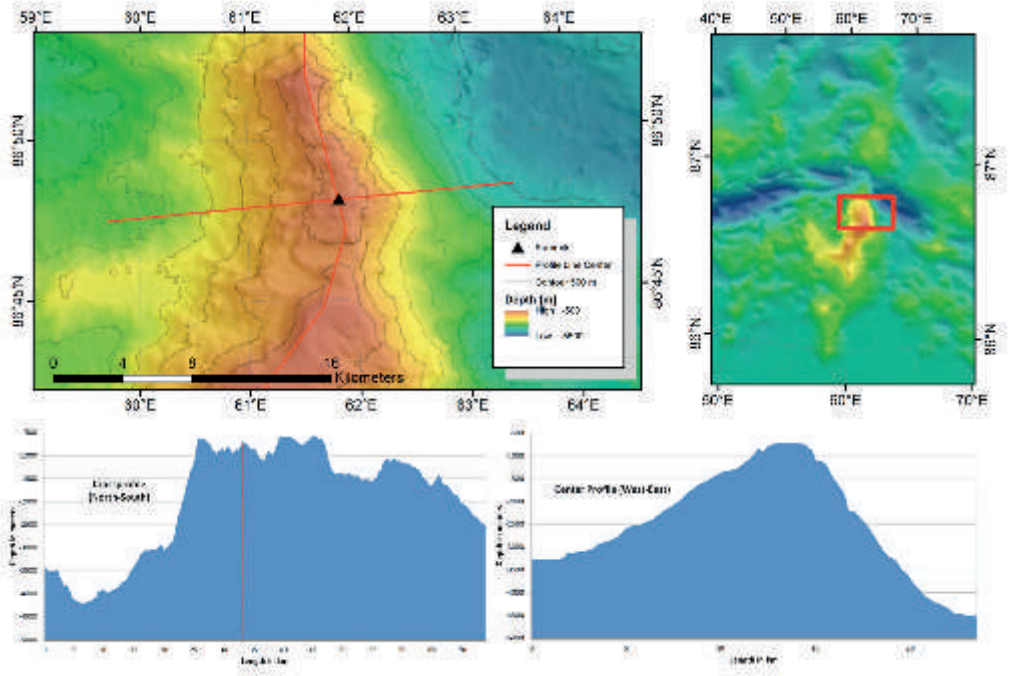

Fig. 3.5.3: Bathymetry of the central summit of the Langseth Ridge (Central Mount)

Northern Mount

The northern summit is located at 86°51.86'N 61°34'E with an elevation of 630.6 m below sea level. A steep slope drops from this peak into the northerly Gakkel Ridge rift valley, down to a depth of 4,000 m (Fig. 3.5.4).

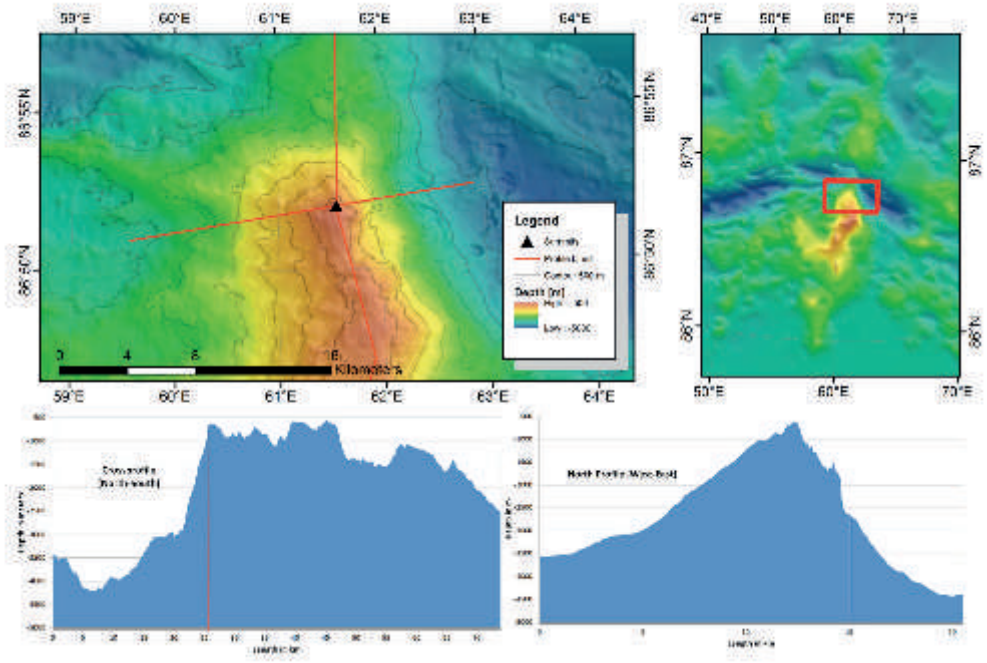

Fig. 3.5.4: Bathymetry of the northern summit of the Langseth Ridge (Northern Mount)

Leninskiy Komsomol Seamount

During our hydroacoustic survey we were not able verify the existence of a seamount reaching a depth of 391 meters below sea level. The depth at the proposed location, 86°40.5'N 60°50.0'E, was by our surveying at a depth of 1420 meters. Thus, we will propose to use the name Leninskiy Komsomol Seamount for the nearest seamount located at 86°36.0'N 60°8.39'E. This seamount is found 14 kilometers southwest of the Karasik Seamount and climbs 1,015 meters above the surrounding seafloor, which is 3,200 meters deep (Fig. 3.5.5).

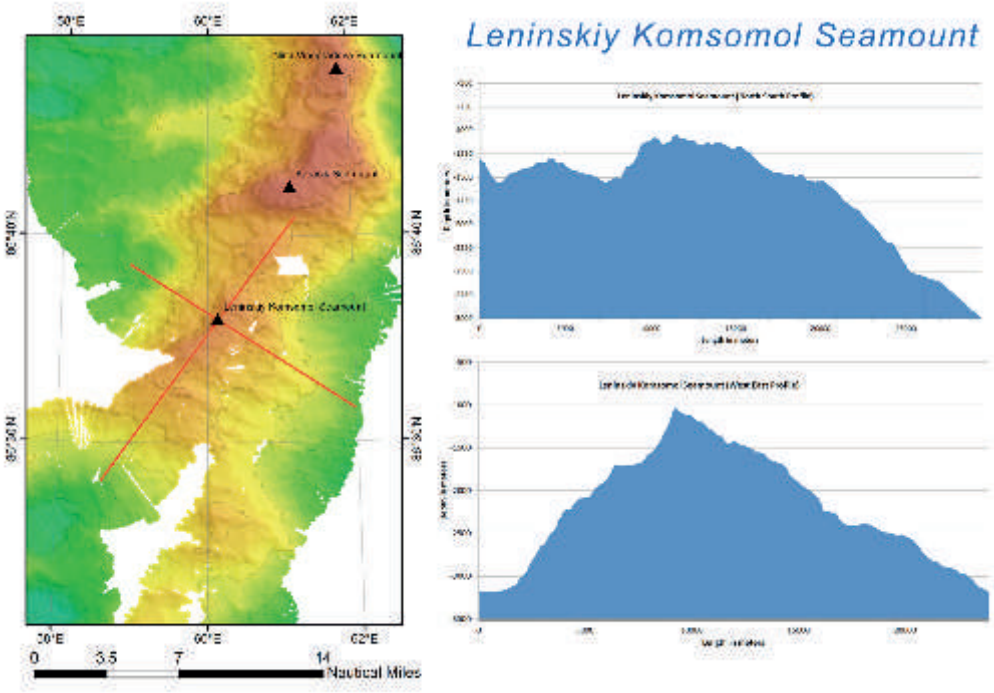

Fig. 3.5.5: Bathymetry of the seamount proposed to be renamed

Unnamed seamounts

At the beginning of our cruise we discovered a seamount in the Nansen Basin, which has not been surveyed so far. It is approximately 7 km away from the next large feature in the IBCAO data. The seamount stretches from north to south, is elevated over 1500 m compared to the surrounding area and is located at 85° 44.47'N 59°20.72'E (Fig. 3.5.6).

Also, the seamount in the Gakkel Ridge, which was investigated during PS101 for hydrothermal vent activity has not as yet been officially named. The seamount is aligned from west to east and is nearly 1,800 m above the deep Gakkel Ridge sea bottom. It is located at 86° 57.1'N 55° 46'E (Fig. 3.5.7).

Data management

See chapter 3.1.

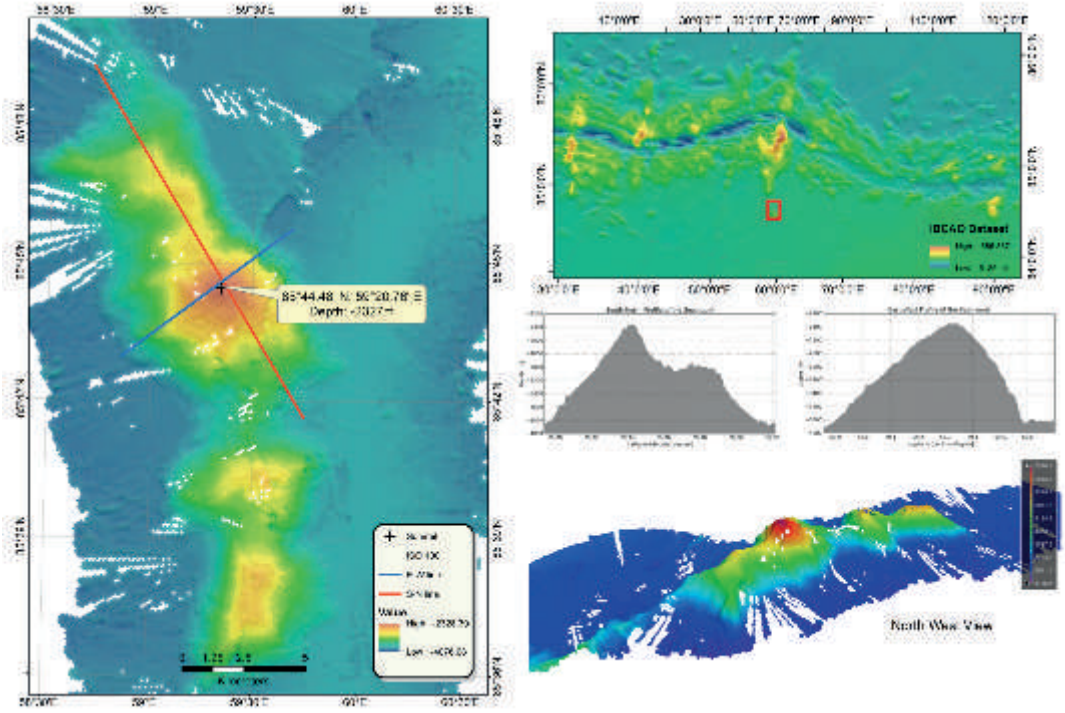

Fig. 3.5.6: Bathymetry of the unnamed seamount in the Nansen Basin

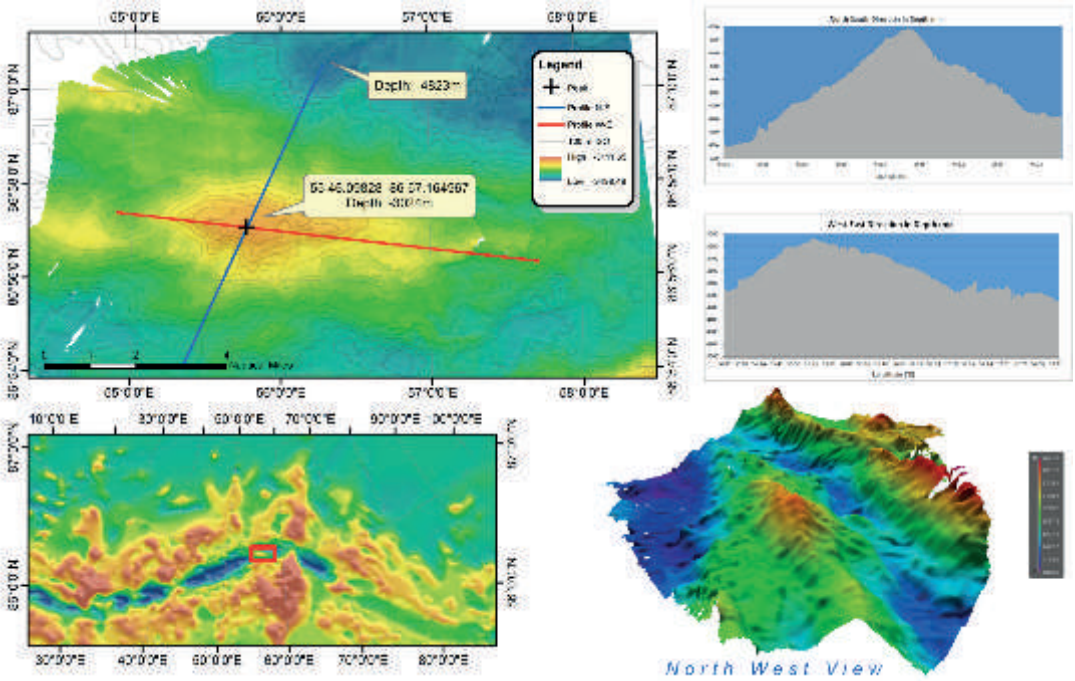

Fig. 3.5.7: Bathymetry of the unnamed vent seamount in the Gakkel Ridge

References

International Oceanographic Commission (IOC), International Hydrographic Organization (IHO)(2003): Sixteenth Meeting of the GEBCO Sub-Committee on Undersea Feature Names (SCUFN) – Summary Report. International Hydrographic Bureau, Monaco, 55 p. (IOC-IHO/GEBCO SCUFN-XVI/3)

4. GEOLOGY AND HARD ROCK PETROLOGY

Alexander Diehl[1], Elmar Albers[1], Christopher R. German[2], Kevin P. Hand[3], Wolfgang Bach[1] (not on board)

[1]MARUM/UHB-GEO
[2]WHOI
[3]NASA-JPL

Grant No. AWI_PS101_01

Objectives

Geologic processes at the ultra slow spreading Gakkel Ridge are far from being understood, partly because the area is situated in an area where the sea surface remains constantly covered and therefore difficult to reach. At present, there are only few high precision seafloor maps available and very few rock samples, in particular from the Eastern Volcanic Zone and its seamounts. As a result, few inferences on the relative roles of magmatic versus tectonic processes related to the accretion of new lithosphere in this region have yet been made. Some studies, however, suggest that the Gakkel Ridge seamounts are volcanic in origin, while others promote the role of tectonic accretion in formation.

The Langseth Ridge is one of the most striking geological features of the Gakkel Ridge, intersecting it at 61.5 °E. Until now only a few rocks of primarily altered diabase from the very most northerly slope (Michael et al., 2003) and some fresh basalts from the top of Karasik seamount (Michael et al., 2003; Schauer et al., 2012) have been sampled. The existing samples could point to a volcanic origin for the ridge but its position at an inside corner of the Gakkel Ridge spreading center, between two long volcanic segments, together with its general appearance, could also be consistent with a tectonic origin, e.g., as a core complex.

Our main objectives were to investigate the geological processes that formed the Langseth Ridge and the Vent Mount and any hydrothermal systems that they host(ed). Mapping and sampling of rocks were aimed at indicating if the Langseth Ridge is indeed an entirely volcanic edifice; exposures of plutonic and mantle-derived rocks would indicate otherwise. Specific questions we hoped to address included: How much did the mantle melt? How deep did melting take place? How deep were crustal magma reservoirs? What are the relations to active venting? A further goal was to collect hydrothermal precipitates from the vent sites. Such mineral deposits allow insights into the vent fluid composition and temperature as well as near-seafloor mixing and precipitation processes (e.g., Vanko et al., 2004; Craddock and Bach, 2010). Vent fluid compositions on the other hand, depend on the fluid's reactions with different lithologies in the sub-seafloor and thus provide hints for the deeper geological construction of the vent sites.

Work at sea

The geomorphologies of the Langseth Ridge and the Vent Mount were continuously updated throughout the cruise by improved seafloor mapping and imagery (*cf*. Chapter 3). These data were used to determine sampling locations of rocks, hydrothermal precipitates, and sediments from the slopes and summits of the seamounts. Samples were collected by targeted dredging stations as well as through serendipitous sampling of rock specimens collected in gravity, box and TV-MUC sediment coring.

The chain bag dredge (Fig. 4.1) was employed to recover rock samples from the Langseth Ridge and the Vent Mount. The use of this device was challenging not only because of the rough ocean floor topography that had to be taken into account, but also because of strong winds and the drift (direction and velocity) of the sea ice. The dredge was lowered to the seafloor at a rope speed of about 0.5 m/s. A strong decline in the rope tension profile was used to indicate when ground contact had been made. At that point a further total of 500 to 700 m of rope was paid out, laid along the seafloor. The wire was then pulled back in over this distance, dredging uphill along the seafloor at wire speeds of 0.5 m/s. The rope tension profile was monitored continuously and showed strong fluctuations while dredging the rough seafloor. These fluctuations stopped once enough wire had been hauled back in for the device to be lifted off the seabed. The dredge was thereupon heaved back to the surface at about 1 m/s (Fig. 4.1). In addition, many small rock samples were obtained from the numerous box and multi-corer stations occupied by the benthic biology group (*cf*. Chapter 8).

Fig. 4.1: Chain bag dredge back on board after successful deployment at the Vent Site

Representative samples of the different lithologies were picked for systematic examination and rock identification. The samples were broken with a hammer to provide fresh surfaces and studied macroscopically as well as with a reflected light stereomicroscope. Representative hand specimens were photographed and documented via short descriptions of their major features. Hand samples from stations PS101/186-1 and PS101/203-1 were also examined onboard with an Analytical Spectral Devices FieldSpec Pro visible to near-infrared spectrometer. This spectrometer covers the wavelength range from 0.35–2.5 µm at a resolution of approximately 0.003 µm at 0.7 µm and 0.01 µm beyond 1.4 µm. The spectrometer was used with a contact probe, in which the instrument fiber is oriented at 23° to a halogen-krypton light source, which is held normal to the rock surface. Sample surfaces were not altered in any way, nor were rocks ground to produce fines for enhancing spectroscopy.

Sediments were sampled using a gravity corer with a 1,600 kg weight stack. At five of six stations a 5.75 m long steel pipe was used. A 3 m long pipe was used at the final station. The gravity corer was equipped with a *POSIDONIA* (*cf*. Chapter 3), attached about 50 m above the corer, and at a subset of stations it was also equipped with temperature sensors attached to the steel tube (*cf*. Chapter 5). The device was lowered to the seafloor and penetrated into it at pay-out speeds of about 1 m/s. From a total of six gravity corer deployments two stations failed to recover material at all (PS101/105-1, PS101/161-1). At station PS101/105-1 the rope tension profile indicated that the corer fell over, presumably due to a poor penetration depth at that location (i.e., thin sediment cover). Station PS101/161-1 on the Vent Mount was aborted because the targeted small sediment terrace was missed as consequence of a change in drift direction mid-deployment. Very little material, with no preservation of stratigraphy, was

recovered at three further stations (PS101/104-1, PS101/160-1, and PS101/180-1). Presumably this was also due to very little sediment cover on top of the rocky basement. In the case of successful recovery, the plastic liner holding the core material was cut into 1 m long segments and split lengthwise into archive and working halves. The archive halves were photographed and systematically described. Exemplary smear slides were taken to identify the sediment material. Eventually both halves were placed into D-tubes and stored at 4 °C for return to the shore laboratory.

In addition, the TV multi-corer was used to recover hydrothermal sediments from close to the active vent site at the Vent Mount (*cf*. Chapter 8).

Preliminary results

Langseth Ridge

South of the rift valley, the Langseth Ridge forms a north–south aligned ridge structure that may also continue across-axis to the north of Gakkel Ridge. While its eastern slopes drop steeply into the rift valley, the western slopes are less steep and several smaller east–west aligned ridges can be made out. The Langseth Ridge consists of three distinct peaks (*cf*. Chapter 3), of which the southernmost and the central one are separated by a saddle structure. Numerous bedrock outcrops could be identified at the seamount slopes but their summits are to a large extent covered by a profuse biomass and geologic outcrops are extremely rare.

Dredging of the northernmost slope of the Langseth Ridge (PS101/203-1), closest to the ridge-axis, recovered samples from three different lithologies. The first lithology shows a greenish to brownish matrix containing cm-size phenocrysts of transparent to white plagioclase and white to pale green pyroxene (samples PS101/203-R1, PS101/203-R4; Fig. 4.2b, c). Subhedral crystals in the matrix can just be recognized in hand specimen, without magnification. Many of the rocks appear to be orthogonally shaped and some of the samples show a layering with regard to phenocryst size (PS101/203-R1; Fig. 4.2b). Some rocks are cut by veins of light green crystals with perfect cleavage in two directions. From the dominant colour, cleavage and their crystal shape these are interpreted as epidote veins (PS101/203-R4; Fig. 4.2c, d). The host rock type is presumed to not be extrusive in origin and, instead, may be doleritic or gabbroic. The second lithology is strikingly green coloured and exhibits rare anhedral, possibly resorbed, black crystals (PS101/203-R2; Fig. 4.2a). A hardness test of the green matrix produced a white powder typical for chlorite and/or serpentine, both representatives of the phyllosilicates group and challenging to discriminate. This interpretation was further supported by spectral analyses at sea that show significant alteration to phyllosilicates. Fig. 4.3 shows a comparison between the spectrum for sample PS101/203-R2 and several minerals from the USGS (United States Geological Survey) spectral library. The dredge sample shows the characteristic absorptions of bound and adsorbed water, –OH vibration, and bending modes associated with altered phyllosilicates. At the short wavelength (visible) end of the spectrum we see a broad peak likely due to the electronic excitation of iron, possibly indicative of mafic minerals in the host material, e.g., pyroxene. Moving to longer wavelengths, the feature observed at approximately 1.4 µm in the dredge sample is likely due to the combination of bound water and vibrational modes associated with Mg_2OH. In the region near 1.9 µm, absorptions due to both bound and adsorbed water on and within phyllosilicates are observed, again consistent with significant alteration. Finally, in the region between 2.2 and 2.4 µm additional –OH and Mg_2OH absorptions can be seen. By initial comparison to a host of USGS library spectra (examples are shown in Fig 4.4) a reasonable fit for the sample spectrum is a composition of chlorite (light blue spectrum) or serpentine (light green spectrum), both of which would imply strong sub-seafloor alteration (mafic crust alteration under greenschist facies conditions and serpentinization of ultramafic rocks, respectively) of the host material found on the seafloor.

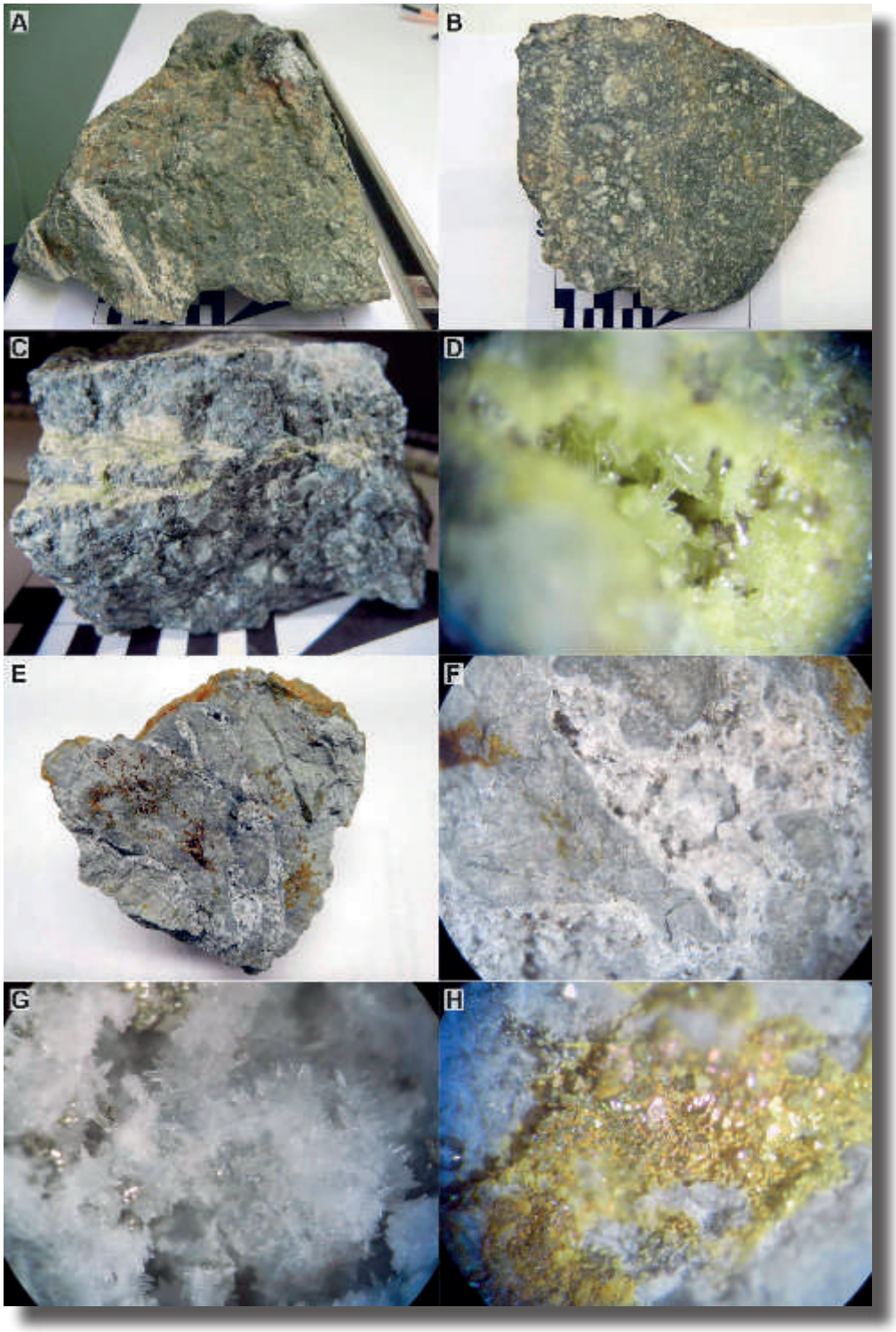

Fig. 4.2: Rock samples recovered at the northern Langseth Ridge slope (PS101/203-1). A: Possibly serpentinized rock with a greenish colour (sample PS101/203-R2); B: gabbroic to doleritic sample with large phenocrysts (PS101/203-R1); C: gabbro or dolerite with plagioclase and pyroxene phenocrysts, cut by green epidote veins (PS101/203-R4); D: close-up of epidote vein (field of view approx. 3 mm); E: hydrothermally altered rock (PS101/203-R3) with close-ups of sulfide and possibly sulfate precipitates in F, G, and H (field of view approx. 2 cm for F, 3 mm for G and H).

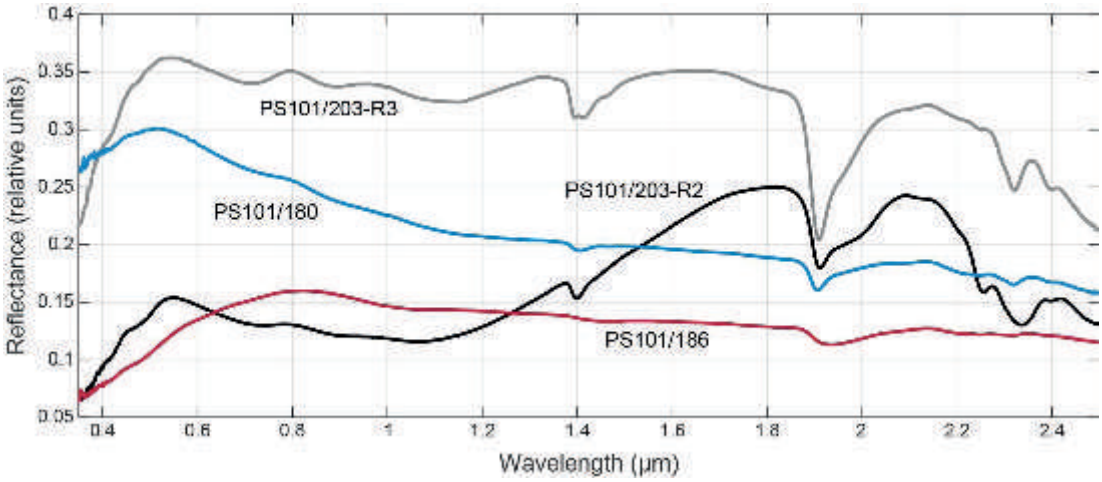

Fig. 4.3: Visible to near-infrared spectra of hand samples collected during dredges at stations PS101/186-1 and PS101/203-1.

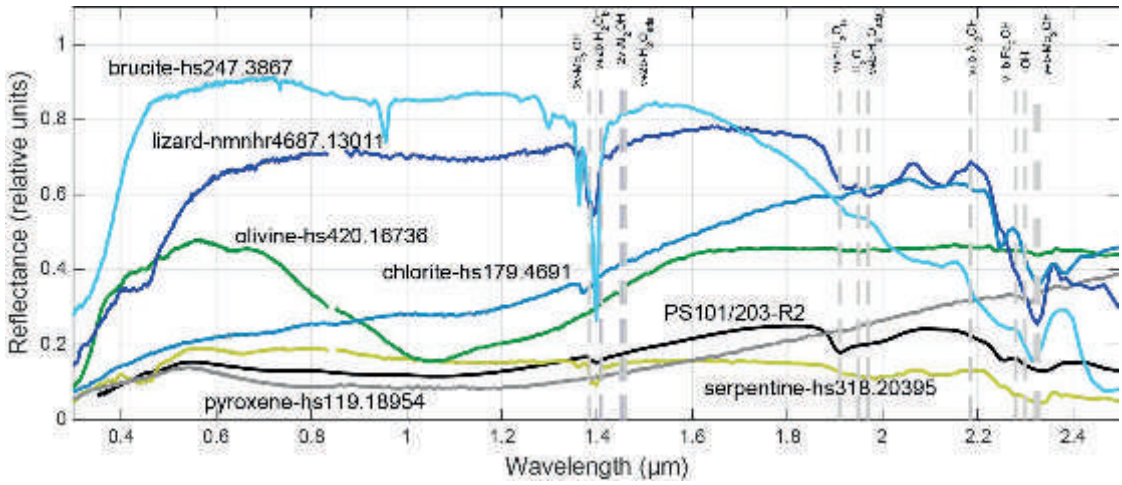

Fig. 4.4: Spectral comparison between the sample PS101/203-R2 (black spectrum) and several USGS spectral library samples (coloured spectra). Names of the library minerals are indicated in the labels, and all spectra were from hand samples. Several lines of key absorptions are provided and labelled for comparison.

In general, the occurrence of these deep crustal or mantle rocks strongly suggests tectonic uplift and possibly also tilting of the northern slope of the Langseth Ridge. Various OFOS and NUI seafloor images of banked, layered, and/or orthogonally fractured rocks as well as clear evidence for geological faults with visible offsets all strengthen these interpretations (Fig. 4.5; *cf*. Chapters 3 and 8).

The third lithology appears light-grey to slightly blue in colour (PS101/203-R3; Fig. 4.2e–h). It does not show any primary crystal phases and appears highly altered, which again is confirmed by spectroscopy (Fig. 4.4). The samples contain white to colourless veins probably composed of sulfates that also contain interbedded yellow–gold sulfide precipitates. We conclude that hydrothermal circulation has led to an intensive alteration of at least some of these rocks together with the precipitation of a range of sulfur bearing minerals.

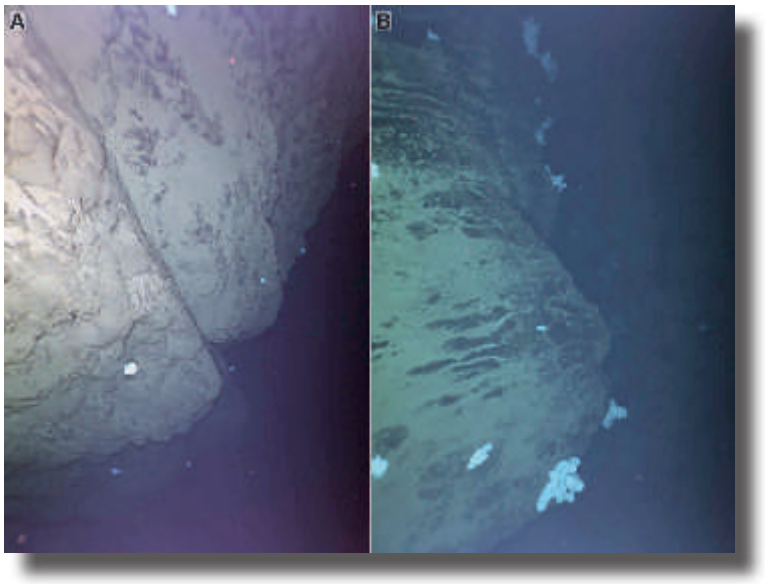

Fig. 4.5: Hints towards tectonic movements at Langseth Ridge. A: Fault plane with visible offset; B: outcrop of banked rocks (Photographs by AWI OFOS-Team).

Dredge PS101/193-1 brought up several distinct lithologies from the northwestern slope of the Karasik seamount, further from the ridge-axis. Besides very fine-grained aphyric basalts containing minute plagioclase laths (PS101/193-R1, PS101/193-R2; Fig. 4.6a), we also recovered variably weathered rocks interpreted as olivine tholeiitic basalts (PS101/193-R3, PS101/193-R4; Fig. 4.6b). These contain large phenocrysts of mainly olivine, which has been partly iddingsitized, and some plagioclase. Furthermore, we identified brecciated rocks with a yellowish-brown groundmass and angular and poorly sorted fragments of mainly basaltic material (PS101/193-R5; Fig. 4.6c). The groundmass also holds fragments with crusts reminiscent of variably weathered glass, as well as single crystals.

The samples of aphyric basalt point to a rapid rise and cooling of magma without prolonged reservoir residence time. The presence of large phenocrysts in the porphyritic samples are, in contrast, indicative of growth during a prolonged period of magma storage at depth below the seafloor. The breccias could be tectonic in origin, which would—as well—fit with an interpretation that the origin of Langseth Ridge is not entirely volcanic.

The NUI vehicle was used to map the northern and southern summits of Karasik seamount itself and revealed a 35 m scarp/gulley feature in the north that was not apparent in the ship's lower-resolution multibeam data (*cf*. Chapter 9). A single pass across this scarp with OFOS (PS101/089-1) revealed rock outcrops at this location. Multiple subsequent passes for down-looking photography with NUI showed both that (a) the scarp was represented by a steep vertical cliff exposing outcrop and (b) that individual outcrops revealed the same orthogonal shapes and layered textures to the rocks that were also seen at the hand specimen scale in the samples collected from dredge PS101/203-1.

Few of the rock samples recovered by box or multiple coring were larger than about 3 cm in diameter. One larger specimen (PS101/093-R1; Fig. 4.7) was brought up near the Karasik summit. It has a fine-grained groundmass with many altered olivine as well as some plagioclase and pyroxene phenocrysts, hence, very similar to the olivine tholeiites recovered from PS101/193-1. Most of the remaining clasts recovered by box or multi-corer from the Karasik seamount also seem to be volcanic in origin.

Fig. 4.6: Recovery from station PS101/193-1 at the northwestern Karasik slope. A: Fine grained basalt (PS101/193-R1); B: basaltic rock with large phenocrysts of olivine and plagioclase (PS101/193-R3); C: brecciated rock with volcanic rock clasts (PS101/193-R5).

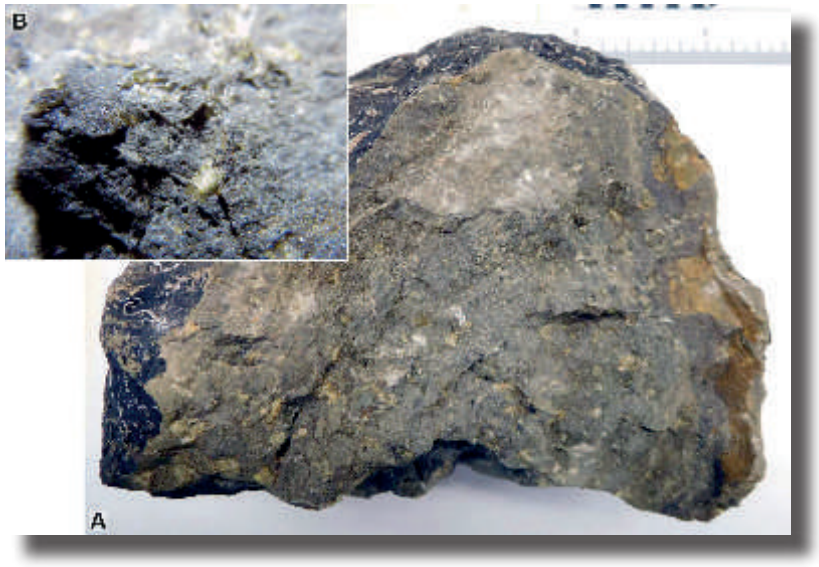

Fig. 4.7: Basalt with large phenocrysts recovered at box corer station PS101/093-1. A: Strongly weathered hand specimen (approx. 20 cm in size); B: close-up of the fine groundmass with greenish olivine crystals.

Using the gravity corer, we recovered sponge needles, minor amounts of sediments, and small rocks as well as weathered glass fragments from near the summit of Karasik (PS101/104-1). At the reference site on the western Karasik slope (PS101/148-1) we cored 2.95 m of sediment with preserved stratification (photograph and detailed description in Appendix A.5.1). It mainly consists of brownish to greyish mud. In the uppermost meter, several layers of fine sand with well-sorted siliciclastic particles in the size range 100–500 µm interrupt the mud. The mud presumably represents background deep-sea sedimentation away from the ridge axis, in which case the change in is most probably due to diagenetic processes (reduction, remobilization, and/or oxidative colour reprecipitation of Mn). The sand layers most probably represent event deposits, e.g., turbidity flows, although they could, instead, represent deposition during short-term periods of environmental (± climate) perturbation.

To summarize, recovered rock samples as well as seafloor image data indicate combined volcanic and tectonic activity in the origin of the Langseth Ridge. Basalts from the three summits provide evidence of typical ocean crustal material, with occasional evidence for prolonged storage of magma at depth prior to eruption. But the recovery of deeper crustal or mantle lithologies from the steepest slopes close to the ridge axis, as well as the brecciated rocks and independent visual evidence for fault structures, are all consistent with tectonic uplift.

Vent Mount

Dredging at the Vent Mount (PS101/186-1) recovered exclusively pillow basalts (Fig. 4.8). The samples are fine grained with some euhedral olivine (<2 mm in size) and pyroxene crystals (<1 mm). The glassy crusts are partly oxidized and orange-brown in colour. Spectral analyses show a relatively uniform, flat spectrum typical for pillow basalts (Fig. 4.3). Some absorption at 1.9 µm can be seen and this is likely due to bound water associated with the slightly altered surface of the rock.

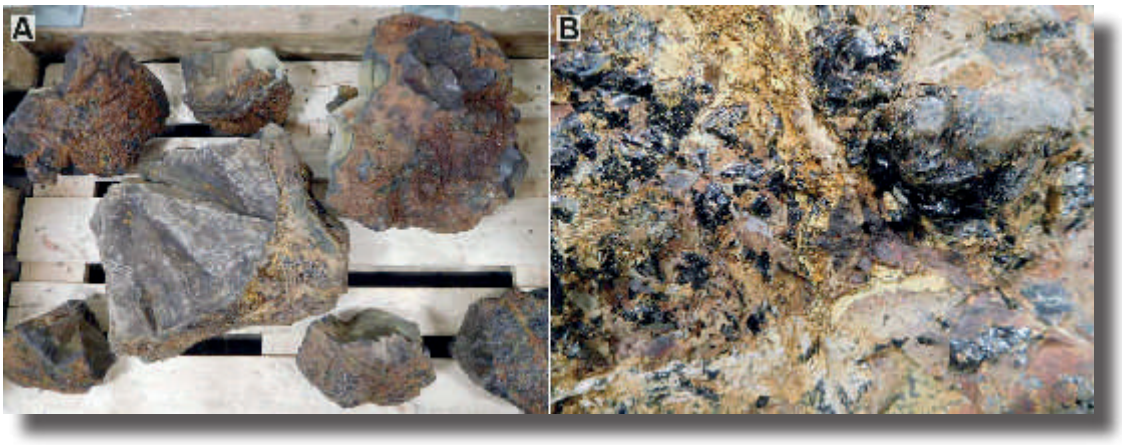

Fig. 4.8: Pillow basalt recovered at the vent mount (PS101/186-1). A: Large pillows with chilled margins of obsidian; B: slightly weathered glass crust (field of view approx. 5 cm).

Together with seafloor image data from several OFOS dives (Fig. 4.9a; *cf*. Chapter 3) it is very likely that the Vent Mount was entirely volcanic in its initial origin. There are, however, a couple of sedimented terraces separated by steep east–west oriented walls that cut through the northern slope that could hint to post-eruptive tectonic activity in this area. Similarly oriented fractures to the south of the Vent Mount summit, also imaged by OFOS, showed no vertical offset across the fractures. They could either result from dike emplacement or, instead, represent a more recent generation of spreading direction parallel extensional faulting similar to that invoked for the north flank.

Tracing of hydrothermal plume signals narrowed down the location of the discharge site to be located with, and presumably directly associated with, the terracing on the north side of the Vent Mount. Subsequent OFOS seafloor image data revealed numerous examples of hydrothermal deposits including intact but inactive chimneys and apparent dewatering structures within the sediments in this area (Fig. 4.9b, c). From one of these terraces, the gravity corer (PS101/180-1) only brought up few sediments but, importantly, it did also recover strongly hydrothermally altered basement rocks containing sulfides and sulfates as well as sandy to blocky material composed of hydrothermal crusts and precipitates (Fig. 4.10). Interestingly, the altered rocks appear similar to the hydrothermally altered sample PS101/203-R3 recovered from the northern Langseth Ridge. The spectra for these samples also show significant alteration to phyllosilicates (Fig. 4.4).

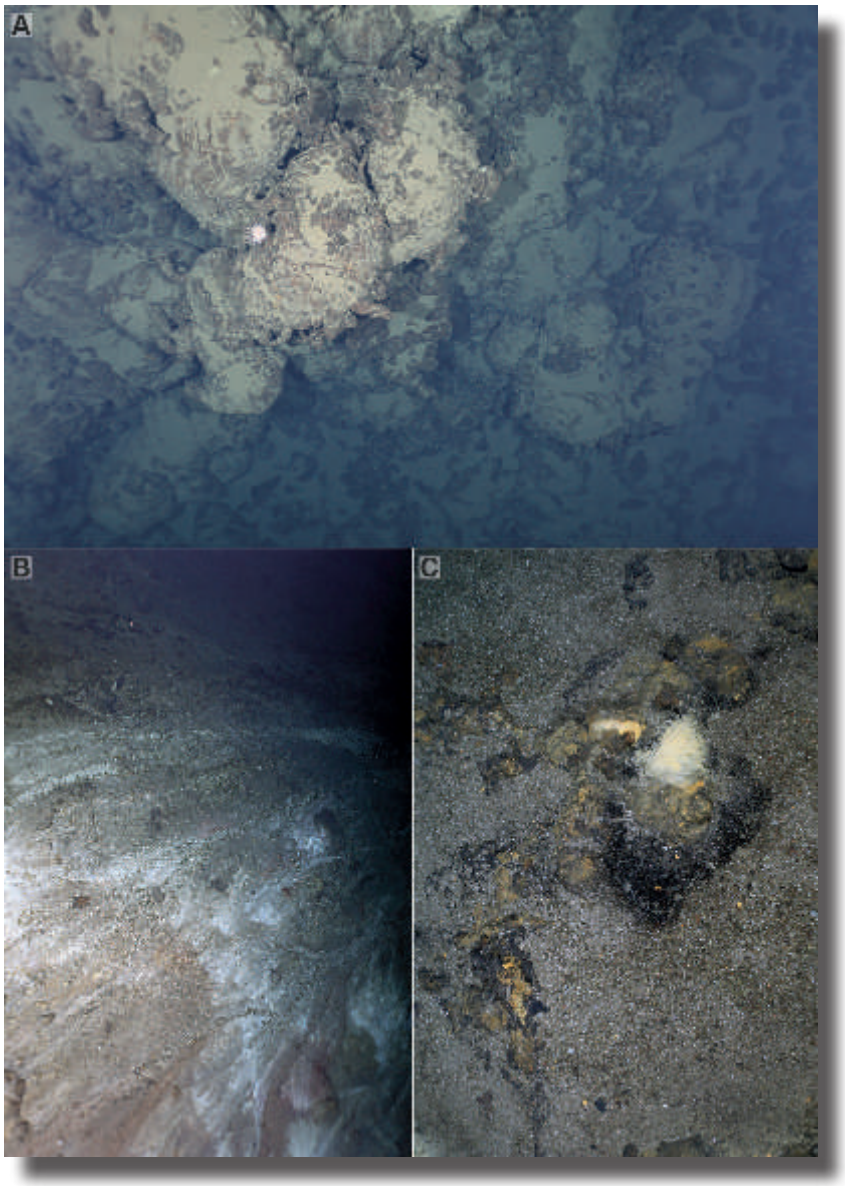

Fig. 4.9: Seafloor images from the Vent Mount. A: Fresh pillow basalts; B: hydrothermal sediments (field of view approx. 3 m); C: small hydrothermal vent and discoloured sediments (field of view approx. 1 m). Photographs by AWI OFOS-Team.

Fig. 4.10: Recovery from gravity corer PS101/180-1 from the Vent Mount. A: Altered host rocks, hydrothermal precipitates, and sediments; B: sulfidized basaltic host rock (specimen approx. 7 cm in width); C: oxidized precipitates; D: hydrothermal precipitates as seen through a binocular, presumably opaline silica or azurite (field of view approx. 1.5 cm).

Finally, we stored two ~25 cm long sediment cores from near the active vent site, recovered by multiple coring (*cf*. Chapter 8). To ensure that we did not disturb the stratigraphy, these cores were preserved at sea so that they can be examined in detail and intact at the home laboratory in Bremen. Additionally, gravity corer PS101/160-1 brought up one single piece of glass stuck between the liner and the steel tube.

OFOS images and rock samples of very fresh basaltic pillows suggest that the Vent Mount is geologically young and may still be volcanically active. The recent volcanism and associated magmatic supply provides heat from the Earth's interior and, hence, the energy to drive hydrothermal circulation. Measured anomalies in temperature, turbidity, and redox potential in the hydrothermal plume point towards an extensive discharge site with hot fluids close to 300 °C (*cf*. Chapter 5). High methane and dihydrogen concentrations in the plume water further indicate deep fluid circulation through mantle rock.

Data management

Data and core descriptions will be made available in PANGAEA upon completion. Rock and mineral analyses will additionally be submitted to the PetDB petrological database of Columbia University.

References

Michael PJ, Langmuir CH, Dick HJB, Snow JE, Goldstein SL, Graham DW, Lehnert K, Kurras G, Jokat W, Mühe R, Edmonds HN (2003) Magmatic and amagmatic seafloor generation at the ultraslow-spreading Gakkel Ridge, Arctic Ocean. Nature, 423, 956–961.

Schauer U (2012) The expedition of the research vessel "Polarstern" to the Arctic in 2011 (ARK-XXVI/3 – TransArc). Berichte zur Polar- und Meeresforschung, 649, 1–205.

Vanko DA, Bach W, Roberts S, Yeats CJ, Scott SD (2004) Fluid inclusion evidence for subsurface phase separation and variable fluid mixing regimes beneath the deep-sea PACMANUS hydrothermal field, Manus Basin back-arc rift, Papua New Guinea. Journal of Geophysical Research, 109, B03201.

Craddock PR, Bach W (2010) Insights to magmatic–hydrothermal processes in the Manus Back-Arc Basin as recorded by anhydrite. Geochimica et Cosmochimica Acta, 74(19), 5514–5536.

5. SEAFLOOR HEATFLOW AT THE ULTRASLOW SPREADING GAKKEL RIDGE

Mechthild Doll[1], Paulina Müller[1] [1]UHB-GEO
Norbert Kaul[1] (not on board)

Grant No. AWI_PS101_01

Objectives

The determination of geothermal heat flow density is a method to characterise the pattern of thermal energy distribution in heterogeneous environments at the Earth's surface. For heat flow density determination in the Arctic Ocean during cruise PS101, information about the undisturbed temperature gradients as well as thermal conductivity in the seabed is essential. This information contributes to our understanding of the thermal characteristics of an ultra-slow spreading centre like the Gakkel Ridge and for detecting hydrothermal activity at the Karasik Seamount. Hydrothermalism can be spectacular as black smokers, visible as shimmering water, measurable as cold and warm fluid flow in deviations of the temperature curve in the data or it can be measured simply as enhanced geothermal heat flow. Even slow spreading ridge systems as the Gakkel Ridge show effects of vigorous hydrothermalism.

At ultra-slow spreading centres, small volcanic seamounts are a dominant morphological feature and are important in building up the morphology of the ocean crust. Furthermore, Gakkel Ridge shows variations in the extent and distribution of such volcanic features, which indicate differences in thermal structure of the crust, localised potential for hydrothermal venting as well as a spectrum of heat and mass fluxes from the Earth's crust and mantle (Cochran, 2008; Drachev et al., 2009). However, ultraslow spreading ridges such as the Gakkel Ridge are supposed to be "cold" ridges with minor amounts of melt. Nevertheless, observations of concentrated magmatic activity indicate that there still should be a transport of magma and energy in the direction of the magmatic centres (Brown and White, 1994; Michael et al., 2003; Standish et al., 2008). Successful heat flow measurements on another ultra-slow spreading ridge, the South West Indian Ridge, carried out during *Polarstern* cruise PS81 (ANT-XXIX/8) in 2013 showed rather low heat-flow rates. In contrast, from the cruises AMORE (PS59, 2001) and AURORA (PS86 2014) we know that the ultra-slow spreading Gakkel Ridge contains sites of very high heat flow density up to more than > 1,000 mW/m² (Baker et al., 2004; Boetius ,2015).

Generally heat flow data points for the Arctic Ocean as of 2016, especially for the area of the Langseth Ridge, are rare. Heat flow data published in the global heat flow database shows some very low as well as very high heat flow values in other areas of the Gakkel Ridge but there is very little known about the thermal energy distribution in the vicinity of the Karasik Seamount.

During *Polarstern* cruise PS101 in 2016, extended heat flow investigations were carried out, which focused on improving the understanding of the thermal environment of the Karasik Seamount, a region of what has been assumed to be very young crust. We were able to detect advective processes with fluid flow recharge sites and very low heat flow values in this area. With these results we contribute to the understanding and better characterisation of hydrothermal activity and its distribution along the Gakkel Ridge.

Work at sea

The temperature gradient was measured at deployment stations using a temperature gradient lance (LIRlance, see Fig. 5.1 and Gradient Lance) onto which miniaturized temperature data loggers (MTLs) were mounted. The temperature range of these loggers is -4°C up to 55°C. The loggers have a resolution of 0.001 K and an accuracy of approximately 0.1 K (Pfender and Villinger, 2002). They were deployed with CTD Profile PS101/044-1 and CTD Profile PS101/055-1 during this cruise for calibration.

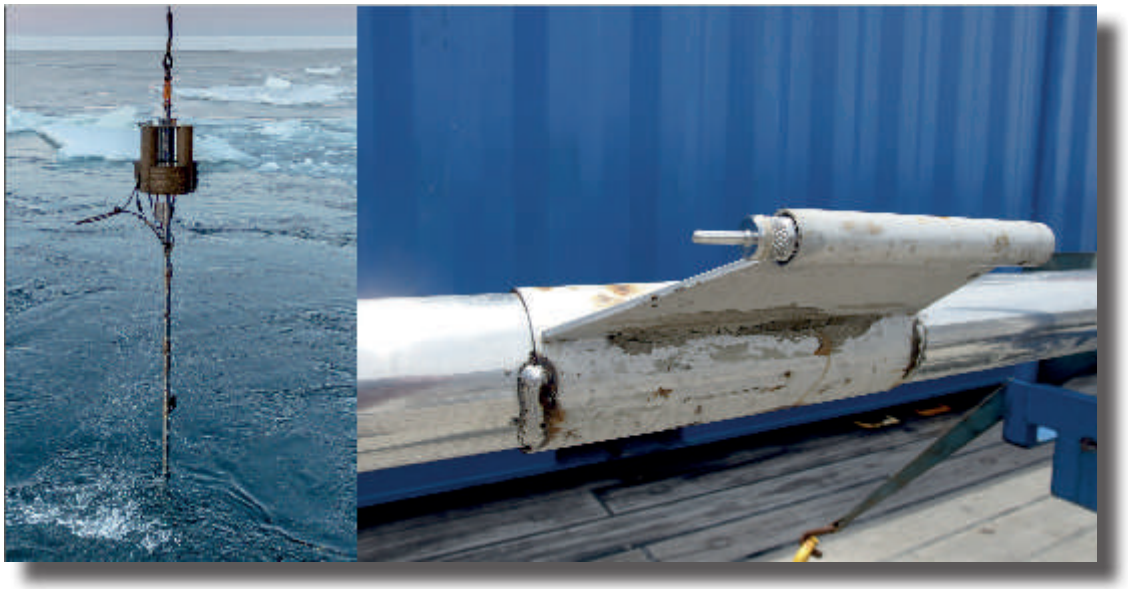

Fig. 5.1: The 5 m long temperature lance immediately after recovery with six miniaturized temperature data loggers mounted on the outside wall of the strength member (left). MTL in clamp mounted on the temperature lance (right).

For measurements of the temperature gradient in the sediment, five to seven MTLs were mounted on one of the temperature lances or on the gravity corer (3 and 6 m). Additional loggers for bottom water temperature and tilt were attached to the top of the devices. The relative depth positions of the loggers along the lance varied between 0.5 m (temperature lance transects) up to 0.8 m (6 m gravity corer) spacing. For gravity core sites the spacing between the sensors was closer towards the tip.

Four short heat flow profiles were attempted on and around the Langseth Ridge. Due to the ice coverage of 90 – 100 % and a significant ice drift in varying directions, we usually aimed at one target per profile and proceeded according to the drift.

Visual inspections of both the Langseth Ridge and the Vent Mount by the Ocean Floor Observation System (OFOS) showed steep flanks and areas of exposed rock or talus flows with only a thin sediment dusting, which we needed to avoid in order not to damage the heat flow probe. Therefore most of the positions were located at the foot or on the slope of Langseth Ridge (see Fig. 5.2 and Fig. 5.4), except for one station in the sedimented saddle between Karasik Seamount and Central Mount. A reference site was chosen some 150 km S of the rift axis in the Nansen Basin (see Fig. 5.3).

At each site several penetrations were carried out in a local spread. One station consisted of four to eight single penetrations, commonly positioned 150-200 m apart, depending on the speed of the ice drift at the time. The transit was done in pogo style with the instrument

approximately 200 m above ground between penetrations. Depending on the drift conditions, the time the instrument could be left in the ground varied between 7 and 10 min. Our stations usually covered a time of five to six hours. Fig. 5.4 shows all heat flow stations in the working area during cruise PS101.

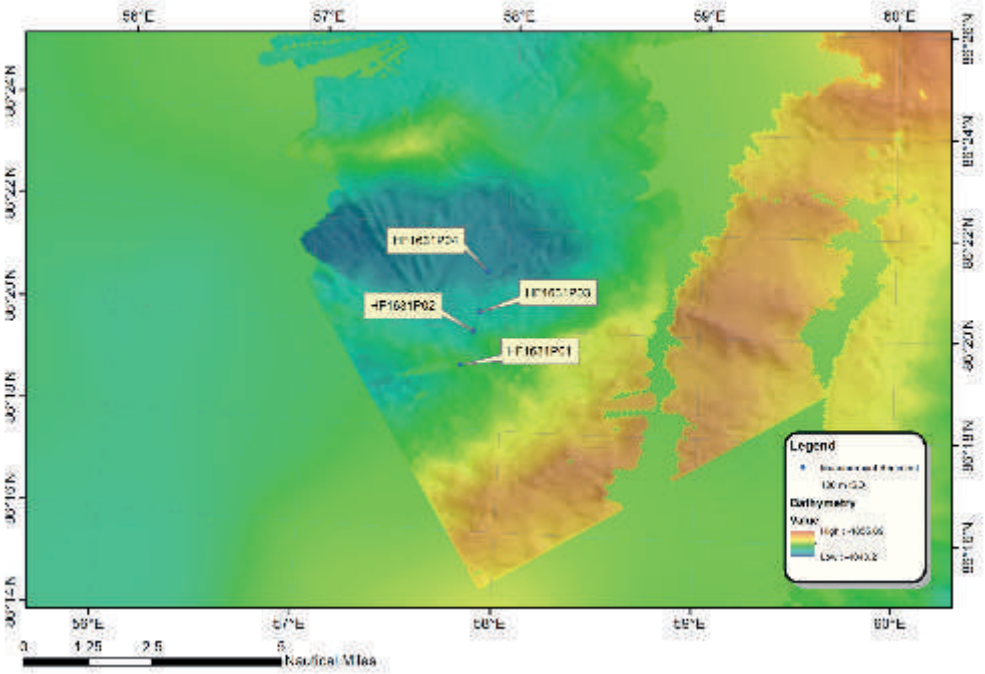

Fig. 5.2: Four penetrations of the heat flow probe were carried out in a basin southeast of the Karasik Seamount

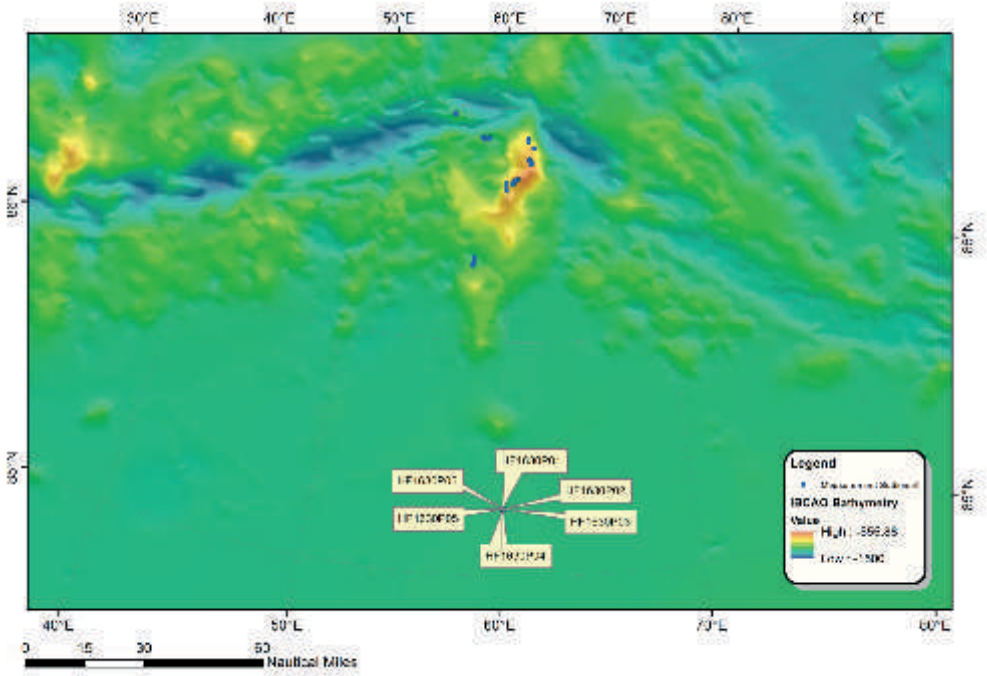

Fig. 5.3: Six penetrations of the heat flow probe were carried out at the first reference site and Mooring 1 position in the Nansen Basin

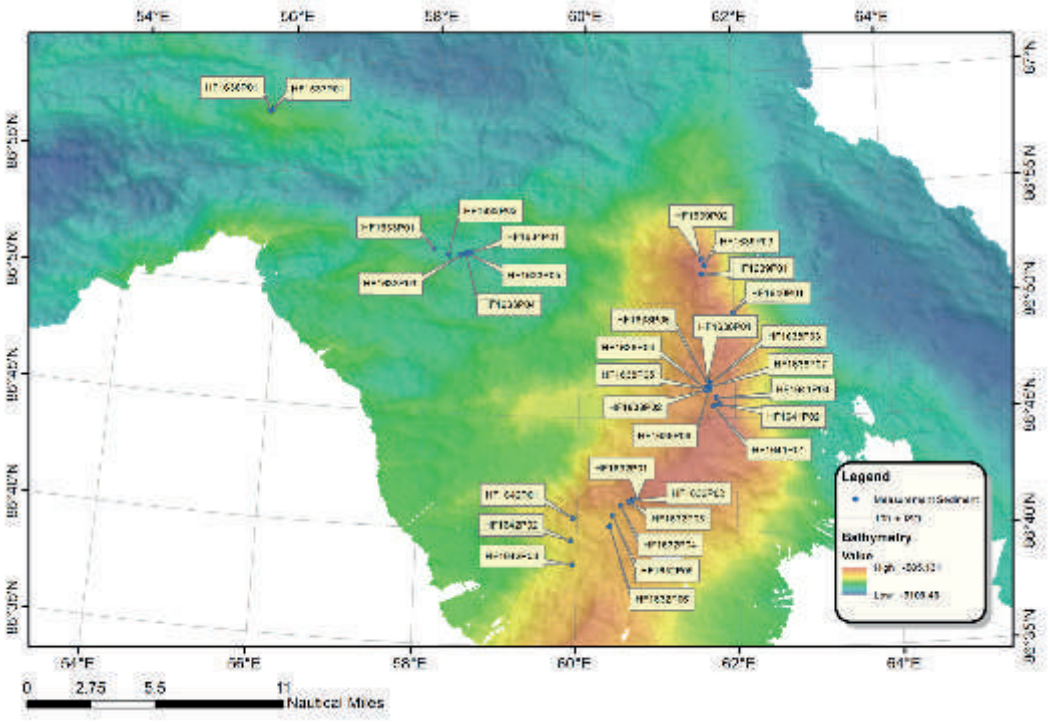

Fig. 5.4: Map of all penetrations of the heat flow probe as well as temperature measurements in the seabed carried out using the gravity corer and modified TV-MUC in the working area

For thermal conductivity measurements, the DECAGON DEVICES thermal properties meter KD2 Pro was employed with the 6 cm single needle. The instrument is rated at 5 % accuracy in conductivity. Thermal conductivity k was measured on core material from the gravity corer, sampled at 10-20 cm intervals and at the depth at which MTLs had been mounted on the gravity corer, as well as on core material from the box corer after the benthic sampling was finished (Fig. 5.5).

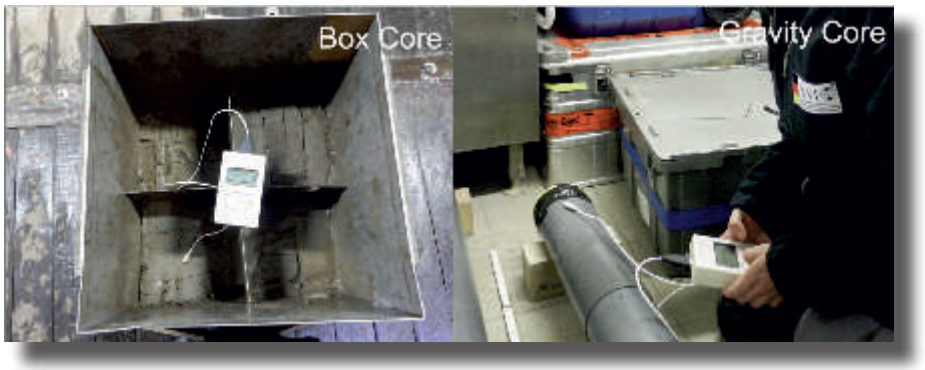

Fig. 5.5: Thermal conductivity measurements in core material

In addition to measuring sediment temperatures, MTLs were mounted onto the frames of the OFOS and of the Tv-Multicorer (TV-MUC) during surveys to monitor the temperature at dive height, nominally 4 m above ground. Fig 5.6 and Fig. 5.7 show the OFOS and TV-MUC stations and sites of other devices equipped with an MTL with the exact “on ground” positions. A special set up was devised that allowed the mounting of up to 2*4 MTLs on the TV-MUC on steel rods between the coring tubes (Fig. 5.8).

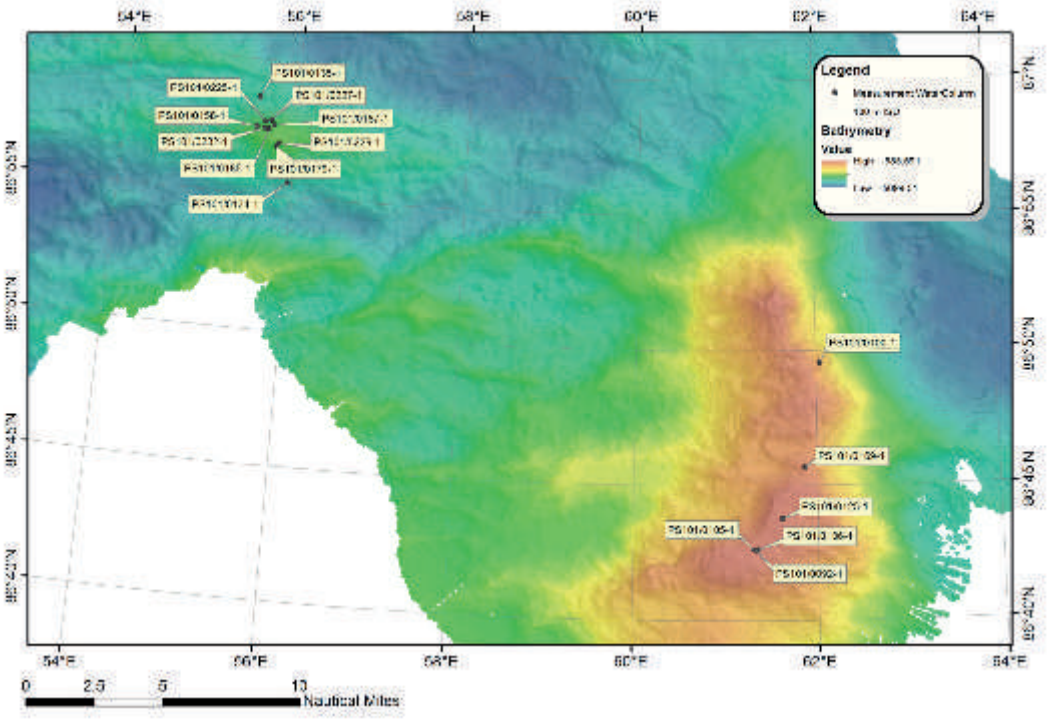

Fig. 5.6: Location of stations PS101/0092-1 to PS101|0232-1

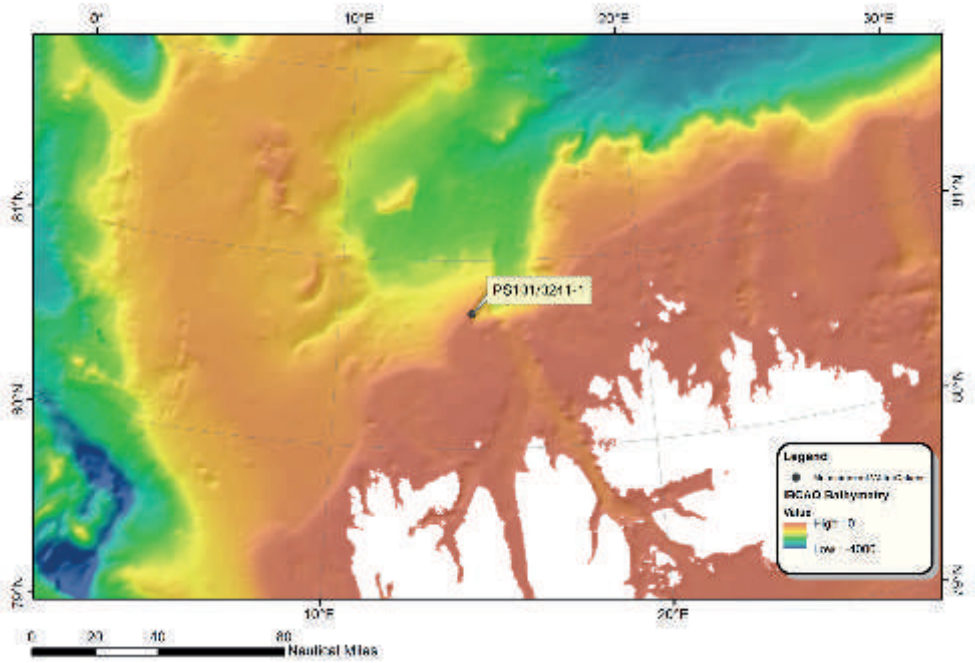

Fig. 5.7: Location of OFOS station PS101/0241-1 on the Yermak Plateau in the Arctic Ocean onto which two MTLs were mounted to measure the bottom water temperature

Fig. 5.8: Set-up of OFOS and TV-MUC

Preliminary (expected) results

Heat Flow

During PS101, 45 heat flow measurements were attempted on 13 different stations, and 40 of those were successful penetrations. Most of the data gathered with the gradient lance yielded temperature gradients of good or very good quality. The data gathered with the TV-MUC were more difficult to interpret. The temperature gradients on and around Langseth Ridge ranged from -0.080 K/m up to 0.151 K/m, often without distinguishable geographic or morphological trend. The lowest calculated heat flow was 110.17 mW/m² and the highest 151.31 mW/m². Both values come from measurements taken with the TV-MUC. The lowest and highest heat flow measured with a long heat flow probe were 0.27 mW/m² and 47.75 mW/m², respectively.

The variability of heat flow in the study area is an expected feature of very young crust, and mainly caused by hydrothermalism in the new seafloor. Hydrothermal activity can cause extremely high, extremely low or even negative temperature gradients and heat flow estimations. Heat flow close to the rift valley should show values in excess of 300 mW/m², and decrease further away from the ridge as the crust ages (Hasterok, 2013). However, a low melt production under Langseth Ridge would result in slow spreading rates due to low mantle temperatures. This would, in turn, result in a reduced heat flow in this area with regional deviations due to hydrothermalism. Our results show the expected variability, but also very low values overall. A vigorous hydrothermal circulation could be supposed as the reason for such effective cooling of the crust, particularly in conjunction with the very limited sediment input into the area, which leaves the permeable rock exposed. At the bottom of Langseth Ridge strong signs for recharge of cold seawater and fluid flow through a sediment pond can be seen in the data (Fig. 5.9). We did not find areas of the expectedly high or significantly elevated heat flow, only relatively high temperature gradients. The rough terrain with significant effects of topography might be a second reason for measurements of quite different temperature gradients in the seabed. No corrections for slope features like turbidites or landslides or topographical effects have been conducted on the data as yet.

Unusual results were the negative temperature gradients measured during TV-MUC deployments on top of the mounts on Langseth Ridge, where the sediment was notably colder than the bottom water. This phenomenon remains enigmatic.

Fig. 5.9 shows the analysed temperature gradients for heat flow station PS101/0082-1 (A), PS101/0148-1 (A) and PS101/0187-1 (C). It represents the high variability of the temperature gradients in this area. Fig. 5.9A shows the effect of downward fluid advection, which can be seen in the deviation of the temperature curve from its steady-state conductive heat flow. Fig. 5.9B shows an extremely low temperature increase with depth whereas Fig. 5.9C, which was carried out on a sedimented terrace on the northern flank of the Vent Mount, shows results likely more affected by comparatively recent volcanic or hydrothermal activity in that area.

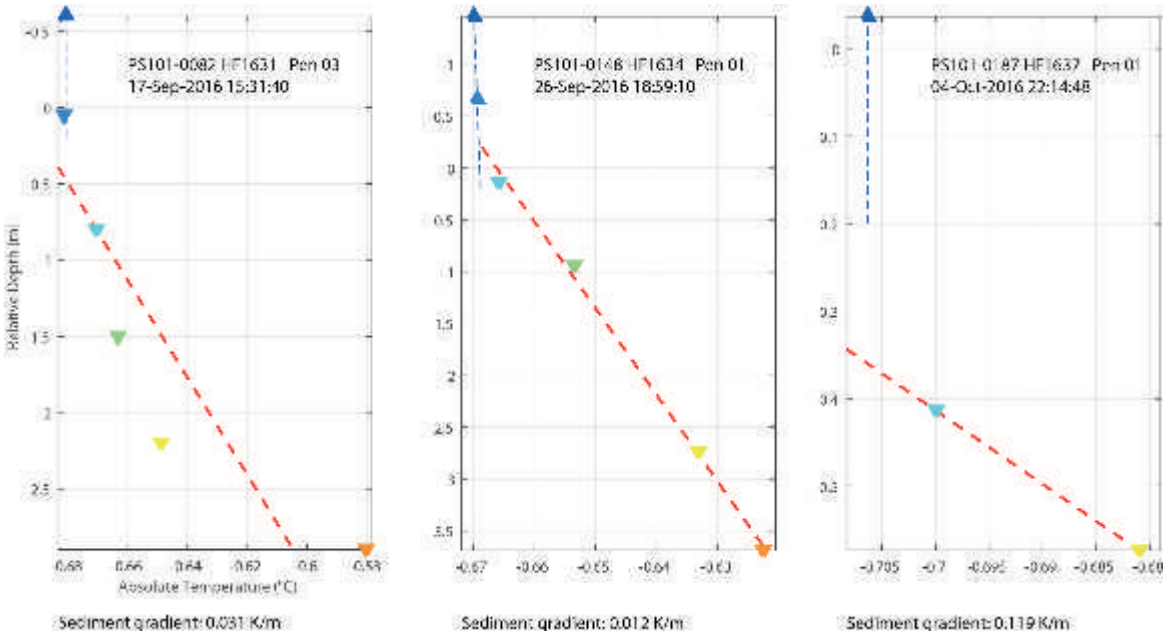

Fig. 5.9: Temperature gradients for heat flow station: (A) PS101/0082-1 (left), (B) PS101/0148-1 (middle) and (C) PS101/0187-1 (right)

A list of all heat flow stations is summarized in Tab. 5.1. In a few instances penetration failed due to hard ground. Data reduction and processing of measured time series was done using the programme MHFRED according to an algorithm published by Villinger and Davis (1987).

The thermal conductivity data measured on board on recovered core material of one gravity corer results in very good, regionally representative estimations. The mean value for thermal conductivity is estimated at 0.983 W/mK. We attribute this to a high content of volcanogenic material e.g. volcanic glass, fragments of basalts. Those particles were found in abundance in gravity corer PS101/0148-1 and different box corer sites. The thermal conductivity measurements of cruise PS101 fit with results of other cruises on the Gakkel Ridge indicating values between 0.9 up to 1.5 W/mK (e.g. Drachev et al., 2003).

Tab. 5.1: List of all heat flow stations during research cruise PS101. Thermal conductivities marked with an asterisk (*) are assumed. The exact coordinates are listed in the appendix.

PS-Name	Station	Probe type	Date	Pen. Time (Ship UTC)	Water depth [m]	Pen. Depth [m]	Temp. Grad [mK/m]	th. Conducti-vity [W/mK]	Heat flow [mW/m²]
PS101/0069-1	HF1630P01	T-Lance	16.09.16	19:22:00	3890	1,71	0,010	1,00	10,19
PS101/0069-1	HF1630P02	T-Lance	16.09.16	20:10:00	3885	3,72	0,003	1,00	3,49
PS101/0069-1	HF1630P03	T-Lance	16.09.16	20:25:00	3882	3,71	0,014	1,00	13,6
PS101/0069-1	HF1630P04	T-Lance	16.09.16	21:01:00	3880	3,61	0,012	1,00	12,23
PS101/0069-1	HF1630P05	T-Lance	16.09.16	21:17:00	3882	1,99	0,025	1,00	25,34
PS101/0069-1	HF1630P06	T-Lance	16.09.16	21:53:00	3884	2,80	0,016	1,00	15,89
PS101/0082-1	HF1631P01	T-Lance	17.09.16	13:26:00	3181	3,68	0,048	1,00	47,75
PS101/0082-1	HF1631P02	T-Lance	17.09.16	14:53:00	3595	no pen.	NaN	NaN	NaN
PS101/0082-1	HF1631P03	T-Lance	17.09.16	15:32:00	3655	3,16	0,031	1,00	31,41
PS101/0082-1	HF1631P04	T-Lance	17.09.16	16:58:00	3872	3,15	0,030	1,00	29,64
PS101/0107-1	HF1632P01	T-Lance	20.09.16	01:11:00	1035	2,42	0,012	1,00	11,79
PS101/0107-1	HF1632P02	T-Lance	20.09.16	01:33:00	1099	1,78	0,023	1,00	22,62
PS101/0107-1	HF1632P03	T-Lance	20.09.16	02:17:00	1237	3,12	0,016	1,00	16,03
PS101/0107-1	HF1632P04	T-Lance	20.09.16	02:50:00	1406	no pen.	NaN	NaN	NaN
PS101/0107-1	HF1632P05	T-Lance	20.09.16	04:10:00	1590	2,87	0,020	1,00	20,05
PS101/0107-1	HF1632P06	T-Lance	20.09.16	05:03:00	1590	2,80	0,012	1,00	11,68
PS101/0119-1	HF1633P01	T-Lance	22.09.16	01:57:00	3819	3,50	0,009	1,00	8,69
PS101/0119-1	HF1633P02	T-Lance	22.09.16	03:15:00	3836	2,76	0,003	1,00	2,54
PS101/0119-1	HF1633P03	T-Lance	22.09.16	03:48:00	3840	3,50	0,000	1,00	0,42
PS101/0119-1	HF1633P04	T-Lance	22.09.16	04:16:00	3835	3,50	0,003	1,00	3,07
PS101/0119-1	HF1633P05	T-Lance	22.09.16	04:30:00	3835	3,50	0,008	1,00	7,68
PS101/0148-1	HF1634P01	Gravity Corer	26.09.16	19:00:00	3792	3,71	0,012	1,00	11,87
PS101/0160-1	HF1635P01	Gravity Corer	29.09.16	00:17:00	3376	no pen.	NaN	NaN	NaN
PS101/0161-1	HF1635P02	Gravity Corer	29.09.16	02:51:00	3292	no pen.	NaN	NaN	NaN
PS101/0180-1	HF1636P01	Gravity Corer	03.10.16	15:53:00	3157	no pen.	NaN	NaN	NaN
PS101/0187-1	HF1637P01	TV-MUC	04.10.16	22:16:00	3200	0,38	0,131	1,00	130,55
PS101/0187-1	HF1637P02	TV-MUC	04.10.16	22:16:00	3200	0,38	0,121	1,00	121,28

PS-Name	Station	Probe type	Date	Pen. Time (Ship UTC)	Water depth [m]	Pen. Depth [m]	Temp. Grad [mK/m]	th. Conducti-vity [W/mK]	Heat flow [mW/m²]
PS101/0189-1	HF1638P01	T-Lance	05.10.16	15:57:00	1220	3,33	0,001	1,00	0,74
PS101/0189-2	HF1638P02	T-Lance	05.10.16	17:25:00	1153	0,75	0,151	1,00	151,31
PS101/0189-2	HF1638P03	T-Lance	05.10.16	17:45:00	1144	3,24	0,026	1,00	25,65
PS101/0189-3	HF1638P04	T-Lance	05.10.16	19:24:00	1157	2,06	0,013	1,00	12,88
PS101/0189-3	HF1638P05	T-Lance	05.10.16	19:45:00	1155	2,77	0,007	1,00	6,61
PS101/0189-3	HF1638P06	T-Lance	05.10.16	20:23:00	1151	2,21	0,008	1,00	7,67
PS101/0189-3	HF1638P07	T-Lance	05.10.16	21:02:00	1151	1,79	0,029	1,00	29,25
PS101/0189-3	HF1638P08	T-Lance	05.10.16	21:25:00	1153	2,14	0,017	1,00	17,19
PS101/0194-1	HF1639P01	TV-MUC	06.10.16	14:35:00	724	0,40	-0,006	1,00	-66,24
PS101/0195-1	HF1639P02	TV-MUC	06.10.16	16:40:00	639	0,38	-0,080	1,00	-79,91
PS101/0196-1	HF1639P03	TV-MUC	06.10.16	17:36:00	656	0,38	-0,077	1,00	-77,24
PS101/0205-1	HF1640P01	TV-MUC	07.10.16	07:21:00	1134	0,61	-0,008	1,00	-8,37
PS101/0210-1	HF1641P01	TV-MUC	07.10.16	15:15:00	1014	0,62	0,031	1,00	31,25
PS101/0211-1	HF1641P02	TV-MUC	07.10.16	17:09:00	927	0,61	-0,038	1,00	-38,27
PS101/0212-1	HF1641P03	TV-MUC	07.10.16	18:36:00	936	0,61	0,001	1,00	1,4
PS101/0218-1	HF1642P01	TV-MUC	08.10.16	16:29:00	1830	0,61	-0,003	1,00	-3,33
PS101/0219-1	HF1642P02	TV-MUC	08.10.16	18:15:00	2005	0,61	0,008	1,00	8,29
PS101/0220-1	HF1642P03	TV-MUC	08.10.16	19:58:00	2017	0,61	0,001	1,00	0,99

Bottom Water Temperatures

While CTD-casts map the vertical distribution of properties in the water column, mounting sensors on instruments that travel long lateral distances over the seafloor gives a fascinating insight in the distribution and variability of the properties of the bottom water. Our temperature loggers were deployed parallel to a MAPR on the OFOS and the TV-MUC. The temperature data from both instruments were in good agreement, but our sampling rate of 1 Hz to the MAPR's 0.2 Hz gave a better dynamic range.

Our interest in bottom water temperatures was mainly the detection of (warm) fluid outflow to match the cold fluid inflow we observed in our heat flow data, and particularly during the dives on the Vent Mount in the rift valley we saw temperature peaks that reached up to 150 mK. All anomalies higher than 10 mK were counted as significant signals, and could always be linked to observations of anomalous features on the seafloor or unusual occurrences of fauna. Fig. 5.10 gives an example of a dive temperature log from station PS101/0229-1. This illustrates the first step of interpretation, by putting together seafloor observations with a time stamp with the temperatures logged at that time. Shown here are not only near-bottom temperatures, but also data from the water column, most notably the plume discovered by the CTD at about 2,900 m depth that we passed both during down- and upcast.

Our secondary aim of finding the source of the plume was unsuccessful, but our data indicates that we might well have passed close to the main vent site. Fig. 5.11 shows all temperatures recorded with our MTLs during OFOS-dives on Vent Mount in the rift valley. The temperature increase with depth on the tracks that go into the valleys is the adiabatic increase due to the pressure of the water column. Of particular interest were the marked anomalies in temperature on the northern flank of Vent Mount. The red star marks station PS101/0187-1, where we recorded a heat flow of 130 mW/m², which is significantly elevated compared to other measurements in the area.

The data collected during two dives on Langseth Ridge was less spectacular, but showed cold water in surprising places.

A list of all MTL temperature data of the water column is shown in Tab. 5.2.

Tab. 5.2: List of all MTL temperature data in the water column. The exact coordinates are listed in the appendix.

PS-Name	Probe type	Date	On ground (Ship UTC)	Off ground (Ship UTC)	Water depth [m]
PS101/0092-1	Box Corer	18.09.2016	19:45:00	19:47:00	663.3
PS101/0093-1	Box Corer	18.09.2016	20:34:00	20:36:00	635.4
PS101/0094-1	Box Corer	18.09.2016	21:23:00	21:25:00	640.7
PS101/0100-1	OFOS	19.09.2016	13:48:00	17:24:00	1217
PS101/0105-1	Gravity Corer	19.09.2016	23:00:00	23:02:00	521
PS101/0106-1	Gravity Corer	19.09.2016	23:40:00	23:42:00	644
PS101/0125-1	TV-MUC	22.09.2016	20:14:00	20:16:00	664
PS101/0134-1	OFOS	24.09.2016	12:39:01	13:52:00	4023
PS101/0135-1	OFOS	24.09.2016	18:08:00	22:17:00	3708
PS101/0158-1	OFOS	28.09.2016	07:50:00	13:30:00	3322
PS101/0169-1	OFOS	30.09.2016	20:25:00	00:42:00	878
PS101/0179-1	OFOS	03.10.2016	10:19:00	12:27:00	3216
PS101/0185-1	OFOS	04.10.2016	11:36:00	13:09:00	3190
PS101/0187-1	TV-MUC	04.10.2016	22:16:00	22:18:00	3200
PS101/0225-1	OFOS	09.10.2016	16:27:00	22:06:00	3052
PS101/0227-1	TV-MUC	10.10.2016	12:20:00	12:22:00	3422
PS101/0229-1	OFOS	10.10.2016	17:54:00	19:54:00	3079
PS101/0232-1	OFOS	11.10.2016	07:32:00	09:40:00	3173
PS101/0241-1	OFOS	16.10.2016	10:46:00	12:24:00	407

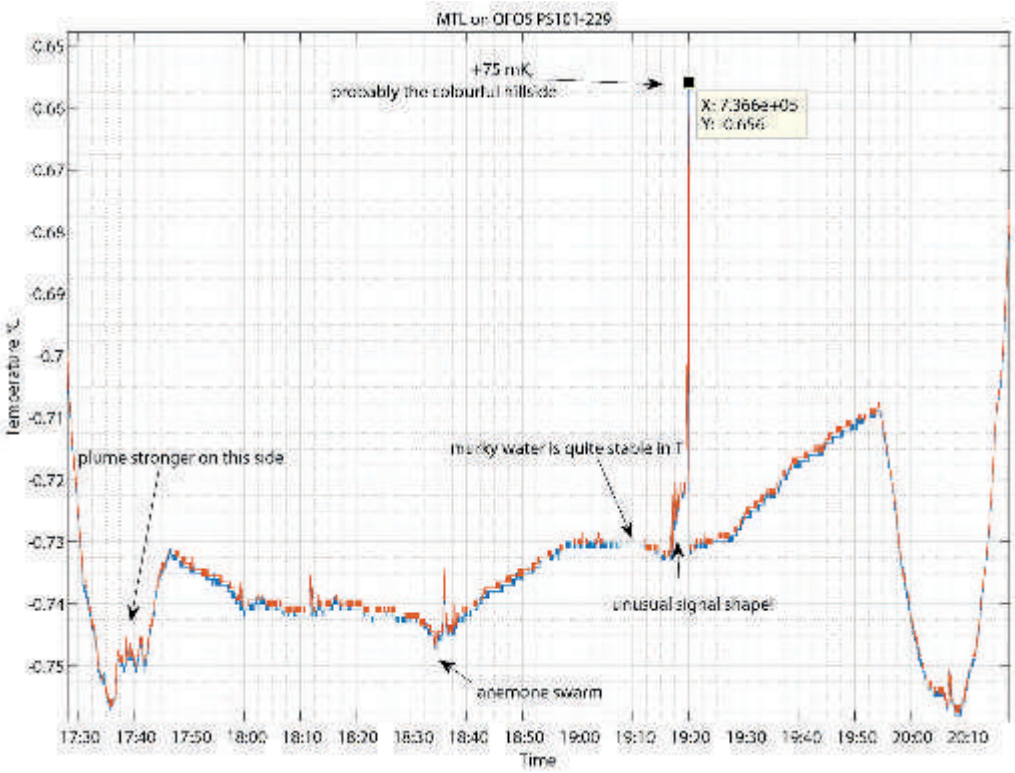

Fig. 5.10: Dive temperature log at station PS101/0229-1

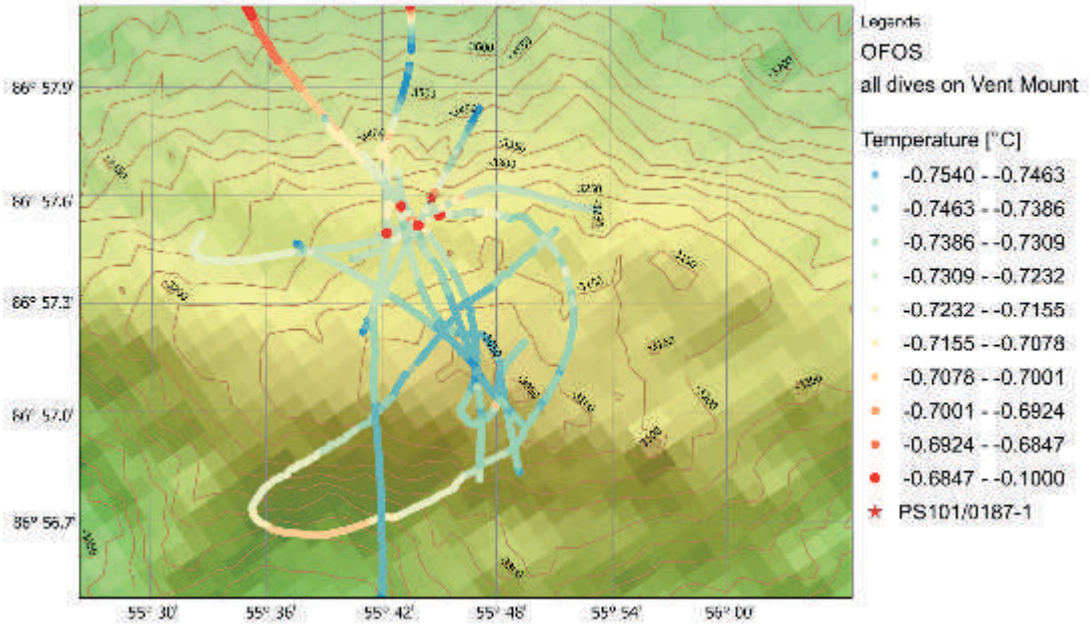

Fig. 5.11: All temperatures recorded with MTLs during OFOS-dives on Vent Mount in the rift valley

Data management

Data from all MAPR deployments is available directly from the PANGAEA archive:

https://doi.pangaea.de/10.1594/PANGAEA.869114

Processed data will be stored as soon as they are available and after their publication in peer-reviewed papers along with other geophysical results of this cruise. Heat flow data will be freely available on PANGAEA two years from the end of the cruise.

References

Baker E, Edmonds HN, Michael PJ, Bach W, Dick HJ, Snow JE, Walker SL, Banerjee NR, Langmuir CH (2004) Hydrothermal venting in magma deserts: The ultraslow-spreading Gakkel and Southwest Indian Ridges. G3 - Geochemistry, Geophysics, Geosystems, 5 (8), 1-29.

Boetius A (2015) The Expedition PS86 of the Research Vessel POLARSTERN to the Arctic Ocean in 2014. Berichte zur Polar- und Meeresforschung = Reports on polar and marine research, Bremerhaven, Alfred Wegener Institute for Polar and Marine Research, 685, 133 p.

Brown J, White R (1994) Variation with spreading rate of oceanic crustal thickness and geochemistry. Earth and Planetary Science Letters, 121 (3), 435-449.

Cochran JR (2008) Seamount volcanism along the Gakkel Ridge, Arctic Ocean. Geophysical Journal International, 174, 1153–1173.

Drachev SS, Kaul N, Beliaev VN (2003) Eurasia spreading basin to Laptev Shelf transition: structural pattern and heat flow. Geophysical Journal International, 152, 688–698.

Hasterok D (2013) Global patterns and vigor of ventilated hydrothermal circulation through young seafloor. Earth and Planetary Science Letters, 380, 12-20.

Michael PJ, Langmuir CH, Dick HB, Snow JE, Goldstein SL, Graham DW, Lehnert K, Kurras G, Jokat W, Mühe R, Edmonds HN (2003) Magmatic and amagmatic seafloor generation at the ultraslow-spreading Gakkel ridge, Arctic Ocean. Nature, 423, 956-961.

Pfender M, Villinger H (2002) Miniaturized data loggers for deep sea sediment temperature gradient measurements. Marine Geology, 186, 557–570.

Standish JJ, Dick HJB, Michael PJ, Melson WG, O'Hearn T (2008) MORB generation beneath the ultraslow spreading Southwest Indian Ridge (9–25°E): Major element chemistry and the importance of process versus source. G3 - Geochemistry, Geophysics, Geosystems, 9, Q05004.

Urlaub M, Schmidt-Aursch MC, Jokat W, Kaul N (2009) Gravity crustal models and heat flow measurements for the Eurasia Basin, Arctic Ocean. Marine Geophysical Researches, 30, 277–292.

Villinger H, Davis EE (1987) A new reduction algorithm for marine heat flow measurements. Journal of Geophysical Research, 92 (B12), 12846-12856.

6. PHYSICAL OCEANOGRAPHY AND BIOGEOCHEMISTRY OF HYDROTHERMAL PLUMES

Maren Walter[1], Elmar Albers[2], Jana Bäger[3], Alexander Diehl[2], Chris German[4], Kevin P. Hand[5], Myriel Horn[2], Janna Köhler[1], Jill McDermott[6], Massimiliano Molari[7], Bermann Steimacher[2], Gunter Wegener[7], Laura Wischnewski[3] (not on board:) Christian Mertens[1], Jürgen Sültenfuß[1], Mario Hoppmann[3], Ellen Damm[3], Wolfgang Bach[2], Jeff Seewald[4]

[1]MARUM/UHB-IUP
[2]MARUM/UHB-GEO
[3]AWI
[4]WHOI
[5]NASA-JPL
[6]LU
[7]MPI

Grant No. AWI_PS101_01

Objectives

The main objectives of the oceanography group were to locate and explain the dispersal of hydrothermal plumes from the vent field of the ultraslow spreading ridge Gakkel Ridge around the Karasik Seamount and to understand the influence of the emitted potential energy and carbon sources on the water column microbiota. We aimed to determine the heat and mass fluxes of the field, and to estimate the vertical mixing of the water above the ridge and in the axial valley. First we identified the hydrothermal plumes in the water column, which also helped to locate the vent areas on the seafloor. A hydrothermal plume signal can be identified either by anomalies in temperature and/or an increase in turbidity and drop of oxygen reduction potential (Eh). Hence, measurements of temperature, salinity, turbidity, redox and velocity were conducted to study the extent of plume dispersal. As important parameters within plume chemistry, concentrations of hydrogen, methane and sulfide and of the macronutrients (i.e., ammonium, silicate) were measured. Furthermore we used *in-situ* pump deployments to sample microbial biomass and mineral precipitates for further analyses. Another aspect of our work was to characterize the mineral composition of hydrothermal plumes. A reconnaissance study revealed that the Gakkel Ridge showed a higher plume incidence than expected, based on the slow rate of spreading and hence assumed low magma budget (Baker et al., 2004). We analyzed methane concentrations in the water column sampled by CTD/Niskin water sampler rosette along tow-yo transects. We also sampled for post-cruise measurements of dissolved metals (specifically Fe and Mn) in these samples. From methane, metal, heat, and turbidity data collected during these surveys, inferences can be made about the nature of the vent (Edmonds et al., 2003; German et al., 2010).

The water column of the plumes and reference depths was sampled with high vertical resolution using the CTD sampling rosette. Samples were analyzed on board for hydrogen, methane and sulfide concentrations, and in addition for nutrients such as silicate. Helium and neon isotopes will be measured in the noble gas laboratory (University of Bremen). Most hydrothermal plumes were highly enriched in Helium (Isotopes: ^{3}He and ^{4}He) leading to He/Ne ratios, 5-8 times higher than those observed outside the plumes. The helium isotopic composition is an important tracer for the distribution of vent fluids in the water column, since the inert gas helium is non-reactive and detectable over long distances away from the source. Direct current measurements made in parallel to the CTD casts will be used for the calculation of fine-scale velocity shear to estimate diapycnal mixing above the seamount area and along valley.

Microorganisms are key players in the pelagic carbon cycle. Heterotrophic bacteria degrade particulate and dissolved organic matter, whereas autotrophic bacteria are producers of biomass. Within the dark oceans energy sources supporting autotrophic carbon fixation are quite limited however hydrothermal vents plumes may provide energy sources for autotrophic activity. The relative contribution of these compounds varies with the vent temperature and geological background of the vent, and hence the plume composition gives insights into the vent chemistry. On board we measured the *in-situ* concentrations of hydrogen and methane, the likely most accessible energy sources expelled from vents in the buoyant plume and outer area. Furthermore, we performed experiments on the turnover of these species in bottle incubations and we investigated the influence on carbon fixation using a ^{14}C-radiotracer assay. Moreover we sampled microbial biomass using different on board and *in-situ* filtration techniques to determine microbial community compositions at the Karasik Seamount, in the hydrothermal plume and at reference sites.

With these experiments the biogeochemistry teams aims were (i) to quantify the emission of hydrocarbons and redox active metals into the water column; (ii) to track the consumption of methane and hydrogen as the most important anticipated energy sources; (iii) to determine the increase of autotrophic carbon fixation; (iv) to deduce/predict the source vent-fluid compositions, hence, likely geologic origins, based on our interpretation of the evolving plume composition at increasing distance from the source.

Work at sea

Hydrography and current measurements

The aim of the oceanographic measurements was to obtain the spatial distribution of hydrothermal plume material in the water column, as well as characterize the background hydrographic properties at the Langseth Ridge and the Karasik Seamount. Three types of casts were employed: (i) Single casts at the mooring sites (*cf*. Chapter 10) and above Langseth Ridge to obtain vertical profiles of temperature, salinity, pressure, oxygen, fluorescence, turbidity, redox potential and currents. (ii) Tow-yo casts, where the instrument package was lowered and heaved in a seesaw manner while the ship drifted slowly with the ice, were used in an exploratory fashion to identify and map the hydrothermal plume. (iii) Drift casts, where the CTD system was kept at plume level as the ship drifted to obtain horizontal plume transects; these casts were additionally equipped with *in-situ* pumps to collect cell material from the water column. Typical ship velocities during the drift were between 0 and 0.6 kn.

Conductivity-temperature-depth (CTD) casts were carried out using the ships Sea-Bird Electronics, Inc. SBE911plus system, initially equipped with two temperature probes, two conductivity probes, a Digiquarz pressure sensor, an SBE 43 oxygen sensor, a WET Labs ECO-AFL/FL fluorometer, a WET Labs C-Star transmissometer and an altimeter. Additionally a custom built Seapoint Turbidity Meter (5x normal gain), and two redox potential (Eh) sensors were used to identify hydrothermal plume signals in the water column. The first Eh-sensor was designed and built by K. Nakamura (AIST, Japan), the second one was the CTD version of the MAPR Eh sensor, the Oxygen Reduction Potential (ORP) sensor buildt at NOAA PMEL by E. Baker and S. Walker. The latter was only used in exchange for the oxygen sensor during tow-yo and drift casts because of the limited number of auxiliary ports available on the CTD. The underwater unit was attached to a SBE 32 carousel water sampler with 22 or 24 Niskin bottles. The two remaining spaces for bottles were taken up by the lowered acoustic Doppler current profiler system (LADCP) during parts of the cruise. 28 salinity samples, typically two replicates at two depths every two or three days, were collected and analyzed on board for post-cruise salinity calibration.

In total 32 CTD stations were carried out (Fig. 6.1). Twelve of those were dedicated to plume mapping at the vent site, the rest to characterize the environmental conditions at Langseth Ridge, reference sites and mooring calibration.

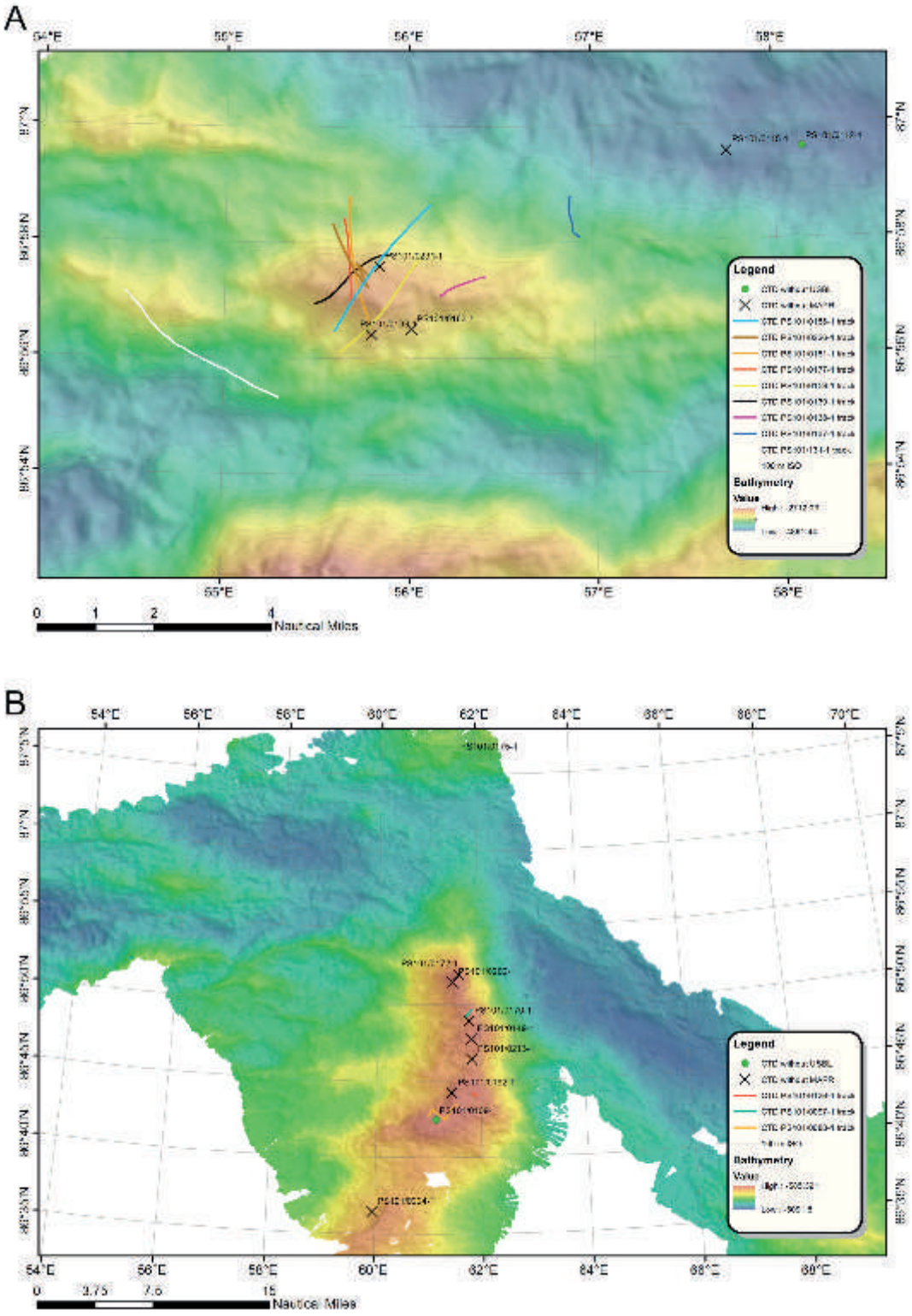

Fig. 6.1: Positions of CTD casts in the vent area (a) and at Langseth Ridge (b). Map by FIELAX.

Velocity data were collected during some of the CTD stations. The inital setup of the Lowered Acoustic Doppler Profiler (LADCP) system was two RD Instruments 300 kHz Workhorse Monitor ADCPs (AWI Bremerhaven) that were attached to the water sampler. The ADCPs were operated in a synchronized configuration in which the downward looking instrument (S/N 23293) triggers the upward looking instrument (S/N 23292). To overcome problems with the directional information arising from using the instruments internal compasses in the magnetic field of very high latitudes, the instruments were operated via a custom built data logger system (SubCTech) that integrated the data from the ADCPs with external gyro information collected on deck immediately before and after the profile. However, the communication between the two instruments via the logger deteriorated during the initial stations, and the logger was subsequently found to be flooded with seawater. Without the external compass, the heading information of the two instruments was off by approximately 40°. Further, as the abundance of scatterers at depth was extremely sparse, only the uppermost 1,000 m of the water column returned usable data. Therefore, during the second half of the cruise, velocity profiling was restricted to the shallow single-cast profiles above Langseth Ridge, using only one of the instruments (S/N 23293), which was determined to have the lesser heading offset. In addition to the lowered ADCP, upper ocean velocity data were collected along track with the ship's vessel-mounted ADCP, a 150 kHz instrument, mounted permanently into the hull of the ship.

MAPR deployments

Miniature Autonomous Plume Recorders (MAPRs, E. Baker and S. Walker, NOAA, PMEL) were deployed on CTD, OFOS, TVMUC and heat-flow stations. MAPRs are self-contained instruments that record data at pre-set time intervals (5 seconds) from temperature (thermistor mounted in a titanium probe, resolution 0.001°C), pressure (0-6000 psi gauge sensor, resolution 0.2 psi), optical backscatter (Sea Tech Light Backscatter Sensor, in nepheloid turbidity unit - NTU), and oxidation-reduction potential (ORP) sensors to register hydrothermal plume signals (Baker and Milburn, 1997). Six MAPRs (SN 03, 37, 39, 66, 67,70) were rented from the National Oceanographic and Atmospheric Association Pacific Marine Environmental Laboratories (NOAA/PMEL). MAPRs where deployed at 43 casts in total, (Figs. 6.1a,b; 6.2a,b). The instruments were either directly attached to the OFOS or TV-MUC to register near-bottom Eh and or T anomalies, or on the cable of the CTD during tow-yo stations to increase the spatial resolution of the plume data acquired. A typical tow-yo set-up included five MAPRs at 20, 40, 60, 80 and 100 m above the instrument. All MAPRs worked well, except SN 39, which exhibited a low signal to noise ratio as well as drift in the backscatter signal.

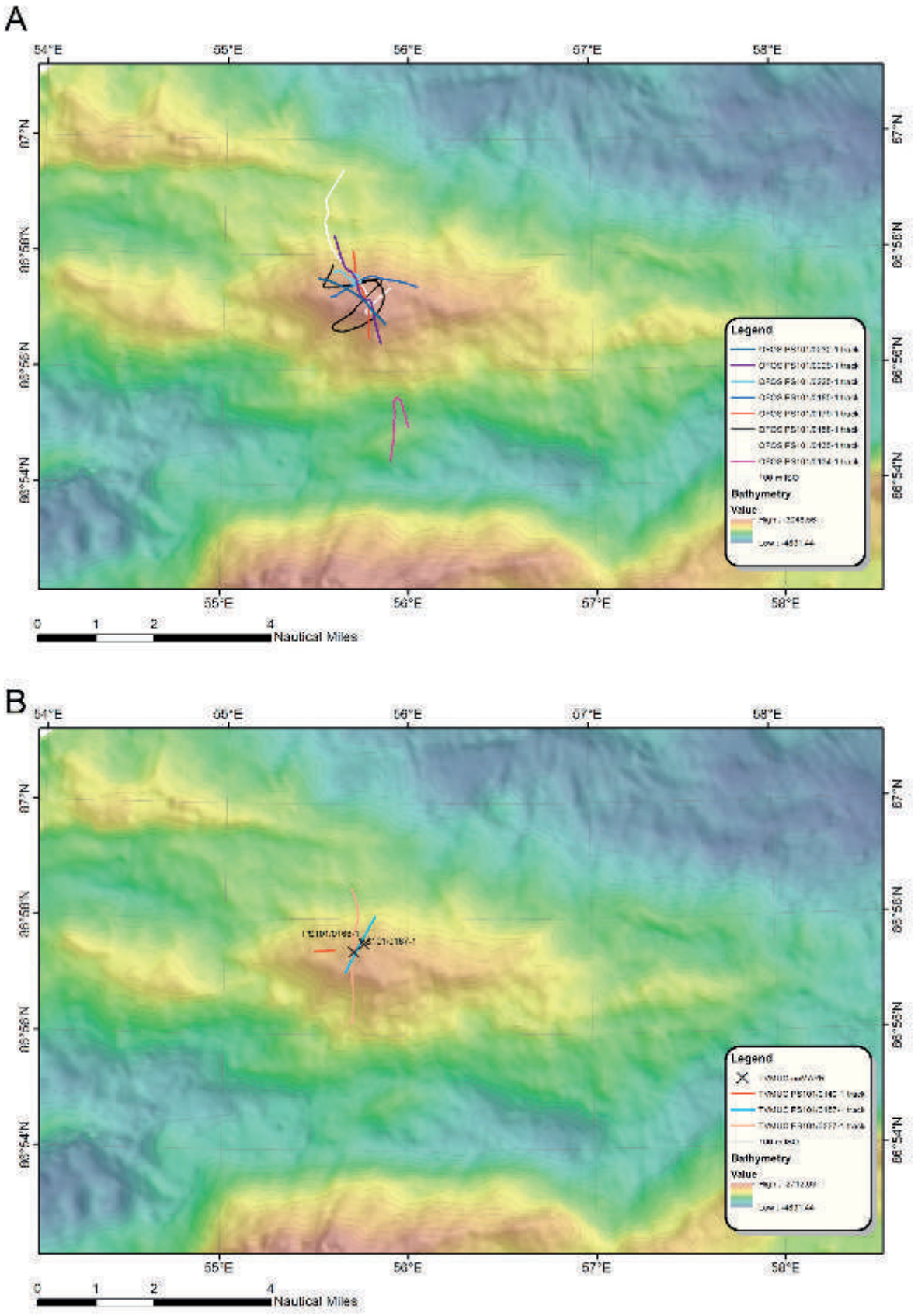

Fig. 6.2: Positions of OFOS (a) and MUC (b) deployments in the vent (a,b) area with MAPR attached as indicated. Map by FIELAX.

Tab. 6.1: Overview of water samples collected from CTD casts

Station/CTD profile	Tow-yo	Pump station	LADCP	MAPR	Samples
PS101_009/1			x		Nuts, S, Microb. Activity, CH4
PS101_044/2			x		Nuts, S, He, 3H, SF6/CFC, Metal, DNA, FISH, O2, Microb. Activity, CH4
PS101_055/3		x		x	Nuts, TA/DIC, S, He, 3H, SF6/CFC, Microbiome, Metal, DNA, FISH, O2, POC/PON, POP, PbSi, Seston, Microb. Activity, CH4
PS101_058/4					Nuts, TA/DIC, He, 3H, SF6/CFC, O2, POC/PON, POP, PbSi, Chl, Seston, Microscopy
PS101_088/5	x			x	H2, He, SF6/CFC, Microbiome, CH4
PS101_097/6	x			x	H2, He, 3H, SF6/CFC, DNA, FISH, Microb. Activity, CH4
PS101_109/7				x	
PS101_112/8		x		x	Nuts, TA/DIC, He, 3H, SF6/CFC, Microbiome, DNA, FISH, O2, POC/PON, POP, PbSi, Chl, Seston, Microb. Activity, CH4
PS101_115/9					Nuts, TA/DIC, He, 3H, SF6/CFC, O2, POC/PON, POP, PbSi, Chl, Seston, Microscopy
PS101_126/10		x		x	Nuts, DNA, FISH, O2, Microb. Activity
PS101_131/11	x			x	Nuts, S, He, POC/PON, POP, PbSi, Chl, Microscopy, Microb. Activity, CH4
PS101_133/12					Nuts, He, Microbiome, Metal, DNA, FISH, CH4
PS101_137/13	x			x	H2, CH4
PS101_138/14	x			x	CH4
PS101_139/15	x			x	Nuts, H2/CH4 Exp., H2, S, He, SF6/CFC, Metal, DNA, FISH, Microb. Activity, CH4, 13C-CH4
PS101_149/16		x			Nuts, DNA, FISH, O2, POC/PON, POP, PbSi, Chl, Microscopy, POC/PON stable isotope, Microb. Activity
PS101_159/17	x			x	Nuts, H2/CH4 Exp., H2, He, 3H, SF6/CFC, Metal, DNA, FISH, O2, Microb. Activity, CH4, 13C-CH4
PS101_163/18					POC/PON, POP, PbSi, Chl, Microscopy, POC/PON stable isotope
PS101_170/19					Nuts, Microbiome
PS101_172/20		x			Nuts, Microbiome, DNA, FISH, O2, Microb. Activity
PS101_175/21			x	x	Nuts, H2/CH4 Exp., S, He, DNA, O2, POC/PON, POP, PbSi, Chl, Microscopy, Microb. Activity
PS101_177/22	x			x	Nuts, H2/CH4 Exp., H2, He, Metal, DNA, FISH, O2, Microb. Activity, CH4, 13C-CH4

Station/CTD profile	Tow-yo	Pump station	LADCP	MAPR	Samples
PS101_181/23		x		x	Nuts, TA/DIC, H2/CH4 Exp., S, He, Metal, DNA, FISH, POC/PON, POP, PbSi, Chl, Microscopy
PS101_188/24		x		x	Nuts, H2/CH4 Exp., H2, He, DNA, FISH, O2, Microb. Activity, CH4, 13C-CH4
PS101_192/25			x		Nuts, POC/PON, POP, PbSi, Chl, Microscopy, POC/PON stable isotope
PS101_202/26			x		POC/PON, POP, PbSi, Chl, Microscopy, POC/PON stable isotope
PS101_213/27			x		Nuts, POC/PON, POP, PbSi, Chl, Microscopy, POC/PON stable isotope
PS101_224/28			x		Nuts, POC/PON, POP, PbSi, Chl, Microscopy
PS101_226/29	(x)			x	Nuts, H2/CH4 Exp., H2, He, 3H, SF6/CFC, Metal, Microscopy, Microb. Activity, CH4, 13C-CH4
PS101_231/30					Microb. Activity
PS101_239/31					POC/PON, POP, PbSi, Chl, Seston, Microscopy, HPLC, POC/PON stable isotope, RNA Fungi
PS101_240/32					Nuts, S, He, 3H, SF6/CFC

Plume water sampling for geochemical and microbiological measurement

The plume water was sampled for a large set of samples to assure a detailed geochemical and microbiological description. First noble gases were sampled followed by other gases and dissolved ions. A summary of CTD rosette samples taken on the cruise is displayed in Tab. 6.1, a detailed version can be found in the Appendix.

Concentrations and isotopic compositions of noble gases

To determine helium and neon concentrations and their isotopic signature, 103 water samples were collected from the Niskin bottles in gas tight copper tubes for later analysis in the home laboratory. Helium isotope measurements will be carried at the University of Bremen with a fully automated UHV mass spectrometric system, including gas extraction in a controlled high vacuum system. Helium and neon are separated from permanent gases in a cryo system at 25 K. A split of the sample is analyzed for ^{4}He, ^{20}Ne and ^{22}Ne with a quadrupole mass spectrometer. At 14 K helium is separated from neon and released into the sector field mass spectrometer for analysis of ^{3}He and ^{4}He. The facility achieves about ± 0.2% precision for $^{3}He/^{4}He$ ratios, and ± 0.5% or better for helium and neon concentrations (Sültenfuß et al., 2009). Since the background signal for ^{3}He in this area may be altered by tritiugenic helium, 20 samples for the analysis of tritium were taken in 1L glass bottles from water collected at hydrothermal plume level and from background profiles. Additionally, samples were taken to test for contamination from the ship and from precipitation (snow). Further, 41 samples for SF6 and CFC-12 were taken concurrent with helium samples to determine the age of the respective water. For this analysis, samples were taken in gas tight glass ampoules that were flushed prior to sampling. After equilibrating to room temperature, these samples were flame sealed and will be analyzed after the cruise in the Bremen Trace Gas Laboratory.

Methane measurement

Niskin bottles were sampled for CH_4 following noble gas and/or SF_6 sampling, when applicable, or were the first sample collected after the CTD was secure. Air-free aliquots were collected in syringes directly from the Niskin bottles, equilibrated at room temperature, and immediately analyzed via headspace extraction gas chromatography using flame ionization detection. Standard calibration was performed daily using NIST-traceable 100.0 ppm CH_4 in N_2 balance. In total, 184 water column samples were analyzed for dissolved CH_4 (80 single and 52 replicate analyses), including 73 at Karasik Seamount and 111 at the Gakkel Ridge.

Methane isotopic compositions

Methane concentrations, carbon dioxide concentrations, and $\delta^{13}C_{CH4}$ analyses of plume water samples from the CTD casts 139/15, 159/17, 177/22, 188/24, and 226/29 were also measured on board during PS101 with a Picarro cavity ringdown spectrometer. Regions of high Eh and turbidity excursions observed during downcasts and upcasts were targeted as proxies for methane since the isotopic analyses require concentrations of >1 nM for sufficient gas extraction. Several background bottom water and shallower water column samples were analyzed during each of the above listed CTD casts. For all Niskin bottles fired during a large Eh or turbidity excursion at least two evacuated serum vials were filled directly from the Niskin bottle for subsequent measurement on the spectrometer. Sample bottles were backfilled with clean nitrogen as a carrier gas, warmed to 25°C, and shaken thoroughly before each analysis. A total of 80 samples were measured on the spectrometer for isotopic analysis (14, 14, 16, 14, and 22 samples were collected from each of the CTD casts listed above, respectively). Six bottles were prepared for cross-comparison with a mass spectrometer upon return.

Measurements of hydrogen concentrations

To determine hydrogen concentrations in the plume, 60 ml syringes were filled with 40 ml seawater samples retrieved by CTD rosette sampling. A 10 ml (1 atm) headspace of hydrogen-depleted synthetic air (N_2:CO_2; 90:10) was added to the syringe and after 30 seconds of vigorous shaking the hydrogen gas content was quantitatively transferred into the headspace. The gas mixture was pushed into a *Peak performer 1* gas chromatograph equipped with a reducing compound photometer and a 250 µL sample loop. It allowed quantitative determination of hydrogen concentrations from 0.2 to 2000 nM.

Concentrations of dissolved iron and manganese species

Water samples from the CTD-rosette were taken for post-cruise measurements of dissolved metals (specifically Fe and Mn) in these samples. Aliquots of the fluid samples were filtered (0.45 µm) and acidified with nitric acid to a pH of 1.7 and stored at 4 °C for the remainder of the cruise. Metal concentrations will be measured by ICP-MS at the Geosciences Department of the University of Bremen.

Macronutrients in the water column

Surface and near surface nutrient concentrations have been measured in the context of FRAM (cf. Chapter 9). To study the nutrient signal of the hydrothermal plume, also deep nutrient samples in the plume layer as well as above and below were taken and analyzed for NO_x, NO_2, (NO_3), NH_4, PO_4 und SiO_2 concentrations with a Continuous Flow Nutrient Analyzer "QuAAtro 39" by Seal Analyticals.

Determination of trace methane turnover in water column samples

Experiments at the Aurora vent field in 2014 (PS86) showed a lack of methane oxidation in the water column hydrothermal plume. Hence, on PS101, we performed $^{14}CH_4$ incubations to track methane turnover. Plume water from the CTD rosette was filled headspace-free into butyl rubber stopper sealed 256 ml Serum vials (4-5 replicates per sampled depth). From each sample approx. 4 kBq ^{14}C-tracer dissolved in 20 µL anoxic water was retrieved via injection through the septum. All samples were incubated at 0°C, and either stopped in a time series (2 days to 2 weeks) or after 1 week of incubation by replacing 5 ml of medium with 1 ml of NaOH and 4 ml of air. Killed-controls were fixed as described above, but before the addition of the radiotracer.

Fixation of water samples for δ^{13}C-methane measurements in the home laboratories

The carbon isotopic composition of water column methane is an important parameter to determine the origin and fate of the methane. To stabilize samples for later analysis, seawater from the CTD rosette was transferred into 256 ml serum bottles that already contained 0.5 ml NaOH (50 % w/v). Samples were immediately sealed with gas-tight rubber stoppers and stored at 0°C to await shore-based analysis. Since no headspace was added the temperature of the samples will need to be kept stable until analysis.

Preparations of seawater samples for fluorescence microscopy and molecular analyses

To fix cells for microscopic analyses 500 ml of sampled seawater were treated with formaldehyde (2% final concentration). After an incubation period of 6 to 8 hours at 0°C samples were filtered onto 0.2 µm polycarbonate filters (47 mm diameter) using a vacuum pump system. Formaldehyde was washed out with sterile seawater and 70% Ethanol to dry the filters. After that filters were stored in petri dishes at -20°C for further analysis.

To retrieve material for gene amplification-based tag sequencing analyses10 L of CTD water were filtered onto Sterivex filters (Merck) using a peristaltic pump system installed in the cold room (0°C). Retrieved filters were immediately stored at -20°C for further analyses.

In-situ filtration of seawater for molecular and geochemical analysis

To retrieve larger quantities of water column biomass for transcriptomic and genomic analysis, 9 CTD rosette casts were equipped with pre-programmed *in-situ* pumps (MacLane) equipped with polycarbonate filters (142 mm diameter; 0.2 µm pore size). For the Karasik seamount and reference sites, pumps were operated at 180 min at a specific depth. To retrieve the microbial communities established within the hydrothermal plume, pumps were installed 10 to 60 meters above the CTD rosette. Guided by the characteristic Eh and temperature profile of the CTD the pumps were then positioned at the plume depth. To ensure continuous placement within the plume, and to avoid dilution with background water due to the ship drifting out of the plume area, at the Vent Mount pumping times were limited to 90 min for casts. On average 200 liters of water were filtered. Directly after retrieval on deck, pumps were opened, filters were sectioned into four equal pieces and shock-frozen in liquid nitrogen (two pieces each, into 50 ml Sarstedt centrifuge tubes) and stored at -80°C until undergoing analysis at the home laboratory.

To retrieve particulate inorganic matter from the plume and from reference sites three *in-situ* pumps were equipped with preconditioned and pre-weighed hydrophilic Polyethersulfon filters (HPWP1425; Millipore Express PLUS membrane filters, pore size 0.2 µm; washed with trace metal free solvents according to GEOTRACES protocols) including a programme as above. After retrieval filters were percolated with MilliQ grade water (>18.2 MΩ) using the *in-situ* pumps in the manual operation mode. The amount and compositions of metals will be determined in the home laboratory at the University of Bremen.

A summary of the *in-situ* pump operation depths, pumped volumes, and filter types can be found in Appendix. A.5.2

Time series of hydrogen and methane development in plume and reference waters.

To track possible consumption of hydrogen and methane in plume and reference waters CTD water samples were transferred into 9 to 18 replicates of 256 ml serum vials and sealed, headspace-free, with gas-tight butyl rubber stoppers. When indicated additional hydrogen and methane was added dissolved in sterile (0.2 µm pore size filtered) seawater to achieve measurable concentrations. The development of dissolved gas concentrations was performed in three biological replicates, and each sample was measured twice. Therefore, in each replicate 24.1 ml of medium were exchanged with 1 mmol synthetic air. The sample was agitated as described above and its hydrogen concentration was measured with the RCP-GC by transferring 2.5 ml of headspace gas into the sampling loop that was replaced with sterile-filtered seawater (technical replicates were performed). By the same method 5 ml of headspace gas was retrieved to measure methane using flame ionization mass spectrometry. The residual liquid was treated with formaldehyde solution (final concentration 2%), stored 8 to 12 hours at 0°C, and the 3 replicates of each time point (together 690 ml original culture) were filtered onto polycarbonate filter for fluorescence microscopy in the home laboratory (see above). In total 10 time series experiments with 320 measurements were performed.

Assessment of dark carbon fixation in plume and reference waters

Dark inorganic carbon fixation (DCF) was assessed using a radiotracer method as previously applied to deep-sea environments (e.g. Herndl et al., 2005). Water samples were collected from Niskin bottles using 60 ml sterilized plastic syringes. Within 30 minutes after sampling ^{14}C-bicarbonate (37 kBq per ml water) was added. For each water depth three live replicates and two formaldehyde killed control samples were processed. The samples were then incubated in the dark at *in situ* temperature (-2°C) for 48 hours (deep-sea samples) and for 3-24 hours (plume samples). The incubation was stopped by injection of formaldehyde (2% final concentration) and samples were processed as previously described (Herndl et al. 2005). To optimize the incubation time in what were anticipated to be the most active plume water samples, a time series was carried out with the first plume sample.

Furthermore several experiments were performed to assess the role of different reduced compounds (i.e. CH_4, H_2, CO, NH_4^+, $S_2O_3^+$) in causing microbial biomass production. These compounds were added with final concentrations of 100-150 nM into triplicates of the culture and DCF was measured after 24 hours of pre-incubation with the substrate.

The relationship between energy source, DCF and bacterial biomass production was investigated by transferring inocula of 240 and 540 ml plume water, depleted from grazers by filtration with 0.45 to 0.6 µm pore size, to 760 and 1710 ml of plume water, sterile-filtered on 0.22 µm filters, respectively. Replicate samples were transferred into 256 ml serum glass bottles sealed with rubber stopper and clamps, and incubated in the dark at *in situ* temperatures (-2°C) for 4 to 8 days. Two batch culture experiments were carried out with the addition of H_2 (at ca. 1.5 µM and 0.6 µM final concentration), one with addition of CH_4 (at ca. 0.4 µM), and one control without the addition of any substrates. At each stop time, 5 ml was collected in order to determine concentrations of H_2 and CH_4 using the gas chromatograph with reduced compound photometer (RCP) and flame ionization detection as described above. Aliquots of 40 ml were subjected to DCF (measured as described above) and the remaining water was fixed with formaldehyde (2% final concentration) and filtered onto 0.22-µm polycarbonate filters, then stored at -20°C for later microscopy. Additionally, at the start and end of the experiments residual water samples were taken for DNA analysis.

Preliminary (expected) results

Plume Observations CTD/MAPR (Chris German, Maren Walter, Janna Köhler)

The CTD/MAPR casts, coupled with associated MAPR deployments on both the OFOS system and the TV-MUC, provided valuable insights into both the location and the nature of hydrothermal venting on the Vent Mount during the course of the cruise. While tow-yo 137/13 showed only a transient optical backscatter plume to the SW of the Vent Mount, the following tow-yo, 139/15 intercepted the same particle-rich plume to the SW of the Vent Mount but then intercepted a fresh Eh anomaly at plume height at its NE limit, immediately to the north of the shallowest point on the seamount. Interestingly, there was only a very weak optical signal associated with this Eh anomaly during the final upcast. The following two tow-yos passed to the East and West of the central summit, respectively, oriented along approximately N-S lines. Station 159/17 was a tow-yo from North to South that started in background then intercepted a fresh Eh and optical plume which became progressively weaker in Eh and stronger in optical backscatter before returning to background profiles south of the Vent Mount where the cast was ended. Station 177/22 followed the reverse direction, from south to north, passing by the West side of the Vent Mount summit. Here, the trace again started with a background profile in the downcast but then revealed increasing optical backscatter plumes which then declined at the same time as an Eh anomaly first appeared (Fig. 6.3), just as the CTD passed due West of where the larger Eh anomaly had been observed on Station 139/15.

Following these CTD tow-yo operations, two *in-situ* pump drift stations with the CTD were occupied, CTD 181/23 and CTD 188/24 which also recorded useful *in-situ* sensor data at plume height. CTD 181/23 drifted SSE-NNW, just to the East of the line followed by CTD177/22 and transitioned from background signals into strong Eh anomalies as it passed through the same location as the most pronounced anomaly from CTD 139/15. CTD 188/24 was oriented SW-NE, parallel to CTD 139/15 but offset to the South. Strongest plume signals were observed just as the CTD passed through the same latitude range as the signals seen further West at CTDs 177/22, 181/23 and 139/15. However, the anomalies seen at this station were not as strong as at CTD 139/15 showing that this cast must be to the East of the vent-source, just as CTDs 177/22 and 181/23 must have passed the source to its West. In addition to our CTD operations, MAPRs were also deployed routinely on all OFOS and TV-MUC deployments over the Vent Mount and, wherever the downcast or upcast passed through the non-buoyant plume depths, these data could also be used to help us constrain the source of venting more precisely. Specifically, both the upcast from OFOS Station 179 and the upcast from TV-MUC 187 recorded Eh anomalies at plume height at locations to the north and northeast of the CTD139/15 station that were not as strong as at CTD139/15, confirming that CTD139/15 remained our point of closest approach to the vent-source to date.

Informed by these surveys, our final CTD tow-yo, station CTD 226/29, was a drift-yo that lowered the CTD to plume depth to the south of our predicted vent-site where a strong optical backscatter anomaly was encountered. Over time, this plume signal transitioned from an optical plume with little to no Eh anomaly to a plume, still at the same depth, with a much stronger Eh anomaly and potential temperature anomaly but no particulate back-scatter (Fig. 6.4). Lowering the CTD to the seafloor and then raising it back up to collect water samples, the CTD intercepted the buoyant stem of the hydrothermal plume during the upcast at ~2,900 m depth, approximately 200 m deeper than the non-buoyant plume although still about 200 m above the underlying seabed. Assuming weak bottom currents in the area, we believe that this now allows us to predict the source of venting on the seafloor to within ~100 m radius. Further, the evolution from chemically-fresh (high Eh anomaly) but particle-free (low optical back-scatter) to a particle-laden plume (high optical backscatter) as Eh anomalies diminish is important. It allows us to predict that the source vent fluids must not initially contain high

concentrations of polymetallic sulfides (absence of particles) but that it likely does still contain high concentrations of dissolved Fe, which - upon oxidation within the dispersing plume - would be consistent with the observed „grow-in“ of optical back-scatter signals. From these deductions we might predict a clear vent fluid source of ~300°C (cooler than 350°C, hotter than 200°C) to be responsible for the plume signatures observed – but shorebased geochemical analyses will be required to confirm this – particularly the Fe and Mn content of the samples and their relationship to He isotopic signatures as well as the already-obtained *in-situ* sensor data.

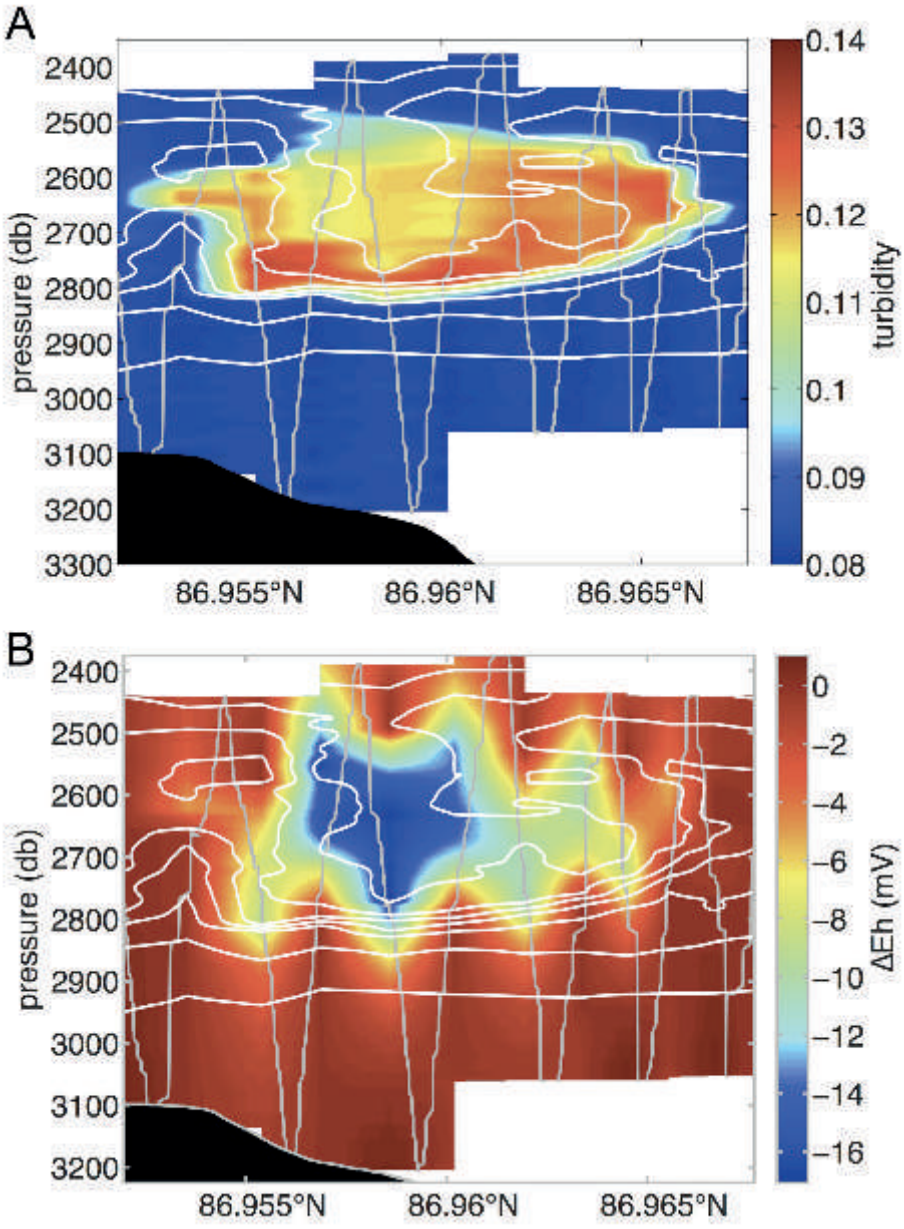

Fig. 6.3: Anomaly in (a) turbidity (NTU) and (b) Eh relative to background values during station PS101/177 going south-north on the west site of the vent mound. Grey lines denote the position of the CTD, isotherms are shown in white. Note that the area of the strongest Eh anomaly does not coincide with the strongest turbidity signal.

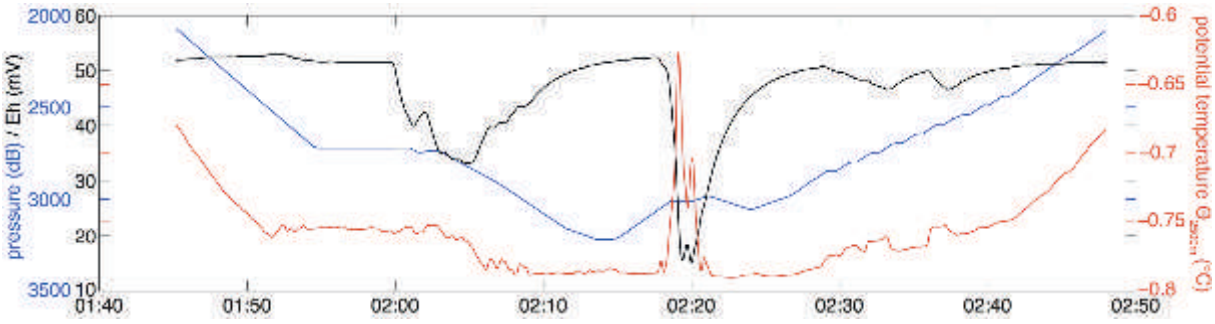

Fig. 6.4: Potential temperature (red), pressure (blue) and Eh (black) versus time during drift station PS101/226. The point at which the rising plume was intercepted is clearly visible in the sharp drop in Eh and increase in potential temperature at about 2:20 hours into the cast. Note that these were transient signals that were absent from the record when the CTD was lowered back down through the same depths just 5-10 minutes later (2:20-2:30).

Plume chemistry (Jill McDermott, Gunter Wegener)

At Karasik Seamount, there were no hydrothermal signals identified in 6 casts, and both CH_4 and hydrogen concentrations were always below 3 nM. Both values can be considered as deep seawater concentrations (CTD 009, 044, 055, 088, 097, 112). Three casts over the Gakkel Ridge did not intercept any discernable plume and likewise contained <3 nM background CH_4 (131/11, 137/13 and 138/14). Gakkel Ridge hydrothermal plume waters at 2500 to 2950m were identified by turbidity, Eh, and temperature anomalies in six CTD casts on which CH_4 abundance was also determined (133/12, 139/15, 159/17, 177/22, 188/24 and 226/29).

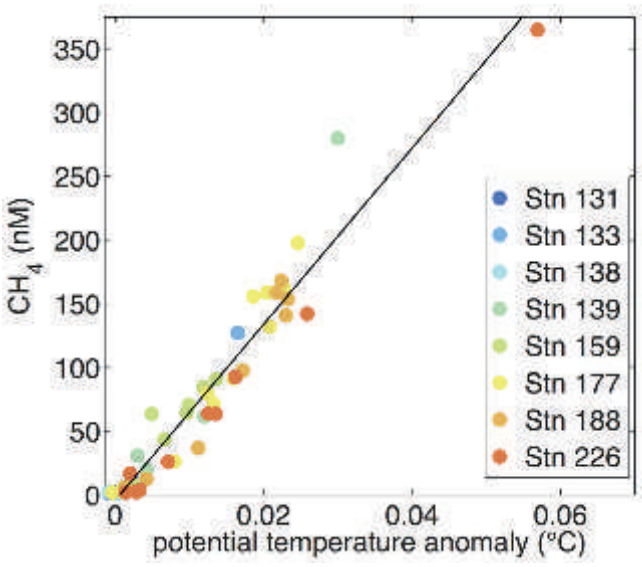

Fig. 6.5: Methane concentrations vs. observed temperature anomaly in the plume. For position of the individual casts see Fig. 6.1.

Gakkel ridge CTD Cast 226/29 intercepted the strongest plume containing the highest fraction of source hydrothermal fluid, at 2950 m depth. This sample was characterized by pronounced Eh and potential temperature anomalies that were devoid of high turbidity. It is most physically and geochemically similar to the lower magnitude signal intercepted at 2646m depth in CTD 139/15, while other plume signals had comparatively lower Eh and temperature anomalies, and higher turbidity.

This sample contained nearly equivalent dissolved CH_4 (365 nM) and H_2 (360 nM), resulting in a low [CH_4] to [H_2] ratio. In plumes with weaker Eh signals and higher turbidity, CH_4 contents tended to be higher relative to H_2. All successful casts collected CH_4-rich water within plume depths, relative to the <1nM CH_4 abundance in ambient seawater. However, many samples contained far less H_2 than CH_4, which is reflected in higher [CH_4] to [H_2] ratios and potentially indicates faster H_2 oxidation rates. A positive relationship is observed between dissolved CH_4 abundance and potential temperature anomaly (Fig. 6.5), indicating that all plume waters likely derive from the same high temperature source.

$\delta^{13}CH_4$ isotopes (Kevin Hand, Jill McDermott)

Results of the on-board gas chromatography and $\delta^{13}CH_4$ isotopic analyses with the Picarro method of Gakkel Ridge plume water indicate high concentrations (>200 nM, Fig. 6.6) of methane directly over the northern slope, which OFOS identified to be populated with many small chimneys, and orange, white, and black talus. Commensurate with those high methane concentrations are $\delta^{13}C_{CH4}$ values of -11‰ to -12‰, possibly indicating a low-temperature ultramafic plume source comparable to Lost City or Von Damm. Regions sampled around the top and periphery of the Vent Mount indicate $\delta^{13}C_{CH4}$ values of -7‰ to -9‰, which may result from preferential microbial consumption of lighter methane.

Water collected from the region measured to have the largest *in situ* Eh change (during 139/15) was found to have a methane concentration of 285.3 nM and a $\delta^{13}C_{CH4}$ of -11.8‰. Three separate water samples from the same Niskin bottle (#20, depth 2,646 m) were analyzed to generate this average. The measured values for the three samples were 233, 235, and 300 nM for methane concentration, and -11.9, -11.5, and -12‰ for $\delta^{13}C_{CH4}$. Two other regions within the water column were found to have high methane concentrations, although the Eh signal there was either weak or non-existent. Niskin bottle #8, from a depth of 2,530 m, was measured to have 70 nM methane with $\delta^{13}C_{CH4}$ of -6.49‰. Two separate samples were analyzed from bottle #8. Niskin bottle #18 was measured to have 18 nM methane, with an isotopic signature of -6.63 ‰. Tab. 6.2 provides measurements made for each bottle during Station 139/15 and serves as a representative example of preliminary results from each CTD cast analyzed. Fig. 6.6 provides a 3-D perspective view of the preliminary results for methane concentration and isotopic measurements from the Picarro method at all of the above listed CTD casts, except 226/29. The size of the circle scales with methane concentration and the color scales from white (heavy methane) to black (light background methane). The green diamond on the terrain map indicates the region with small chimneys and discolored slope terrain, as observed by OFOS believed to be within ±100-200m of the hydrothermal plume source.

Tab. 6.2: Preliminary analyses of the $\delta^{13}C_{CH4}$ isotopic excursions in the plume seawater of Gakkel Ridge. Data are from the September 25th, 2016 PS101/139/15 CTD cast.

Bottle	Depth below surface [m]	Methane concentration [nM]	$d^{13}CH_4$ [‰]
23	1000	1.0	NA
21	2000	1.4	NA
12	2300	0.8	NA
8	2530	70	-6.49
20	2646	285	-11.8
18	2700	18	-6.63
2	3050	2.3	-38.0

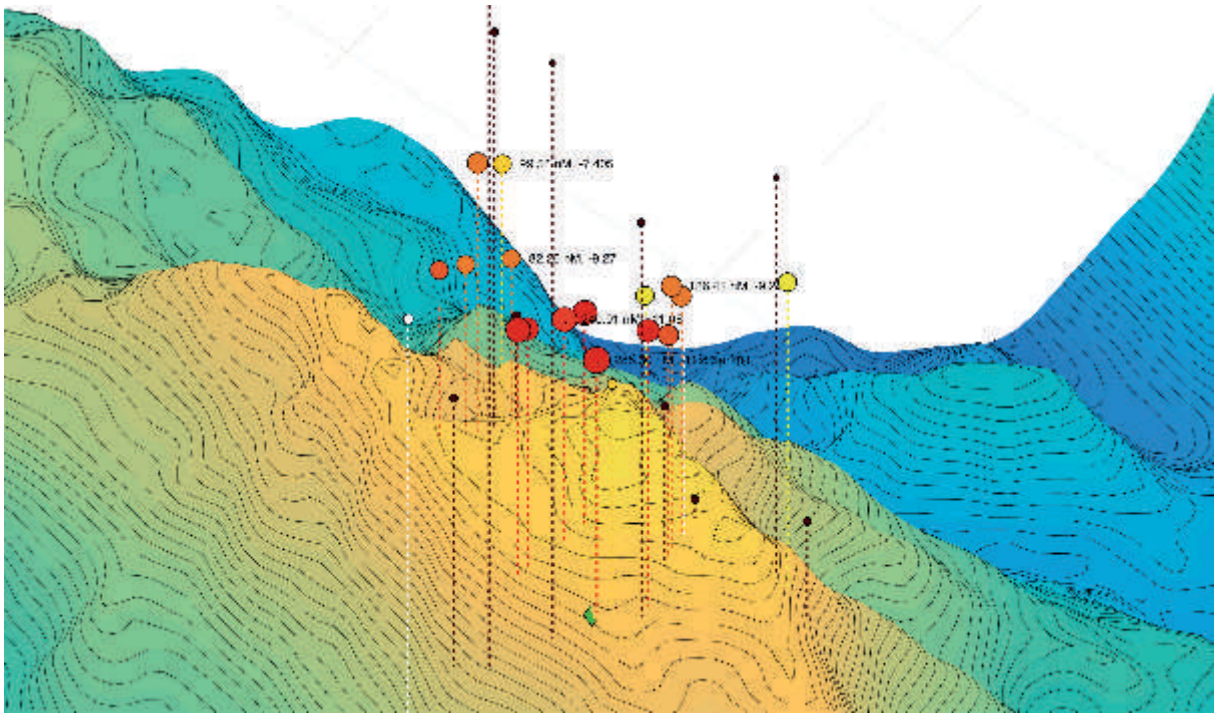

Fig. 6.6: Mapping of methane concentration and $\delta^{13}C_{CH4}$ isotopic analyses of CTD water collected in and around the Gakkel Ridge plume site at 87°N, 56° E

Microbial activity (Gunter Wegener, Massimo Molinari)

For later analyses about 300 polycarbonate filters of particles > 0.2 µm have been prepared for phylogenetic fluorescence-specific in quantitative community analysis. Within the plumes we will count total cells and specific phylogenetic groups. The microbial biomass collected in the Sterivex filters will be used to assess microbial community compositions based on massive parallel tag sequencing of amplified archaeal and bacterial 16S rRNA genes. To reduce amplification transcriptomic and metagenomic work will be preferentially performed on material retrieved by *in-situ* filtration.

Outside of detected hydrothermal plumes, dissolved methane concentrations in the deep water column around the Vent Mount were only slightly elevated compared to marine background concentrations (≤ 2 nM). By contrast, the buoyant plume sample associated with distinct temperature anomalies of up to 0.3 K exhibited methane concentrations of 300 nM. In the same sample hydrogen concentrations reached similar or even slightly higher values (up to 360 nM). Two different trends can be observed with increasing distance from the plume center. Closest to the vent-source, samples showed relatively stable ratios between methane and hydrogen of approximately 1:1. Other samples including many from stations 159 and 189 showed a larger variety in methane/hydrogen ratios consistent with a significant loss of hydrogen in the periphery, which we propose results from preferential microbial consumption of hydrogen in these samples (Fig. 6.7a).

The substrate turnover experiments conducted at sea were designed to follow microbial consumption of methane and hydrogen. Two opposing patterns were observed: In samples from the outer (older) plume environmental or artificially resupplied hydrogen is oxidized whereas in the buoyant plume samples neither consumption of methane nor hydrogen was detected (Fig. 6.7b-d). These data indicate that the buoyant plume does not host significant number

of hydrogen oxidation microorganisms, but, instead, that those strains must be incorporated into the plume further downstream, as it disperses. In parallel carbon fixation rates of up to 30 nMol C L^{-1} d^{-1} were measured in plume-height samples, compared to background water in which carbon fixation rates were close to the detection limit (1 mMol C L^{-1} d^{-1}). This indicates an important, at least local, role for hydrothermal fluids in providing an energy source for deep-sea microorganisms and their predators. The upcoming microbial community analysis of the different samples will aim to identify the microbial taxa that directly benefit from the vent derived energy sources.

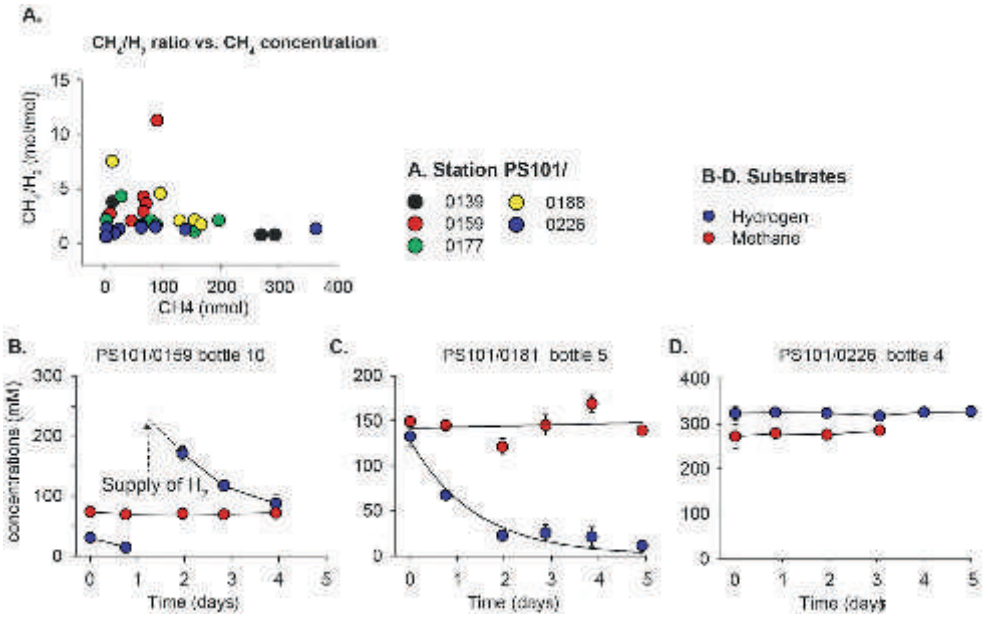

Fig. 6.7: Methane and hydrogen in the hydrothermal plume and in time course experiments. a) Ratios of methane and hydrogen as function of the methane concentration. The 1:1 stoichiometry observed at high concentrations likely reflects the ratio at the source. b)-d) Development of hydrogen concentrations in plume waters incubated at in situ temperature. Plume samples taken further away from the source (b-c) show rapid consumption of the original hydrogen or artificially supplied substrate, whereas samples from the buoyant plume do neither consume methane nor hydrogen.

Hydrography Langseth Ridge (Maren Walter, Janna Köhler)

The high abundance of biomass on top of the Langseth Ridge raised the question of the food source for such a rich ecosystem. We collected data to characterize the physical environment of the seamount chain and to study the flow field atop the seamounts, with the aim to identify possible seamount specific circulation patterns that might help to retain plankton and larvae in the water column above the seamount. The summits of the seamounts reach into a depth that lies in the gradient between the relatively warm and salty layer of Atlantic Water and the European Basin Deep Water below, and is therefore characterized by a relatively high amount of small scale spatial variability (Fig. 6.8). The current profiles collected above the ridge showed no preferred direction of the flow, but generally weak velocities (< 0.1 m/s), that were occassionally bottom intensified. A large scale survey along and across the ridge with the ships' ADCP showed also very weak velocities in the upper 200 m (50 bins, the instruments range) with typical magnitudes of only a few centimeter per second, and no large scale structure. Since the magnitude of the observed flow is in the same order of magnitude

as the instrument error, it is at this stage of data processing not possible to infer a circulation pattern and to refute or confirm the theory that the abundance of biomass is fueled by a seamount specific circulation. However, the vertical distribution of the amount of scatterers visible in the received signal of the acoustic current measurements (Fig. 6.9) clearly shows that the majority of the planktonic biomass is concentrated in the Atlantic layer, which is also high in oxygen (Fig. 6.8). Therefore the food source for the ecosystem may well be advected towards the seamount chain from upstream within the Atlantic inflow.

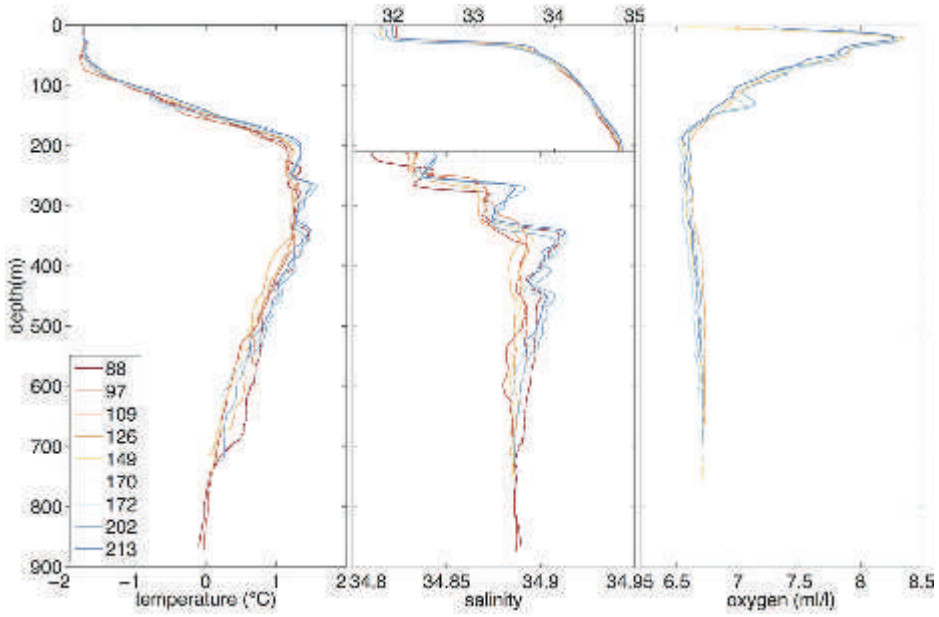

Fig. 6.8: Profiles of temperature, salinity and oxygen (both uncalibrated) from stations at the Langseth Ridge, including Karasik Seamount, Central Mound Saddle, Northern and Central Mount. The signature of North Atlantic water can clearly be seen between approximately 200 m and 500 m. Note the change of scale for salinity at 200 m depth.

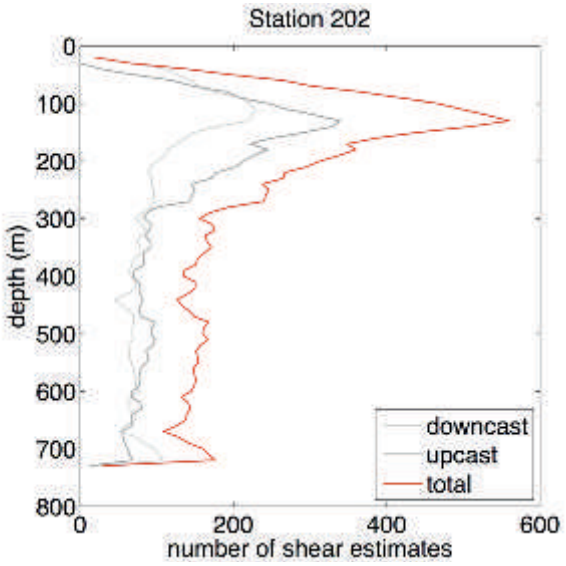

Fig. 6.9: Number of shear estimates per depth cell measured by the LADCP during Station PS101/0202-1. The abundance of scatterers in the Atlantic Water atop the seamount with a peak at ~150m depth is clearly visible.

Data management

CTD data was made available for all cruise participants on board and data uploaded to PANGAEA on return to shore. The trace-gas data will be made public on the PANGAEA database as soon as available (approx. one year after the cruise), carefully quality controlled, and published in a peer-reviewed journal. Genomic data will be published via INSDC, the international public database collaboration (DDBJ, EMBL-EBI and NCBI).

ADCP data from the continuous VM-ADCP current profiler is available from PANGAEA: https://doi.pangaea.de/10.1594/PANGAEA.867799

References

Baker ET, Milburn H (1997) MAPR: a new instrument for hydrothermal plume mapping. Ridge Events 8(1), 23–25.

Baker ET, Edmonds HN, Michael PJ, Bach W, Dick HJB, Snow JE, Walker SL, Banerjee NR, Langmuir CH (2004) Hydrothermal venting in a magma desert: The ultraslow-spreading Gakkel and Southwest Indian Ridges. Geochem. Geophys. Geosys. 5(8) Q08002.

Edmonds HN, Michael PJ, Baker ET, et al. (2003) Discovery of abundant hydrothermal venting on the ultraslow-spreading Gakkel ridge in the Arctic Ocean. Nature 421, 252–256.

German CR, Thurnherr AM, Knoery J, Charlou JL, Jean-Baptiste P, Edmonds HN (2010) Heat, Volume and Chemical Fluxes from Submarine Venting: A Synthesis of Results from the Rainbow Hydrothermal Field, 36°N MAR. Deep-Sea Res. I 57, 518–527.

Herndl GJ, Reinthaler T, Teira E, van Aken H, Veth C, Pernthaler A, Pernthaler J (2005) Contribution of Archaea to total prokaryotic production in the deep Atlantic Ocean. Appl. Environ. Microbiol., 71 2303-2309.

Sültenfuß J, Rhein M, Roether W (2009) The Bremen mass spectrometric facility for the measurement of helium isotopes, neon, and tritium in water. Isotopes Environ. Health Stud. 45(2), 1–13.

7. PLANKTON OF KARASIK SEAMOUNT

Nicole Hildebrandt[1], Mirta Jacobs[1], Ksenia Kosobokova[2], Anique Stecher[1], Bernd Christiansen[3] , not on board: Barbara Niehoff[1], Eva-Maria M Nöthig[1]

[1]AWI
[2]IORAS
[3]UHH

Grant No. AWI_PS101_01

Objectives

Since the 1990s, ecological investigations of phyto- and zooplankton have been carried out in the central Arctic Ocean with *Polarstern* in order to document basic characteristics of plankton ecosystems, relate them to environmental parameters and processes and understand how they are influenced by ongoing and projected climate change. These studies demonstrated that species composition, community structure and distribution patterns of zooplankton in the Arctic Ocean are strongly affected at regional and even basin scales by water circulation patterns, bottom topography, ice conditions and primary productivity (Hirche & Mumm, 1992; Mumm, 1993; Kosobokova & Hirche, 2000, 2009).

Since 1995 zooplankton sampling was carried out throughout the water column at most visited locations, including the deepest samplings in the Arctic deep basins at bottom depths of >3,000 and even >4,000 m. The aim of these studies was to document the poorly known and unique deep-water fauna of the Arctic Ocean to better understand its origin, distribution and role in pelagic trophodynamics. The studies carried out in the vicinity of underwater ridges, and the Lomonosov Ridge in particular, indicated that the ridge areas are characterized by peculiar fauna and enriched plankton life (Kosobokova & Hirche, 2000, 2009; Kosobokova, 2012). However, the knowledge on diversity and productivity of pelagic organisms and the effects of underwater ridges and mountains on zooplankton distribution is very limited. In particular, the information on plankton communities associated with the Arctic underwater seamounts and hydrothermal vents is completely missing.

The main research questions to be answered during this mission regarding zooplankton were therefore:

1. **Elucidate patterns:** To relate composition, abundance and biomass of zooplankton to the bathymetry and water circulation pattern in the Karasik seamount and the Gakkel Ridge vent area to better understand the role of underwater seamounts in shaping the regional variability of zooplankton distribution in the Arctic Ocean.

2. **Investigate pre-winter physiological state of populations of key species:** to assess lipid content, dry mass and ion concentrations in the dominant species.

3. **Genetics:** Collection of material for building the DNA sequence library needed to assess zooplankton community structure using molecular approaches.

4. **Zooplankton fauna photo-documentation:** To continue photographic inventory of all zooplankton taxa throughout the entire water column to contribute to global catalogues of marine life and the catalogue of Arctic pelagic fauna, in particular.

Fig. 7.1: The Multinet Maxi with the attached side net. Picture: Frederick Tardeck (FIELAX)

The main focus of **phytoplankton sampling** was on *Melosira arctica*, a filamentous sea ice diatom populating the sub-ice habitat of the Arctic Ocean. It was proposed that this diatom is responsible for a large amount of the sub-sea ice productivity and plays a significant role for the carbon export to the deep sea in ice-covered Arctic basins (Boetius et al., 2013). Thus, genetic analyses were planned to complement our understanding of the ability of this diatom to cope with changing conditions in the light of climate change.

Work at sea

For the investigation of large-scale distribution and species composition, zooplankton were collected by a multiple closing net (Type MAXI, 0.5 m^2 mouth opening, Hydrobios, Kiel; Fig. 7.1). The multinet (MN) was equipped with nine nets (150 µm mesh size) and provided stratified sampling of the entire water column from the bottom to the surface.

Sampling was carried out in three regions: at one station in the deep Nansen Basin, five stations in the area of underwater seamounts of Langseth Ridge, and four stations in the Gakkel Ridge vent area. In total, the multinet was deployed at 10 stations (Tab. 7.1, Fig. 7.2).

In the Langseth Ridge area, we carried out deep casts up the western and southern flanks of Karasik seamount (1,250 and 1,650 m depth, respectively) and shallow ones in the vicinity of the tops of the three mounts (Karasik, Central and Northern Mount).

Our sampling protocol followed standard procedures as applied during previous *Polarstern* Arctic cruises (1993-2015). At the deepest stations of the vent area (>2,000 m) the following sampling intervals were taken: bottom-4,000-3,000-2,000-1,000-500-300(-200)-100-50(-25)-0 m. In the shallower regions in vicinity of underwater seamounts the sampling intervals in the upper 500 m were as follows: 500-400-300-200-100-50-25-0 m, while below 500 m they depended on the bottom depth (Tab. 7.1).

Tab. 7.1: Station list of Multinet and LOKI/Aquascat casts

Station	Date	Time UTC (start profile)	Gear	Net #	Depth interval [m]	Mesh size [µm]
PS101/0059-1	15.09.2016	11:21	LOKI/Aquascat		1000-0	150
PS101/0060-1	15.09.2016	14:00	Side net		3860-0	200
PS101/0060-1	15.09.2016	14:00	Multinet Maxi	MN1	3860-3000	150
PS101/0060-1	15.09.2016	14:30	Multinet Maxi	MN2	3000-2000	150
PS101/0060-1	15.09.2016	15:06	Multinet Maxi	MN3	2000-1000	150
PS101/0060-1	15.09.2016	15:43	Multinet Maxi	MN4	1000-500	150
PS101/0060-1	15.09.2016	16:01	Multinet Maxi	MN5	500-300	150
PS101/0060-1	15.09.2016	16:08	Multinet Maxi	MN6	300-200	150
PS101/0060-1	15.09.2016	16:13	Multinet Maxi	MN7	200-100	150
PS101/0060-1	15.09.2016	16:17	Multinet Maxi	MN8	100-50	150
PS101/0060-1	15.09.2016	16:19	Multinet Maxi	MN9	50-0	150
PS101/0067-1	16.09.2016	12:40	LOKI/Aquascat		1000-0	150
PS101/0090-1	18.09.2016	16:55	LOKI/Aquascat		640-0	150
PS101/0091-1	18.09.2016	18:08	Side net		660-0	200
PS101/0091-1	18.09.2016	18:08	Multinet Maxi	MN1	660-600	150
PS101/0091-1	18.09.2016	18:11	Multinet Maxi	MN2	600-500	150
PS101/0091-1	18.09.2016	18:15	Multinet Maxi	MN3	500-400	150
PS101/0091-1	18.09.2016	18:19	Multinet Maxi	MN4	400-300	150
PS101/0091-1	18.09.2016	18:23	Multinet Maxi	MN5	300-200	150
PS101/0091-1	18.09.2016	18:27	Multinet Maxi	MN6	200-100	150
PS101/0091-1	18.09.2016	18:31	Multinet Maxi	MN7	100-50	150
PS101/0091-1	18.09.2016	18:33	Multinet Maxi	MN8	50-0	150
PS101/0099-1	19.09.2016	11:33	Side net		850-0	200
PS101/0099-1	19.09.2016	11:33	Multinet Maxi	MN1	850-750	150
PS101/0099-1	19.09.2016	11:37	Multinet Maxi	MN2	750-500	150
PS101/0099-1	19.09.2016	11:46	Multinet Maxi	MN3	500-400	150
PS101/0099-1	19.09.2016	11:50	Multinet Maxi	MN4	400-300	150
PS101/0099-1	19.09.2016	11:54	Multinet Maxi	MN5	300-200	150
PS101/0099-1	19.09.2016	11:58	Multinet Maxi	MN6	200-100	150
PS101/0099-1	19.09.2016	12:02	Multinet Maxi	MN7	100-50	150
PS101/0099-1	19.09.2016	12:05	Multinet Maxi	MN8	50-25	150
PS101/0099-1	19.09.2016	12:06	Multinet Maxi	MN9	25-0	150
PS101/0108-1	20.09.2016	08:55	Side net		1250-0	200
PS101/0108-1	20.09.2016	08:55	Multinet Maxi	MN1	1250-1000	150
PS101/0108-1	20.09.2016	09:04	Multinet Maxi	MN2	1000-750	150
PS101/0108-1	20.09.2016	09:14	Multinet Maxi	MN3	750-500	150
PS101/0108-1	20.09.2016	09:23	Multinet Maxi	MN4	500-300	150
PS101/0108-1	20.09.2016	09:30	Multinet Maxi	MN5	300-200	150
PS101/0108-1	20.09.2016	09:34	Multinet Maxi	MN6	200-100	150

Station	Date	Time UTC (start profile)	Gear	Net #	Depth interval [m]	Mesh size [µm]
PS101/0108-1	20.09.2016	09:38	Multinet Maxi	MN7	100-50	150
PS101/0108-1	20.09.2016	09:40	Multinet Maxi	MN8	50-25	150
PS101/0108-1	20.09.2016	09:41	Multinet Maxi	MN9	25-0	150
PS101/0116-1	21.09.2016	11:34	LOKI/Aquascat		1000-0	150
PS101/0117-1	21.09.2016	14:36	Side net		4830-0	200
PS101/0117-1	21.09.2016	14:36	Multinet Maxi	MN1	4830-4000	150
PS101/0117-1	21.09.2016	15:07	Multinet Maxi	MN2	4000-3000	150
PS101/0117-1	21.09.2016	15:44	Multinet Maxi	MN3	3000-2000	150
PS101/0117-1	21.09.2016	16:24	Multinet Maxi	MN4	2000-1000	150
PS101/0117-1	21.09.2016	17:01	Multinet Maxi	MN5	1000-500	150
PS101/0117-1	21.09.2016	17:18	Multinet Maxi	MN6	500-200	150
PS101/0117-1	21.09.2016	17:30	Multinet Maxi	MN7	200-100	150
PS101/0117-1	21.09.2016	17:34	Multinet Maxi	MN8	100-50	150
PS101/0117-1	21.09.2016	17:36	Multinet Maxi	MN9	50-0	150
PS101/0136-1	25.09.2016	00:05	LOKI/Aquascat		1000-0	150
PS101/0141-1	25.09.2016	22:51	Side net		3450-0	200
PS101/0141-1	25.09.2016	22:51	Multinet Maxi	MN1	3450-2500	150
PS101/0141-1	25.09.2016	23:25	Multinet Maxi	MN2	2500-2000	150
PS101/0141-1	25.09.2016	23:43	Multinet Maxi	MN3	2000-1000	150
PS101/0141-1	26.09.2016	00:19	Multinet Maxi	MN4	1000-500	150
PS101/0141-1	26.09.2016	00:39	Multinet Maxi	MN5	500-300	150
PS101/0141-1	26.09.2016	00:47	Multinet Maxi	MN6	300-200	150
PS101/0141-1	26.09.2016	00:50	Multinet Maxi	MN7	200-100	150
PS101/0141-1	26.09.2016	00:54	Multinet Maxi	MN8	100-50	150
PS101/0141-1	26.09.2016	00:57	Multinet Maxi	MN9	50-0	150
PS101/0164-1	29.09.2016	09:30	LOKI/Aquascat		1000-0	150
PS101/0165-1	29.09.2016	12:21	Side net		3950-0	200
PS101/0165-1	29.09.2016	12:21	Multinet Maxi	MN1	3950-2800	150
PS101/0165-1	29.09.2016	13:02	Multinet Maxi	MN2	2800-2500	150
PS101/0165-1	29.09.2016	13:13	Multinet Maxi	MN3	2500-2000	150
PS101/0165-1	29.09.2016	13:31	Multinet Maxi	MN4	2000-1000	150
PS101/0165-1	29.09.2016	14:08	Multinet Maxi	MN5	1000-500	150
PS101/0165-1	29.09.2016	14:27	Multinet Maxi	MN6	500-200	150
PS101/0165-1	29.09.2016	14:39	Multinet Maxi	MN7	200-100	150
PS101/0165-1	29.09.2016	14:43	Multinet Maxi	MN8	100-50	150
PS101/0165-1	29.09.2016	14:45	Multinet Maxi	MN9	50-0	150
PS101/0173-1	01.10.2016	11:32	LOKI/Aquascat		1000-0	150
PS101/0182-1	03.10.2016	23:27	LOKI/Aquascat		1000-0	150
PS101/0183-1	04.10.2016	02:31	Side net		4400-0	200
PS101/0183-1	04.10.2016	02:31	Multinet Maxi	MN1	4400-2800	150

Station	Date	Time UTC (start profile)	Gear	Net #	Depth interval [m]	Mesh size [µm]
PS101/0183-1	04.10.2016	03:33	Multinet Maxi	MN2	2800-2500	150
PS101/0183-1	04.10.2016	03:44	Multinet Maxi	MN3	2500-2000	150
PS101/0183-1	04.10.2016	04:03	Multinet Maxi	MN4	2000-1000	150
PS101/0183-1	04.10.2016	04:41	Multinet Maxi	MN5	1000-500	150
PS101/0183-1	04.10.2016	05:00	Multinet Maxi	MN6	500-200	150
PS101/0183-1	04.10.2016	05:12	Multinet Maxi	MN7	200-100	150
PS101/0183-1	04.10.2016	05:16	Multinet Maxi	MN8	100-50	150
PS101/0183-1	04.10.2016	05:18	Multinet Maxi	MN9	50-0	150
PS101/0201-1	06.10.2016	22:46	Side net		725-0	300
PS101/0201-1	06.10.2016	22:46	Multinet Maxi	MN1	725-600	150
PS101/0201-1	06.10.2016	ND	Multinet Maxi	MN2	600-500	150
PS101/0201-1	06.10.2016	22:55	Multinet Maxi	MN3	500-400	150
PS101/0201-1	06.10.2016	22:58	Multinet Maxi	MN4	400-300	150
PS101/0201-1	06.10.2016	23:03	Multinet Maxi	MN5	300-200	150
PS101/0201-1	06.10.2016	ND	Multinet Maxi	MN6	200-100	150
PS101/0201-1	06.10.2016	23:11	Multinet Maxi	MN7	100-50	150
PS101/0201-1	06.10.2016	23:13	Multinet Maxi	MN8	50-25	150
PS101/0201-1	06.10.2016	23:14	Multinet Maxi	MN9	25-0	150
PS101/0214-1	07.10.2016	20:40	LOKI/Aquascat		951-0	150
PS101/0215-1	08.10.2016	01:02	Side net		1650-0	300
PS101/0215-1	08.10.2016	01:02	Multinet Maxi	MN1	1650-1000	150
PS101/0215-1	08.10.2016	01:25	Multinet Maxi	MN2	1000-500	150
PS101/0215-1	08.10.2016	01:44	Multinet Maxi	MN3	500-400	150
PS101/0215-1	08.10.2016	01:48	Multinet Maxi	MN4	400-300	150
PS101/0215-1	08.10.2016	01:52	Multinet Maxi	MN5	300-200	150
PS101/0215-1	08.10.2016	01:57	Multinet Maxi	MN6	200-100	150
PS101/0215-1	08.10.2016	02:01	Multinet Maxi	MN7	100-50	150
PS101/0215-1	08.10.2016	02:03	Multinet Maxi	MN8	50-25	150
PS101/0215-1	08.10.2016	02:05	Multinet Maxi	MN9	25-0	150
PS101/0223-1	09.10.2016	02:55	LOKI/Aquascat		1000-0	150

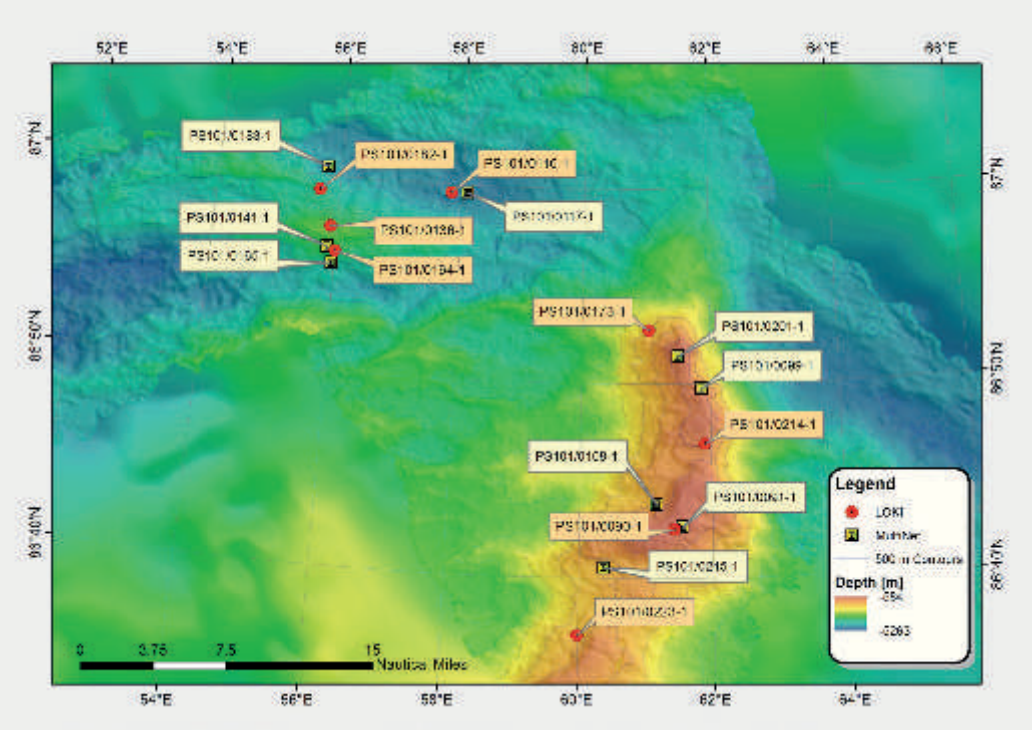

Fig. 7.2: Station map of Multinet and LOKI/Aquascat casts

The zooplankton samples were preserved in 4% formaldehyde buffered with hexamethylen-tetramine and will later be processed at the home laboratories.

In addition to the MN samples, optical (LOKI) and acoustical methods (Aquascat) were used to investigate the small-scale distribution of zooplankton species in the upper 1000 m of the water column at 10 stations (Tab. 7.1, Fig. 7.2). The LOKI system (Lightframe On-sight Key species Investigation; Fig. 7.3) was equipped with a high-resolution digital camera as well as sensors for measuring temperature, salinity, depth, oxygen and fluorescence, thus allowing us to relate zooplankton distribution patterns directly to the hydrography. The Aquascat system was mounted to the upper part of the LOKI frame (Fig. 7.3), facing sideward, and recorded the acoustic backscatter at 0.5, 1, 2 and 4 MHz. By combining all approaches (MN, LOKI and Aquascat), we will be able to analyze the zooplankton distribution patterns at the Langseth Ridge seamounts as well as in the Gakkel Ridge vent areas. In addition, comparing these data with data gathered during previous cruises will help us to analyze and better understand changes in the zooplankton communities under changing environmental conditions.

To test the hypothesis that the dominant Arctic herbivorous *Calanus* spp. (Copepoda) which undergo diapause during winter alter their extracellular cation concentration to regulate buoyancy at depth, individuals of *Calanus hyperboreus* and *C. glacialis* from different depth layers were sorted from the multinet samples. Then, hemolymph was extracted and stored at -20 °C for later analyses of ion contents at the home laboratory. For comparison with non-diapausing copepods, samples were also taken from the omnivorous copepod species *Metridia longa* and *Scaphocalanus magnus,* as well as the carnivorous species *Gaetanus brevispinus* and *Paraeuchaeta glacialis*.

Live animals for molecular genetics and stable C and N isotope analyses were collected by a 60 cm diameter live net (200 or 300 µm mesh-size) attached to the outside of the multinet (Fig. 7.1). Representatives of target species to be used for molecular genetic analyses were removed from live samples, photographed alive under a stereomicroscope using a digital

stereomicroscope camera and preserved in 96% ethanol. These samples were stored at 0 °C for later determination of COI sequences in target species plus some additional mitochondrial or nuclear target regions. For the two copepod species, *Calanus glacialis* and *C. finmarchicus,* and the chaetognath *Pseudosagitta maxima* samples were prepared to explore population genetics at a high spatial resolution.

To assess the amount of lipids stored for overwintering by the key herbivorous Arctic copepods *Calanus hyperboreus* and *C. glacialis*, photos of individual live animals were taken under a stereomicroscope, prosome length of each individual was measured, and animals were frozen in pre-weighted tin cups at -20°C for further extraction of total lipids and/or dry weight assessment.

Animals for stable C and N isotope analyses were also sorted out from live samples and stored at -20 °C for later analyses.

The remainders of non-quantitative catches collected by a live net in the regions with high abundance of sponges on the seafloor were frozen at -20°C for bulk stable C and N isotope analyses aimed at understanding the pelagic food source for these benthic inhabitants. The remaining non-quantitative catches were frozen at -20°C for further analysis of the Hg content of the Arctic zooplankton at IORAS.

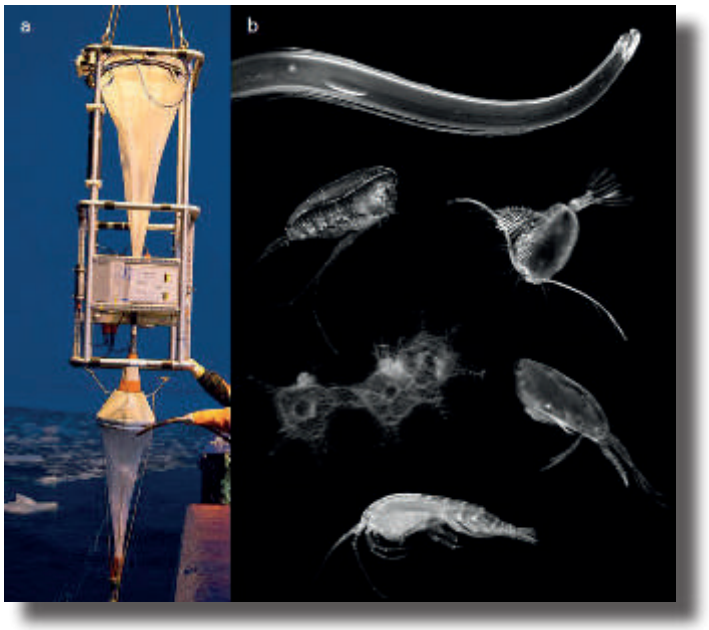

Fig. 7.3: (a) The LOKI/Aquascat system. (b) Zooplankton pictures taken with the LOKI, in clockwise direction: the chaetognath Eukrohnia hamata, the calanoid copepods Gaetanus sp. and Scaphocalanus magnus, the amphipod Apherusa glacialis, radiolarians and the calanoid copepod Calanus hyperboreus. Pictures: Marcel Nicolaus/Nicole Hildebrandt (AWI).

Phytoplankton

Unfortunately, it was not possible to sample algal mats at all. At the beginning of the cruise, some mats were seen, but it was not possible to collect them. Additional attempts to sample mats directly from under the ice flow by an under ice robot (ROV, 15.09.2016, PS101/0057, Fig. 7.4) were unsuccessful. At the end of the cruise, only remnants of *Melosira arctica* were left which also were not possible to sample (Fig. 7.5)

Fig. 7.4: Camera view of the ROV Beast diving under the ice at station PS101/0057-1. Algal mats were tried so sample by a custom made sampling device ("slime slurp gun"). Picture: AWI Meereisphysik.

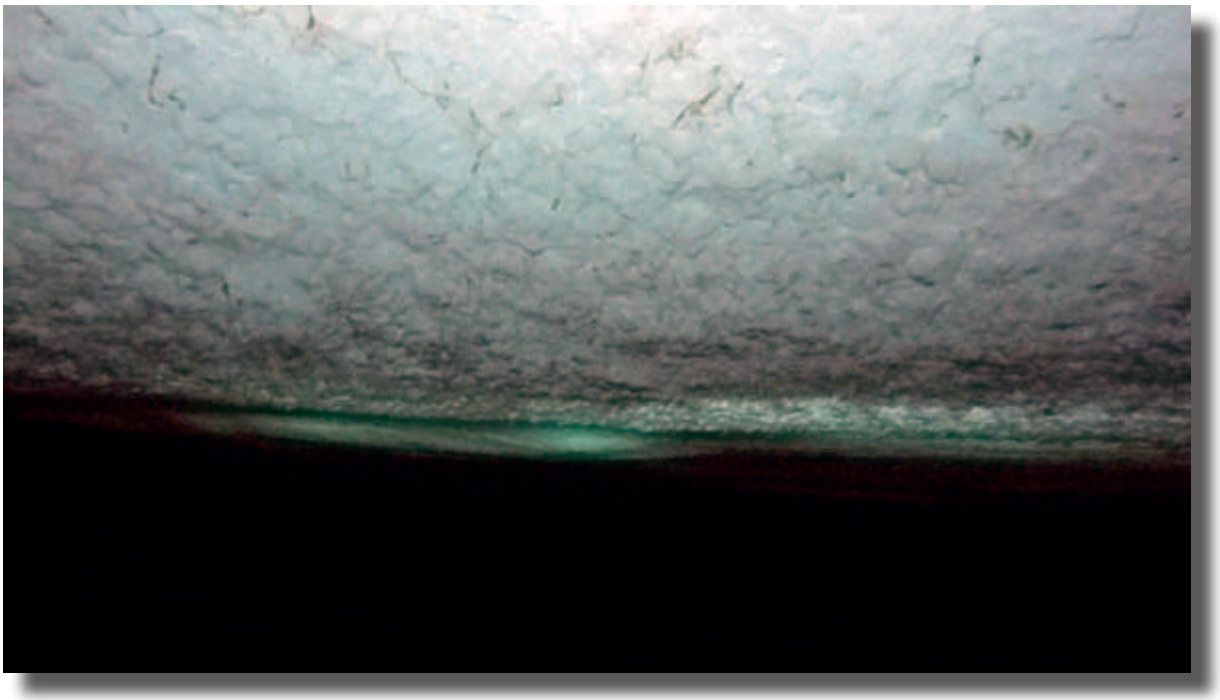

Fig. 7.5: Under ice view of an ice floe at station PS101/0162-1. Only remnants of former Melosira arctica mats are still attached to the ice. Picture: Kevin Hand (NASA JPL).

Preliminary (expected) results

Zooplankton

LOKI pictures revealed that the mesozooplankton community in the upper 1000 m of the water column was clearly dominated by copepods (Calanoida and Cyclopoida). The larvaceans *Oikopleura* spp. were also abundant at many locations. Chaetognaths, ostracods, hydrozoan medusa and amphipods occurred regularly, but in relatively low numbers. The MN data confirmed these observations.

The cruise took place at the end of the primary productive season, which gave us an opportunity to investigate the pre-winter distribution patterns of the zooplankton community and physiological state of populations of key players in the Arctic pelagic ecosystem - predominantly herbivorous filter-feeders, i.e. the copepods *Calanus hyperboreus* and *C. glacialis*. The preliminary results based on express examination of live MN catches showed that populations of these copepods consisted almost exceptionally of late copepodite stages CIV-CVI. From the stage composition of the population, vertical distribution and reduced swimming activity of *Calanus hyperboreus*, we can conclude that this species was entering its overwintering state. The *C. hyperboreus* females were not feeding and were currently descending to depths between 200 and 1000 m where they will hibernate till next spring. In contrast, the *Calanus glacialis* population was still concentrated in the upper water layers, and some adult females were feeding on available particles producing fecal pellets. The Atlantic expatriate species *C. finmarchicus,* advected into this region with the Atlantic inflow (Kosobokova, 2012; Bluhm et al., 2015; Wassmann et al., 2015), was found in low numbers and was represented exceptionally by late copepodites CV and adult females.

The preliminary examination of samples from deep-water locations showed that planktonic life at great depths between 2 and 4.8 km in the vent area is much richer in terms of biomass and specimens numbers than we have ever observed on earlier expeditions to the central Arctic (1995-2015). Further procession of MN material at home laboratories will allow us to relate the species composition, abundance, biomass and spatial distribution of zooplankton to specific local bathymetric conditions and water circulation patterns of the study area. This will help us to answer the questions whether the high abundance of zooplankton at great depths is a specific feature of the Gakkel Ridge vent area, an effect of advection of particles with the Atlantic inflow, or it is shaped by a peculiar water circulation pattern in the vicinity of the sea mounts. The comparison of data obtained during PS101 with historical data will then be also implemented for assessing changes in the Arctic pelagic biota related to degrading sea ice cover.

Our preliminary species inventory based on examination of live MN samples shows that the species composition of zooplankton in our study area was typical of the deep Arctic Basins with the communities clearly structured by depth (Kosobokova et al., 2011). We found more than 120 different zooplankton species that represent more than half of the known diversity for the deep Arctic basins.

The most striking result is a record of several mesozooplankton species that have not been found earlier in the Arctic Basins and are therefore not included in the most recent species inventories (Kosobokova et al., 2011; Kosobokova, 2012). Most of them were found at the deepest locations in the Gakkel vent area. This includes two species of pelagic Polychaeta, three species of Hydromedusae, and two species of Copepoda from Augaptilidae family. Specimens of all these species were sorted out from live MN and side net catches, imaged and preserved with 96% ethanol and 4% formaldehyde for further identification by experts at home laboratories. After a detailed examination of the formalin-preserved samples the list of new records may be extended.

In the non-quantitative zooplankton samples used for molecular genetics, a total of 97 planktonic metazoan species were identified and imaged to build a molecular library of Arctic biodiversity illustrated by the species images. This yield represents >50 % of the zooplankton species known from the Arctic basins, with only the rarest species still remaining unsampled.

For stable isotope analyses 15 species of most common herbivorous, omnivorous and carnivorous copepods (12 species), amphipods (2 species), and decapods (1 species) were collected to assess relative ratios of grazers versus omnivores and predators. These collections include 65 samples from 4 stations (1-14 replicates for each species).

Quantitative multinet samples as well as LOKI pictures will be analyzed for species abundance and depth distribution at IORAS and AWI. The molecular genetic samples collected for DNA barcoding will be analyzed in cooperation with IORAS at facilities of the White Sea Biological Station of the Moscow State University (WSBS MSU). Stable isotope samples will be analyzed at the AWI and MARUM, samples for analyses of Hg content will be analyzed at IORAS.

Phytoplankton

Melosira arctica seemed to already have sunken down to the seafloor as observed during an OFOS dive on this cruise (PS101/0068-1; Fig. 7.6) and on a previous *Polarstern* cruise PS78 (ARK-XXVII/3) (Boetius et al., 2013) due to the season and the accompanied sea ice melt.

Fig. 7.6: Picture of the seafloor at 3882.1 m depth, taken by the OFOS system (station PS101/0068-1). Red circles indicate Melosira arctica mats fallen down to the sea floor. Picture: PS101 AWI OFOS system.

Data management

We plan that the full data set will be available at latest three years after the cruise. Most of species samples and samples which will not be analysed immediately will be stored at the AWI at least for another 10 years and will be available for other colleagues. Data will be made available to the public via PANGAEA upon analysis completion.

References

Bluhm BA, Kosobokova KN, Carmack EC (2015) A tale of two basins: An integrated physical and biological perspective of the deep Arctic Ocean. Progress in Oceanography, 139, 89-121.

Boetius A, Albrecht S, Bakker K, Bienhold C, Felden J, Fernandez-Mendez M, Hendricks S, Katlein C, Lalande C, Krumpen T, Nicolaus M, Peeken I, Rabe B, Rogacheva A, Rybakova E, Somavilla R, Wenzhofer F, RV Polarstern ARK27-3-Shipboard Science Party (2013) Export of algal bio- mass from the melting Arctic sea ice. Science, 339, 1430-1432.

Hirche HJ, Mumm N (1992) Distribution of dominant copepods in the Nansen Basin, Arctic Ocean, in summer. Deep-Sea Research, 39, Suppl. 2, S485-S505.

Kosobokova KN (2012) Zooplankton of the Arctic Ocean: community structure, ecology, spatial distribution. MOSCOW: GEOS, 212 pp. (in Russian).

Kosobokova KN, Hirche H-J (2000) Zooplankton distribution across the Lomonosov Ridge, Arctic Ocean: species inventory, biomass and vertical structure. Deep-Sea Research I, 47, 2029-2060.

Kosobokova KN, Hirche H-J (2009) Biomass of zooplankton in the eastern Arctic Ocean - a base line study. Progress in Oceanography, 82, 265-280.

Kosobokova KN, Hopcroft RR, Hirche H-J (2011) Patterns of zooplankton diversity through the depths of the Arctic's central basins. Marine Biodiversity, 41, 29-50.

Mumm N (1993) Composition and distribution of mesozooplankton in the Nansen Basin, Arctic Ocean, during summer. Polar Biology, 13, 451-461.

Wassmann P, Carmack E, Kosobokova KN, Slagstad D, Drinkwater K, Hopcroft RR, Moore SE, Ellingsen I, Nelson RJ, Popova E, Berge J (2015) The contiguous domains of Arctic Ocean advection: Trails of life and death. Progress in Oceanography, 139, 42-65.

8. BENTHOS OF KARASIK SEAMOUNT

Kai Horst George[1], Antje Boetius[2,3,4], Jana Bäger[2], Jakob Barz[2], Jennifer Dannheim[2], Alexander Kieneke[1], Massimiliano Molari[3], Axel Nordhausen[3] Autun Purser[2], Linn Schmidtmann[2],Fabian Schramm[3], Beate Slaby[5], Tobias Vonnahme[3], Gunter Wegener[2,3], not on board: Ute Hentschel[5] , Hans Tore Rapp[6], Jutta Wollenburg[1]

[1]Senckenberg
[2]AWI
[3]MPI
[4]MARUM
[4]Senckenberg
[5]GEOMAR
[6]UiB

Grant No. AWI_PS101_01

8.1 Megabenthos

Objectives

The main objective of the study of megabenthos on and in the vicinity of the Karasik seamount was to (a) analyze the faunal distribution, diversity and production along depth gradients from seamount base to peak, (b) evaluate potential species endemism within the seamount fauna and (c) compare the fauna of chemosynthetic and non-chemosynthetic habitats around vent fields. Given a sufficiently successful cruise, the intention was to as thoroughly assess the faunal ecology of the Karasik Seamount and any surrounding active vent regions, and to place this analysis in context with research carried out both at other northerly active vent sites on the Mohns and Knipovich Ridges, such as Loki's Castle (Pedersen et al., 2010; Schander et al., 2010), as well as with communities observed at other spreading ridges elsewhere in the world ocean. Community compositions in several distinct reference locations were also investigated for comparison; the Nansen Basin and the upper region of a canyon running from the Yermak Plateau.

Work at sea

A selection of devices were used to identify and determine the distribution of the megabenthic communities across the surveyed areas (The Karasik Seamount, the central and northern mounts of the Langseth Ridge, the Vent Mount of the Gakkel Ridge Rift Valley and the reference stations). The Ocean Floor Observation System (OFOS) and TV-Multicorer (TV-MUC) systems were used to film the seafloor over distances of several meters to several kilometres. Detailed description of these devices, their specifications and the precise locations of their deployments is given in Chapter 3. Additionally, the NUI HROV was used to fly autonomously over a region of the Karasik Seamount, imaging swathes of seafloor from a height of ~2 m with high definition still cameras. The preliminary output of this HROV survey is described in Chapter 9.

By utilising the ROV functionality of the NUI vehicle, direct samples of key fauna from the Karasik seamount were taken, with these samples being stored on return to surface for detailed molecular and taxonomic study.

Following OFOS deployments, still images collected automatically every 20 seconds throughout each survey dive could be analysed using the PaparaZZi 2.0 software application (Marcon and

Purser, 2016). This software allows species or morphotype densities to be rapidly assessed for individual still images. By analysing numerous images from the various survey regions, some broad characterisation of community structures could be made whilst still at sea.

Data collected via the oblique cameras mounted on NUI for ROV deployments and on the TV-MUC were assessed qualitatively after each deployment, and all data recorded for more detailed analysis on shore.

The image data collected automatically via NUI in AUV mode will be compared with that collected by OFOS at a later date, and a comparison of the relative suitability of each research platform for spatial analysis of seamount megabenthic communities made.

Preliminary (expected) results

Initial analysis of the seafloor images collected by the OFOS, TV-MUC and NUI systems shows the various surveyed areas to each contain a range of subhabitats and communities, and in the case of the Langseth Ridge, perhaps surprisingly distinct communities of megafauna at the Karasik Seamount, the North Mount and Central Mount. Direct megafauna samples were collected via box corer and TV-MUC from a number of locations though the only live megafauna collected from within these were shrimp and sponges. A number of fauna samples were collected directly from the Karasik Seamount via NUI in ROV mode, using the grab manipulator and an array of sampling tools.

Megafauna of the Karasik Seamount

The Karasik seamount was the most southerly of those surveyed during PS101, with megafauna investigated by OFOS, TV-MUC, box corer, and NUI. A fairly gentle upper peak tops rather steep flanks to the east, south and west, whereas to the north the seamount drops ~500 meters to merge with the central saddle. The seafloor of the central peak area was observed to be ~90% covered by live bacterial sponges and infilling thick carpet of sponge needles (see Fig. 8.1.1).

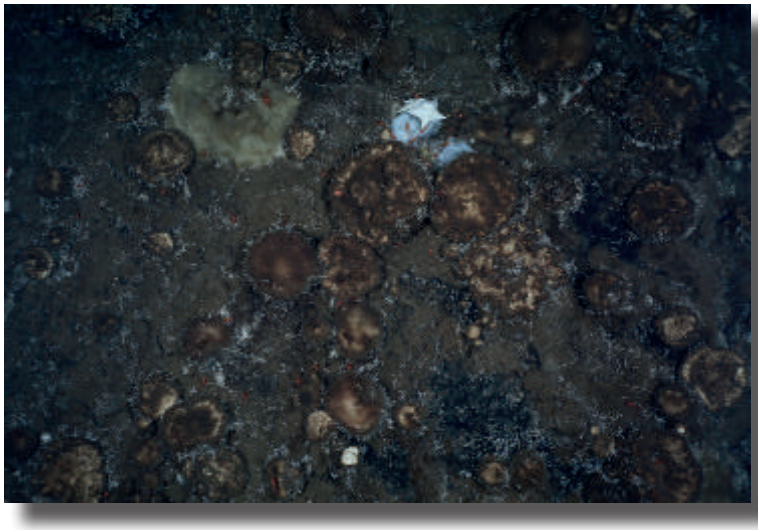

Fig. 8.1.1: Typical view of the central peak area of the Karasik Seamount. The brown circular objects are bacterial sponges, with the green/brown infilling material being made up of sponge spines. The black areas are predominantly dead polychaete casts, a strata of several centimetres thickness covering the majority of the central peak below the sponges. The starfish and shrimp toward the top of the image are feeding either on a dead sponge or the bacterial matt growing on the sponge. Photo: AWI OFOS-Launcher team.

Four key morphotypes of sponges were observed on the mount. The majority of these sponges were colonized by what appeared to be small bryzoan colonies and several species of tube-dwelling polychaetes. The remaining ~10% of surveyed seafloor was covered predominantly with black, dead polychaete casts. Occasional glass sponges of several distinct species were also observed growing directly on bacterial sponges. Starfish, isopods, several species of shrimps were reasonably abundant at densities of >1 ind. m^{-2}. At much lower density were what

Fig. 8.1.2: Light pink/orange 'octocoral' collected by NUI in ROV mode., photographed with microscopic camera in the laboratory. Polyp diameter is several mm. Photo: Autun Purser.

appeared to be occasional octocoral colonies (soft- and gorgonians), also observed growing on sponges.

There was the opportunity to collect direct samples of megafauna from Karasik Seamount using the NUI ROV. In Fig. 8.1.2 the sample collected in Fig. 9.8d (*cf*. Chapter 9) can be seen. From this image, and following consultation with an onshore expert (Santiago Herrera, Lehigh University, USA) we are tentatively identifying the sample as an 'octocoral'. In addition to this unexpected sample, sponges (both alive and dying with bacterial coverage) and starfish were also taken (see Chapter 9). These samples will be taken to AWI and Senckenberg for analysis.

Megafauna of the Central Saddle

The Central Saddle consists of a north-south ridge feature which separates the Karasik Seamount from the Central Mount. OFOS dive PS101_169 collected video and still images of the megafauna on the flanks of these two seamounts, and across the 1,000 m deep Central Saddle.

The north and south flanks of the saddle were found to consist of several steep vertical rock-faced steps, populated by tubeworms and on plateaus within the vertical steps, the familiar colonies of astrophoroid sponges and associates described in the Karasik Seamount section above. The seafloor across the saddle itself was however distinct. Here, the thick layer of sponges and needles, with infilling mix of dead polychaetes and needles was replaced by a lower density of sponges and sponge spicules (< 50 %), intermixed with sand, occasional rocky outcrops and small stones (Fig. 8.1.3). Fish and shrimps were abundant across the saddle, and anemones more numerous that on the Karasik Seamount.

Fig. 8.1.3: Compact sponge community within the central section of the Central Saddle. There is a much thinner layer of polychaete tubes evident at the seafloor. Sand is directly visible below the intermittent layer of sponge spicules (also called spicule mats), as are occasional broken rocks. Photo: AWI OFOS-Launcher team.

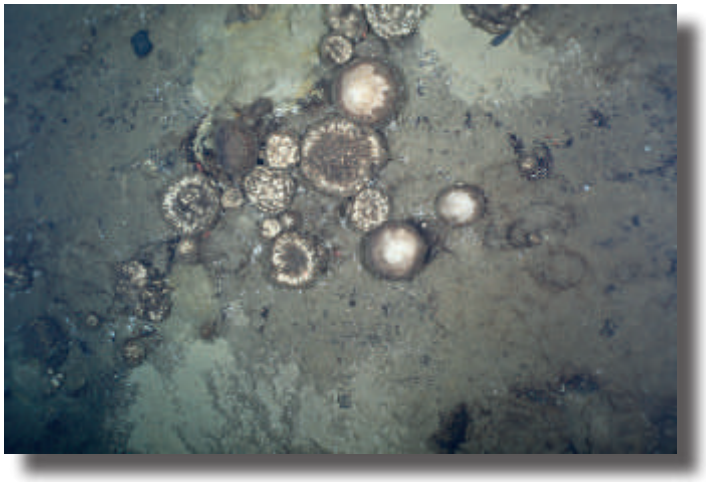

Megafauna of the Central Mount

The Central Mount exhibited a generally similar mix of megabenthic species to the Karasik Seamount, but with a much lower density of live sponges (<20% coverage). Spicule mats mixed with dead polychaete tubes are quite abundant and again the underlying layer obscures any underlying rock or sediment strata across much of the surveyed area of the mount. Anemones appear to be more abundant at the Central Mount than at the Karasik Seamount, as are starfish. The starfish were commonly observed feeding on the dead remains or bacterial growth upon the dying/dead sponges (see Fig. 8.1.4).

Megafauna of the Northern Mount

The Northern Mount of the Langseth Ridge is the most exposed, running north into the Gakkel Ridge. As with the other mounts on the Langseth Ridge, the flanks are steep and populated by occasional stalked and unstalked glass sponges, polychaete tubes and astrophoroid sponges only on the occasional small plateaus amongst the steeply jointed rock.

The upper megafaunal communities of the mount, towards the summit, are at first sight quite reminiscent of those observed at the Karasik Seamount, with a near total coverage of the underlying rock/sediment by sponges, spicules and dead polychaete tubes.

On closer examination many of the sponges can be observed to have been partially colonised by soft corals and/or small gorgonians (see Fig. 8.1.2 and 8.1.5). Although these fauna elements were observed in extremely low density at the Karasik Seamount, they were present on every sponge adult in some regions of the Northern Mount. Higher abundances of small glass sponges were also observed on the Northern Mount, and also, on top of the spicule mat, what appeared to be small <5 cm sized colonies of what may be stylasterid corals or erect bryozoans were also observed in great abundance (some present in Fig. 8.1.6). High resolution images of the various ‘corals’ will be forwarded to appropriate experts for better identification on return to shore.

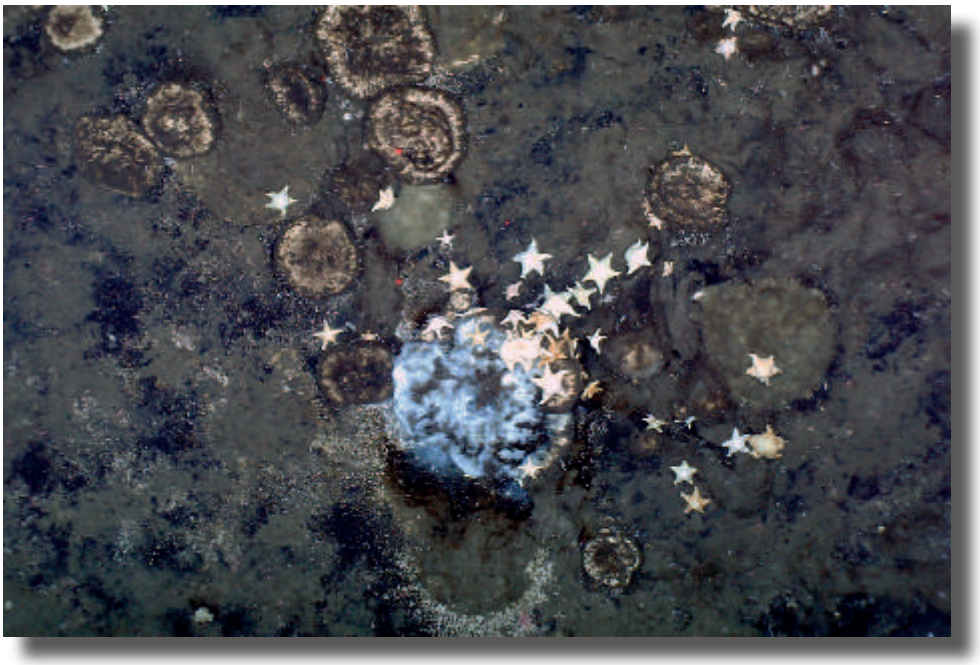

Fig. 8.1.4: Bacterial mat covering dead/dying sponge. Numerous starfish have been attracted to the sponge and are likely actively feeding upon it or on the bacterial growth directly. Photo: AWI OFOS-Launcher team.

Megafauna of the Vent Mount

The Vent Mount within the Gakkel Ridge was observed to support a range of different megabenthic communities. Much of the mount was made up of pillow basalts of varying degrees of freshness. These supported at low densities individual and occasionally clustered anemones, individual glass sponges and some fish and jellyfish.

The northwest region of the Vent Mount, below the hydrothermal plume measured in the water column (*cf*. Chapter 6), supported various distinct communities. The composition of these communities seemed to be at least partially determined by distance from the small, active vents observed during dives, and the makeup of the seafloor.

Amongst the small vents, areas of several to tens of sq. m. are covered by broken precipitate rocks. These areas, which also exhibit shimmering water, support communities of Kolga sp. holothurians, brittlestars, bacterial mats, polychaetes and fish (see Fig. 8.1.6.). An interesting observation was that many dead fish remains were also visible in these areas, but not anywhere else on Vent Mount.

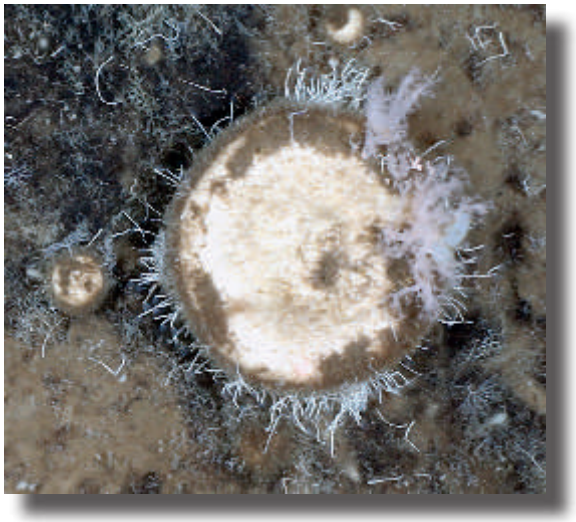

Fig. 8.1.5: Soft coral and small octocorals colonizing the flanks of a astrophorid sponge. Small branched colonial animals can be seen arounf the image, potentially stylasterid corals or erect bryozoans. Photo: AWI OFOS-Launcher team.

The vents themselves only supported occasional amphipods, again Kolga sp. Individuals and at least two species of mobile polychaete, as well as bacterial mats.

Surrounding the region of precipitate rocks, a megafaunal community of stalked crinoids, anemones and ophiuroids extended some 10 m over soft sediment covered basaltic pillows.

Megafauna of the Nansen Basin

An initial test dive within the Nansen Basin (PS101_68) imaged a flat, fine sediment covered area of seafloor with a scattered distribution of Melosira arctica ice algae, dead on the seafloor (Fig. 8.1.7). Megafauna consisted of occasional anemones (densities of <0.01 ind. m^{-2}), small occasional fish and very few holothurians.

Megafauna of the Vermak Plateau canyon

OFOS dive PS101_241 surveyed the upper canyon and lip of the Vermak Plateau, ~70km north of Svalbard. The dive covered a depth range of ~500 m to 170 m depth; throughout the dive abundances of sponge and coral megafauna were high. Glass, encrusting and demosponges were all abundant (Fig. 8.1.8). Soft corals, octocorals and stylasterid corals of many species were also present. Several regions of surveyed seafloor were covered in egg aggregates. Fish and shrimp megafauna were also present throughout the dive transect. Tunicates, hydroids, bryozoans, bivalves, polychaetes, hermit crabs, anemones, starfish, ophiuroids and many other distinct fauna categories were also present in the surveyed area. On return to shore the collected images will be forwarded to appropriate experts for a more detailed analysis of the species present.

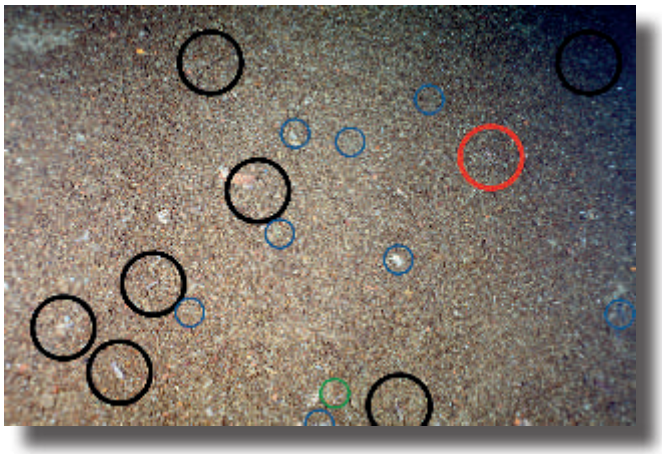

Fig. 8.1.6: Typical region in close vicinity to small vents. A broken substrate of precipitate rock fragments supports Kolga sp. holothurians (black circles), bacterial mats (blue circles), ophiuroids (red circle) and polychaete tubes (green circle). Photo: AWI OFOS-Launcher team.

Fig.8.1.7: Typical image taken of the Nansen Basin seafloor during OFOS dive PS101_68. Occasional anemones are the predominant megafauna. Occasional strands of dead Melosira arctica algae are scattered across the seafloor, and there are clear signs of surface reworking by fauna. Photo: AWI OFOS-Launcher team.

Fig.8.1.8: Typical image from OFOS dive PS101_241. Numerous encrusting sponge species, stylasterid corals, hydroids and anemones have colonised all pebbles, boulders and hardground outcrops of the edge of the Vermak plateau. Photo: AWI OFOS-Launcher team.

Data management

All still image and video data of megabenthos collected with the OFOS camera system or the TV-MUC will be made available on return to shore via the scientific data warehouse PANGAEA. All still image and video data collected with the NUI HROV will be made available online via the WHOI website following return to shore.

References

Marcon Y, Purser A (2016) PAPARA(ZZ)I: an open-source software interface for annotating deep-sea imagery data. doi:10.1594/PANGAEA.855568.

8.2 Macrobenthos

Objectives

The macrozoobenthos, particularly in deep waters, is a good ecological indicator for environmental changes and habitat description, as communities are generally relatively stationary and long-lived and reflect changes in environmental conditions in the oceans (e.g., organic flux to the seabed) at integrated scales (Gage and Tyler, 1991; Piepenburg, 2005). However, the benthos of central Arctic basins is poorly studied compared to other deep-sea areas (Bluhm et al., 2011). The few existing studies have provided evidence of strong gradients in faunal abundance, biomass and production from slopes to basins (Cusson and Bourget, 2005; Bluhm et al., 2011), caused by low surface-water production, small flux of particulate organic matter to the seafloor and, hence, general food limitation of the benthos (Wassmann et al., 2010; Degen et al., 2015). Seamounts should therefore reflect the same gradient on rather local scales being generally remote islands of diversity and production (e.g., Henrich et al., 1992) within the Arctic deep-sea plains. Vent ecosystems are typically dominated by benthic invertebrates that host symbiotic, chemoautotrophic microorganisms (van Dover, 2014). Therefore, benthic production and biomass is very high at vents, while species richness is comparably low. However, nothing is known about the benthos of the vent fields in the area and nearly nothing is known about the benthos of Arctic seamounts.

Our objectives were to (a) analyze the macrofaunal distribution, diversity and production along a depth gradient from seamount base to top, (b) evaluate potential species endemism within the seamount fauna and (c) compare the fauna of chemosynthetic and non-chemosynthetic habitats around vent fields. The expected findings will serve as a base to characterize and potentially map different habitats of macrozoobenthos at the seamount.

Work at sea

At the Langseth Ridge and in the adjacent sea areas (Fig. 8.2.1) we were able to take 21 samples (26 deployments, of which five failed due to uneven seafloor, Tab. 8.2.1) at seven target areas. All mounts of the Langseth Ridge, i.e. the Karasik seamount (mean depth: 660 m), the Central Mount (822 m) and the Northern Mount (693 m) were sampled. The mounts were compared to deeper areas in the Karasik surrounding, i.e. the Karasik Central Mount saddle (1,055 m), Southern (1583 m) and Western slope (3,563 m), as well as to the area of the Nansen basin (3,863 m). Macrozoobenthic samples were obtained by USNEL box corer (0.25 m²) which was equipped with a POSIDONIA transponder for geo-referencing. Box corer is a preferred sampling gear, as it provides reliably deep and relatively undisturbed sediment samples adequate for macrofauna sampling (Gage & Bett, 2005). The unique samples allow for comparisons of macrozoobenthos between the different mounts of the Langseth Ridge and along depth gradients from the top to deeper adjacent areas.

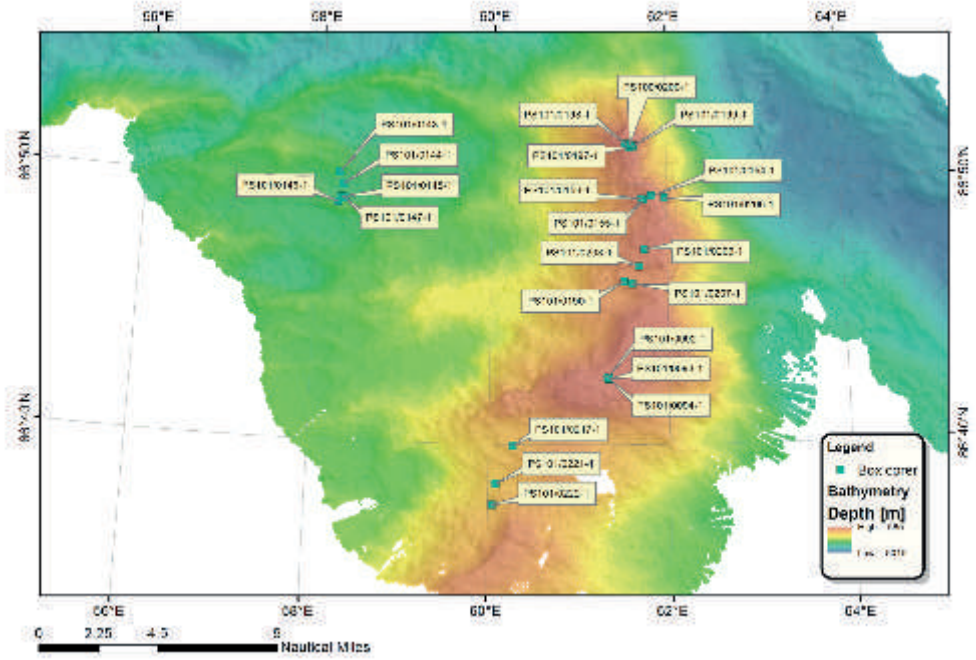

Fig. 8.2.1: Bathymetric map of the Langseth Ridge of the expedition PS101 with deployment positions of box corers. The 'Nansen Basin (mooring 1)' area is not shown on this map.

Unfortunately, we were unable to obtain box-core samples from the vent area. There were only small areas within this predominantly hard-bottom habitat of sediments, areas too small to hit blindly, as the PS101 box core was not equipped with camera guidance.

For further processing, box-corer samples were divided into four equal subsamples of which two were taken for quantitative taxonomic and community analysis, one for qualitative analyses for later DNA analysis and one for sediment analysis (Tab. 8.2.1). The upper 12 cm of each subsample sediment and the supernatant seawater to catch epibenthic animals from the fluffy layer on top of the sediment, were taken for further sample processing. Quantitative and qualitative samples were sifted over a 500 µm mesh size sieve. Quantitative macrofaunal samples in the sieve residues were preserved in 10 % buffered formalin.

Tab. 8.2.1: Station, depth (m), target area and number of macrozoobenthic samples collected for qualitative-community, species-DNA and sediment analysis during PS101 at the Langseth Ridge (LR), the Karasik Western and Southern Slope, as well as the Nansen Basin.

Station	Depth [m]	Target area	Macrozoobenthic samples	DNA	Sediment	Total
PS101/0064-1	3848	Nansen Basin (mooring 1)	2	1	2	5
PS101/0065-1	3903	Nansen Basin (mooring 1)	2	1	2	5
PS101/0066-1	3837	Nansen Basin (mooring 1)	2	1	2	5
PS101/0092-1	663	Karasik Seamount	2	1	2	5
PS101/0093-1	622	Karasik Seamount	2	1	2	5
PS101/0094-1	700	Karasik Seamount	2	1	2	5
PS101/0143-1	3481	Karasik Western Slope	Failed			

Station	Depth [m]	Target area	Macrozoobenthic samples	DNA	Sediment	Total
PS101/0144-1	3628	Karasik Western Slope	2	1	2	5
PS101/0145-1	3601	Karasik Western Slope	2	1	2	5
PS101/0146-1	3394	Karasik Western Slope	Failed			
PS101/0147-1	3587	Karasik Western Slope	2	1	2	5
PS101/0154-1	795	LR Central Mount	2	1	2	5
PS101/0155-1	796	LR Central Mount	2	1	2	5
PS101/0156-1	683	LR Central Mount	Failed			
PS101/0190-1	1156	Karasik Central Mount Saddle	2	1	2	5
PS101/0197-1	648	LR Northern Mount	2	1	2	5
PS101/0198-1	679	LR Northern Mount	2	1	2	5
PS101/0199-1	760	LR Northern Mount	Failed			
PS101/0200-1	684	LR Northern Mount	2	1	2	5
PS101/0206-1	1012	LR Central Mount	2	1	2	5
PS101/0207-1	1055	Karasik Central Mount Saddle	2	1	2	5
PS101/0208-1	1122	Karasik Central Mount Saddle	Failed			
PS101/0209-1	890	Karasik Central Mount Saddle	2	0	2	5
PS101/0217-1	1686	Karasik Southern Slope	2	1	2	5
PS101/0221-1	1868	Karasik Southern Slope	2	1	2	5
PS101/0222-1	1195	Karasik Southern Slope	2	1	2	5
sum: 21 box corer			42	20	42	104

At the laboratory at AWI species will be determined to the lowest possible taxonomic level, counted and wet mass will be determined per species. Qualitative samples were stored in cooled sea water (0 °C) and sorted alive on board. Animals picked from these samples were fixed in 95 % ethanol for future taxonomic and DNA-studies in the AWI laboratory. Two surface sediment samples were derived from each station with 8 and 5 cm^3 PVC cores. Samples were stored at -20°C until further analysis on (a) median grain size and sorting coefficient and (b) on carbon, nitrogen and organic carbon content. In total, benthic sampling with the box corer yielded 104 samples, i.e. 42 samples for quantitative community and sediment analysis as well as 20 samples for future genetic analysis (Tab. 8.2.1).

Preliminary (expected) results

Sediment inspections of all box-core samples provide already first hints on differences between habitats. The Karasik mount, the Central and the Northern Mount of Langseth Ridge were dominated by sponge communities/grounds (*Geodia* spp. and *Stelletta* spp.). All sediment surfaces were covered with a dense spicule mat (Fig. 8.2.2, rows B, D and E) up to 5-15 cm depth.

The spicule mats consist mainly of sponge spicules but also of polychaete tubes and dead bryozoans. Underneath the spicule mats we found homogenous clayish fine sediment. Some

sponges had a size of up to one meter and thus form a major part of the biomass in this sponge-dominated community. Besides the sponges, live sorting of the mount samples on board revealed several taxonomic groups that are associated with this sponge community: Amphipoda, Tanaidacea, Gastropoda, Polychaeta and Bryozoa. Most of the macrozoobenthic organisms found seem to be filter feeders, i.e. they filter food particles from the water column. However, it is still unclear where the nutrients come from to maintain such a high concentration of macrozoobenthic biomass.

The Karasik Central Mount Saddle (Fig. 8.2.3, row A) displays a transition community between the sponge communities on the mounts and the deeper areas sampled. Some of the saddle samples resembled the mount communities with sponges (PS101/0208-1) and a thin layer of spicule mats (PS101/0209-1) while the first station in this area (PS101/0190-1) resembled deeper stations (see below).

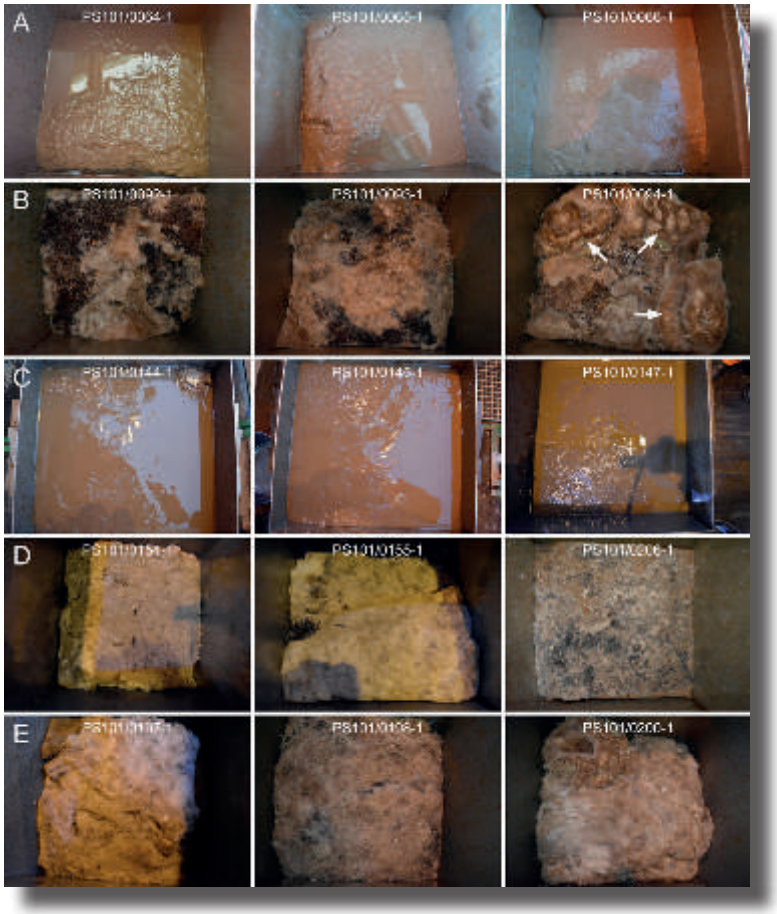

Fig. 8.2.2: Surface images of the box corer samples of Polarstern expedition PS101 after removal of the supernatant seawater. Size of the box is 50 x 50 cm. Note the three sponge individuals in box PS101/0094-1 (arrows). Row A: Nansen Basin (mooring 1), row B: Karasik Seamount, row C: Karasik Western Slope, row D: Langseth Ridge Central Mount, row E: Langseth Ridge Northern Mount.

The sediments of the deeper target areas of Karasik Western (Fig. 8.2.2, row C), and Southern Slope (Fig. 8.2.3, row B) as well as the Nansen Basin area (Fig. 8.2.2, row A) were characterized by homogenous clayish fine sediment which was strongly compacted. At the Karasik Southern Slope the clay was mixed with pebbles and cobbles and probably lower diversity and abundances of macrobenthic species.

The sampled target areas show large sediment differences and thus we also expect differences in the macrofaunal community between the mount samples and the deep sea reference areas: the slopes, the saddle of the Langseth Ridge and the Nansen Basin. We are confident that we can characterize macrofaunal distribution, diversity and production by the unique samples taken and potentially map different habitats on the seamount and the surrounding deeper areas. Further, we will be able to evaluate potential species endemism within the seamount fauna and expect to find new species which will be described taxonomically and genetically by the samples we took during the *Polarstern* expedition PS101.

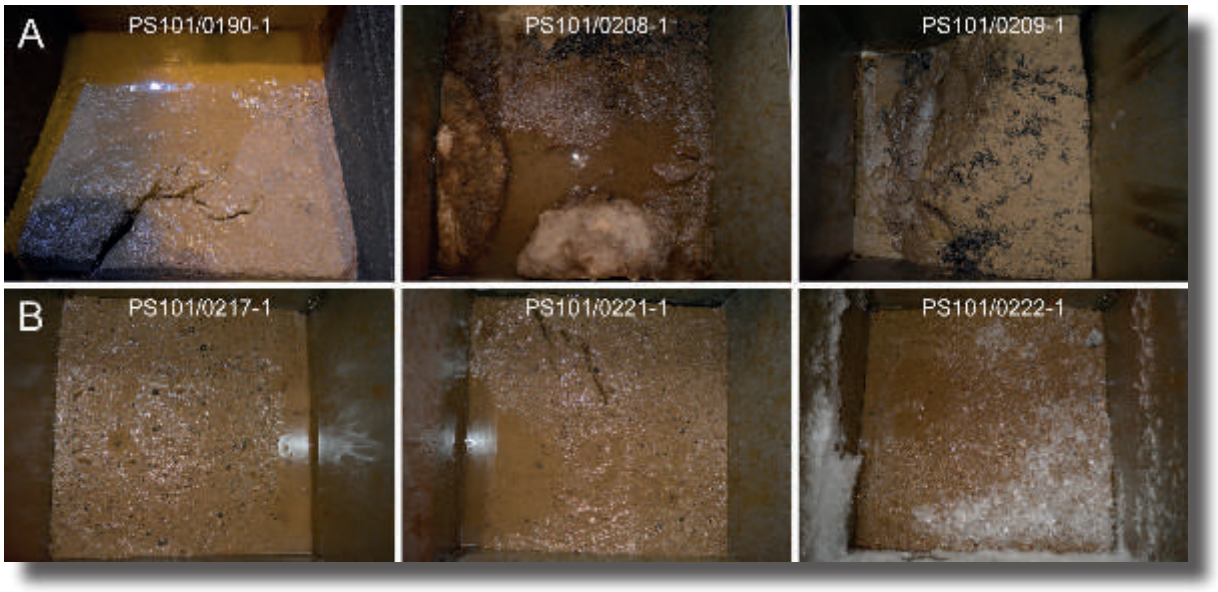

Fig. 8.2.3: Surface images of the box corer samples of Polarstern expedition PS101 after removal of the supernatant seawater. Size of the box is 50 x 50 cm. Row A: Karasik - Central Mount Saddle, row B: Karasik Southern Slope.

Data management

All data will be obtained through laboratory analyses after the cruise. Processed data will be deposited in the Arctic Benthos-Database at AWI and be publically available via PANGAEA and the Pan-Arctic Inventory, currently being built by Piepenburg et al. (*cf*. Piepenburg et al. 2011).

References

Bluhm BA, Ambrose WG Jr, Bergmann M, Clough LM, Gebruk AV, Hasemann C, Iken K, Klages M, MacDonald IR, Renaud PE, Schewe I, Soltwedel T, Włodarska-Kowalczuk M (2011) Diversity of the Arctic deep-sea benthos. Marine Biodiversity, 41, 87-107.

Cusson M, Bourget E (2005) Global patterns of macroinvertebrate production in marine benthic habitats. Marine Ecology Progress Series, 297, 1–14.

Degen R, Vedenin A, Gusky M, Boetius A, Brey T (2015) Patterns and trends of macrobenthic abundance, biomass and production in the deep Arctic Ocean, Polar Research 34.

Gage JD, Tyler PA (1991) Deep-sea biology: a natural history of organisms at the deep-sea floor. London: Cambridge University Press.

Gage JD, Bett BJ (2005) Deep-Sea Benthic Sampling. In Eleftheriou and McIntyre (eds.), Methods for the Study of Marine Benthos, Pp. 273–325. Oxford: Blackwell Science.

Henrich R, Hartmann M, Reitner J, Schäfer P, Freiwald A, Steinmetz S, Dietrich P, Thiede J (1992) Facies belts and communities of the arctic Vesterisbanken Seamount (Central Greenland Sea), Facies, 27, 71-103.

Pedersen RB, Rapp HT, Thorseth IH, Lilley M, Barriga F, Baumberger T, Flesland K, Fonseca R, Früh-Green GL, Jørgensen SL (2010) Discovery of a black smoker field and a novel vent fauna at the ultraslow spreading Arctic Mid-Ocean Ridges. Nature Communications. DOI:10.1038/ncomms1124.

Piepenburg D (2005) Recent research on Arctic benthos: common notions need to be revised, Polar Biology, 28, 733-755.

Piepenburg D, Archambault P, Ambrose W Jr, Blanchard A, Bluhm B, Carroll M, Conlan K, Cusson M, Feder H, Grebmeier J, Jewett S, Lévesque M, Petryashev V, Sejr M, Sirenko B, Włodarska-Kowalczuk M (2011) Towards a pan-Arctic inventory of the species diversity of the macro- and megabenthic fauna of the Arctic shelf seas. Marine Biodiversity, 41, 51-70.

Schander C, Rapp HT, Kongsrud JA, Bakken T, Berge J, Cochrane S, Oug E, Byrkjedal I, Cedhagen T, Fosshagen A, Gebruk A, Larsen K, Nygren A, Obst M, Plejel F, Stöhr S, Todt C, Warén A, Handler-Jacobsen S, Kuening R, Levin L, Mikkelsen NT,Petersen KK,ThorsethI, Pedersen RB (2010) The fauna of the hydrothermal vents on the Mohn Ridge (North Atlantic). Marine Biology Research 6(2): 155-171

Van Dover CL (2014) Impacts of anthropogenic disturbances at deep-sea hydrothermal vent ecosystems: A review. Marine Environmental Research, 102, 59-72.

Wassmann P, Slagstad D, Ellingsen I (2010) Primary production and climatic variability in the European sector of the Arctic Ocean prior to 2007: preliminary results. Polar Biology, 33, 1641-1650.

8.3 Meiobenthos

Objectives

The Senckenberg am Meer Meiofauna Group aimed to investigate the meiofaunal communities at both the summits of the Langseth Ridge and the surrounding deep sea seafloor, focusing primarily on three meiobenthic major groups: Copepoda, Gastrotricha, and Tardigrada. The analyses aimed to cover taxonomic, faunistic and biogeographical aspects. Main topics being the comparison of the meiobenthic seamount communities with (i) associations of other Atlantic seamounts (George, 2013), (ii) with the vent fauna of Atlantic and Pacific hydrothermal fields (Gollner et al., 2011), and (iii) with anchialine cave fauna (Huys, 1996, George and Martínez Arbizu, 2005). A major aim regarding the biogeography of the meiofauna from oceanic seamounts was to clarify the role of such geological submerged structures for the dispersal of these microscopic organisms (George, 2013). Seamounts can be regarded as isolated, submerged “islands” that may foster the formation of endemic meiofauna species. Alternatively, they could serve as “stepping stones” for the trans-oceanic dispersal of these microscopic animals that mostly lack free swimming larvae (Gad and Schminke, 2004).

Work at sea

For sampling the meiobenthic communities of the Langseth Ridge (Fig. 8.3.1) and adjacent sites of the Arctic Basin, we have solely used the camera-guided multiple corer (TV-MUC) deployed from the *Polarstern* using a fibre optics wire (LWL). The TV-MUC was additionally equipped with a POSIDONIA transponder for geo-referencing.

The obtained cores were directly processed on board of *Polarstern*. For subsequent extraction of the whole meiofauna community at our home laboratory, the upper 5 cm of each sediment core was cut, filled into 750 ml Kautex® bottles and fixed with borax-buffered formaldehyde solution (final concentration between 4 and 8 %) or preserved with DESS, a solution of dimethyl sulfoxide, disodium EDTA, and saturated NaCl. DESS was invented for simultaneous preservation of genomic DNA and for a good conservation of the morphology of nematodes (Yoder et al., 2006). However, for several years DESS has been successfully used at our institute for preserving other meiobenthic organisms such as harpacticoid copepods. The DESS supernatant was poured over a 40 µm sieve in order to retain every meiofauna specimen and the samples bottle was filled with fresh DESS within 24 h after fixation.

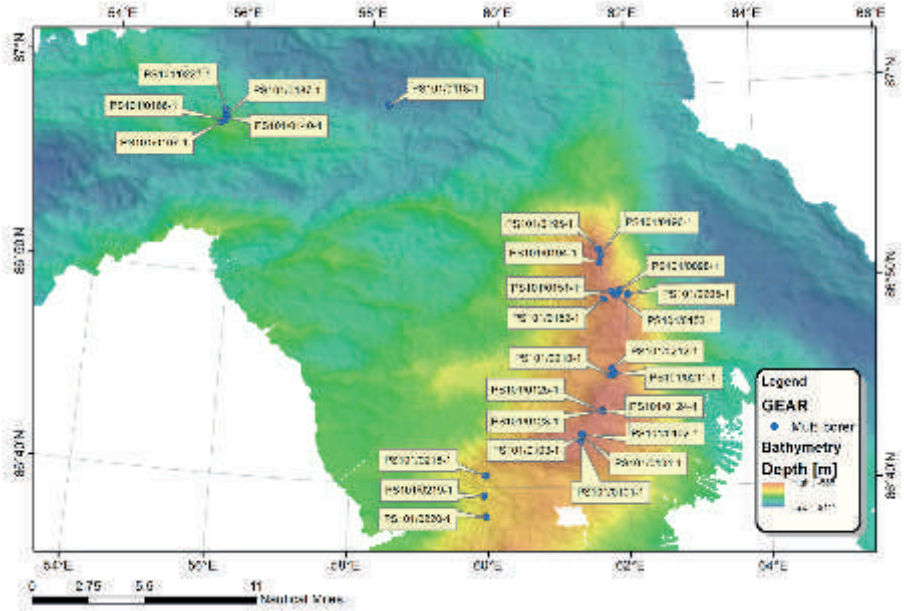

Fig. 8.3.1: Bathymetric map of the main working area of the expedition PS101 with the positions of deployments of the camera-guided multiple corer (TV-MUC). The target areas 'Nansen Basin (mooring 1)' and 'Yermak Plateau' are not in the range of this map.

Before fixing each MUC core, either with formaldehyde or with DESS, the supernatant seawater was also filtered over a 40 µm sieve in order to catch epi-/hyperbenthic animals that might be present in the fine fluffy layer on top of the sediment. For most cores that were fixed with formalin, the sieve and shovel were rinsed with a 7% (w/v) aqueous solution of $MgCl_2$ in order to anaesthetise the meiobenthic organisms prior to fixation. This step is recommended for soft-bodied meiofauna such as gastrotrichs (e.g. Todaro and Hummon, 2008).

Preliminary (expected) results

In total, there were 31 deployments of the TV-MUC during the expedition PS101 (Fig. 8.3.1). Three deployments were only for video imaging without any sampling since the seafloor of the target area was either too steep or had a rocky bottom, preventing coring. Two deployments failed. Once, the TV-MUC landed on a dense assemblage of arctic sponges and during another deployment, the device triggered before ground contact with all cores closing within the water column. The success of the remaining 26 hauls was generally very good (Tab. 8.3.1). Especially on the summits of the Langseth Ridge few cores did not close properly and the sample was washed away during heaving to surface. This poor closure was mainly due to the heterogeneous texture of the samples, with some bigger debris that hindered a complete closure of the lower lids. The underwater video equipment of the TV-MUC was a big advantage for our sampling campaign. Especially in areas were narrow corridors of sediment bottom were flanked by steep cliffs of volcanic bedrock (as at the Vent Mount) a successful benthic coring would not have been possible without the video and telemetry systems. In total, benthic sampling with the TV-MUC yielded 183 cores. Of these, 31 will be used for the study of benthic foraminiferans (see 8.4), 40 cores serve for geo-microbiological analyses (see 8.6) and from 111 cores the meiofauna will be extracted for subsequent taxonomic, faunistic and biogeographical analyses. A single core contained a part of a sponge individual, and that sample will be analysed by GEOMAR (see 8.5).

From the 111 cores dedicated to the study of the meiofauna, 81 cores were fixed with formaldehyde (14 cores were only qualitative) and 30 were treated with DESS (5 qualitative

cores). 33 of the cores from the summits of the Langseth Ridge had to be split into two subsamples A and B (Tab. 8.3.1). The A horizon covers a filthy mat of sponge spicules and empty tubes of sessile polychaetes (Fig. 8.3.2 B-D). The thickness of this layer of organic carbonate and silicate debris varied between a few and up to 20 cm. Underneath the mat, there was again a sediment layer (horizon B) in most cores that consisted of fine, clayish material mixed with empty calcareous tubes. We retained the upper 5 cm of this sediment layer. The sediment of the saddle between the Karasik Seamount and the Central Mount of the Langseth Ridge was comparable to that of the summits, however, with less organic debris from sponges and polychaetes. The sediment of the southern reference station in the Nansen Basin (mooring 1) consisted of rather homogenous clayish fine sediment that was strongly compacted. The sediment of the southern slope of the Karasik Seamount was comparable to the aforementioned (Fig. 8.3.2 E-F). Somehow different was the sediment consistence at the Vent Mount within the Gakkel Ridge Rift Valley. It also consisted of fine clayish sediment but not that strongly compacted as at the southern reference station. It seemed that at least the upper centimetres had a higher proportion of pore water. Furthermore, the sediment surface was abundant in small gravel particles, possibly precipitates of the adjacent vent flows (Fig. 8.3.2 A).

Tab. 8.3.1: Deployments of the camera equipped multiple corer (TV-MUC) and remainder of each of the maximum 8 cores per haul. If the total number is less than 8, single cores did not close or were washed during hieving. AWI, Alfred-Wegener-Institut für Polar- und Meeresforschung (Foraminifera); DE, DESS solution; DZMB, Deutsches Zentrum für Marine Biodiversitätsforschung (Meiofauna); FA, formaldehyde; GEO, GeoMar (sponges); LR, Langseth Ridge; MPI, Max Planck Institut für Marine Mikrobiologie (pore water analyses and geomicrobiology). The letter q indicates qualitative samples (e.g. if the core was obviously disturbed) and A+B indicates if cores for the analysis of the meiofauna were split into two subsamples (see text for details). For more information such as the positions see the full station list in the appendix.

Station	Depth [m]	Target area	AWI	DZMB						GEO	MPI	Total
				DE	DE (q)	FA	FA (q)	sum DZMB	A+B			
PS101/0061-1	3882,7	Nansen Basin (mooring 1)	3			3		3	0		2	8
PS101/0062-1	3880,4	Nansen Basin (mooring 1)		2		3		5	0		1	6
PS101/0063-1	3879,9	Nansen Basin (mooring 1)		1		3		4	0		3	7
PS101/0098-1	1101,4	LR Central Mount	imaging only									
PS101/0101-1	635	Karasik Seamount	3				1	1	1		2	6
PS101/0102-1	643,1	Karasik Seamount		2		4		6	6		1	7
PS101/0103-1	634,6	Karasik Seamount			1	3		4	4			4
PS101/0104-1	637,4	Karasik Seamount				3		3	3		2	5
PS101/0118-1	4726,1	Gakkel Ridge Rift Valley	imaging only									
PS101/0123-1	650,9	Karasik Seamount			1	2	1	4	2		3	7
PS101/0124-1	650,1	Karasik Seamount	sampling failed									
PS101/0125-1	655,8	Karasik Seamount	3				1	1	1		3	7
PS101/0140-1	3263,8	Vent Mount		2		3		5	0		3	8
PS101/0151-1	859,2	LR Central Mount	3				1	1	1		2	6
PS101/0152-1	903,2	LR Central Mount		1	1	3	1	6	0		1	7
PS101/0153-1	847,8	LR Central Mount					3	3	0			3
PS101/0166-1	3213,7	Vent Mount	sampling failed									
PS101/0167-1	3175,7	Vent Mount	3	1		3		4	0		1	8

Station	Depth [m]	Target area	AWI	DZMB						GEO	MPI	Total
				DE	DE (q)	FA	FA (q)	sum DZMB	A+B			
PS101/0187-1	3410,5	Vent Mount		2		4		6	0		2	8
PS101/0194-1	724,4	LR Northern Mount	3				4	4	2		1	8
PS101/0195-1	639,4	LR Northern Mount			2	2	1	5	0	1	2	8
PS101/0196-1	657,2	LR Northern Mount		2		5		7	2		1	8
PS101/0205-1	1182,6	LR Central Mount		2		5		7	0		1	8
PS101/0210-1	1020,6	Karasik Central Mount Saddle	3	1		2		3	0		1	7
PS101/0211-1	908,9	Karasik Central Mount Saddle		2		4		6	5		2	8
PS101/0212-1	956,6	Karasik Central Mount Saddle		2		3	1	6	6		2	8
PS101/0218-1	1852,3	Karasik South Slope		2		4		6	0		2	8
PS101/0219-1	2049,2	Karasik South Slope	3	1		3		4	0		1	8
PS101/0220-1	2001,7	Karasik South Slope		2		5		7	0		1	8
PS101/0227-1	3596,2	Vent Mount	imaging only									
PS101/0242-1	866,6	Yermak Plateau	7									7
sum:			31	25	5	67	14	111	33	1	40	183

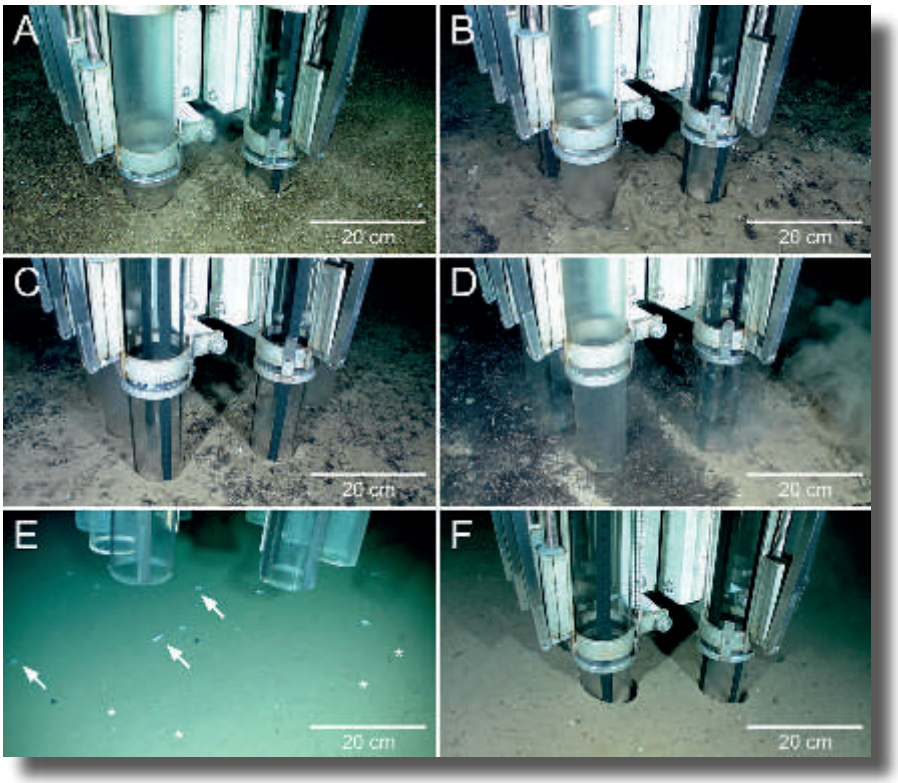

Fig. 8.3.2: Penetration of the TV-MUC into the seafloor at selected stations. A Station PS101/140-1 (Vent Mount) with soft sediment mixed with gravel (possibly vent fluid precipitates). B Station PS101/151-1 (Langseth Ridge Central Mount) with a filthy cover of sponge spicules. C Station PS101/152-1 (Central Mount) with soft sediment and some spots of sponge spicules and tubeworm debris. D Station PS101/153-1 (Central Mount) with soft sediment covered with a layer tubeworm debris. E-F Station PS101/219-1 (Karasik South Slope) shortly before (E) and after penetration (F). Note the numerous sea cucumbers (arrows) and the slender polychaete tubes (asterisks) on/in the soft sediment.

Back in our home laboratory, the fixed meiofauna specimens will be separated from the sediment and the organic debris (sponge spicules and calcareous tubes) using the silica gel gradient centrifugation technique (Pfannkuche & Thiel 1988) with the colloidal silica Levasil©. Subsequently, the extracted fauna will be sorted, mounted on microscopic slides and investigated by taxonomic specialists. Due to the great heterogeneity of sediments between the different target areas, we expect different meiofauna communities in the deep sea, the slope and summits of the Langseth Ridge as well as on the vent mount within the Gakkel Ridge Rift Valley. On the summits there might even be different communities when comparing the meiofauna species of the spicule mats with the soft sediments below the mats.

During the cruise we were able to rinse and sieve the mats from two qualitative cores before fixation (PS101/101-1 core 1 and PS101/125-1 core 6, see Fig. 8.3.3 and 8.3.4), in order to get a first insight to the inhabiting meiofauna. The samples were poured into a petri dish and screened for animals under a Leica MZ 9.5 stereo microscope.

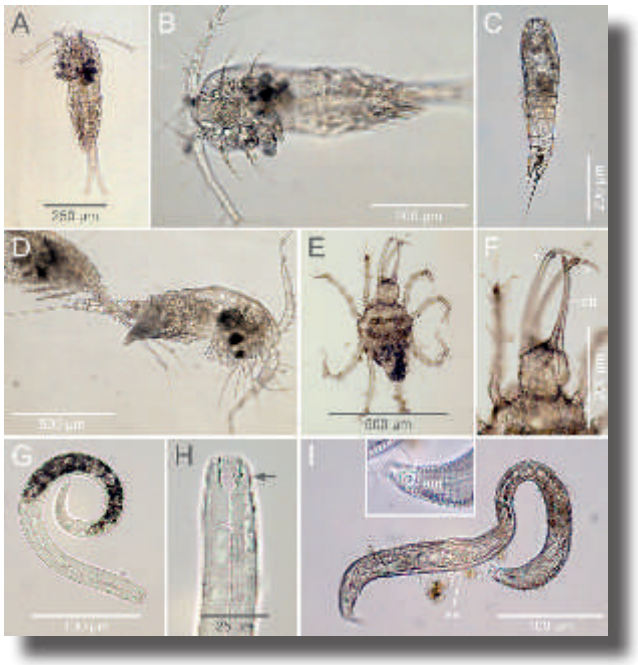

Fig. 8.3.3: Meiofauna organisms from the mat of sponge spicules and tubeworm debris at station PS101/101-1 (gear: MUC, tube #1, depth: 635 m). A, B, D Interstitial copepods of the order Cyclopoida. C A harpacticoid copepod, taxon Ectinosomatidae. E-F A marine mite of the taxon Halacarida. Note the elongated palps (*) and chelicerae (ch) on the close-up of the gnathosoma (F). G-H A subadult nematode. Note the big tooth inside the spaceous buccal cavity (arrow) that indicates a predatory lifestyle (H). I An epifaunal nematode of the taxon Epsilonematidae. These animals move over the substratum by aid of their ambulatory setae (as). Note the chemoreceptive amphid (am) at the anterior end (inset image).

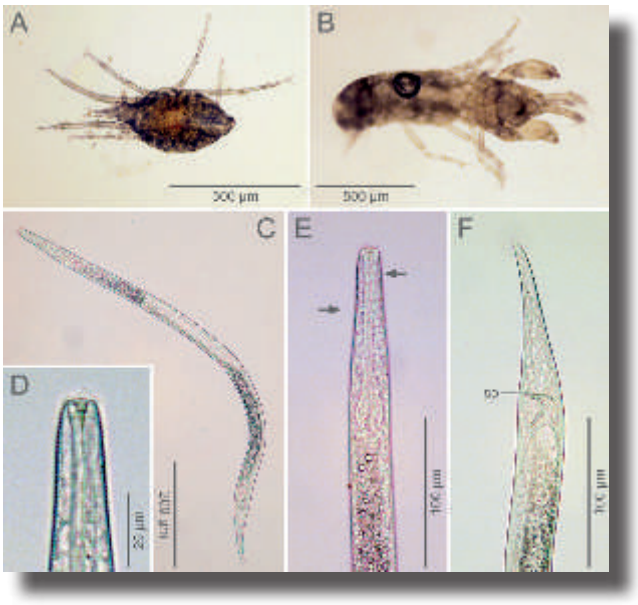

Fig. 8.3.4: Meiofauna organisms from the mat of sponge spicules and tubeworm debris at station PS101/125-1 (gear: MUC, tube #6, depth: 655.8 m). Light microscopic images. A A marine mite of the taxon Halacarida. B A meiobenthic specimen of the crustacean taxon Tanaidacea. C-F An unidentified species of Nematoda, male specimen. C shows the whole specimen, anterior to the upper left. The close up in D shows the anterior end with a narrow buccal cavity, possibly indicating a bacterivorous species. In E and F you can see the anterior and posterior end. Note the annulated cuticle and sensory setae (arrows) in E and the male spicules (sp) close to the cloaca in F.

Selected specimens were prepared as fresh slides in seawater and inspected and documented with an Olympus CX41 microscope with an adapted digital camera Olympus E520. Sample PS101/101-1 core 1 yielded at least two different species of Nematoda (one of the subtaxon Epsilonematidae), a halacarid mite and Copepoda from the taxa Cyclopoida, Misophrioida and Harpacticoida. Within the latter group, the families Ectinosomatidae and Tisbidae (?) could already be identified (Fig. 8.3.3 A-I). In sample PS101/125-1 core 6, we could find another species of Nematoda, another species of Halacarida, and a specimen of Tanaidacea (Fig. 8.3.4 A-F). There were furthermore the copepod taxa Calanoida and Harpacticoida with specimens of the harpacticoid families Ameirinae, Laophontidae, Cerviniinae, Paranannopinae and Tisbidae. This very first glance to our meiobenthic samples may already indicate a species-rich meiofauna community at the bottom of the high arctic Langseth Ridge.

Data management

Fixed specimens for morphological taxonomic and phylogenetic analyses will be sent to the corresponding taxonomic experts, in collaboration with Senckenberg Research Institute and Natural History Museum. Biological data (determined taxa, locations and depth) will be submitted to the OBIS data base. Meiofauna sequence data will be archived in GenBank after publication.

References

Gad G, Schminke HK **(**2004) How important are seamounts for the dispersal of meiofauna? Archive of Fishery and Marine Research, 5, 43-54.

George KH (2013) Faunistic research on metazoan meiofauna from seamounts—a review. Meiofauna Marina, 20, 1-32.

George KH, Martínez Arbizu P (2005) Discovery of Superornatiremidae Huys (Copepoda, Harpacticoida) outside anchialine caves, with the description of *Gideonia noncavernicola* gen. et sp. nov. from the Patagonian continental slope (Chile). Meiofauna Marina, 14, 75-89.

Gollner S, Fontaneto D, Martínez Arbizu P (2011) Molecular taxonomy confirms morphological classification of deep-sea hydrothermal vent copepods (Dirivultidae) and suggests broad physiological tolerance of species and frequent dispersal along ridges. Marine Biology, 158, 221-231.

Huys R (1996) Superornatiremidae fam.nov. (Copepoda: Harpacticoida): An enigmatic family from North Atlantic anchialine caves. Scientia Marina, 60, 497-542.

Pfannkuche O, Thiel H (1988) Sampling processing. In: Higgins RP, Thiel H (eds) Introduction to the study of meiofauna, pp. 134-145. Smithsonian Institution, Press. Washington, D.C.

Todaro MA, Hummon WD (2008) An overview and a dichotomous key to genera of the phylum Gastrotricha. Meiofauna Marina, 16, 3-20.

Yoder M, Tandindan de Ley IW, Mundo-Ocampo Mann J, Blexter M, Poiras L, de Ley P (2006) DESS: A versatile solution for preserving morphology and extractable DNA of nematodes. Nematology, 8, 367-376.

Background literature (not cited in text):

Rossi S, Bramanti L, Gori A, Orejas C (eds) (2017) Animal Forests: the ecology of benthic biodiversity hotspots. Springer International Publishing, doi:10.1007/978-3-319-17001-5, pp 1-39.

8.4 Foraminifera

Objectives

Benthic foraminiferal analyses on sediment samples from venting sites of the Gakkel Ridge collected in 1987 to 2008, revealed *Placosilinella aurantiaca,* a primitive organic walled epizoic foraminifera as the only living species. Until the *Polarstern* expedition in 2011, when the first samples from the Karasik Seamount were collected, the origin from the highly diverse benthic foraminiferal thaphocoenoses observed at other Gakkel Ridge sites remained unclear. The Karasik Seamount reveals an oasis-like diverse benthic foraminiferal assemblage that stands out from the common desert-alike Gakkel Ridge environment. The Rose Bengal-stained samples collected during PS101 will supplement the sparse sample set collected in 2011. Rose Bengal-stained samples will furthermore be used to increase the 27-years old data set on the distribution of living foraminifers in the Arctic Ocean in the more general context. Starting with this year's expedition our morphological taxonomic approach will be supplemented by DNA-barcoding. Shells of foraminifers will be used for trace metal (especially B/Ca ratio and B isotope) analyses. Sediments collected during the final multiple corer cast will be used within our high-pressure culturing laboratory. In this laboratory deep-sea foraminifers will be reproduced under variable pressure and pH conditions. Experimental offspring will be used to generate the first B/Ca and Boron isotope calibration curves on benthic foraminifers in the Arctic Ocean or for cultured deep-sea benthic foraminifers in general.

Work at sea

During the expedition a total of 8 multiple corer casts were carried out and sampled for benthic foraminifers (Tab. 8.4.1). At 7 sites 3 multiple corer tubes were sampled in 1 cm-intervals from the sediment surface to 10 cm sediment depth. From one tube the surface sediment centimetre was frozen and will be used for DNA-barcoding, the remaining 1cm-thick subsamples from that tube and all subsamples from the remaining two tubes were transferred in Kautex bottles. A sediment volume equivalent volume of Ethanol-Rose Bengal mixture (2 g Rose Bengal per l Ethanol) was added to the respective subsamples carefully mixed and stored at 4°C for further investigations in our home laboratory.

Tab. 8.4.1: List of stations sampled for Foraminifera with the TV-MUC, including sampling dates, geographical location, and sampling depth

Station	Date	Position Lat	Position Lon	Depth [m]	Gear
PS101/0062-1	15.09.16	85° 13.85‘ N	060° 0.16‘ E	3824.9	TV-MUC
PS101/0101-1	19.09.16	86° 42.29‘ N	061° 18.36‘ E	635.3	TV-MUC
PS101/0125-1	22.09.16	86° 43.77‘ N	061° 36.76‘ E	664	TV-MUC
PS101/0151-1	27.09.16	86° 49.76‘ N	061° 47.07‘ E	854.7	TV-MUC
PS101/0166-1	29.09.16	86° 57.86‘ N	055° 47.01‘ E	3030.8	TV-MUC
PS101/0194-1	06.10.16	86° 51.22‘ N	061° 34.87‘ E	732.4	TV-MUC
PS101/0219-1	08.10.16	86° 39.64‘ N	059° 55.34‘ E	2005.3	TV-MUC
PS101/0242-1	17.10.16	79° 27.09‘ N	007° 30.93‘ E	855.9	TV-MUC

Preliminary (expected) results

Treatment of samples, faunal and geochemical analyses will be carried out in our laboratories at the Alfred Wegener Institute. This work will be carried out by Jutta Wollenburg. Expected results will aid in understanding the environmental causes of the Karasik Seamount oasis and the complex interaction between different benthic foraminiferal and macrofaunal taxa at this distinct central Arctic Ocean site. Sediments transferred in our culturing devices will help us to generate the first deep-sea benthic foraminiferal calibration curves for boron-calcium ratios and boron stable isotopes.

Data management

Raw and processed data will be made available to all shipboard and shore based, and submitted to PANGAEA for long-term storage.

8.5 Porifera

Objectives

An objective of this cruise was to characterize the sponge (Porifera) communities of Langseth Ridge regarding diversity, abundance, their associated microbial communities, and microbial gene activity. The different communities of Karasik Seamount, the North Mount and the Central Mount will be compared to each other and to other deep-sea sponge grounds in the framework of H2020 EU project SponGES, grant agreement No 679849 (Cárdenas and Rapp, 2015; Maldonado et al., 2016; Rapp, Xavier, et al. 2016). Post cruise, the GEOMAR Kiel Marine Microbiology group will investigate the microbial diversity and microbial gene activity of a selected number of arctic deep-sea sponges by metagenomic and metatranscriptomic sequencing as well as amplicon sequencing of the V4 region of the 16S rRNA gene following protocols of the Earth Microbiome Project (http://www.earthmicrobiome.org/) for comparability with previous sponge microbiome projects (Thomas et al. 2016). Microscopy (electron microscopy and otherwise) will be performed alongside to visualize the presence and abundance of microbial consortia within the sponge extracellular matrix. Further effort will be placed on understanding the taxonomy, phylogeographical position and functional role of sponges on the Langseth Ridge ecosystem in collaboration with University Bergen's experts on Northern hydrothermal vents and the ecology of sponge grounds on seamounts.

Work at sea

Sponge samples of different morphotypes were collected via box corer, multiple corer systems (TV-MUC), dredge with chain bag, and NUI ROV. The animals were photographed and samples were fixed for genetics, (meta)genomics, (meta)transcriptomics, transmission electron microscopy, raster electron microscopy, and morphological analyses. As references for the microbial community, sediment was sampled from box corers and bottom water was collected by CTD rosette and filtered through 0.22 µm PVDF filters. Seawater filters as well as sediment samples were frozen at -80°C. Sediment subcores were taken for analyses of the sponge spicule mats and frozen at -20°C.

Preliminary (expected) results

The sponge community on Karasik, Central, and Northern seamount was dominated by few main morphotypes of Demospongia: round, disk-shaped, and nest-shaped (different *Geodia*

spp. and *Stelletta* spp.), all of which had external spicules (Figs. 8.5.1, 8.5.2, and 8.5.3). The ground around and beneath the sponges was covered by a thick spicule mat. Buds of both sponge morphotypes were frequently observed and sampled whenever possible (Tab. 8.5.1). Glass sponges (Hexactinellida) were not dominant, but also observed frequently. Three vase-shaped glass sponges were sampled by box corer at the Northern mount and frozen whole at -80°C (PS101/200 #1-3, Tab. 8.5.1, Figs. 8.5.3 and 8.5.4). An attempt to sample more hexactinellids at Karasik with the NUI ROV failed due to the fragility of these sponges. All sponge samples collected during PS101 are listed in Tab. 8.5.1, all reference samples (sediment and sea water) in Tab. 8.5.2.

Fig. 8.5.1 Box corer (50cm side length) of station PS101/0093 with a sponge specimen of the round morphotype on top of a spicule mat (Photo: B. Slaby).

Fig. 8.5.2 Box corer (50cm side length) of station PS101/0094 with sponge specimens of the disk-shaped morphotype on top of a spicule mat (Photo: B. Slaby).

Fig. 8.5.3 Box corer (50cm side length) of station PS101/0200 with a sponge specimen of the nest-shaped morphotype (top left) and three specimens of vase-shaped Hexactinellida *(right) on top of a spicule mat (Photo: J. Dannheim).*

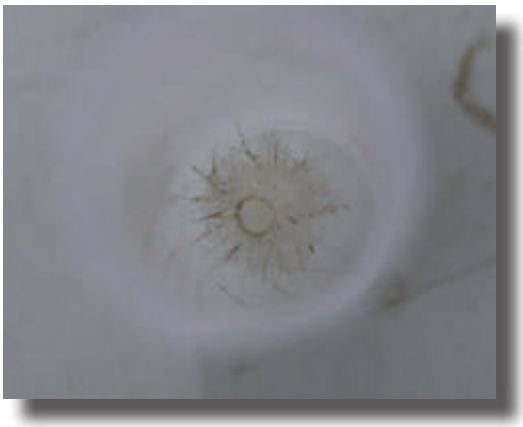

Fig. 8.5.4 vase-shaped Hexactinellida *specimen PS101/200 #3 (diameter ca. 1cm) (Photo: B. Slaby).*

Tab. 8.5.1: Sponge samples collected during PS101 at Karasik seamount, Central mount, Northern mount and the saddle between Karasik and Central mount. Abbreviations: BC – box corer, MUC – multicorer, DCB – dredge and chain bag, NUI ROV – remotely operated vehicle "NUI", REM – raster electron microscopy, TEM – transmission electron microscopy, EtOH - ethanol.

Station	Gear	Sample no.	Species	REM	TEM	RNA later	EtOH (2ml)	-80°C (2ml)	EtOH (50ml)	-80°C (50ml)	Other
Karasik seamount											
PS101/ 0092-1	BC	PS101/ 092 #1	Demospongia	2	2	4	5	4	-	-	at -20°C (x2)
PS101/ 0092-1	BC	PS101/ 092 #1A	Demospongia buds						-	1	-
PS101/ 0093-1	BC	PS101/ 093 #1	Demospongia	2	2	4	5	4	-	-	at -20°C; at -20°C
PS101/ 0093-1	BC	PS101/ 093 #1 A	Demospongiabuds	-	-	-	-	-	1	-	-
PS101/ 0093-1	BC	PS101/ 093 #2	Demospongia	-	-	-	-	-	-	-	Whole sponge in 96% EtOH at -20°C
PS101/ 0094-1	BC	PS101/ 094 #1	Demospongia	2	2	4	5	4	1	1	at -20°C (x2)
PS101/ 0094-1	BC	PS101/ 094 #2 A	Demospongiabuds	-	-	-	-	-	1	-	-
PS101/ 0094-1	BC	PS101/ 094 #2	Demospongia	2	2	4	5	4	1	1	at -20°C (x3)
PS101/ 0094-1	BC	PS101/ 094 #3	Demospongia	2	2	4	5	4	-	1	at -20°C (x4)
PS101/ 0123-1	MUC	PS101/ 123 #1	Demospongia	2	2	4	5	4	-	2	at -20°C
PS101/ 0193-1	DCB	PS101/ 193 #1	Demospongia	2	2	-	5	4	1	1	at -20°C
PS101/ 0193-1	DCB	PS101/ 193 #2	Demospongia	2	2	-	5	4	-	1	at -20°C
PS101/ 0193-1	DCB	PS101/ 193 #3	Demospongia	2	2	-	5	4	-	1	at -20°C
PS101/ 0193-1	DCB	PS101/ 193 #4	Demospongia	2	2	-	5	4	-	1	at -20°C
PS101/ 0193-1	DCB	PS101/ 193 #5	Demospongia	2	2	-	5	4	-	1	at -20°C
PS101/ 0193-1	DCB	PS101/ 193 #6	Demospongia	2	2	-	5	4	-	1	at -20°C
PS101/ 0193-1	DCB	PS101/ 193 #7-9	Demospongia	-	-	-	-	-	-	-	in EtOH at -20°C
PS101/ 0193-1	DCB	PS101/ 193 Rest	Demospongia	-	-	-	-	-	-	-	at -20°C
PS101/ 0216-1	NUI ROV	PS101/ 216 rotting sponge	Demospongia	-	-	-	-	-	-	-	in EtOH at -20°C; at -80°C
PS101/ 0216-1	NUI ROV	PS101/ 216 #1	Demospongia	2	2	4	5	4	1	1	at -20°C (x2)
PS101/ 0216-1	NUI ROV	PS101/ 216 #2	Demospongia	2	2	-	5	4	1	2	-
PS101/ 0216-1	NUI ROV	PS101/ 216 #2 A	Demospongiabuds	-	-	-	-	-	1	-	-

Station	Gear	Sample no.	Species	REM	TEM	RNA later	EtOH (2ml)	-80°C (2ml)	EtOH (50ml)	-80°C (50ml)	Other
Central mount											
PS101/ 0154-1	BC	PS101/ 154 #1	Demospongia	2	2	4	5	4	-	1	at -20°C
PS101/ 0155-1	BC	PS101/ 155 #1	Demospongia	2	2	4	5	4	1	1	at -20°C
Northern mount											
PS101/ 0194-1	MUC	PS101/ 194 #1	Demospongia	2	2	4	5	4	-	1	-
PS101/ 0195-1	MUC	PS101/ 196 #1	Demospongia	2	2	4	5	4	-	1	at -20°C
PS101/ 0197-1	BC	PS101/ 197 #1	Demospongia	2	2	4	5	4	1	1	at -20°C
PS101/ 0197-1	BC	PS101/ 197 #2	Demospongia	2	2	4	5	4	-	1	in EtOH at -20°C
PS101/ 0197-1	BC	PS101/ 197 #3	Demospongia	2	2	4	5	4	-	1	-
PS101/ 0198-1	BC	PS101/ 198 #1	Demospongia	2	2	4	5	4	-	1	-
PS101/ 0198-1	BC	PS101/ 198 #2	Demospongia	2	2	4	5	4	-	-	in EtOH at -20°C
PS101/ 0200-1	BC	PS101/ 200 #1	Hexactinellida	-	-	-	-	-	-	-	frozen whole at -80°C
PS101/ 0200-1	BC	PS101/ 200 #2	Hexactinellida	-	-	-	-	-	-	-	frozen whole at -80°C
PS101/ 0200-1	BC	PS101/ 200 #3	Hexactinellida	-	-	-	-	-	-	-	frozen whole at -80°C
PS101/ 0200-1	BC	PS101/ 200 #4	Demospongia	2	2	4	5	4	1	1	at -20°C
PS101/ 0200-1	BC	PS101/ 200 #4A	Demospongiabuds	2	2	4	5	4	-	-	-
PS101/ 0200-1	BC	PS101/ 200 #5	Demospongia	2	2	4	5	4	1	1	at -20°C
Karasik - Central mount saddle											
PS101/ 0208-1	BC	PS101/ 208 #2	Demospongia	2	2	4	5	4	1	1	at -20°C
PS101/ 0208-1	BC	PS101/ 208 #1	Demospongia	2	2	4	5	4	1	1	at -20°C
Station	**Gear**	**Sample no.**	**Species**	**REM**	**TEM**	**RNA later**	**EtOH (2ml)**	**-80°C (2ml)**	**EtOH (50ml)**	**-80°C (50ml)**	**Other**
Karasik seamount											
PS101/ 0092-1	BC	PS101/ 092 #1	Demospongia	2	2	4	5	4	-	-	at -20°C (x2)
PS101/ 0092-1	BC	PS101/ 092 #1A	Demospongia buds						-	1	-
PS101/ 0093-1	BC	PS101/ 093 #1	Demospongia	2	2	4	5	4	-	-	at -20°C; at -20°C
PS101/ 0093-1	BC	PS101/ 093 #1 A	Demospongiabuds	-	-	-	-	-	1	-	-

Station	Gear	Sample no.	Species	REM	TEM	RNA later	EtOH (2ml)	-80°C (2ml)	EtOH (50ml)	-80°C (50ml)	Other
PS101/ 0093-1	BC	PS101/ 093 #2	Demospongia	-	-	-	-	-	-	-	Whole sponge in 96% EtOH at -20°C
PS101/ 0094-1	BC	PS101/ 094 #1	Demospongia	2	2	4	5	4	1	1	at -20°C (x2)
PS101/ 0094-1	BC	PS101/ 094 #2 A	Demospongiabuds	-	-	-	-	-	1	-	-
PS101/ 0094-1	BC	PS101/ 094 #2	Demospongia	2	2	4	5	4	1	1	at -20°C (x3)
PS101/ 0094-1	BC	PS101/ 094 #3	Demospongia	2	2	4	5	4	-	1	at -20°C (x4)
PS101/ 0123-1	MUC	PS101/ 123 #1	Demospongia	2	2	4	5	4	-	2	at -20°C
PS101/ 0193-1	DCB	PS101/ 193 #1	Demospongia	2	2	-	5	4	1	1	at -20°C
PS101/ 0193-1	DCB	PS101/ 193 #2	Demospongia	2	2	-	5	4	-	1	at -20°C
PS101/ 0193-1	DCB	PS101/ 193 #3	Demospongia	2	2	-	5	4	-	1	at -20°C
PS101/ 0193-1	DCB	PS101/ 193 #4	Demospongia	2	2	-	5	4	-	1	at -20°C
PS101/ 0193-1	DCB	PS101/ 193 #5	Demospongia	2	2	-	5	4	-	1	at -20°C
PS101/ 0193-1	DCB	PS101/ 193 #6	Demospongia	2	2	-	5	4	-	1	at -20°C
PS101/ 0193-1	DCB	PS101/ 193 #7-9	Demospongia	-	-	-	-	-	-	-	in EtOH at -20°C
PS101/ 0193-1	DCB	PS101/ 193 Rest	Demospongia	-	-	-	-	-	-	-	at -20°C
PS101/ 0216-1	NUI ROV	PS101/ 216 rotting sponge	Demospongia	-	-	-	-	-	-	-	in EtOH at -20°C; at -80°C
PS101/ 0216-1	NUI ROV	PS101/ 216 #1	Demospongia	2	2	4	5	4	1	1	at -20°C (x2)
PS101/ 0216-1	NUI ROV	PS101/ 216 #2	Demospongia	2	2	-	5	4	1	2	-
PS101/ 0216-1	NUI ROV	PS101/ 216 #2 A	Demospongiabuds	-	-	-	-	-	1	-	-
Central mount											
PS101/ 0154-1	BC	PS101/ 154 #1	Demospongia	2	2	4	5	4	-	1	at -20°C
PS101/ 0155-1	BC	PS101/ 155 #1	Demospongia	2	2	4	5	4	1	1	at -20°C
Northern mount											
PS101/ 0194-1	MUC	PS101/ 194 #1	Demospongia	2	2	4	5	4	-	1	-
PS101/ 0195-1	MUC	PS101/ 196 #1	Demospongia	2	2	4	5	4	-	1	at -20°C
PS101/ 0197-1	BC	PS101/ 197 #1	Demospongia	2	2	4	5	4	1	1	at -20°C
PS101/ 0197-1	BC	PS101/ 197 #2	Demospongia	2	2	4	5	4	-	1	in EtOH at -20°C

Station	Gear	Sample no.	Species	REM	TEM	RNA later	EtOH (2ml)	-80°C (2ml)	EtOH (50ml)	-80°C (50ml)	Other
PS101/ 0197-1	BC	PS101/ 197 #3	Demospongia	2	2	4	5	4	-	1	-
PS101/ 0198-1	BC	PS101/ 198 #1	Demospongia	2	2	4	5	4	-	1	-
PS101/ 0198-1	BC	PS101/ 198 #2	Demospongia	2	2	4	5	4	-	-	in EtOH at -20°C
PS101/ 0200-1	BC	PS101/ 200 #1	Hexactinellida	-	-	-	-	1	-	-	frozen whole at -80°C
PS101/ 0200-1	BC	PS101/ 200 #2	Hexactinellida	-	-	-	-	1	-	-	frozen whole at -80°C
PS101/ 0200-1	BC	PS101/ 200 #3	Hexactinellida	-	-	-	-	1	-	-	frozen whole at -80°C
PS101/ 0200-1	BC	PS101/ 200 #4	Demospongia	2	2	4	5	4	1	1	at -20°C
PS101/ 0200-1	BC	PS101/ 200 #4A	Demospongiabuds	2	2	4	5	4	-	-	-
PS101/ 0200-1	BC	PS101/ 200 #5	Demospongia	2	2	4	5	4	1	1	at -20°C
Karasik - Central mount saddle											
PS101/ 0208-1	BC	PS101/ 208 #2	Demospongia	2	2	4	5	4	1	1	at -20°C
PS101/ 0208-1	BC	PS101/ 208 #1	Demospongia	2	2	4	5	4	1	1	at -20°C

Tab. 8.5.2: Reference seawater and sediment samples collected for sponge microbiology during PS101 at Karasik seamount, Central mount, Northern mount, the saddle between Karasik and Central mount, at two mooring stations and the investigated vent area. Abbreviations: CTD/r – conductivity, temperature, depth and seawater sampling rosette, BC – box corer.

Station	Gear	Sample no.	Sample type and number	Notes
Karasik				
PS101/0088-1	CTD/r	PS101/088 filter #1-4	4 filters at -80°C	each filter 2L of CTD bottle #1
PS101/0092-1	BC	PS101/092 sediment	4 15ml tubes with sediment sample at -80°C	-
PS101/0092-1	BC	PS101/092 sediment core	sediment core in aluminum foil at -20°C	-
PS101/0093-1	BC	PS101/093 sediment	3 15ml tubes with sediment sample at -80°C	-
PS101/0094-1	BC	PS101/094 sediment	4 15ml tubes with sediment sample at -80°C	-
Central mount				
PS101/0154-1	BC	PS101/154 sediment core	sediment core in aluminum foil at -20°C	-

Station	Gear	Sample no.	Sample type and number	Notes
PS101/0154-1	BC	PS101/154 sediment	4 15ml tubes with sediment sample at -80°C	
PS101/0155-1	BC	PS101/155 sediment core	sediment core in aluminum foil at -20°C	-
PS101/0155-1	BC	PS101/155 sediment	4 15ml tubes with sediment sample at -80°C	
PS101/0170-1	CTD/r	PS101/170 filter #1-4	4 filters at -80°C	each filter 2L of CTD bottle #1
Northern mount				
PS101/0172-1	CTD/r	PS101/172 filter #1-4	4 filters at -80°C	each filter 2L of CTD bottle #2
PS101/0197-1	BC	PS101/197 sediment core	sediment core in aluminum foil at -20°C	-
PS101/0197-1	BC	PS101/197 sediment	4 15ml tubes with sediment sample at -80°C	
PS101/0198-1	BC	PS101/198 sediment	4 15ml tubes with sediment sample at -80°C	
PS101/0200-1	BC	PS101/200 sediment core	sediment core in aluminum foil at -20°C	-
PS101/0200-1	BC	PS101/200 sediment	4 15ml tubes with sediment sample at -80°C	
Karasik - Central mount saddle				
PS101/0208-1	BC	PS101/208 sediment core	sediment core in aluminum foil at -20°C	-
PS101/0208-1	BC	PS101/208 sediment	4 15ml tubes with sediment sample at -80°C	
other				
PS101/0055-1	CTD/r	PS101/055 filter #1-2	2 filters at -80°C	Mooring 1; each filter 2L of CTD bottle #1; no other samples from this station (no sponges)
PS101/0112-1	CTD/r	PS101/112 filter #1-2	2 filters at -80°C	Mooring 2; each filter 2L of CTD bottle #1; no other samples from this station (no sponges)
PS101/0133-1	CTD/r	PS101/133 filter #1-2	2 filters at -80°C	Vent area; each filter 2L of CTD bottle #3; no other samples from this station (no sponges)

Data management

The collected specimens will be analysed by cruise participants and other sponge experts. All metadata will be made available through PANGAEA and all quality-filtered sequence data will be archived in GenBank after publication.

References

Cárdenas P, Rapp HT (2015) Demosponges from the Northern Mid-Atlantic Ridge shed more light on the diversity and biogeography of North Atlantic deep-sea sponges. Journal of the Marine Biological Association of the United Kingdom, 95, 1475-1516.

Thomas T, Moitinho-Silva L, Lurgi M, Björk JR, Easson C, et al. (2016) Diversity, structure and convergent evolution of the global sponge microbiome. Nature Communications, 7, 11870.

Maldonado M, Aguilar R, Bannister RJ, Bell JJ, Conway KW et al. (2016) Sponge grounds as key marine habitats: a synthetic review of types, structure, functional roles, and conservation concerns. Marine Animal Forests: the ecology of benthic biodiversity hotspots, 1-39.

8.6 Microbiology

Objectives

The main objectives were to investigate microbial community compositions, abundances, and metabolic activities related to the presence of the Langseth Ridge and hydrothermally active areas. On the Langseth Ridge the high density of sponge mats can support high microbial activities and specific sponge associated microbial communities. Furthermore, degradation of sponge biomass is a potential energy sources for sulphur- and ammonia oxidizing bacteria. Hydrothermal activities can be responsible for releasing reduced compounds (i.e. CH_4, H_2, H_2S) that may change microbial community compositions and abundances, enhancing microbial metabolic activities (e.g. chemosynthesis). The reference areas in the Nansen Basin and south of the Langseth Ridge are expected to host the typical deep-sea communities of the central Arctic Ocean with low activities.

Work at sea

Sediment samples for microbiological and biogeochemical analyses were sampled with a TV-guided multicorer (TV-MUC). An additional sample of bacterial mats was taken with a NUI-ROV. Promising sampling spots on the seamount were identified with an ocean floor observation system (OFOS) prior to the TV-MUC sampling. On the Langseth Ridge three sea mount peaks and a saddle were sampled. Additional samples were taken from a hydrothermal vent field on a seamount nearby, and from the Nansen Basin. All benthic samples for microbial studies are listed in Tab. 8.6.1.

In a cooled container at 0°C the cores were subsampled in layers of 0-1 cm, 1-2 cm, 2-3 cm, 3-5 cm and where possible 4-16 cm depth below sea floor. The subsamples were preserved at -20°C for later measurements of phytopigments, porosity, total organic carbon and nitrogen contents, and phospholipid composition. Additional samples were preserved for DNA (-20°C) and RNA (-80°C) extractions, which will help to investigate the microbial community structures via different molecular approaches. Further samples were fixed for Fluorescent *in-situ* hybridisations (FISH), another method to investigate the microbial community structures, and for total cell counts via the acridine orange direct cell count method (AODC). Potential extracellular enzymatic activities (EEA) for beta-glucosidase, chitobiase, aminopeptidase, and esterase were measured on board via assays with fluorescent substrates. For dark inorganic carbon fixation (DCF), samples at 0-1 cm, 3-5 cm, and 14-16 cm depth below sea floor were incubated with ^{14}C-DIC for 24 h, killed with Formaldehyde (2% final concentration) and stored at 4°C for later measurements (Molari et al., 2013). Samples of surface sediment layer were prepared for later tracer FISH studies, which allows quantifying the contribution of different taxonomic groups to the DCF via FISH, cell sorting, and scintillation counting. For investigating the potential energy source for microbial activities in the hydrothermal

vent field, DCF measurements were carried out in presence of different reduced inorganic compounds (i.e. CH_4, H_2, SO_4, and NH_4). For determining the biomass produced per moles of DIC or leucine incorporation, a biomass experiment with the first 5 cm of top sediment from the Nansen basin was carried out for 19 days. Extracellular enzymatic activities and DCF rates were measured in some sponges. DCF in sponge tissues were also measured in presence of different energy source (i.e. CH_4, H_2, NH_4 SO_4, CO), in order to clarify the metabolic ability of microbial associated communities. DCF and leucine uptake measurements were carried out in the dark and at *in situ* temperature, killed with formaldehyde (2% final concentration) and stored at 4°C for later analyses. Extracellular enzymatic activities were measured on board. The rotten sponges and microbial mat sampled with the NUI-ROV were fixed for DNA analysis, FISH and AODC and directly observed under an inverse microscope with 10x40 magnification.

Tab. 8.6.1: Sampled cores for porewater analysis (DIC, Alkalinity, Fe, Mn, SO_4, HS, Si, PO_4, NH_4, NO_3, NO_2), sediment analysis (Phytopigments, porosity, TOC/TON, phospholipids, DNA, RNA, FISH, AODC, EEA, ^{14}C-DIC uptake, Tracer FISH, and extra samples and cores for experiments.

Date	Gear	Station	Site/Area	Depth [m]	Pore-water	Sedi-ment	Extra
15/09/2016	MUC	PS101/061-1	Nansen Basin (Mooring 1)	3883		1	3 cores for biomass experiment
16/09/2016	MUC	PS101/062-1	Nansen Basin (Mooring 1)	3880		1	
16/09/2016	MUC	PS101/063-1	Nansen Basin (Mooring 1)	3880	1	1	
19/09/2016	MUC	PS101/101-1	Karasik Sea Mount	635	1	1	
20/09/2016	MUC	PS101/102-1	Karasik Sea Mount	643		1	
20/09/2016	MUC	PS101/104-1	Karasik Sea Mount	637	1	1	
22/09/2016	MUC	PS101/123-1	Karasik Sea Mount	651	2	1	additional cores sliced in 1 cm steps from 0-7 cm bsf for later sulphide and nutrient analyses, stored at 4°C (core 2)/ black surface material frozen at -20°C from core 1
23/09/2016	MUC	PS101/125-1	Karasik Sea Mount	656	1	2	
25/09/2016	MUC	PS101/140-1	Vent Mount	3263	1	2	additional cores sliced (0-1,3,5,7,9,11,17 cm bsf) for sulphide analyses stored at 4°C/ sponge and stone samples preserved at -20°C (core 1 and 2)
27/09/2016	MUC	PS101/151-1	Langseth Ridge central mount	860	1	1	
28/09/2016	MUC	PS101/152-1	Langseth Ridge central mount	903		1	
30/09/2016	MUC	PS101/167-1	Vent Mount	3176	1	1	porewater core sliced and stored at -20°C
05/10/2016	MUC	PS101/187-1	Vent Mount	3410	1	1	substrate experiment with porewater core
06/10/2016	MUC	PS101/194-1	Langseth Ridge northern mount	724	1	1	

Date	Gear	Station	Site/Area	Depth [m]	Pore-water	Sedi-ment	Extra
06/10/2016	MUC	PS101/195-1	Langseth Ridge northern mount	639		2	
06/10/2016	MUC	PS101/196-1	Langseth Ridge northern mount	657		1	
07/10/2016	MUC	PS101/205-1	Langseth Ridge central mount	1183		1	
07/10/2016	MUC	PS101/210-1	Langseth Ridge saddle	888		1	
07/10/2016	MUC	PS101/211-1	Langseth Ridge saddle	909	1	1	
07/10/2016	MUC	PS101/212-1	Langseth Ridge saddle	957		1	1 sponge core for sponge incubations
08/10/2016	NUI/ ROV	PS101/216-1	Reference South	739			3 cores for rotten sponges and microbial mats (AODC, FISH, DNA, microscopy)
08/10/2016	MUC	PS101/218-1	Reference South	1852	1	1	
08/10/2016	MUC	PS101/219-1	Reference South	2049		1	
08/10/2016	MUC	PS101/220-1	Reference South	2002		1	

The porewater was sampled from intact cores (every cm from the top to 10 cm, in deeper depth every 2 cm) using Rhizons. The porewater was split and fixed for later determination of dissolved inorganic carbon, alkalinity, iron, manganese, sulfate and sulfide in the home laboratory. Nutrients (silicate, phosphate, ammonium, nitrate, nitrite) were directly measured on board.

Preliminary results

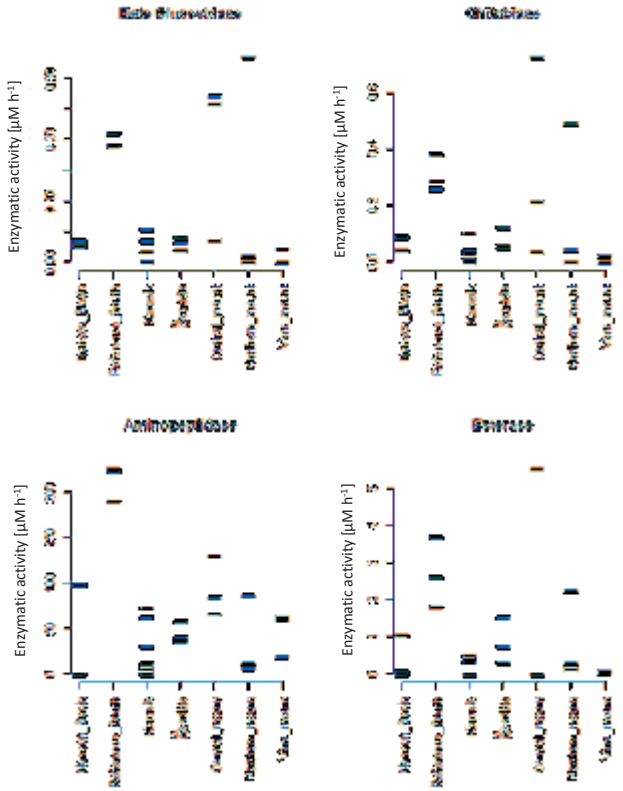

Fig. 8.6.1: Extracellular enzymatic activites of beta glucosidase, chitobiase, aminopeptidase, and esterase in the surface sediment layer (0-1 cm) of all sites. Each data point represents one core.

On sea, microbial and biogeochemical analyses were limited to extracellular enzymatic activities, nutrient measurements, and microscopic observations of the rotten sponges and bacterial mats. Most enzymatic activities show a high variation (Fig. 8.6.1) with values in the range of similar studies (Boetius et al., 2015). In the reference area south of the Langseth Ridge aminopeptidase activities were higher compared to all other sampled sites. Beta-glucosidase, chitobiase, and esterase activities were generally higher in the southern reference area, too, but one to two cores of the central and northern mounts of the Langseth Ridge showed activities even higher. All enzymatic activities, except aminopeptidase have reduced activities at the vent mount. Enzymatic activities at the Karasik seamount and the saddle of the Langseth Ridge are comparable to activities at the Nansen Basin. Beta-glucosidase and chitobiase activities decrease along the sediment profiles, while aminopeptidase and esterase do not show any dependent pattern, as observed in the Aurora vent area in southern Gakkel Ridge (Boetius et al., 2015). All enzymatic activites in the sponge samples were highly increased by one (Beta glucosidase, chitobiase, aminopeptidase) or two (esterase) orders of magnitude. The mean Beta glucosidase activity is 5 µM h^{-1}, the mean chitobiase activity is 6.5 µM h^{-1}, the mean aminopeptidase activity is 4678 µM h^{-1}, and the mean Esterase activity 124.8 µM h^{-1}.

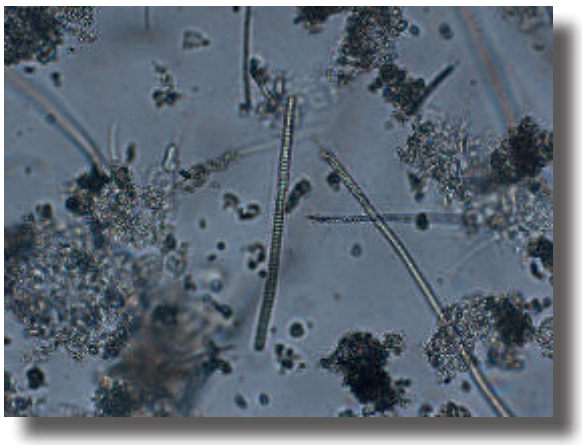

Fig. 8.6.2: chains of sulphur-oxidizing bacteria on a rotten sponge. 10x40 magnification on an inverse microscope. Picture taken with AcioVision.

The bacterial mats on a freshly degrading sponge contained long and thick bacterial chains (Fig. 8.6.2), which are presumably sulphur-oxidizing bacteria, which is supported by a sulfidic smell. In addition, high abundances of ciliates and copepods, but no nematodes have been found. Neither the meiofauna nor the bacterial mats were present in significant amounts in samples of a completely degraded yellow looking sponge.

Data management

All data will be quality-checked, stored and be available after publication in peer-reviewed journals through PANGAEA Data Publisher for Earth & Environmental Science. Gene sequences of processes sediment microbiota will be publicly available via GenBank after publication aimed within the next two years.

References

Boetius A (2015) The Expedition PS86 of the Research Vessel Polarstern to the Arctic Ocean in 2014. Reports on Polar and Marine Research, 685, doi:10.2312/BzPM_0685_2015.

Molari M, Manini E, Dell'Anno A (2013) Dark inorganic carbon fixation sustains the functioning of benthic deep-sea ecosystems. Global Biogeochemical Cycles, 27(1), 212-221.

9. USE OF HROV NUI FOR UNDER ICE EXTREME ENVIRONMENT EXPLORATION (PSTAR&ROBEX)

Chris German[1], Mike Jakuba[1], John Bailey[1], Antje Boetius[2,3,4], Andrew Branch[5], Kevin P. Hand[5], Casey Machado[1], Jill McDermott[6], Autun Purser[2], Stefano Suman[1], Louis Whitcomb[1,7]
not on board: Wolfgang Bach[4,8], Andy Bowen[1], Steve Chien[5], James Kinsey[1] , Ko-ichi Nakamura[9], Oscar Pizarro[1,10], Steve Schaffer[5],

[1]WHOI
[2]AWI
[3]MPI
[4]MARUM
[5]NASA-JPL
[6]LU
[7]JHU
[8]UHB-GEO
[9]AIST
[10]ACFR

Grant No. AWI_PS101_01 / NASA PSTAR Grant Number NNX16AL04G

Objectives

Our programme sought to explore for and characterize (geochemically and microbiologically) new sites of seafloor fluid flow at the Karasik Seamount which rises from 4,700 m to 566 m deep on the Gakkel Ridge (87°N, 61°E) beneath the permanent ice-cover of the northern Arctic. Our programme aimed to identify biosignatures generated by any chemosynthetic ecosystems and to investigate the fate of those biosignatures as they are transported upwards via hydrothermal plumes into the water column and/or the overlying ice-cover. Our field campaign used the novel NUI vehicle in a range from fully autonomous to real-time human-directed modes for survey and sampling missions during the course of the cruise.

Work at sea

Technology

The NUI vehicle is uniquely well-suited for the exploration undertaken during PS101 – both as an autonomous underwater vehicle (AUV) and as a remotely operated vehicle (ROV) in which an unprotected, expendable glass fiber is used as a communication tether for human-supervised under-ice operations and exploration. Its compact size, low weight and horizontal mobility provide more maneuverability than conventional ROVs while offering the full bandwidth data return unavailable to conventional AUVs. Bi-directional telemetry enables direct control of the vehicle over relatively extended distances (up to 20 km) from a central location (in this project, *Polarstern*). While *Polarstern* was also equipped with a CTD-rosette to conduct water column surveys and the OFOS camera system that could be used survey the seafloor directly beneath the ship, addition of NUI's freedom to move laterally as well as vertically added an important new capability for systematic exploration of the Karasik Seamount and precise sampling, independent of the ship's track.

In AUV configuration (Fig. 9.1a) the primary sensors were an Imagenex 837b DeltaT multibeam sonar and a bespoke down-looking stereo camera pair with synchronized strobes provided by O. Pizarro, Australian Centre for Field Robotics, University of Sydney, Australia. Bathymetric surveys using the multibeam were flown at 1 m/s and 50 m above bottom, nominal. Camera surveys using the stereo camera pair were flown at 0.7 m/s nominal and 3 m above bottom. Additional physical oceanographic and chemical data were collected per dive Tab. 9.1).

Examples of data collected are illustrated in the Preliminary results section below.

Tab. 9.1: A list of the sensor suites employed on each NUI dive

Dive	HD Video	DeltaT multibeam	Wetlabs ECO Chl/ NTU	Eh sensor	CTD (SBE 49 FastCAT)	Down-looking Stereo Camera
PS101/150-1 NUI 014 (AUV)	N	Y	Y	Y	Y	N
PS101/168-1 NUI 015 (AUV)	N	Y	Y	Y	Y	Y
PS101/216-1 NUI 016 (ROV)	Y	Y	N	Y	Y	N

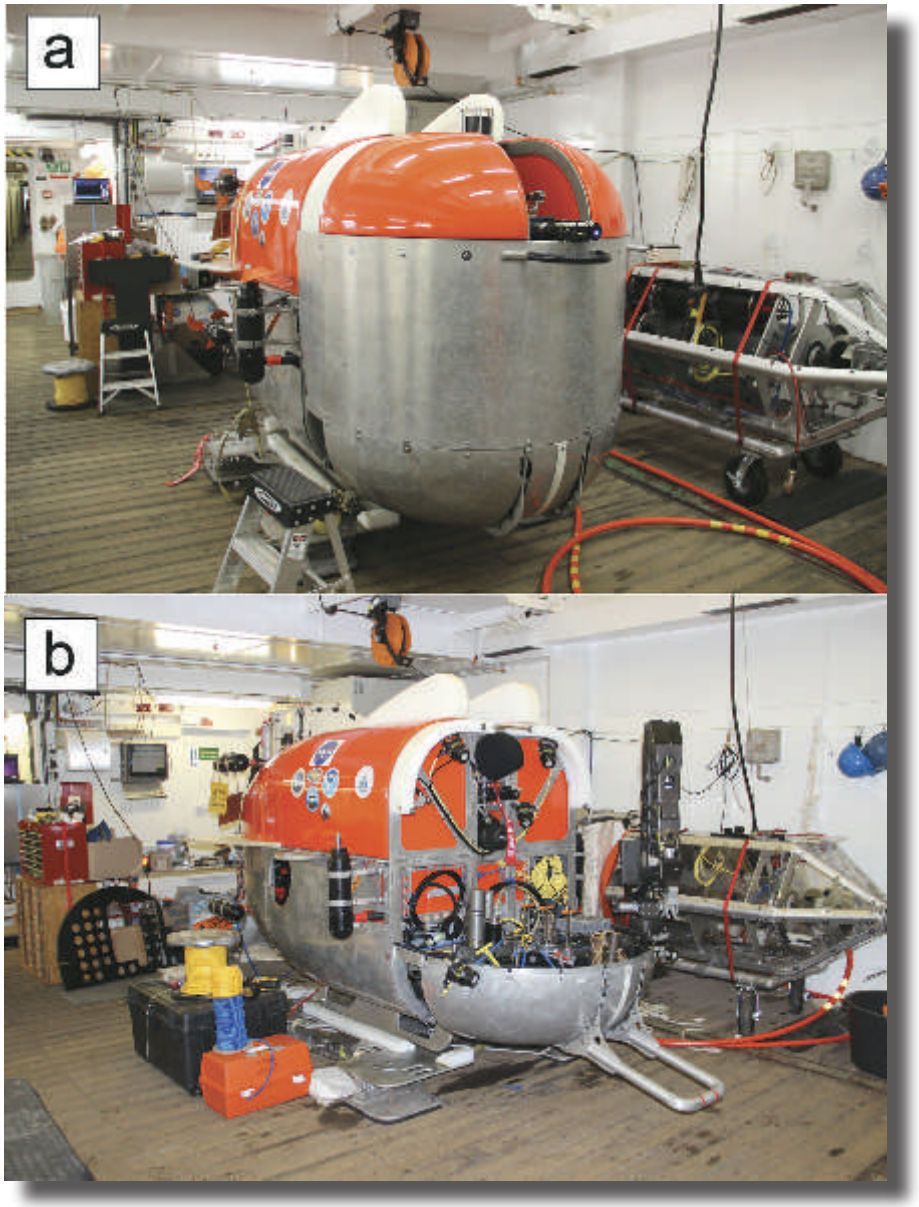

Fig.9.1: Photographs of NUI in the hangar of Polarstern: (a) NUI in AUV mode with in situ sensors for CTD, Eh and optical back scatter (blue light visible) mounted high on the forehead of NUI above the aluminium skins fitted to the front of the vehicle for optimum hydrodynamic efficiency when conducting AUV surveys; (b) NUI in ROV mode with manipulator and sample basket installed in place of the aluminium AUV skins.

In ROV configuration (Fig. 9.1b), the vehicle was equipped with a Kraft Telerobotics 7-function electro-hydraulic manipulator arm and the nose reconfigured for sampling. Sampling equipment consisted of push cores (3), nets (2), a four-chamber bio-box, and one IGT (isobaric gas-tight) fluid sampler. In ROV configuration HD video from a Kongsberg hyperdome internal pan and tilt camera system was recorded. All sampling activities were undertaken with the vehicle thrusting actively against the seafloor to hold position. Additional physical oceanographic and chemical data were collected per Tab. 9.1. Examples of data collected are illustrated in the Preliminary results section, below.

Dive operations

Four NUI dives were attempted, 3 in AUV configuration (NUI 013, NUI 014, NUI 015) and 1 in ROV configuration (NUI 016). Dive NUI 013 (PS101/129-1) was unsuccessful and failed to leave the sea surface. Statistics for the remaining dives are detailed in Tab. 9.2. Launch and recovery times denote the time of release and the on-hook time, respectively.

Tab. 9.2: NUI Dive Operations

Dive	Launch Time [UTC]	Recovery Time [UTC]	Dive Duration [hh:mm]	Time on Bottom [hh:mm]	Maximum Depth [m]
NUI 014 (AUV) (PS101/150-1)	2016-09-27 06:41:00	2016-09-27 15:05:00	08:24	06:32	662
NUI 015 (AUV) (PS101/168-1	2016-09-30 07:13:00	2016-09-30 18:42:00	11:55:00	06:32	687
NUI 016 (ROV) (PS101/216-1)	2016-10-08 05:20:00	2016-10-08 10:27:00	05:07:00	03:10	686

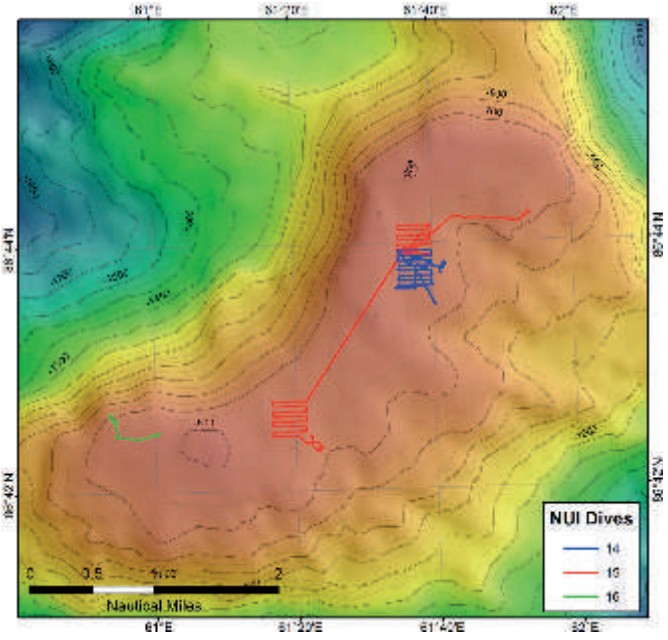

Fig.9.2: Track lines for NUI Dives 014 (PS101/150-1), 015 (PS101/168-1) and 016 (PS101/216-1) superimposed on the background ship-based bathymetry for Karasik Seamount.

Dive tracks for each dive are shown in Fig. 9.2 superimposed upon the background bathymetry for the summit of Karasik Seamount. To aid in seafloor navigation three transponders were deployed at Karasik Seamount: Transponder B (PS101/121-1), Transponder A (PS101/122-1) and Transponder C (PS101/191-1). To save on shiptime costs, none of the transponders were recovered at cruise end. Details are provided in Appendix 5.3.

Preliminary results

In AUV mode, one of the primary results was that detailed multibeam mapping was achieved over the course of NUI dives 014 (PS101/150-1) and 015 (PS101/168-1) over both the primary area selected for benthic biology sampling near the southern Summit of Karasik Seamount (Fig. 9.3) and also at the Northern Summit in an area selected from OFOS Dive 089 which, during that entire dive, was the only location at which any rock outcrops were observed (Fig. 9.4). The area near the Southern Summit, which measured ~500 m x 500 m, was rather featureless and flat, as expected – that was why it was selected for multiple TV-MUC and box-coring activities. In contrast, the northern area (~500 m x 900 m) revealed a deep gulley at the base of the scarp leading up to the Northern Summit – a feature that was not evident in the ship's multibeam bathymetry. The full extent of the gulley was approximately 500 m running NE-SW along the base of a scarp that rose ~35 m to the NW from its base to its upper limit.

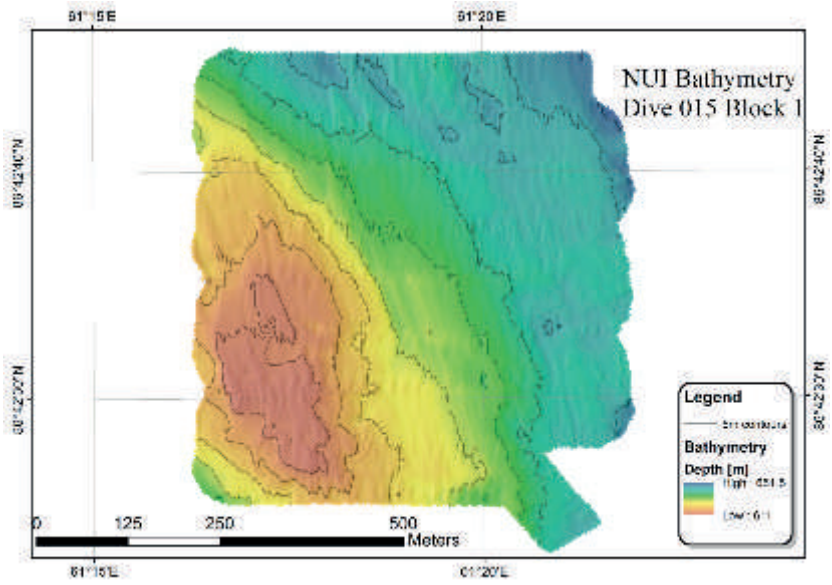

Fig.9.3: High resolution bathymetric map of the seafloor in the benthic biology sampling area near the southern summit of Karasik Seamount as mapped in AUV mode during NUI Dive 015 (PS101/168-1).

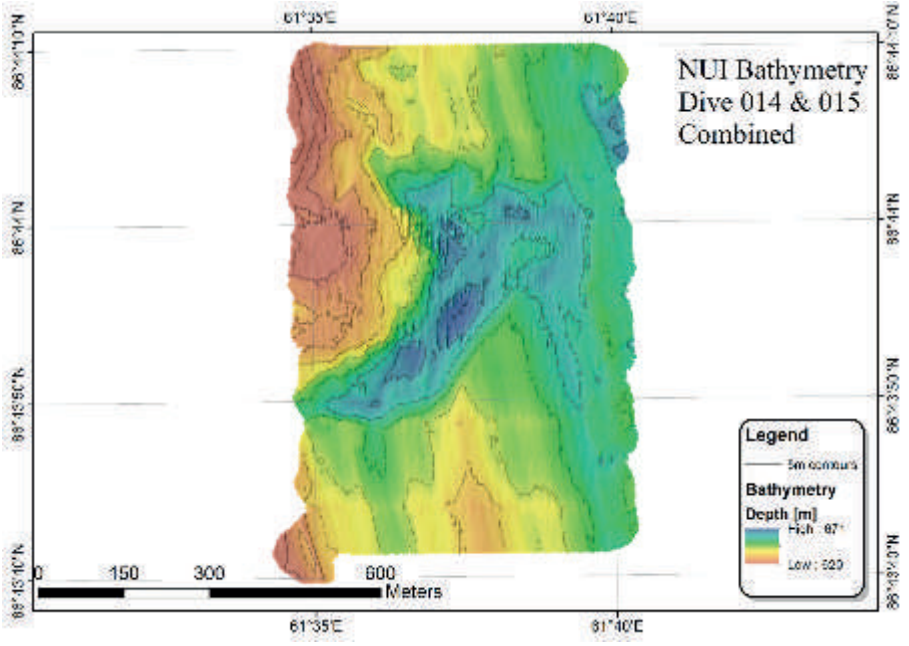

Fig.9.4: High resolution bathymetric map of the seafloor revealing the steep, ~35m tall and ~500m long gulley and scarp feature at the northern summit of Karasik Seamount as mapped in AUV mode during NUI Dives 014 (PS101/150-1) and 015 (PS101/168-1).

During NUI Dive 015, detailed seafloor stereo-photography was also undertaken in the northern Scarp/Gulley area. As elsewhere on Karasik Seamount, sponge fauna dominated what was imaged (Fig. 9.5a) but multiple crossings of the scarp identified from AUV-based mapping revealed a sharp cliff indicative of geological faulting (Fig. 9.5b) that led to rock outcrops being exposed at the seafloor (Fig. 9.5c). Certain of these images revealed clear evidence for foliation consistent with a tectonic and not purely volcanic origin at the summit of Karasik Seamount (Fig. 9.5d).

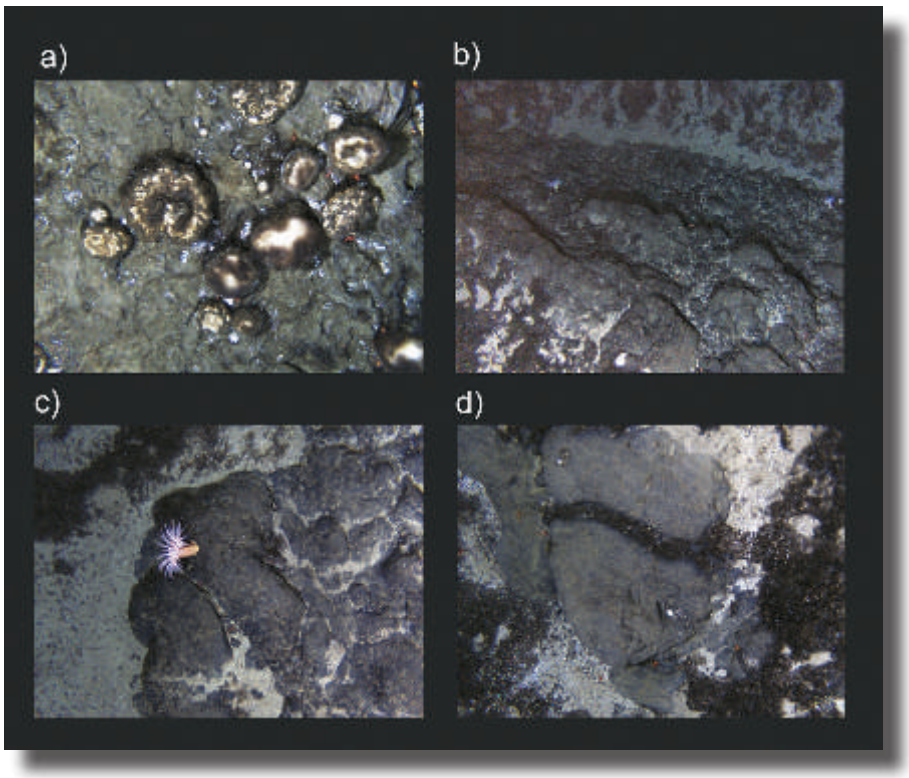

Fig.9.5: Down-looking still images of the seafloor collected in AUV mode during NUI Dive 015 (PS101/168-1): a) Profuse Giant Sponge abundances were typical throughout the survey area; b) the scarp that runs NE-SW through the area is characterised by steep vertical cliffs indicative of geologic faulting at the North Summit of Karasik ; c) the steep scarp/fault yields rock outcrops that are otherwise absent across the entire summit of Karasik Seamount; d) sub-parallel layering in the rocks, coupled with rectilinear fractures, are not typical of the pillow basalts seen at the Vent Mount site with OFOS and speak to a tectonic aspect to the geologic formation of Karasik Seamount. Full 3D versions of these images will be processed, post-cruise, as part of an ongoing collaboration between WHOI and the Australian Centre for Field Robotics.

Pronounced Eh anomalies were observed above the Northern Summit area at Karasik Seamount during both mapping surveys (nominally 50 m off bottom) in the northernmost line from Dive NUI 014 which was re-occupied as the southernmost line in NUI 015 (Fig. 9.6). and also during near-seafloor photographic surveys which placed the strongest near seafloor anomalies in the gulley at the base of the scarp (Fig. 9.6). A marked and enigmatic Eh anomaly was also observed during mapping of the seafloor in the Southern Summit Area in a single survey line (not shown) but the signal could not readily be related to any features in the underlying bathymetry (Fig. 9.3). Unfortunately, the presence of a large thick floe over the intended dive site and impending weather meant that it was not possible to return to either of these locations in ROV mode for NUI Dive 016.

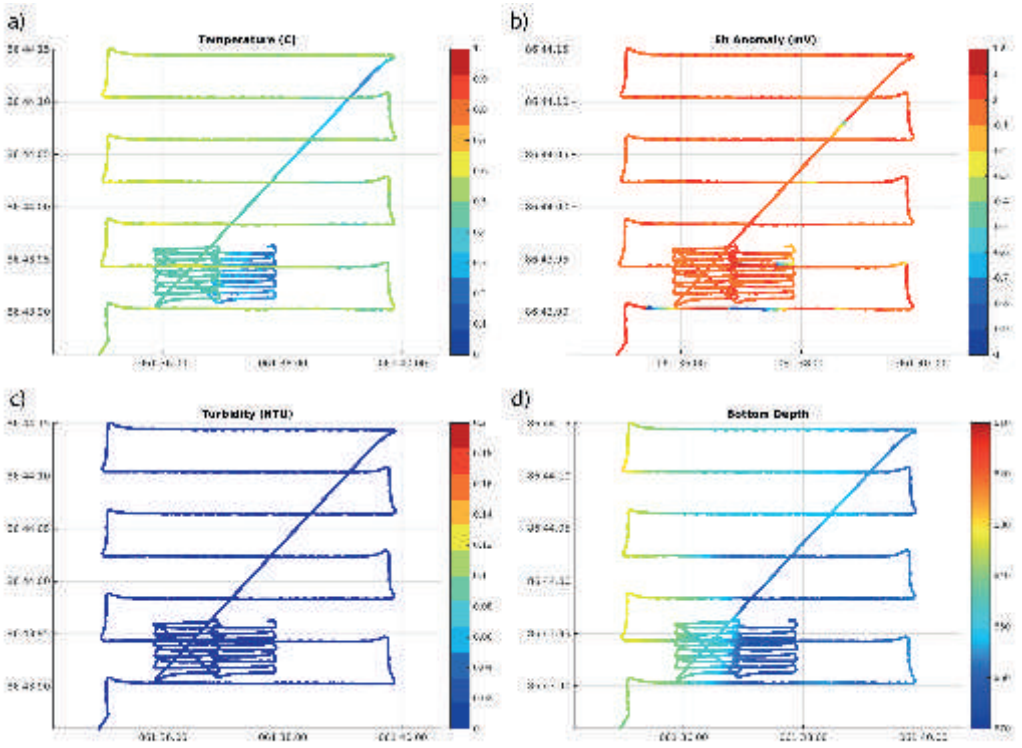

Fig.9.6 Examples of in situ water column data collected by NUI from the northern dive area during NUI Dive 15 (PS101/168-1): (a) temperature (°C); (b) calculated Eh anomaly (mV), (c) turbidity (NTU) and (d) seafloor depth (m). Wide spaced lines were conducted in multibeam mapping mode at 50 m altitude while close spaced lines were from photographic surveys at 3 m altitude above the seafloor.

NUI Dive 016 (PS101/216-1) was the first dive of NUI to the seafloor, in ROV mode, beneath 100% ice cover. The key outcomes of the dive were an ability to conduct detailed examination and video-documentation of animal behavior at the seafloor and also to conduct precise sampling at a number of locations (Tab. 9.3; Fig. 9.7). Sampling included collection of push-core samples of a putative new species of “Yellow Sponge” (Fig. 9.8a) that had been observed extensively from OFOS and NUI AUV images but which had not previously been sampled by the Benthic Biology group. Other sampling included a push core of microbial mat associated with the rotting of a giant sponge as well as a co-located cushion star seen grazing on that microbial mat (Fig. 9.8b). Opportunistic sampling was also conducted to collect an example of an octocoral living on a giant sponge (Fig. 9.8c) and, at a different location, an example of a giant sponge with two glass sponges attached (Fig. 9.8d). Unfortunately, these glass sponge samples – which had only been seen rarely in OFOS imagery and not sampled at all previously – were too delicate to survive return to the surface in the net sample that was placed in NUI’s basket. In addition to multiple additional video clips recorded at the seafloor (polychaetes, starfish grazing, video transects across giant sponges), NUI also recorded HDTV video of the water column all the way from the surface ocean to the seabed at the start of the dive and again, from the seafloor all the way back to the ocean surface, to aid future studies of the biology of the water column.

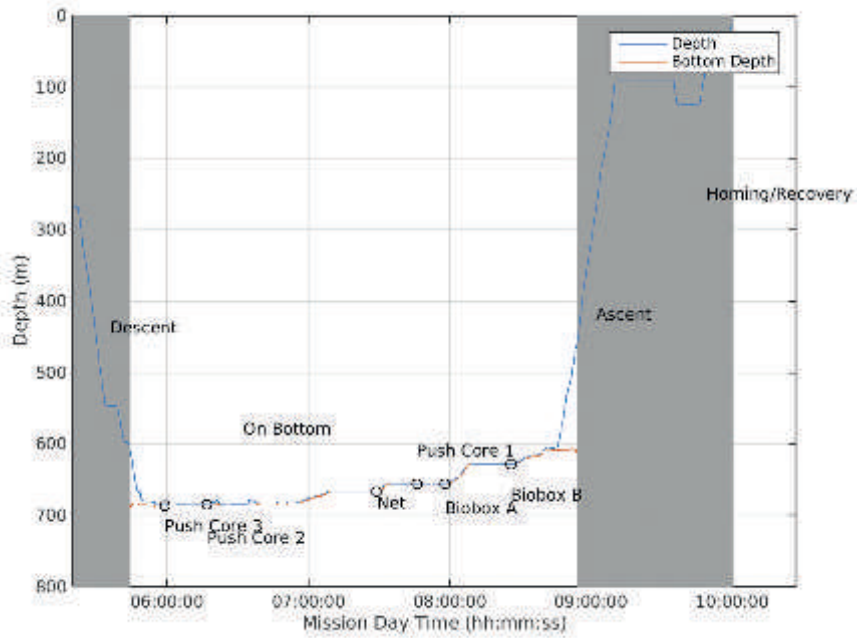

Fig.9.7: Plot of sampling locations vs depth during NUI Dive 016 (PS101/216-1)

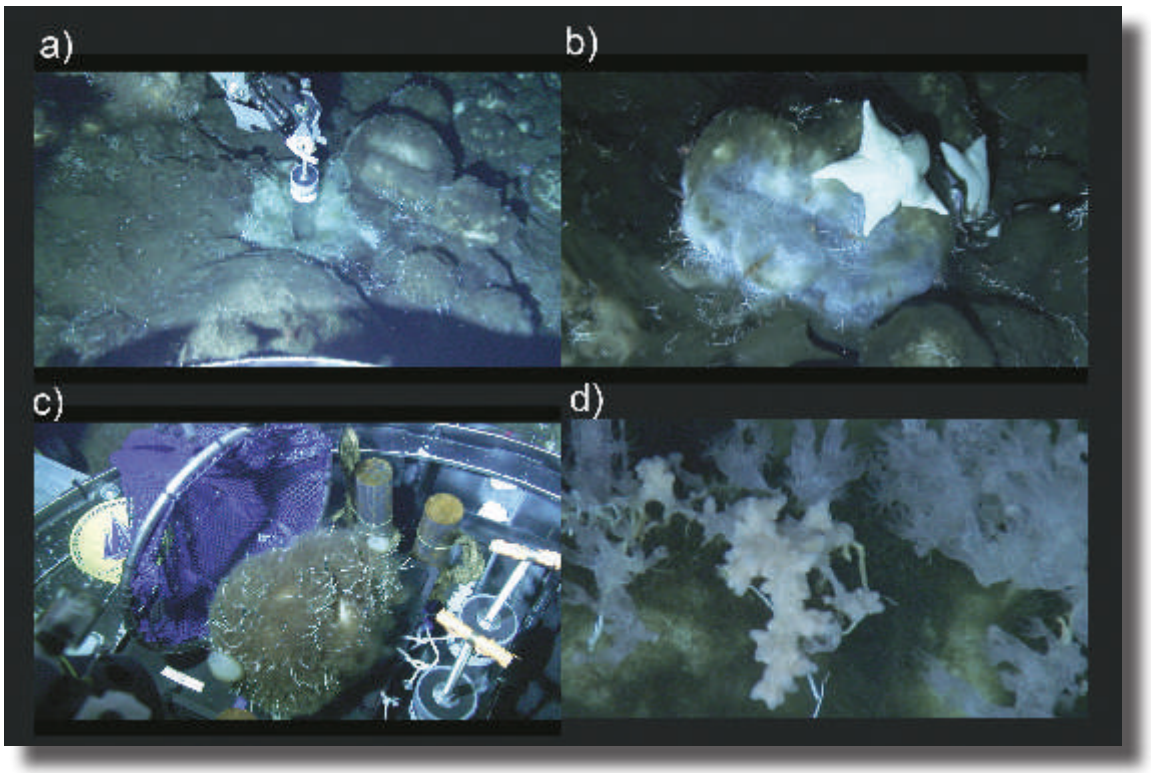

Fig.9.8: Frame grabs from the HDTV video recordings conducted during NUI Dive 16 (PS101/216-1) showing: (a) a region of "yellow sponge" being sampled by push core; (b) an area of microbial mat growing on a decaying giant sponge and being grazed upon, in turn, by both shrimp and "cushion star" starfish; (c) the octocoral sampled by NUI and (d) a rare example of glass sponges growing on a giant sponge.

Tab. 9.3: Samples Collected from NUI Dive 016 (Station PS101/216-1)

Sample	Type	UTC	Lat	Long	Description
N016-01	Push Core #3	05:59	86.7108	60.89850	Yellow Sponge
N016-02	Push Core #2	06:17	86.71054	60.89686	Yellow Sponge
N016-03	Net	07:29	86.70997	60.90571	Giant Sponge with 2 Glass Sponges
N016-04	Push Core #1	07:46	86.70848	60.90935	Microbial Mat
N016-05	Biobox A	07:58	86.70787	60.90693	Cushion Star
N016-06	Biobox B	08:26	86.70743	60.95082	Octocoral

Data management

Multiple data-types were collected during the cruise all of which are directly analogous to those obtained by other AUVs and ROVs designed and operated by WHOI including the Nereus hybrid ROV/AUV and, more pertinent to this section, the Sentry AUV and Jason ROV, both of which are part of the US National Deep Submergence Facility. Standard data products from this cruise include: navigation data, high resolution bathymetric data, time-stamped *in-situ* (physical and biogeochemical) water-column data from the CTD, optical back-scatter and Eh sensors and HD video and still imagery of the seafloor and ocean water column. All sensor and bathymetric data were processed at sea before cruise end. 3D stereographic processing of color still images from NUI Dive 015 will only be completed in collaboration with colleagues at the Australian Center for Field Robotics, post-cruise.

All data acquired using NUI as part of our NASA PSTAR programme will be archived in the *National Deep Submergence Facility* archive at WHOI. A complete duplicate set of the data has been delivered to Cruise PI, Antje Boetius, and will be uploaded to PANGAEA during the first quarter of 2017. Under the conditions of our NASA funding, all NUI data are available immediately for scietific collaboration among the entire PS101 Scientific Team but will only be made publically available by WHOI, 2 years post-collection. For commercial / media purposes, copyright is retained on all video imagery collected by NUI - even after 2 years. Such use should always be licensed through WHOI (media@whoi.edu).

10. FRAM INFRASTRUCTURE AND ARCTIC MONITORING: SEA ICE, OCEAN PHYSICS, AND BIOGEOCHEMISTRY

Antje Boetius[1], Kevin Hand[2], Myriel Horn[1], Mirta Jacobs[1], Christian Katlein[1], Thomas Krumpen[1], Marcel Nicolaus[1], Martin Schiller[1], Daniel Scholz[1], Anique Stecher[1], Bermann Steinmacher[1], Maren Walter[3], Laura Wischnewski[1]
(not on board:) Melanie Behrens[1], Olaf Boebel[1], Jean Louis Bonne[1], Michael Damm[1], Mario Hoppmann[1], Sepp Kipfstuhl[1], Katja Metfies[1], Hanno Meyer[1], Eva-Maria Nöthig[1], Benjamin Rabe[1], Lutz Schönicke[1], Gunnar Spreen[3], Frank Wenzhöfer[1,4], Martin Werner[1]

[1]AWI
[2]NASA
[3]MARUM/UHB-IUP
[4]MPI

Grant No. AWI_PS100_01

Objectives

Developing improved automated and advanced methods for sampling are key aspects of modern polar research. These methods are allowing researchers to expand from classical point measurement data collection to analysis of data sets with much higher spatial and temporal resolutions. At the same time, it is essential to maintain the quality of each single measurement and to ensure that new methods are consistent with previous methods and results. The Helmholtz infrastructure programme FRAM has financed the development of such new methods and measurement systems for in excess of two years, as part of an ongoing programme. During PS101, some of these systems were tested under real polar conditions and, at the same time, results compared with measurements made with established methodologies:

- A prototype of a new sea ice information system, the IceGIS system was installed just before *Polarstern* departure and was used to support operation and decision-making for ice navigation.

- Advanced sea ice buoys were deployed to obtain interdisciplinary data sets from drifting sea ice. In addition, a drifting station was recovered after more than one year of collection of successful measurements of the Arctic Ocean environment.

- The new under-ice ROV system “Beast” was operated for the first time under sea-ice, carrying a very comprehensive sensor suite for bio-physical ice-ocean studies.

- A multi-copter system was tested as a tool for acquisition of aerial images during three sea-ice stations.

- *Polarstern* facilitated the measuring nutrient concentrations and Total Alkalinity (TA) of the upper seawater along the entire cruise track via the new “Underway” systems. The validation of these underway nutrient samples is done by a “QuAAtro” CFA Nutrient Analyzer. For the validation of TA samples discrete samples were taken and will be analyzed in the home laboratory via a VINDTA-System.

- An autonomous filtration unit (AutoFIM) was used for regular water sample analysis. This system was tested and operated along the entire cruise track.
- Aspects of navigation and polar bear protection in darkness were studied with the help of an infrared camera (First Navy) on the crow's nest.
- The quality and reliability of sensor-derived data depends on the sensor's calibration and electrical characteristics, e.g., among others, detection threshold, resolution, accuracy, temperature range, and sensor drift. Based on previous results obtained during PS94, our main objectives were to test the performance of a Satlantic ISUS V3 and SUNA DEEP nitrate sensor, a Contros HydroC pCO_2 sensor as well as the performance of two underway measuring devices, monitoring nutrients, e.g. NO_3, NO_2, PO_4, Si and Total Alkalinity on *Polarstern*'s seawater inlet.

The Arctic Ocean and its sea ice cover are rapidly changing, but data are rare. Next to the dramatic retreat of sea ice, the strongest climatic signals within the Arctic Ocean over the past decade have been changes in temperature and salinity. A strong accumulation of fresh water has been observed in the past decades in the Arctic Ocean; the waters advected from the Atlantic becoming much warmer and saltier, and a high multi-year variability in temperature and salinity of the Pacific Water inflow has been observed. The reduction in ice cover also allows for more light penetration and prolonged growing seasons for phytoplankton, potentially stimulating primary production. Based on these alterations, one could expect the Arctic Ocean to move from a predominantly light-controlled (ice-covered) to a more nutrient-controlled (open water) system. Hence, one aim of the work during PS101 wass to continue time series measurements and monitoring of the Arctic Ocean from a physical, biological, and geochemical point of view:

- The number of oceanographic data for monitoring of the present state of the water mass distribution and circulation in the Eurasian Basin was increased.
- Two moorings were recovered from the Arctic Ocean. These systems included new types of water samplers.
- During ice-stations and helicopter landings ice and snow thickness distributions were measured using electromagnetic induction sounding and snow depth transects.
- The diverse community of pro- and eukaryotes has been studied from sea ice samples, which were obtained during freeze-up from new ice in comparison to sea ice that survived the last summer melt.
- Our work on planktonic protists and biogeochemical fluxes focused on monitoring species and biomass distribution, on biogeochemical parameters and on the vertical particle flux of organic matter in relation to season, sea ice cover, nutrient distribution and water circulation patterns. This continued studies in Arctic waters of the central Arctic Ocean (CAO) during eight cruises between 1993 and 2015 with *Polarstern*.
- The CRDS instrument on board *Polarstern* in combination with surface water sampling provided a unique simultaneous data set of $H_2{}^{18}O$ and HDO in both ocean surface and the atmosphere directly above the ocean surface, allowing the imprint of marine boundary conditions to the isotopic composition of the atmospheric water to be assessed.

Work at sea

Figs. 10.1 and 10.2 give an overview of the Arctic area in which monitoring took place during PS101.

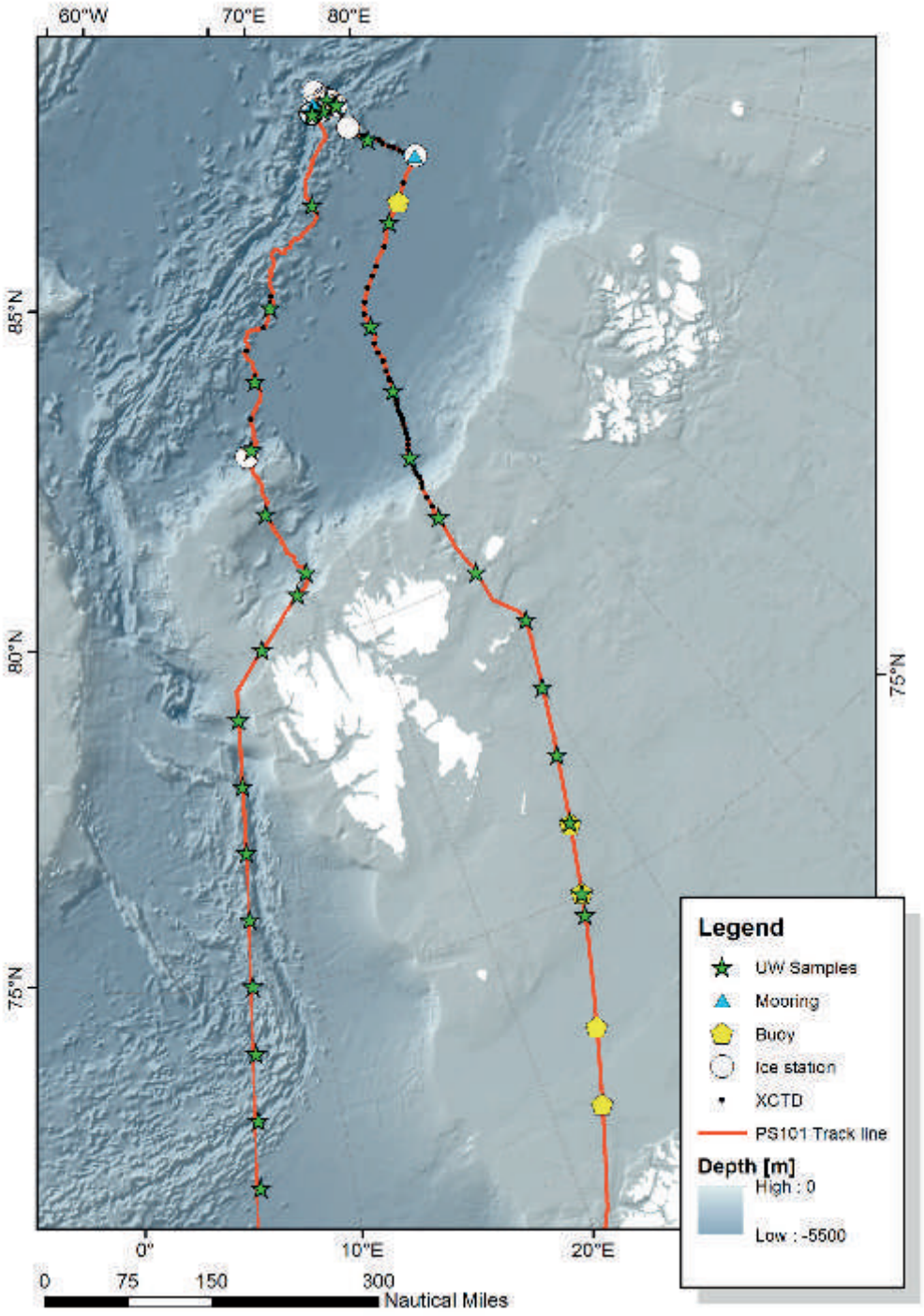

Fig. 10.1: Overview map of all stations of the infrastructure and monitoring programme during PS101. Most stations along the transect refer to underway measurements and expandable CTD (XCTD) casts. A close up of the main study region is given in Fig. 10.2.

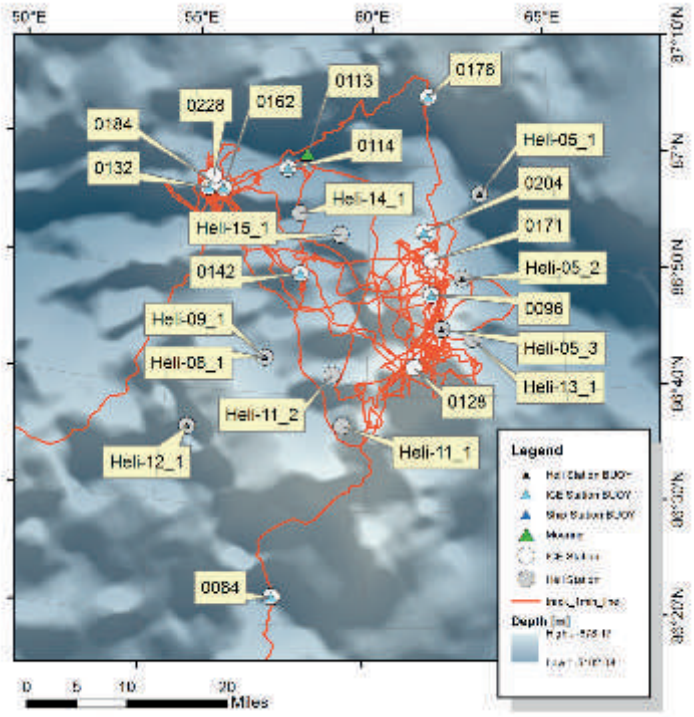

Fig. 10.2: Overview map of all stations of the infrastructure and monitoring programme during PS101: Ice stations (gangway, mummy chair, helicopter), buoy deployments, and mooring sites. An overview of all stations along the cruise track (incl. all underway measurements) is given in Fig. 10.1. Labels give station numbers, but without the leading "PS1010/" string.

Buoys

Five types of autonomous devices (buoys) were deployed for continuous measurements of sea ice, snow, and upper ocean parameters. Photographs of all units are shown in Fig. 10.3:

- Ice Tethered Bio Optical Buoys (ITBOB) prototypes (2 units). ITBOB sensors comprise thermistor chain (air-snow-ice-ocean), solar radiation at the surface and under the ice, web cam, tilt sensor, barometric pressure, as well as an oxygen optode and multi-parameter fluorometer (on 2016M2 only)
- Thermistor String Ice Mass-balance Buoys (IMB, 4 units)
- Snow Buoys (5 units)
- Surface Velocity Profilers (SVP, 4 units with and 4 without drogue)
- GPS trackers (8 units)

In addition to the main parameters, all buoys report their geographical position with each data set. Snow Buoys and SVPs also report directly into the Global Telecommunication System (GTS). Deployment metadata and positions are summarized in Tab. A.5.4.1 and Figs. 10.1 and 10.2.

During ice station PS101/0238-1, three systems were recovered after more than one year of drift through the Arctic Ocean. During PS94, several buoys were deployed together on one floe, as a "Super Buoy Station", on 17 September 2015. Now, we recovered a Snow Buoy (2015S29), a Polar Atmospheric Weather Station (PAWS, 2015A1), and the control unit of a spectral radiation station. Furthermore, the Ice Tethered Profiler (ITP) ITP93 was part of the station, but due to the thick ice (<2m), a recovery was not possible. An IMB was also part of the station, but was completely buried in snow and ice, and thus could not be recovered, too.

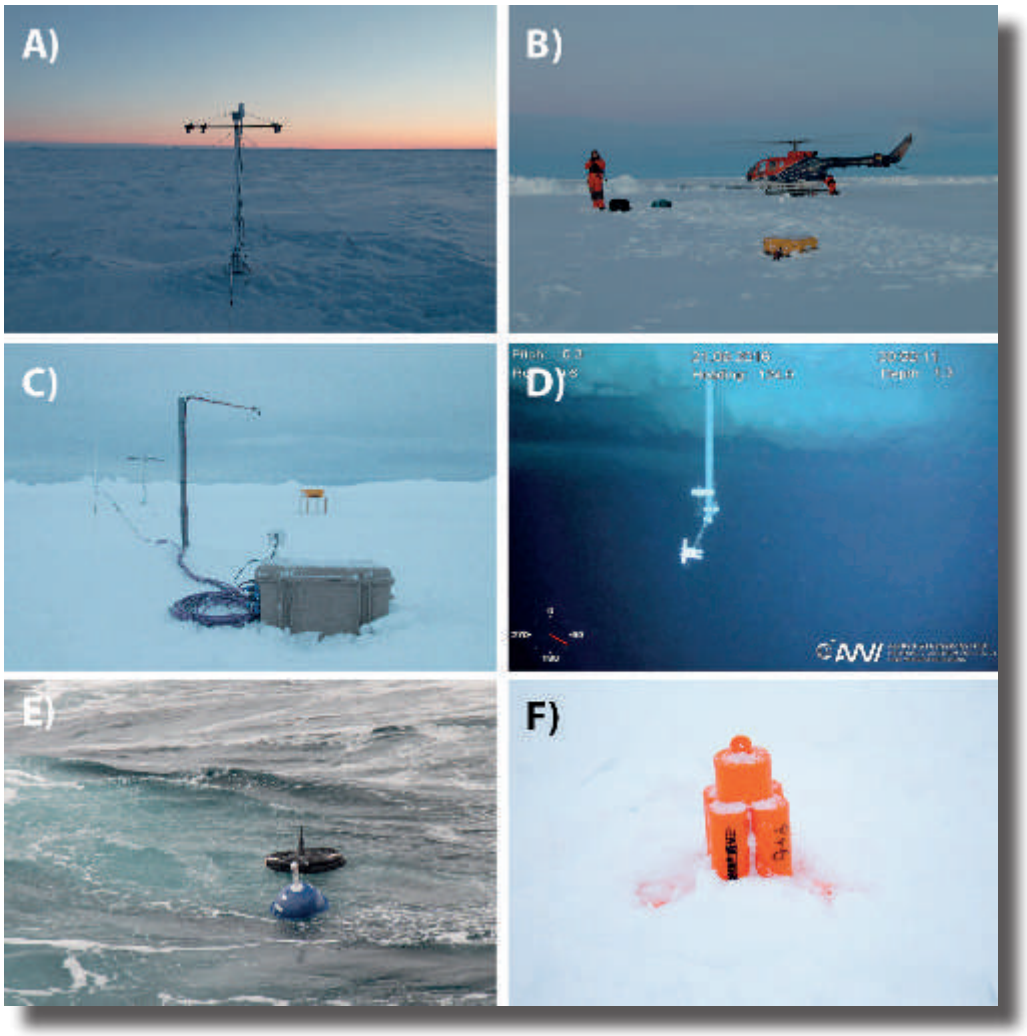

Fig. 10.3: Photographs of the different buoy types deployed during PS101: (a) Snow Buoy 2016S44, (b) Thermistor string Ice Mass-balance Buoy (IMB, yellow box) 2016T35, (c) Ice Tethered Bio Optical Buoy (ITBOB) 2016M2 (with 2016S45 and 2016T21 in the background), (d) Under-ice arm of the ITBOB 2016M2, (e) Surface Velocity Profiler 2016P31, (f) GPS tracker 2016P46.

IceGIS

To ensure safe and efficient ship operations in remote ice covered areas, new satellite and forecast products and sensors systems are currently being developed and validated by a large number of projects. Before the start of the cruise, a concept for a geographical information system was developed, the IceGIS. The system is designed to assist in-field decision making (e.g. sampling, navigation, flight operations, etc.) and improve economic and ecological ship efficiency. The system consists of a web browser-based data viewer (MapViewer, Fig. 10.4) that visualizes relevant satellite and model data together with the ship position and other sensor data. Satellite and model data is provided by space agencies, commercial data providers, weather services and research institutes. Data transfer is done by a separate “pick-up” software. During this cruise, the applicability of different data products, as well as the viewer and pick-up software performance during operations were tested. In addition, various forecast models to simulate ship drift for the next 24 hours were validated. A second aim is to identify strengths and weaknesses of various products. Focus will be placed on the comparison of low and high resolution satellite products (drift, deformation, ice type, etc.), model forecasts from DMI and AWI, and data provided by on-board systems such as an ice radar, thermal

scanner, and a HRPT-receiving station. Whether or not the improved availability of remote sensing and forecast data on board of *Polarstern* has increased vessel performance, will be investigated later by comparing *Polarstern* performance prior and after system installation. The investigation will be based on an analysis of ship performance at different ice conditions using 30 years of engine log data, sea ice observations from bridge and ice conditions obtained from satellite products.

Fig. 10.4: Bridge computer with viewer for data visualization during operation: Here, an up-to-date (3 hours old) Sentinel-1 radar image is displayed together with data from the ship radar and a bathymetric chart.

Ice station work

Characterization of the sea ice cover is crucial for an assessment of the state of the polar climate system. Sea ice thickness datasets are sparse and rarely combine high resolution thickness information and high spatial coverage. Furthermore, instrument design and processing techniques are usually based on a simple 1D representation of the sea ice layer and the ice cover is interpreted as level ice. A multi-frequency device (GEM-2) was used during this expedition. GEM-2 surveys during PS101 are made to resolve with different sounding depths complex and small-scale sea ice thickness and conductivity structures. In addition, snow thickness measurements were made with a Magna Probe along the GEM track. A focus is on the identification of ice and snow thickness values over the 100 x 100 m² transect grid that is surveyed by the ROV from under the ice. In doing so, a later assessment of light transmission through the ice, which is highly dependent on sea-ice and (mainly) snow thicknesses, can be ensured.

The surface properties of sea ice are subject to pronounced changes in the transition from summer to winter. To document surface properties of sea ice in the ROV survey site, a multicopter was equipped with a GoPro camera to obtain aerial images. Images shall help to document spatial variability of surface properties such as ice type, lead position or ridge occurrence.

In the framework of advancing our observational strategies and developing new methods, safety aspects for sea ice work in darkness were evaluated during PS101. Here we made use of the high fidelity infrared camera on the crow's nest of *Polarstern*. The First Navy camera system is usually used for the detection of marine mammals, in particular whales. Here we used it to support the bridge watches for polar bears during ice station work.

To investigate the community living in newly formed sea ice, in total 34 ice cores at 4 stations were taken (see Tab. A.5.4.6). At each station, 3-4 positions with young grey ice (15-30 cm) were drilled, cut into 5-10 cm sections and melted with 70 ‰ PSU salt solution. The melted water was filtered and frozen at -20°C for later analysis. Based on these filters, the 16S and

18S biodiversity of pro- and eukaryotes, respectively, will be analyzed since knowledge about the new ice community is rare. As reference, at each station, one ice core from multiyear ice was sampled and processed in the same way as the new ice samples, except that only the bottom 10 cm were sampled. For each “new ice” DNA core, a temperature and salinity core was taken. Additionally, at each drill hole, a manual CTD cast was performed under newly formed vs. old ice.

A total of 18 sea cores (CORE-MET+CO2) were collected throughout the PS101 cruise, five of which were analyzed at sea for methane and carbon dioxide gas content, as well as $\delta 1^3CCH_4$. One core was subsampled and filtered for organics and biomass. When possible, video footage of the ice core hole and ice-water interface was collected *in-situ* to provide context for the collected core. Of the 18 core holes, nine were recorded with video. Tab. A.5.4.6 provides a summary of the sea ice core collection and analysis.

For comparison to remote sensing data, solar reflectance spectroscopy of the sea ice surface was attempted but low lighting conditions and cloud cover prevented sufficient signal to noise. To circumvent this limitation, surface sea ice samples were then collected, briefly stored at -20°C on the ship, and subsequently analyzed with a visible to near-infrared spectrometer (Analytical Spectral Devices FieldSpec Pro). This spectrometer covers the wavelength range from 0.35-2.5 µm (at a resolution of approximately 0.003 µm at 0.7 µm and 0.01 µm beyond 1.4 µm). The spectrometer was used with a contact probe, in which the instrument fiber is oriented at 23° to a halogen-krypton light source, which is held normal to the sea ice surface. Spectra were also collected of a sea ice core section from a 75-80 cm depth below the surface.

On two ice stations (PS101/0184 and PS101/Heli15/1) a total of additional 9 sea ice cores (CORE-MET) were retrieved and packed for measurements of methane back in Bremerhaven. In addition, snow samples were taken for 3D stratigraphic analysis. For this, the snow pack was cored and samples were stored with minimal disruption of the internal structure.

ROV

The new remotely operated vehicle (ROV) “Beast” was operated for the first time under Arctic sea-ice. The vehicle and respective sensor positions are shown in Fig. 10.5. An overview table of all ROV dives can be found in Tab. A.5.4.2. During six drifting ice-stations a hole was cut through the ice and the ROV deployed into the under-ice environment by using a lifting tripod. Control electronics was mounted in a heated cabin that was lifted by crane onto the ice and pulled with skidoo to the location of the launch hole. Transects were marked both at the surface and underside of the ice using marker sticks lowered through the ice. Along these transects ice and snow thickness were measured by drill holes with additional distributed measurements using a MagnaProbe (SnowHydro) in conjunction with a GEM2 (Geophex) ice-thickness sensor.

During the ROV dives, we characterized the variability of the under-ice light field using hyperspectral Irradiance and Radiance sensors (TriOs RAMSES-ACC/ARC) hyperspectral extinction in seawater was measured along with Salinity, Temperature, dissolved Oxygen concentration, pH and Nitrate concentration both during lateral transects and vertical profiles. Bio-optical properties of the under-ice water were characterized using a Triplet fluorometer (Chlorophyll, CDOM, Backscatter). Sea-ice geometry was scanned with both a high precision altimeter, as well as a upward-looking bathymetric multibeam-sonar. The manipulator arm was used for algae sampling and the setup of under-ice installations. Situational awareness was provided by a scanning imaging sonar as well as a USBL positioning system. All dives were documented with several video-cameras and an upward looking still camera.

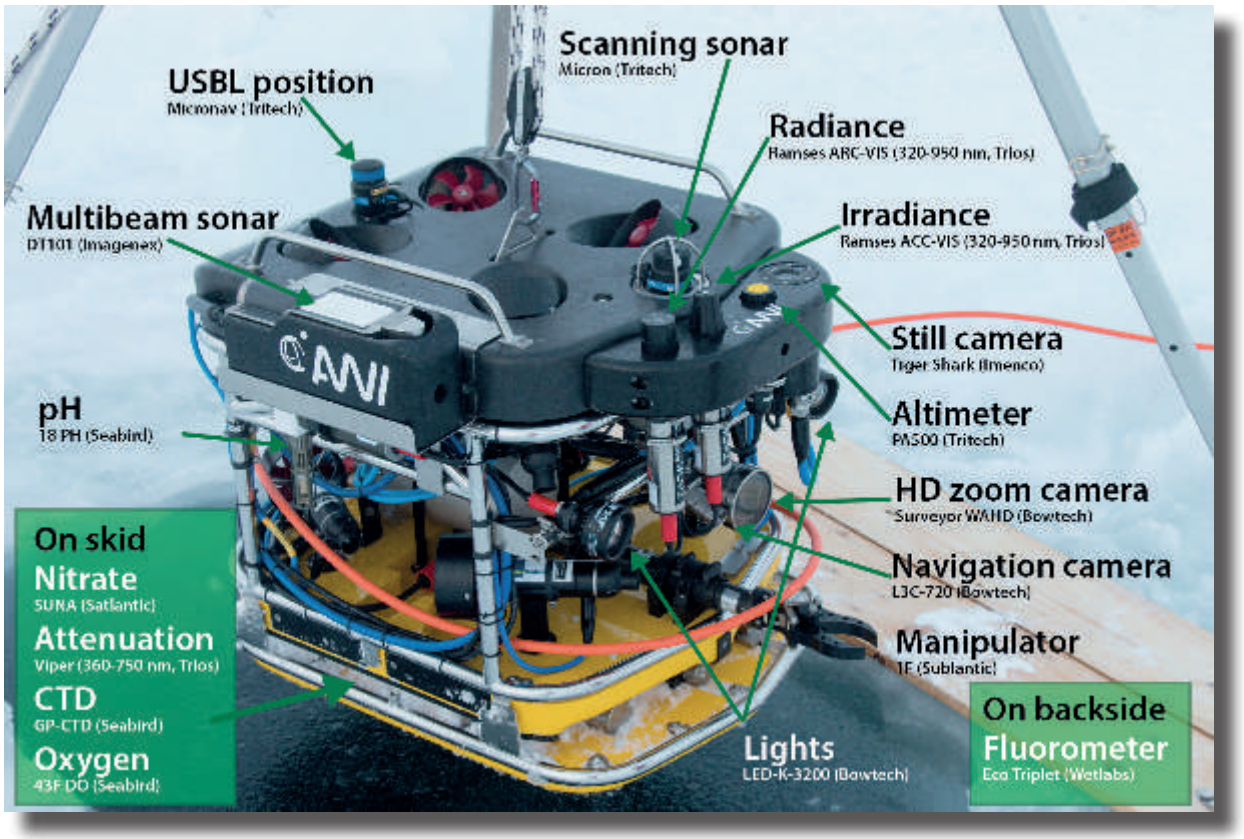

Fig. 10.5: Photograph of the remotely operated vehicle (ROV) "Beast" shortly before deployment through a hole in the sea-ice cover. Sensor positions are indicated by arrows.

Underway sampling and measurements

The nitrate *in-situ* sensors were configured in a pumped system using a SBE5T underwater pump. The Contros HydroC sensor was deployed with its own pump, since it is calibrated by the manufacturer in this configuration. The sensor's behavior and data storage was managed by a central micro controller unit. All sensors and one battery enclosure were combined in a module, deployed on the winch cable, measuring NO_3 and pCO_2 profiles down to about 550 m. To evaluate the sensor's accuracy, discrete water samples were taken from the CTD rosette and analyzed for nitrate using a Quattro auto analyzer (sampled stations and bottles see Tab. A.5.4.4)

Furthermore, a MicroMac nutrient analyzer, developed by the Helmholz-Zentrum Geesthacht, was installed for a second time during the Arctic season, measuring NO_3, NO_2, PO_4 and Si. A Contros HydroFIA TA analyzer was installed to monitor total alkalinity. The data quality of both flow-through systems will be assessed by discrete samples taken from the seawater supply lines. Although nutrients could be directly measured on board with the Quattro analyzer, discrete samples for TA had to be stored for future analysis at AWI using a VINDTA system. The MicroMac nutrient analyzer required calibrating with standard solutions every three days and analytical reagents freshly prepared and loaded into the automated system.

Ice observations from the bridge, using the software based protocol ASSIST were performed during the cruise. The observations are continuations of earlier ice observations made on board of *Polarstern* and are available via the ASSIST database. The aim of the observations is to assist sample and satellite data interpretation and reconstruct ice conditions during the

cruise at a later stage. These underway observations of sea ice were performed from entering the sea ice zone on 12 September until leaving the sea ice on 20 October again. During this time, hourly observations of the sea ice conditions were performed daily from 3:00 to 17:00 UTC as long as sufficient daylight was given.

A First Navy infrared camera system was installed on the crow's nest of *Polarstern*. From this camera, IR photos were recorded in 10 s intervals. The camera was used to observe sea ice conditions, in particular sea ice concentration, along the cruise track, but also to support safe working conditions on the sea ice during darkness. An additional sensor was a hyperspectral radiometer (type Ramses ACC, TriOs GmbH, Rastede, Germany), recording spectral irradiance as a reference for other optical measurements in 10 min intervals. Shorter intervals were set during ice station work as a reference for the ROV measurements.

Additionally, two transects were sampled for analysis of chlorophyll and particulate organic carbon and nitrogen concentration (See Appendix A.5.2) from the seawater supply lines. Over 30 samples were taken at every full degree (latitude) E and W of Svalbard or on a daily basis within the ice covered region (together with the automated sampling, see next part).

Another important point is to monitor phytoplankton species composition and organic parameters like chlorophyll concentration over different temporal and spatial scales. This can also be achieved by automated filtration units that can be controlled via computers. The automated filtration unit (AutoFIM) was successfully tested to collect DNA samples to investigate the species composition over a wide range during previous cruises. However, it is of great interest, whether this system can also be used to sample for other parameters (e.g. chlorophyll concentration or for RNA samples) at very high latitudes.

In total, over 40 stations for Chl, RNA and DNA samples were sampled from the seawater supply lines. First, we sampled a transect E of Svalbard, where samples were taken at every full degree of latitude (74°N until 86°N). A second transect was done on the way back to Bremerhaven west of Svalbard (85°N until 75°N) (see Tab. A.5.4.3 and Fig. 10.1). During the stay in ice covered regions over the Karasik seamount and the vent area, samples were taken on a daily basis or whenever a CTD cast for particular organic matter samples was done (Tab. 10.1).

Physical and biological Oceanography

We started our cruise with a hydrographic section from the Barents Sea shelf at around 81 °N to the Gakkel Ridge (Fig. 10.1). As long as there has been no sea ice we used an underway CTD (UCTD) system which can obtain vertical profiles from the surface to up to 400 m depth. The system (UCTD 10-400) from Oceanscience (Oceanside, USA) was used from the stern of *Polarstern*, mounted on the reeling at the stern portside, to obtain temperature, salinity and pressure profiles while underway. The system contains a Seabird CTD measuring at 16 Hz. The profile depth is limited by the speed of the ship and the length of the cable. We took three profiles of 200 to 250 m depth before we needed to stop because of the first sea ice.

We continued the section with expendable CTDs (XCTD) that can measure vertical profiles from the surface up to 1,000 m depth while underway. The system (XCTD-1) by Tsurumi-Seiki Co. Ltd. (Yokohama, Japan) consisted of a launcher for expendable CTD probes and a mobile deck-unit (MK-150) for data acquisition. The probe sinks down with constant velocity measuring temperature and conductivity. Unfortunately the very thin wire between the probe and the launcher can easily be cut by ice before the profile is finished. That is why we have profiles ranging less than 1,000 m.

At the shelf edge and at Gakkel Ridge we increased the spatial resolution of profiles to better resolve the associated currents. A total of 64 XCTD profiles were taken (See chapter 6). In addition we obtained 32 classical CTD profiles with a rosette system that allows taking water samples at different depths (see chapter 6). These profiles help also monitoring the deeper parts of the Eurasian basin. Temporally distributed over the cruise water samples have been taken parallel to the CTD profiles to measure salinity for the calibration of the conductivity sensors.

The rapid decline in summer sea ice extent and the potential shift of the Arctic Ocean from a light controlled to a nutrient controlled system are strong indicators for a climatic change. Although, the strongest signal is the change in temperature and salinity during the past decade. While waters from the Atlantic became much warmer and saltier, a variability in temperature and salinity of the Pacific inflow over several years has been observed. To monitor these changes affecting the state of water mass distribution and circulation in the Eurasian basin two moorings were deployed during PS94.

To monitor plankton distribution parameters, seawater was analyzed from 14 CTD casts. From the two casts at the mooring positions we analyzed the deeper water layers (500 – 4,000 m) and at the other stations the surface waters (10 – 100 m). At each CTD, different filters for the analysis of organic parameters were taken (see Appendix A.5.2.2). Furthermore, at every shallow CTD, water samples for microscopy were taken and fixed for later classification of species/genera. Additionally, DNA/RNA and chlorophyll filters were taken using the automated filtration device AutoFIM at every CTD position from the ships seawater flow through system from 10 m depth (see Tab. 10.1).

Tab. 10.1: Sample information of AutoFIM sampling events during CTD casts. x indicates data availability.

Date	Station	Latitude	Longitude	Chl filter	DNA filter	RNA filter
2016-09-15	PS101/0055	85°17.726' N	60°02.083' E	x	x	x
2016-09-15	PS101/0058	85°16.646' N	60°09.835' E		x	
2016-09-21	PS101/0112	86°58.794' N	58°.15.434' E	x	x	x
2016-09-21	PS101/0115	86°59.544' N	57°45.338' E		x	
2016-09-24	PS101/0131	86°54.911' N	55°34.115' E	x	x	x
2016-09-27	PS101/0149	86°48.404' N	61°55.702' E	x	x	x
2016-09-30	PS101/0163	86°42.276' N	61°24.704' E	x	x	x
2016-10-02	PS101/0175	87°05.927' N	61°37.476' E	x	x	x
2016-10-03	PS101/0181	86°58.695' N	55°40.723' E	x	x	x
2016-10-06	PS101/0192	86°44.245' N	61°29.302' E	x	x	x
2016-10-06	PS101/0202	86°51.441' N	61°28.736' E	x	x	x
2016-10-07	PS101/0213	86°45.996' N	61°46.873' E	x	x	x
2016-10-15	PS101/0239	82°53.099' N	13°01.418' E	x	x	x
2016-10-16	PS101/0241	80°42.685' N	14°20.277' E	x	x	x

CRDS

During the PS99 to PS101 expeditions, the CRDS instrument was continuously recording the isotopic composition of water vapour in ambient air, alternated with daily measurements of calibration standards. The responsible researchers on board performed daily checks of the instrument and sampling of ocean surface water and carried out small maintenance on the system. This represented an approximate 15 minutes of work per day. Minor troubles were encountered with the calibration system, consisting of a clogging of the glass capillaries used to deliver the liquid water. The frequency of clogging increased from no clogging during the PS99 and PS100 expeditions to about once a week during the last weeks of the PS101 expedition. These problems could be solved easily by cutting the end of the capillary by a researcher, so that the quality of the ambient air isotopic measurements remained unaffected. A full maintenance of the system was planned for the harbour time in Bremerhaven within the end of October/beginning November and will hopefully improve the stability of the calibration system for the next season.

Preliminary (expected) results

Buoys

At the end of the expedition, only two buoys (2016P29 and 2016P32) were not reporting any longer. All other buoys perform as they should. Results will only come in while the buoys report their data over the coming months. Air temperature, barometric pressure, and position are reported in near real time into the Global Telecommunication System (GTS), the International Arctic Buoy Program (IABP), and data are available through meereisportal.de. In addition to these usual results and data streams, buoy positions were imported into the IceGIS system and contributed to drift forecasts to support all the deep sea work.

From the technological point of view, the deployment of the first advanced IMB systems (ITBOB prototypes, 2016M1 and 2016M2) were successful. These units will provide biogeochemical and optical data sets as well as photographs from the sea ice over the coming months. These units will build the basis of further buoy developments in FRAM in the coming years.

IceGIS

During PS101, the performance of individual IceGIS components was assessed. Below, a brief summary of major findings and suggestions for further improvements is given.

Satellite data products obtained on board

- In particular Sentinel-1 data has proven to be a valuable information to support navigation and decision making. On average, Sentinel-1 data provided by Drift & Noise Polar Services were provided 135 minutes after acquisition. Hence, under calm wind conditions with reduced ice drift and rapid data delivery, images can be used to identify bigger lead systems and to reduce travel time between locations. If ice drift velocity increases and data is delivered with a delay of several hours, application for navigation is restricted.

Model/Forecast data products obtained on board

- Different forecast products were tested on board. The HYCOM sea ice forecast provides information about ice drift, ice thickness and concentration. In particular, information about ice drift was of interest for users. Forecasted ice thickness and concentration is

of less applicability. Some ship operations require detailed information about ship drift for the next 12 – 24 hours. To forecast ship drift, 6 different models were tested that made use of local observations, weather forecast data and buoy data. A comparison with the observed ship drift has shown that for short drift stations (less than 4 hours) most accurate drift forecasts are based on local observations only. For longer drift stations and changing wind regimes, forecasts improve if models are driven with weather forecast data from the German Weather Service (DWD).

- *Data transfer on board*
- Transfer of satellite and model/forecast data on board is organized by a “pick-up” software. The software checks various FTP servers of different data providers and downloads data once updates are available. On average, it took 122 minutes for a SAR image to be delivered on board after it was made available by the data provider. The high delay can partially be explained by the intense usage rate and failures of the open port (Iridium) system during the cruise and high demand of other data products. During phases of reduced traffic, SAR data is transmitted within 30 minutes only. To further reduce delay, certain data products such as S1 imagery requires prioritization.

The MapViewer system

The MapViewer system was installed shortly before departure. Therefore, the cruise was used to intensively test the visualization of different data products and report about applicability and user feedback. The overall feedback of scientific users was good and the system itself was widely applied (often as an alternative to ArcGIS or QGIS). The system is complex, but fulfills a wide range of applications such as;

i) Getting a brief overview of current sea ice and weather conditions in the vicinity of the ship and the distance to next waypoint
ii) Planning of ship drift and ice stations
iii) Route planning
iv) Selection of sampling sites
v) Tracking of individual floes

According to scientific users, an improvement of the visualization of vector products (ship track, buoy track, ice drift) is required. A help file for individual data products would further support applicability and data interpretation.

Different to scientific users, the viewer was primarily used by nautical officers to map Sentinel-1 data products. All other remote sensing and model products were of less interest. Officers found the system to be too complex for an easy application. Following changes were requested:

i) Limitation of available data products to Sentinel-1 and ice concentration data
ii) Limitation of the map mode to a “North Up” mode
iii) Improved visualization of delay between image acquisition and delivery

Ice Stations

GEM-2 and magna probe surveys were made during 15 helicopter and ship-based stations. With ship- or handheld-based GPS records, data points were corrected for drift and rotation of the floe relative to the reference position. An example for a resulting grid data file is shown in Fig. 10.6. After the Magna Probe measurements are interpolated to the nearest respective GEM-2 data point the total thickness can be separated into snow and ice thicknesses. Fig. 10.7 summarizes all GEM measurements made between 15 September and 14 October in the survey area. The overall modal thickness (the most frequent ice thickness) amounts

to 1.1 m – 1.3 m. The mean thickness is 1.4 (+- 0.8) m. The average snow thickness obtained from Magna Probe measurements is 0.18 m. Note that although GEM and Magna Probe data were obtained on an almost daily basis at representative locations along the ship track, the ground-based ice and snow thickness surveys are limited to large floes and predominantly level ice thick enough to walk on.

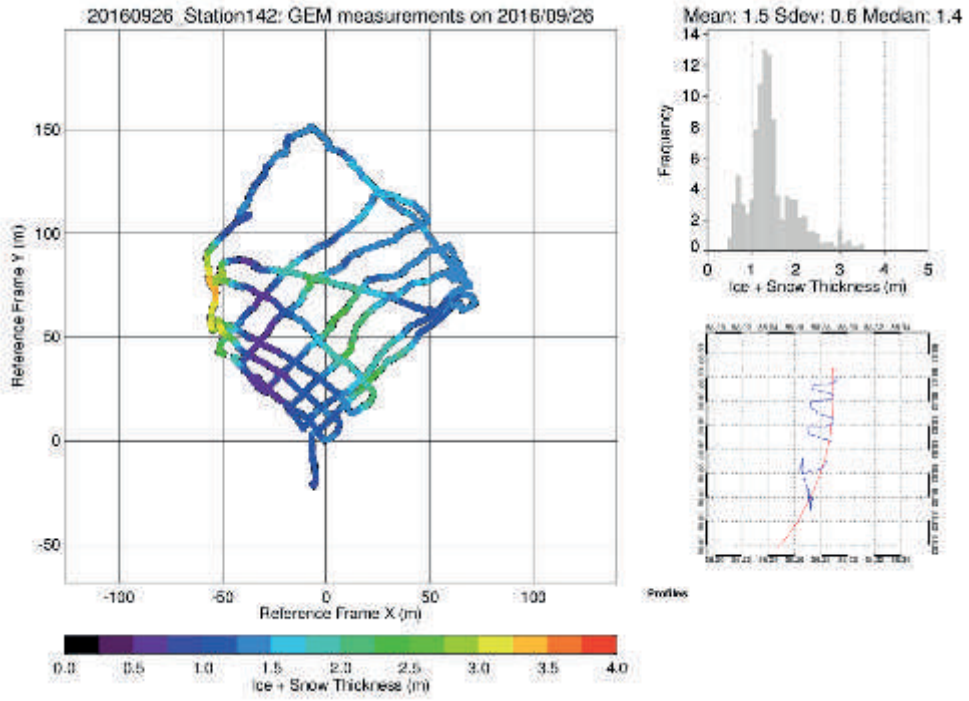

Fig. 10.6: GEM ice thickness grid obtained on ROV survey site on 26 September (Station PS101/0142).The left panel shows the thickness survey. The color coding corresponds to the ice thickness + snow thickness (m) as derived from GEM measurements. The upper right panel shows the corresponding thickness histogram. The lower right panel indicates GPS positions of GEM measurements (blue) and GPS reference station (red).

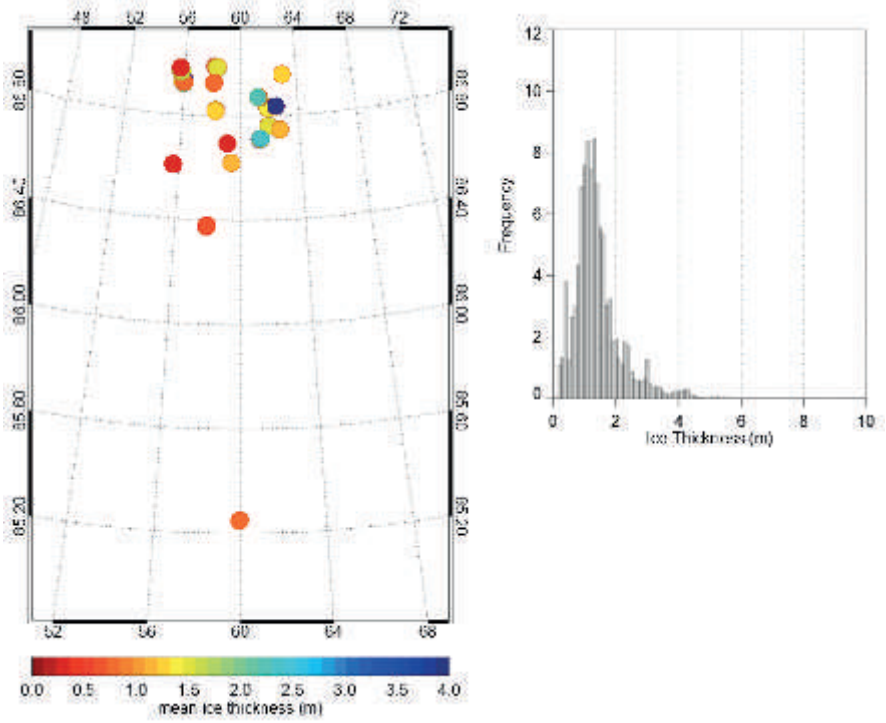

Fig. 10.7: Summary of all 15 GEM surveys made along ship track between 15 September and 14 October. The map shows all positions and the histogram the overall thickness distribution from all stations.

Strong winds and low temperatures limited applicability of the mulitcopter system. Hence, data was obtained only during 2 ice stations: Station PS101/0057 (15 September) and station PS101/0142 (26 September). From the obtained GoPro video, single images were extracted and a mosaic of the ROV site was created. And example is given in Fig. 10.8.

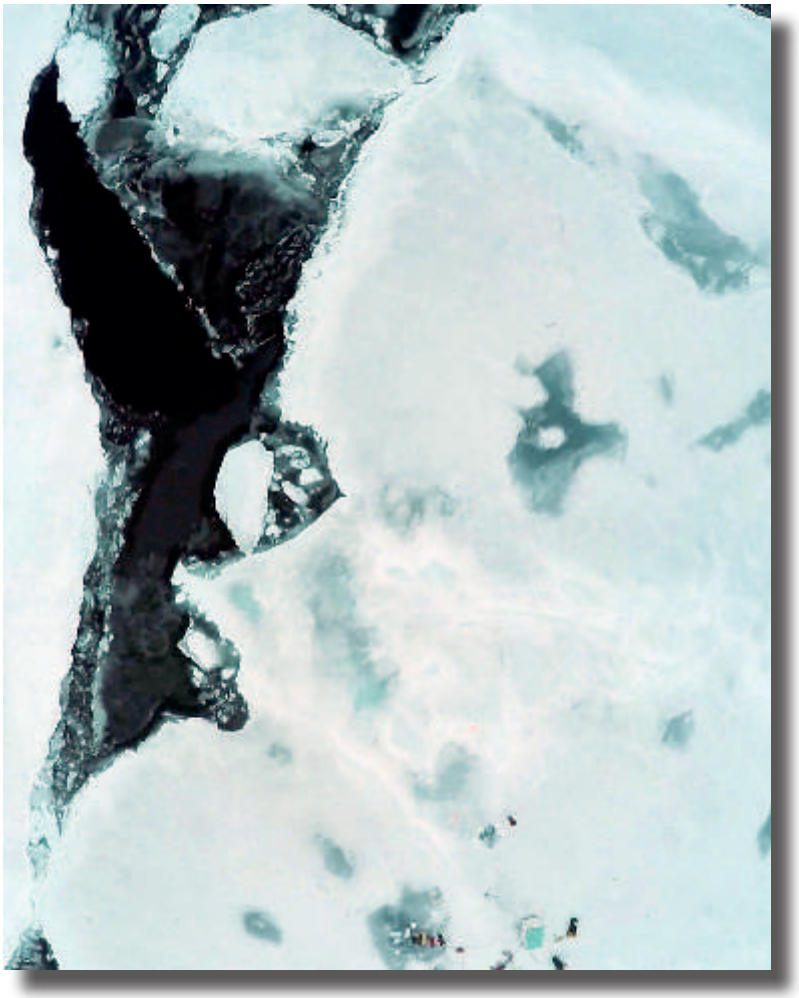

Fig. 10.8: Aerial image obtained over the ROV site on September 15. Images are used to document sea ice conditions and surface properties for ROV data interpretation.

DNA isolation will be performed after the cruise at the laboratories of the AWI in Bremerhaven in cooperation with the MPI in Bremen. First microscopy results show that the first year ice community appears to be similar to the phytoplankton community, with centric diatoms being the most abundant diatoms (Fig. 10.9). In contrast, old ice is mostly inhabited by pennate diatoms, which is in accordance to literature.

Results to date show gas signatures within the upper section of the cores that largely match typical atmospheric and ocean concentrations and isotopic signatures (approximately 2.4 nM and -45‰). No significant venting or plume formation was discovered over the Karasik seamount, or along Langseth Ridge, which eliminated the possibility of plume methane capture in the overlying sea ice. Interestingly, however, the methane-rich plume discovered in the Gakkel Ridge (at approximately 87N, 56E – see Chapter 6) was found to rise to a region 400-600 m above the seafloor, thus validating the hypothesis that an active, shallow seamount or massif could deliver material to the ice water interface.

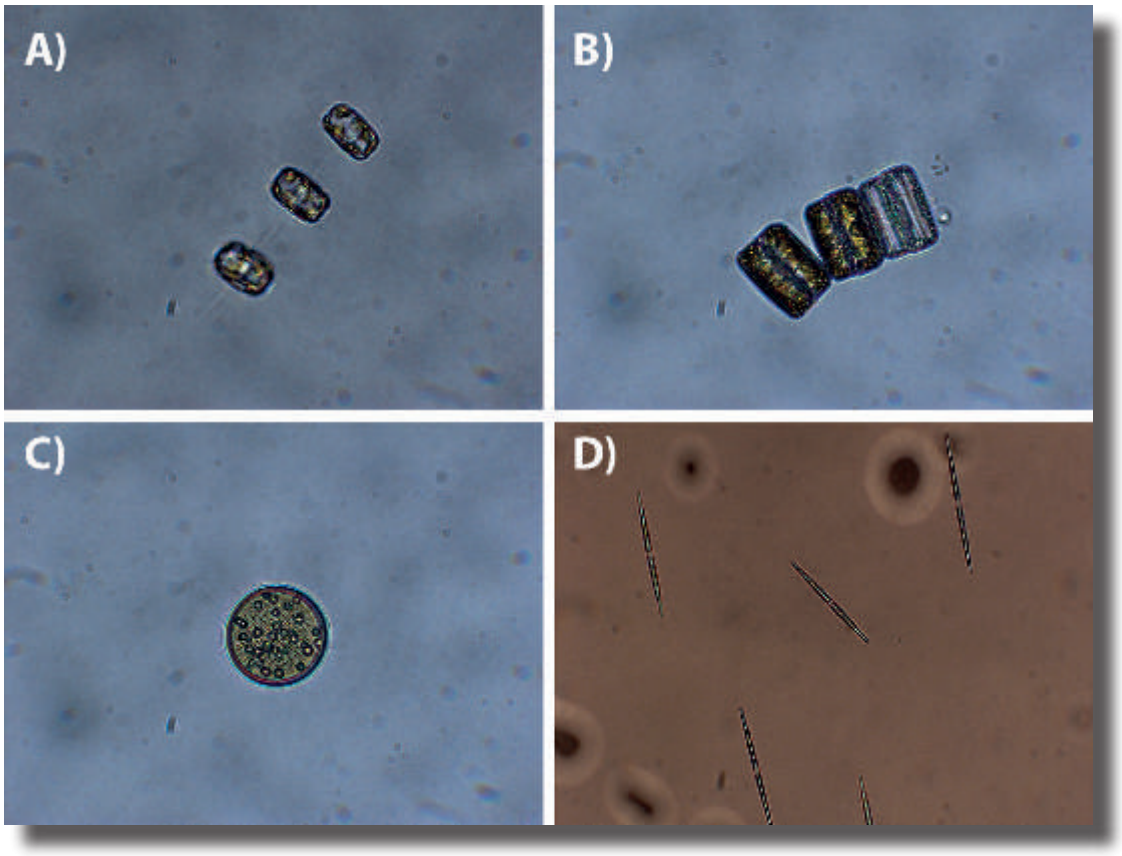

Fig. 10.9: Microscopy pictures of typical diatoms of the two different ice types sampled. A-C: centric diatoms in young grey ice, magnification 40x. D: pennate diatoms in multi-year ice, magnification 25x.

During the video examination of the ice core holes drilled on 29 September 2016 at Station 162, the sea ice algae *Melosira arctica* was observed. *Melosira* can be seen for much of the 360° panoramic view of the ice water interface, and filaments reaching >20 cm in length were recorded. Fig. 10.9 provides an image frame from the video, showing filaments in the foreground.

Visible and near-infrared spectra show nearly pure ice in both the surface and ice core contact spectra. Fig. 10.10 shows the log of ice cores collected. Initial analyses show no indication of salts, brine inclusions, or organic material, but further work is needed. The variation in reflectance between 1 µm and 2.5 µm is highly diagnostic of ice grain size. The sample analyzed and shown in Fig. 10.11 indicates grains of average diameter of 200 µm, 500 µm, and approximately 1 mm, for the upper, middle, and bottom spectra, respectively. Such assessments are important for remote sensing analyses of the sea ice surface and snow cover.

The spectra of the sea ice core were, not surprisingly, dominated by larger grains (e.g. bottom spectrum in Fig. 10.12), but in several regions gas bubbles and fractures increased scattering, likely leading to the increased longer wavelength reflectance seen in the upper spectra. Future work will interrogate these samples, with non-destructive and destructive techniques for organic and salt content, as well as gas composition.

Status	Core #	Date collected	Station ID	Sample ID	Total length (cm)	Number of sections	Section lengths (cm)	Vac sea
Analyzed onboard/Picarro	1	15-Sep-16	PS101/0057-1	PS101.057.PSTAR.IC01	100	3	0-40, 40-70, 70-90	
Analyzed onboard/Picarro	2	"	"	PS101.057.PSTAR.IC02	90	4	0-25, 25-50, 50-70, 70-90	
Stored (-20C)	3	16-Sep-16	PS101/Heli-4/1	PS101.Heli-4.PSTAR.IC03	112	6	0-15, 15-35, 35-55, 55-75, 75-95, 95-112	
Stored (-20C)	4	17-Sep-16	PS101/0084-1	PS101.084.PSTAR.IC04	77	4	~20 cm each: 0-20, 20-40, 40-60, 60-77	
Subsampled	5	19-Sep-16	PS101/0096-1	PS101.096.PSTAR.IC05	190	5	0-40, 40-80, 80-115, 115-150, 150-190	
Stored (-20C)	6	19-Sep-16	"	PS101.096.PSTAR.IC06	180	7	0-30, 40-80 (30-40 was slush), 70-95 (60-70 was slush), 95-115, 115-140, 140-165, 165-182	
Stored (-20C)	7	21-Sep-16	PS101/0114-1	PS101.114.PSTAR.IC07	108	4	0-25, 25-50, 50-75, 75-108	
Analyzed onboard/Picarro-GC	8	21-Sep-16	"	PS101.114.PSTAR.IC08	116	4	0-25, 25-57, 57-80, 80-114	
Stored (-20C)	9	23-Sep-16	PS101/0128-1	PS101.128.PSTAR.IC09	20	1	0-20 cm, Grey	
Stored (-20C)	10	23-Sep-16	"	PS101.128.PSTAR.IC10	20	1	0-20 cm, Grey	
Stored (-20C)	11	23-Sep-16	"	PS101.128.PSTAR.IC11	120	3	0-35, 35-78, 78-120	
Analyzed onboard/Picarro-GC	12	23-Sep-16	"	PS101.128.PSTAR.IC12	117	4	0-37, 37-87, 87-92, 92-117	
Stored (-20C)	13	29-Sep-16	PS101/0162-1	PS101.162.PSTAR.IC13	97	3	0-35, 35-60, 60-97	
Stored (-20C)	14	29-Sep-16	"	PS101.162.PSTAR.IC14	80	3	0-30, 30-43, 43-84	
Stored (-20C)	15	29-Sep-16	"	PS101.162.PSTAR.IC15	76	2	0-35, 35-78, 78-120	
Stored (-20C)	16	10-Oct-16	PS101/0228-1	PS101.228.PSTAR.IC16	24	1	0-24	
Stored (-20C)	17	10-Oct-16	"	PS101.228.PSTAR.IC17	24	1	0-24	
Analyzed onboard/Picarro-GC	18	10-Oct-16	"	PS101.228.PSTAR.IC18	23	1	0-25	

Fig. 10.10: Ice core collection and analysis log for PS101 (K.P. Hand)

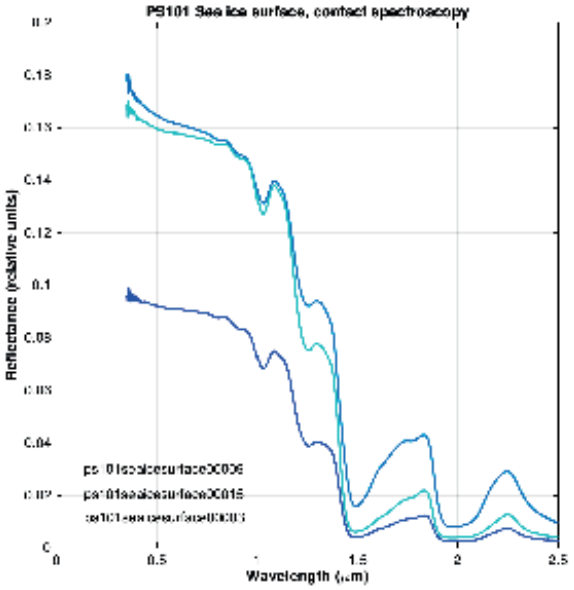

Fig. 10.11: Visible and near-infrared contact spectroscopy of large and small grained sea ice surface. No clear non-ice components were initially measured

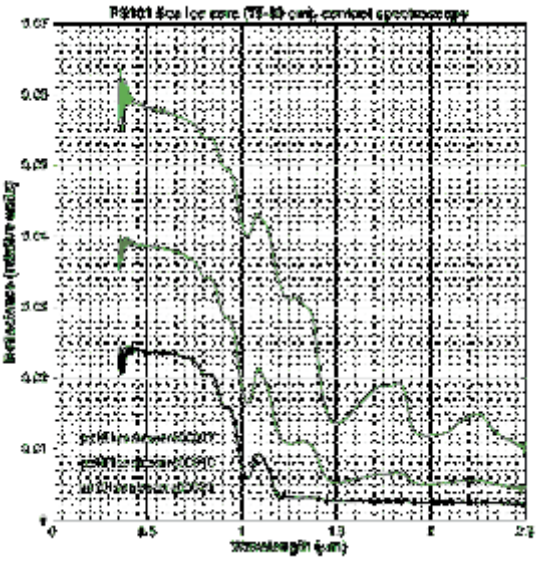

Fig. 10.12: Visible and near-infrared spectra of a core section at a depth of 75 to 80 cm below the surface. Though this section is from deeper in the ice core, and likely grown slower than the uppermost sections, no obvious non-ice components were visible in the initial analyses.

Using the infrared camera system to improve polar bear safety during sea ice stations was highly appreciated by all bear watches on the bridge. The additional possibility to see polar bears in a larger distance through their infrared signature added to the safety aspects especially, but not only, during darkness. However, only one individual polar bear was seen during the entire cruise and this one was more than 500 m away from the ship. Hence, a direct application and more detailed results on the advances could not be achieved, But following persons walking on the ice for sea ice thickness measurements allowed to judge the visibility of persons in a far distance, as it will appear during ice camps in polar night (e.g. with respect to the planned MOSAiC drift in 2019/20). The results also show the strong impact of fog on the infrared visibility. This effect dominated most observations, because of the overall very foggy weather during the expedition.

ROV

The main goal of demonstrating the vehicle's capabilities for under-ice research was reached by successful deployment on six sea-ice stations. Deployment procedures could be easily adapted from earlier work with more lightweight vehicles. Apart from minor issues, the highly complex system performed very well even in the harsh weather conditions prevailing during this cruise. No failures occurred due to cold temperatures and scientific data was successfully acquired on all stations. Several problems located during the first dives could be resolved in the following. One of the main issues was acoustic interference of the MicronNav (Tritech, UK) USBL positioning system with the POSIDONIA transponders whenever devices equipped with POSIDONIA were used on *Polarstern*. Restricting the use of POSIDONIA to times where it was absolutely necessary allowed for good USBL positioning and thus high quality science data.

The ROV proved useful in the deployment of an ITBOB prototype buoy (see above), as the under-ice light sensors were tilted during deployment and ROV intervention successfully re-leveled the sensors. The station work was able to extend existing time series data of sea-ice optical properties into the freeze-up period, also including measurements under newly formed and snow covered sea-ice. An exemplary map of sea-ice light transmittance can be found in

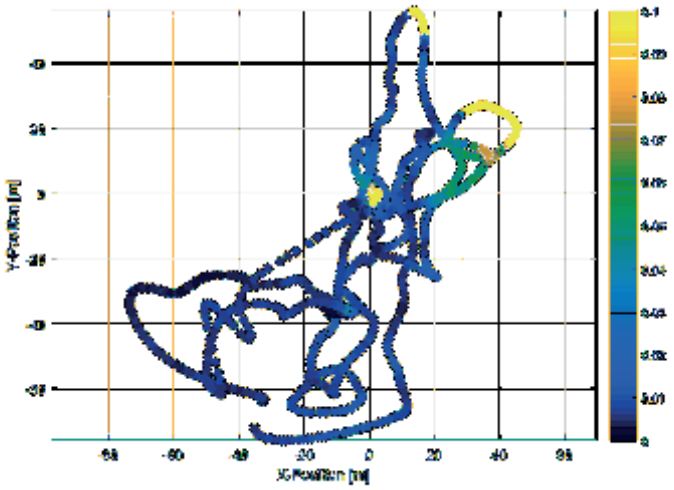

Fig. 10.13: Map of light transmittance as measured with the ROV during sea-ice station PS101/0171. Position is given in a floe-fixed coordinate frame in meters from the deployment hole. Bright colors indicate high light transmittance, as caused by the launch hole and two stretches where the ROV was diving out to open waters in the top right corner.

Fig. 10.13.

Underway sampling and measurements

The deployment of the nitrate and pCO2 sensor module attached to the CTD was successful. A data set of in total 7 stations could be obtained. The water samples taken from the Niskin bottles were analyzed and already used to process the ISUS nitrate data. For the evaluation of the HydroFIA TA analyzer and HydroC pCO_2 sensor discrete samples were taken and will be measured with the VINDTA system at AWI after *Polarstern* returns at the end of October. The flow through nutrient analyzer worked as expected. Only some minor technical issues occurred but could be solved during the cruise. An evaluation of the data will be done in collaboration with the HZG to assure good data quality.

Ice observations started after entering the ice and ended on 17 October, when leaving the ice. During the cruise, observations were carried out from the bridge between 3 am to 17 UTC. In total, 428 observations were made, reporting on sea ice type, topography, snow cover, etc. Data will be processed and made available after the cruise.

Physical and biological Oceanography

Preliminary temperature and salinity profiles from the XCTD measurements show the signature of the Atlantic Water inflow from the Fram Strait as a subsurface warm and salty core hugging the continental slope underneath fresher surface waters (see maps Figs 10.1 and 10.2 and sections in Fig. 10.14).

A backup of all mooring sensor data except for the acoustic recorder was saved. A water sampler (type RAS 500) attached to the Nansen basin mooring was recovered for the first time in the Central Arctic. It provides 24 samples taken on a two-week rhythm for sensor data processing and further biochemical analyzes at AWI. The upper sediment trap of the Nansen basin mooring did not work as expected. Regarding to its log file a technical problem occurred during the transition from sample bottle 11 to sample bottle 12. A reliable operation can be confirmed until the 15. May 2016. Details on the recovered instrumentation may be found in Tab. A.5.4.7.

The AutoFIM device sampled successfully for the first time at high latitudes and very cold conditions. Samples will be analyzed in the laboratory of the AWI Bremerhaven.

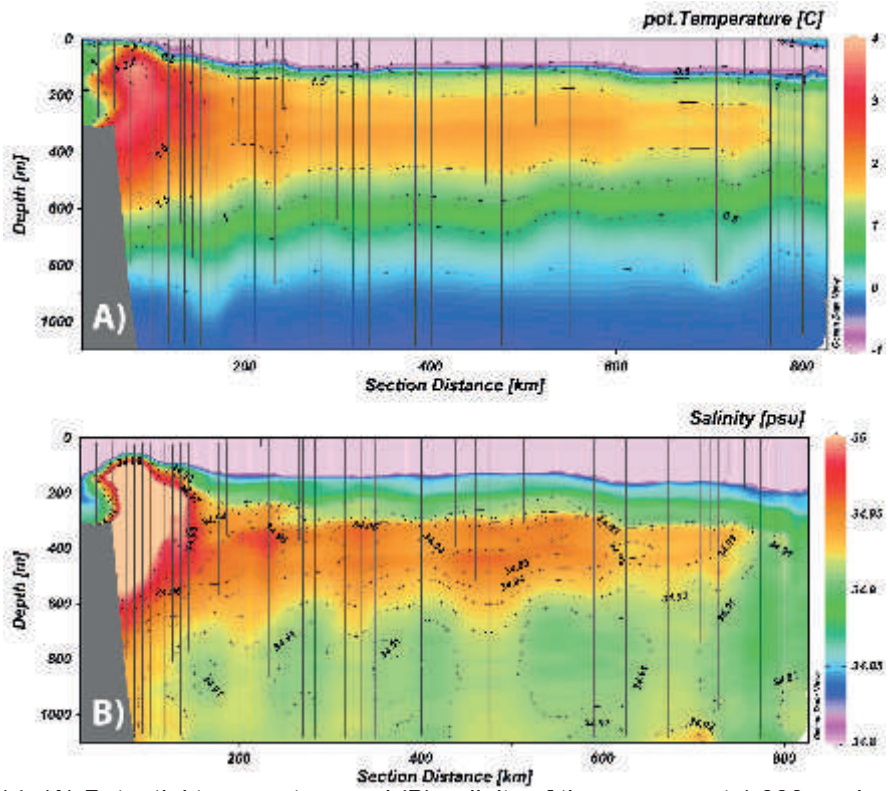

Fig. 10.14: (A) Potential temperature and (B) salinity of the uppermost 1,000 m along the Gakkel Ridge section, as derived from XCTD measurements. The position of all measurements is shown in Fig. 10.1.

Data management

All data from the sea ice stations, incl. the ROV based measurements, require post-processing after the cruise. The sensor data will be made publically available in the PANGAEA database within one year. Video recordings are archived in the AWI data archiving system. Visual sea ice observation data will be distributed by a standardized database at the International Arctic Research Center, University of Alaska, Fairbanks, and are already available through the PANGAEA repository. Buoy data and all associated metadata are available online in near real time through data.meereisportal.de, after completion of their drift, the final data set will be processed and published through PANGAEA. Data obtained by the IceGIS system during PS101 will be archived at the AWI for later use. Whether this data will be made available in the PANGAEA database is currently under discussion.

The calibration and final processing of the mooring data will take place after completion of the mission, and the data will be delivered to the PANGAEA database. The Underway nutrient data will be post processed and quality assured data will be uploaded to PANGAEA.

Data from the rosette-mounted CTD, XCTD, and UCTD collected during PS101 will be delivered after post-cruise calibration to the PANGAEA database and to the appropriate national data centers.

All raw isotopic data will be uploaded to the PANGAEA database. Final data will also be uploaded after processing and post-operative calibration. Unrestricted access to the data will be granted within 2-3 years, pending analysis and publication.

A.1 TEILNEHMENDE INSTITUTE/ PARTICIPATING INSTITUTES

	Address
AWI	Alfred Wegener Institute Helmholtz Centre for Polar and Marine Research Am Handelshafen 12 27515 Bremerhaven Germany
DWD	Deutscher Wetterdienst Geschäftsbereich Wettervorhersage Seeschifffahrtsberatung Bernhard Nocht Str. 76 20359 Hamburg Germany
FIELAX	FIELAX Gesellschaft für wiss. Datenverarbeitung mbH Schleusenstr. 14 D-27568 Bremerhaven Germany
GEOMAR	GEOMAR | Helmholtz Centre for Ocean Research Kiel Marine Microbiology Westshore Campus Düsternbrooker Weg 20 D-24105 Kiel
HeliService	HeliService international GmbH Am Luneort 15 27572 Bremerhaven Germany
iSiTEC	iSiTEC GmbH Bussestr. 27 27570 Bremerhaven Germany
Lehigh University	Lehigh University 27 Memorial Dr W Bethlehem PA 18015 USA
MARUM	MARUM Center for Marine Environmental Research University Bremen Leobener Str. D-28359 Bremen Germany

	Address
MPI-Bremen	HGF MPG Research Group on Deep Sea Ecology and Technology Max-Planck-Institute for Marine Microbiology Celsiusstr. 1 28359 Bremen Germany
NASA-JPL	NASA - Jet Propulsion Laboratory California Institute of Technology M/S 301-260 4800 Oak Grove Drive Pasadena CA 91109-8099 USA
Reederei Laeisz	Reederei F. Laeisz GmbH Trostbrücke 1 20457 Hamburg Germany
Senckenberg	Senckenberg am Meer Abteilung DZMB Südstrand 44 D-26382 Wilhelmshaven
Shirshov Institute (IORAS)	P.P. Shirshov Institute of Oceanology Russian Academy of Sciences Laboratory of Plankton Ecology Biological Department 36 Nakhimova ave. Moscow 117997 Russia
UHB-GEO	Fachbereich 5 Geowissenschaften der Universität Bremen GEO Gebäude Klagenfurter Straße 28359 Bremen Germany
UHB-IUP	Universität Bremen Institut für Umweltphysik/ Sektion Ozeanographie Otto Hahn Allee 1; Gebäude: NW1 28359 Bremen Germany
WHOI	Woods Hole Oceanographic Institution 86 Water St. Woods Hole, MA 02543-1050 USA

Associated Institutes	Address
ACFR	Australian Centre for Field Robotics The Rose Street Building J04 Shepherd Street University of Sidney NSW 2006 Australia
AIST	National Institute of Advanced Industrial Science and Technology Tsukuba Central 7 1-1-1 Higashi Ibaraki 305-8567 Japan
UHH	Universität Hamburg Faculty of Mathematics, Informatics and Natural Sciences Department of Biology Institut für Hydrobiologie und Fischereiwissenschaft Große Elbstraße 133 22767 Hamburg Germany
UiB	University of Bergen Thormøhlensgt. 53 A/B Bergen Norway

A.2 FAHRTTEILNEHMER / CRUISE PARTICIPANTS

Last Name/ Nachname	Given name, Vorname	Institute/ Institut	Profession;/ Beruf	Discipline/ Fachrichtung
Boetius	Antje	AWI	Chief scientist	Biologist
Albers	Elmar	MARUM	PhD student,	Petrology
Baeger	Jana	AWI	Technician,	Geomicrobiology
Bailey	John	WHOI	Engineer, nUI ROV	Mechanical Engineer
Barz	Jakob	AWI	Technician,	Geomicrobiology
Biebow	Harald	iSiTEC	Engineer, OFOS	Electrical Engineering
Branch	Andrew	NASA JPL	Engineer, nUI ROV	Computer Engineering
Dannheim	Jennifer	AWI	Scientist, Fauna	Biology
Diehl	Alexander	MARUM	Group leader, PhD student,	Petrology
Doll	Mechthild	Uni Bremen	Group leader, Student, Heat-flow	Geology
Dreutter	Simon	AWI	Scientist, seafloor observation	Cartography
George	Kai Horst	Senckenberg	Group leader, Fauna	Biology
German	Chris	WHOI	Group leader, nUI ROV	Geology
Gischler	Michael	HeliService	Helicopter	Mechanic
Gregalis	Jan	HeliService	Helicopter	Pilot
Hand	Kevin	NASA JPL	Scientist, nUI ROV	Planetary Science
Hehemann	Laura	AWI	Scientist, seafloor observation	Cartography
Hempelt	Juliane	DWD	DWD	Meteorology
Hildebrandt	Nicole	AWI	Group leader, Zooplankton	Biology
Horn	Myriel	AWI	PhD Student, FRAM	Oceanography
Jacobs	Mirta	AWI	PhD Student, Plankton	Biology
Jager	Harold	HeliService	Helicopter	Pilot
Jakuba	Mike	WHOI	Engineer, nUI ROV	Electrical Engineer
Katlein	Christian	AWI	Scientist, FRAM Sea-ice physics	Ice Physics
Kieneke	Alexander	Senckenberg	Scientist, Fauna	Biology
Köhler	Janna	IUP Uni Bremen	Scientist,	Oceanography
Kosobokova	Ksenia	IORAS	Scientist, Zooplankton	Biology
Krumpen	Thomas	AWI	Scientist, Sea-ice physics	Ice Physics

Last Name/ Nachname	Given name, Vorname	Institute/ Institut	Profession;/ Beruf	Discipline/ Fachrichtung
Machado	Casey	WHOI	Engineer, nUI ROV	ROV Pilot
McDermott	Jill	Lehigh University	Scientist,	Vent chemistry
Miller	Max	DWD	DWD	Meteorolgy
Molari	Massimiliano	AWI	Scientist,	Geomicrobiology
Müller	Paulina	Uni Bremen	Student, Heat-flow	Geology
Nicolaus	Marcel	AWI	Group leader, Sea-ice physics	Ice Physics
Nordhausen	Axel	MPI	Technician, Coring	Mechanical Engineer
Purser	Autun	AWI	Groupleader Seafloor obs.	Biologist
Richter	Roland	HeliService	Helicopter	Engineer
Rößler	Sebastian	FIELAX	GIS, Data management	Cartography
Schiller	Martin	AWI	Engineer, Sea-ice physics	Ice Physics Technician
Schmidtmann	Linn	AWI	Student, Fauna (Foraminifera)	Biology
Scholz	Daniel	AWI	Engineer, FRAM chemistry	Oceanography Technician
Schramm	Fabian	MPI/MARUM	Technician, Coring and OFOS	Technician
Slaby	Beate	GEOMAR	PhD student, Macrofauna	Biology
Stecher	Anique	AWI	Group leader, Plankton	Biology
Steinmacher	Bermann	AWI/Uni Bremen	Student, FRAM	Oceanography
Suman	Stefano	WHOI	Engineer, nUI ROV	Computer Engineering
Tardeck	Frederic	FIELAX	GIS, Data management	Cartography
Vonnahme	Tobias	AWI	Student,	Geomicrobiology
Walter	Maren	Uni Bremen	Group leader,	Oceanography
Wegener	Gunter	AWI	Group leader,	Geomicrobiology
Whitcomb	Louis	JHU, WHOI	Engineer, nUI ROV	Electrical Engineering
Wischnewski	Laura	AWI	Technician, FRAM chemistry	Lab Technician

A.3 SCHIFFSBESATZUNG / SHIP'S CREW

No.	Name	Rank
1.	Schwarze, Stefan	Master
2.	Grundmann, Uwe	1. Offc.
3.	Farysch, Bernd	Ch. Eng.
4.	Fallei, Holger	2. Offc
5.	Hering, Igor	2. Offc
6.	Janik, Michael	2. Offc
7.	Scholl, Thomas	Doctor
8.	Fröb, Martin	R. Offc.
9.	Grafe, Jens	2. Eng.
10.	Krinfeld, Oleksandr	2. Eng.
11.	Holst, Wolfgang	3. Eng.
12.	Redmer, Jens	Elec. Eng.
13.	Christian, Boris	ELO
14.	Hüttebräucker, Olaf	ELO
15.	Pliet, Johannes	ELO
16.	Himmel, Frank	ELO
17.	Loidl, Reiner	Boatsw.
18.	Reise, Lutz	Carpenter
19.	Brück, Sebastian	A.B.
20.	Bäcker, Andreas	A.B.
21.	Hagemann, Manfred	A.B.
22.	Leisner, Bert	A.B.
23.	Scheel, Sebastian	A.B.
24.	Schröder, Horst	A.B.
25.	Völker, Frank Rainer	A.B.
26.	Wende, Uwe	A.B.
27.	Winkler, Michael	A.B.
28.	Preußner, Jörg	Storek.
29.	Lamm, Gerd	Mot-man
30.	Rhau, Lars-Peter	Mot-man
31.	Teichert, Uwe	Mot-man
32.	Schwarz, Uwe	Mot-man
33.	Schünemann, Mario	Mot-man
34.	Redmer, Klaus-Peter	Cook
35.	Martens, Michael	Cooksmate
36.	Silinski, Frank	Cooksmate
37.	Czyborra, Bärbel	1. Stwdess
38.	Wöckener, Martina	2. Stwdess / Nurse
39.	Arendt, René	2. Steward
40.	Dibenau, Torsten	2. Steward
41.	Duka, Maribel	2. Stwdess
42.	Silinski, Carmen	2. Stwdess
43.	Sun, Yong Shen	2. Steward
44.	Yu, Kwok Yuen	Laundrym.

A.4 STATIONSLISTE / STATION LIST PS101

Gear abbreviations:

ADCP	Acoustic Doppler Current Profiler
AUV	Autonomous underwater vehicle
BC	Box corer
BUOY	Buoy
CTD/UW	CTD, underway
CTD/RO	CTD/Rosette
DRG_C	Dredge, chain bag
XCTD	Expendable CTD
GC	Gravity corer
HF	Heat-Flow probe
HS_PS	HydroSweep/ParaSound Profile
ICE	Ice station
ISP	In situ pump
LOKI	Lightframe onsight keyspecies investigation
MAPR	Miniature Autonomous Plume Recorder
MTL	Miniaturized temperature logger
MOR	Mooring
MUC	MultiCorer
TVMUC	Multicorer with television
MN	Multiple opening/closing net
OFOS	Ocean Floor Observation System
ROV	Remotely operated vehicle

In the following list all position and depth information marked from position sensor SHIP are based on GPS positions and multibeam echosounder's center beam depth. Position and depth information from position sensor USBL are based on the acoustic underwater positioning system Posidonia (in the Station List these data are marked in bold in the column "Gear"). The depth is the gear's / transponder depth.

Online Data:

A digital copy of the overleaf station book can be downloaded directly from PANGAEA here: https://doi.pangaea.de/10.1594/PANGAEA.869409

The underwater USBL track data can be downloaded directly from PANGAEA here: https://doi.pangaea.de/10.1594/PANGAEA.869118

Station	Date Time	Position Lat	Position Lon	Depth [m]	Gear	Action
PS101/001-1	2016-09-09 T21:08	72° 00.06' N	022° 27.29' E	361	BUOY	on ground/ max depth
PS101/002-1	2016-09-10 T02:32	73° 05.19' N	023° 41.72' E	359	BUOY	on ground/ max depth
PS101/003-1	2016-09-10 T12:46	74° 59.79' N	026° 00.97' E	216	BUOY	on ground/ max depth
PS101/004-1	2016-09-10 T15:41	75° 33.31' N	026° 41.71' E	191	CTD/ UW	profile start
PS101/004-1	2016-09-10 T15:44	75° 33.90' N	026° 42.45' E	181	CTD/ UW	profile end
PS101/005-1	2016-09-10 T17:57	75° 59.88' N	027° 15.10' E	238	BUOY	on ground/ max depth
PS101/006-1	2016-09-11 T08:15	78° 50.15' N	031° 17.46' E	111	CTD/ UW	profile start
PS101/006-1	2016-09-11 T08:21	78° 51.13' N	031° 19.00' E	128	CTD/ UW	profile end
PS101/007-1	2016-09-11 T12:17	79° 31.20' N	030° 03.14' E		LOKI	profile start
PS101/007-1	2016-09-11 T12:20	79° 31.19' N	030° 03.07' E		LOKI	profile end
PS101/008-1	2016-09-11 T12:54	79° 31.18' N	030° 02.85' E	222	MN	on ground/ max depth
PS101/009-1	2016-09-11 T13:35	79° 31.37' N	030° 03.30' E	220	CTD/ RO	on ground/ max depth
PS101/010-1	2016-09-11 T17:09	80° 01.70' N	030° 03.91' E	271	**OFOS**	profile start
PS101/010-1	2016-09-11 T18:16	80° 01.57' N	030° 08.14' E	258	OFOS	profile end
PS101/011-1	2016-09-11 T22:33	80° 45.48' N	029° 31.66' E	457	CTD/ UW	profile start
PS101/011-1	2016-09-11 T23:29	80° 54.65' N	029° 31.72' E	299	CTD/ UW	profile end
PS101/012-1	2016-09-12 T00:00	81° 01.68' N	029° 31.48' E	300	XCTD	on ground/ max depth
PS101/013-1	2016-09-12 T01:01	81° 11.54' N	029° 31.30' E	314	XCTD	on ground/ max depth
PS101/014-1	2016-09-12 T02:23	81° 20.78' N	029° 31.36' E	305	XCTD	on ground/ max depth
PS101/015-1	2016-09-12 T03:51	81° 30.71' N	029° 34.74' E	902	XCTD	on ground/ max depth
PS101/016-1	2016-09-12 T04:36	81° 34.57' N	029° 47.70' E	1638	XCTD	on ground/ max depth
PS101/017-1	2016-09-12 T05:26	81° 39.76' N	029° 51.52' E	2442	XCTD	on ground/ max depth
PS101/018-1	2016-09-12 T06:12	81° 44.44' N	029° 47.25' E	2830	XCTD	on ground/ max depth
PS101/019-1	2016-09-12 T06:51	81° 48.82' N	029° 50.90' E	3104	XCTD	on ground/ max depth
PS101/020-1	2016-09-12 T07:35	81° 53.55' N	029° 57.15' E	3234	XCTD	on ground/ max depth
PS101/021-1	2016-09-12 T08:24	81° 57.51' N	029° 59.24' E	3284	XCTD	on ground/ max depth

Station	Date Time	Position Lat	Position Lon	Depth [m]	Gear	Action
PS101/021-2	2016-09-12 T08:49	81° 59.65' N	030° 04.25' E	3312	XCTD	on ground/ max depth
PS101/022-1	2016-09-12 T09:18	82° 02.27' N	030° 04.84' E	3388	XCTD	on ground/ max depth
PS101/023-1	2016-09-12 T10:04	82° 06.78' N	030° 14.16' E	3343	XCTD	on ground/ max depth
PS101/024-1	2016-09-12 T10:54	82° 11.30' N	030° 33.99' E	3350	XCTD	on ground/ max depth
PS101/025-1	2016-09-12 T11:40	82° 15.60' N	030° 52.91' E	3315	XCTD	on ground/ max depth
PS101/026-1	2016-09-12 T12:25	82° 20.04' N	031° 02.86' E	3354	XCTD	on ground/ max depth
PS101/027-1	2016-09-12 T13:02	82° 24.14' N	031° 13.68' E	3378	XCTD	on ground/ max depth
PS101/028-1	2016-09-12 T13:50	82° 28.85' N	031° 19.92' E	3431	XCTD	on ground/ max depth
PS101/029-1	2016-09-12 T14:42	82° 33.27' N	031° 32.55' E	3463	XCTD	on ground/ max depth
PS101/030-1	2016-09-12 T14:52	82° 34.21' N	031° 36.03' E	3464	XCTD	on ground/ max depth
PS101/031-1	2016-09-12 T15:36	82° 37.74' N	031° 38.67' E	3512	XCTD	on ground/ max depth
PS101/031-2	2016-09-12 T15:43	82° 38.27' N	031° 39.19' E	3514	XCTD	on ground/ max depth
PS101/032-1	2016-09-12 T17:00	82° 42.31' N	031° 39.95' E	3557	XCTD	on ground/ max depth
PS101/033-1	2016-09-12 T18:03	82° 46.87' N	031° 55.13' E	3583	XCTD	on ground/ max depth
PS101/034-1	2016-09-12 T19:13	82° 51.52' N	032° 05.49' E	3642	XCTD	on ground/ max depth
PS101/035-1	2016-09-12 T20:02	82° 56.02' N	032° 14.20' E	3694	XCTD	on ground/ max depth
PS101/036-1	2016-09-12 T20:50	83° 00.71' N	032° 23.99' E	3728	XCTD	on ground/ max depth
PS101/037-1	2016-09-12 T22:31	83° 09.50' N	032° 45.54' E	3790	XCTD	on ground/ max depth
PS101/038-1	2016-09-12 T22:49	83° 11.18' N	032° 48.50' E	3795	XCTD	on ground/ max depth
PS101/039-1	2016-09-13 T00:18	83° 18.16' N	032° 59.00' E	3838	XCTD	on ground/ max depth
PS101/040-1	2016-09-13 T02:13	83° 27.16' N	033° 22.02' E	3929	XCTD	on ground/ max depth
PS101/041-1	2016-09-13 T04:15	83° 36.19' N	033° 26.72' E	3954	XCTD	on ground/ max depth
PS101/042-1	2016-09-13 T06:00	83° 45.11' N	033° 40.89' E	3968	XCTD	on ground/ max depth
PS101/043-1	2016-09-13 T08:11	83° 54.61' N	034° 23.12' E	3996	XCTD	on ground/ max depth
PS101/044-1	2016-09-13 T11:38	84° 02.87' N	034° 46.78' E	3971	**CTD/ RO**	on ground/ max depth
PS101/045-1	2016-09-13 T15:41	84° 12.15' N	034° 53.05' E	4005	XCTD	on ground/ max depth

Station	Date Time	Position Lat	Position Lon	Depth [m]	Gear	Action
PS101/046-1	2016-09-13 T18:04	84° 20.60' N	035° 56.60' E	4007	XCTD	on ground/ max depth
PS101/047-1	2016-09-13 T20:29	84° 30.01' N	037° 42.19' E	3993	XCTD	on ground/ max depth
PS101/048-1	2016-09-13 T22:31	84° 35.42' N	039° 27.86' E	3984	XCTD	on ground/ max depth
PS101/049-1	2016-09-14 T00:28	84° 40.03' N	040° 53.91' E	3979	XCTD	on ground/ max depth
PS101/050-1	2016-09-14 T04:08	84° 48.43' N	044° 08.99' E	3968	XCTD	on ground/ max depth
PS101/051-1	2016-09-14 T07:49	84° 59.43' N	047° 23.09' E	3952	XCTD	on ground/ max depth
PS101/052-1	2016-09-14 T11:33	85° 07.83' N	051° 08.36' E	3935	XCTD	on ground/ max depth
PS101/053-1	2016-09-14 T11:58	85° 06.09' N	051° 31.87' E	3929	BUOY	on ground/ max depth
PS101/054-1	2016-09-14 T15:28	85° 12.84' N	054° 45.34' E	3921	XCTD	on ground/ max depth
PS101/055-1	2016-09-14 T22:50	85° 17.28' N	060° 09.60' E	3879	CTD/ RO	on ground/ max depth
PS101/055-1a	2016-09-14 T21:24	85° 17.34' N	060° 07.60' E	3882	ISP	profile start
PS101/055-1a	2016-09-15 T04:07	85° 17.78' N	060° 13.01' E	3881	ISP	profile end
PS101/055-1b	2016-09-14 T21:28	85° 17.34' N	060° 07.74' E	3884	ISP	profile start
PS101/055-1b	2016-09-15 T04:03	85° 17.77' N	060° 12.87' E	3880	ISP	profile end
PS101/055-1c	2016-09-14 T21:46	85° 17.32' N	060° 08.31' E	3881	ISP	profile start
PS101/055-1c	2016-09-15 T03:46	85° 17.73' N	060° 12.32' E	3878	ISP	profile end
PS101/055-1d	2016-09-14 T21:48	85° 17.32' N	060° 08.36' E	3880	ISP	profile start
PS101/055-1d	2016-09-15 T03:43	85° 17.72' N	060° 12.24' E	3882	ISP	profile end
PS101/055-1e	2016-09-14 T21:51	85° 17.32' N	060° 08.45' E	3878	ISP	profile start
PS101/055-1e	2016-09-15 T03:42	85° 17.72' N	060° 12.21' E	3879	ISP	profile end
PS101/055-1f	2016-09-14 T22:08	85° 17.30' N	060° 08.87' E	3881	ISP	profile start
PS101/055-1f	2016-09-15 T03:21	85° 17.66' N	060° 11.62' E	3882	ISP	profile end
PS101/055-1g	2016-09-14 T22:11	85° 17.30' N	060° 08.94' E	3881	ISP	profile start
PS101/055-1g	2016-09-15 T03:19	85° 17.65' N	060° 11.57' E	3878	ISP	profile end
PS101/055-1i	2016-09-14 T21:28	85° 17.34' N	060° 07.74' E	3884	MAPR	profile start
PS101/055-1i	2016-09-15 T04:02	85° 17.77' N	060° 12.84' E	3881	MAPR	profile end

Station	Date Time	Position Lat	Position Lon	Depth [m]	Gear	Action
PS101/056-1	2016-09-15 T05:20	85° 17.62' N	060° 03.28' E	3882	MOR	on ground/ max depth
PS101/057-1	2016-09-15 T08:55	85° 17.08' N	060° 10.23' E	3882	ICE	on ground/ max depth
PS101/058-1	2016-09-15 T10:07	85° 16.75' N	060° 10.08' E	3883	CTD/ RO	on ground/ max depth
PS101/059-1	2016-09-15 T10:44	85° 16.55' N	060° 09.56' E	3879	LOKI	profile start
PS101/059-1	2016-09-15 T11:56	85° 16.11' N	060° 07.37' E	3886	LOKI	profile end
PS101/060-1	2016-09-15 T13:59	85° 15.44' N	060° 01.58' E	3882	MN	on ground/ max depth
PS101/061-1	2016-09-15 T18:12	85° 14.70' N	059° 57.57' E	3834	**MUC**	on ground/ max depth
PS101/062-1	2016-09-15 T21:08	85° 13.85' N	060° 00.16' E	3824	**MUC**	on ground/ max depth
PS101/063-1	2016-09-15 T23:59	85° 12.34' N	060° 00.67' E	3880	MUC	on ground/ max depth
PS101/064-1	2016-09-16 T03:33	85° 13.48' N	059° 51.20' E	3847	**BC**	on ground/ max depth
PS101/065-1	2016-09-16 T06:19	85° 13.17' N	059° 50.13' E	3903	**BC**	on ground/ max depth
PS101/066-1	2016-09-16 T09:19	85° 12.71' N	059° 54.22' E	3837	**BC**	on ground/ max depth
PS101/067-1	2016-09-16 T12:07	85° 17.10' N	059° 53.54' E	3888	LOKI	profile start
PS101/067-1	2016-09-16 T13:13	85° 16.87' N	059° 52.36' E	3883	LOKI	profile end
PS101/068-1	2016-09-16 T15:13	85° 16.74' N	059° 50.93' E	3849	**OFOS**	profile start
PS101/068-1	2016-09-16 T17:45	85° 17.03' N	059° 53.56' E	3882	OFOS	profile end
PS101/069-1	2016-09-16 T19:22	85° 17.12' N	059° 59.51' E	3890	HF	profile start
PS101/069-1	2016-09-16 T21:53	85° 17.22' N	060° 05.80' E	3884	HF	profile end
PS101/070-1	2016-09-17 T00:41	85° 22.62' N	059° 43.59' E	3886	XCTD	on ground/ max depth
PS101/071-1	2016-09-17 T01:48	85° 27.25' N	059° 34.03' E	3896	XCTD	on ground/ max depth
PS101/072-1	2016-09-17 T02:52	85° 32.15' N	059° 32.98' E	3892	XCTD	on ground/ max depth
PS101/073-1	2016-09-17 T04:00	85° 37.34' N	059° 24.51' E	3048	XCTD	on ground/ max depth
PS101/074-1	2016-09-17 T04:58	85° 42.48' N	059° 07.63' E	3729	XCTD	on ground/ max depth
PS101/075-1	2016-09-17 T06:01	85° 48.28' N	058° 55.97' E	3552	XCTD	on ground/ max depth
PS101/076-1	2016-09-17 T06:53	85° 52.60' N	059° 14.89' E	3884	XCTD	on ground/ max depth
PS101/077-1	2016-09-17 T07:46	85° 57.62' N	058° 52.95' E	3857	XCTD	on ground/ max depth

Station	Date Time	Position Lat	Position Lon	Depth [m]	Gear	Action
PS101/078-1	2016-09-17 T09:03	86° 03.00' N	058° 16.37' E	2868	XCTD	on ground/ max depth
PS101/079-1	2016-09-17 T09:53	86° 07.24' N	058° 12.29' E	3317	XCTD	on ground/ max depth
PS101/080-1	2016-09-17 T11:18	86° 12.83' N	057° 48.96' E	2427	XCTD	on ground/ max depth
PS101/081-1	2016-09-17 T11:55	86° 17.49' N	057° 56.90' E	2548	XCTD	on ground/ max depth
PS101/082-1	2016-09-17 T13:26	86° 19.27' N	057° 47.09' E	3098	**HF**	profile start
PS101/082-1	2016-09-17 T16:58	86° 21.14' N	057° 53.78' E	3759	**HF**	profile end
PS101/083-1	2016-09-17 T17:36	86° 21.91' N	057° 54.17' E	3873	XCTD	on ground/ max depth
PS101/084-1	2016-09-17 T18:10	86° 22.34' N	057° 54.09' E	3870	ICE	on ground/ max depth
PS101/085-1	2016-09-17 T20:03	86° 27.82' N	057° 41.11' E	2915	XCTD	on ground/ max depth
PS101/086-1	2016-09-17 T21:20	86° 32.23' N	059° 40.22' E	1523	XCTD	on ground/ max depth
PS101/087-1	2016-09-17 T22:27	86° 37.30' N	060° 13.92' E	1457	XCTD	on ground/ max depth
PS101/088-1	2016-09-18 T00:30	86° 42.95' N	061° 01.94' E	825	**CTD/ RO**	on ground/ max depth
PS101/088-10	2016-09-18 T04:24	86° 43.61' N	061° 33.48' E	615	**CTD/ RO**	on ground/ max depth
PS101/088-11	2016-09-18 T04:44	86° 43.74' N	061° 35.98' E	651	**CTD/ RO**	on ground/ max depth
PS101/088-12	2016-09-18 T05:03	86° 43.87' N	061° 38.48' E	644	**CTD/ RO**	on ground/ max depth
PS101/088-13	2016-09-18 T05:24	86° 44.00' N	061° 41.40' E	647	**CTD/ RO**	on ground/ max depth
PS101/088-14	2016-09-18 T06:04	86° 44.24' N	061° 47.49' E	661	**CTD/ RO**	on ground/ max depth
PS101/088-15	2016-09-18 T06:24	86° 44.35' N	061° 50.89' E	639	**CTD/ RO**	on ground/ max depth
PS101/088-16	2016-09-18 T06:45	86° 44.47' N	061° 54.44' E	644	**CTD/ RO**	on ground/ max depth
PS101/088-17	2016-09-18 T07:05	86° 44.56' N	061° 57.65' E	645	**CTD/ RO**	on ground/ max depth
PS101/088-1a	2016-09-18 T00:12	86° 42.85' N	061° 00.84' E	302	**MAPR**	profile start
PS101/088-1a	2016-09-18 T07:18	86° 44.66' N	062° 00.41' E	47	**MAPR**	profile end
PS101/088-1b	2016-09-18 T00:12	86° 42.85' N	061° 00.84' E	302	**MAPR**	profile start
PS101/088-1b	2016-09-18 T07:16	86° 44.65' N	062° 00.19' E	20	**MAPR**	profile end
PS101/088-2	2016-09-18 T00:40	86° 43.03' N	061° 02.73' E	405	**CTD/ RO**	on ground/ max depth
PS101/088-3	2016-09-18 T01:49	86° 42.53' N	061° 19.48' E	611	**CTD/ RO**	on ground/ max depth

Station	Date Time	Position Lat	Position Lon	Depth [m]	Gear	Action
PS101/088-4	2016-09-18 T02:29	86° 42.81' N	061° 22.30' E	639	**CTD/ RO**	on ground/ max depth
PS101/088-5	2016-09-18 T02:50	86° 42.96' N	061° 23.98' E	645	**CTD/ RO**	on ground/ max depth
PS101/088-6	2016-09-18 T03:09	86° 43.09' N	061° 25.57' E	580	**CTD/ RO**	on ground/ max depth
PS101/088-7	2016-09-18 T03:28	86° 43.22' N	061° 27.28' E	622	**CTD/ RO**	on ground/ max depth
PS101/088-8	2016-09-18 T03:47	86° 43.36' N	061° 29.13' E	637	**CTD/ RO**	on ground/ max depth
PS101/088-9	2016-09-18 T04:06	86° 43.49' N	061° 31.31' E	595	**CTD/ RO**	on ground/ max depth
PS101/089-1	2016-09-18 T09:28	86° 42.18' N	061° 13.05' E	567	**OFOS**	profile start
PS101/089-1	2016-09-18 T14:51	86° 44.02' N	061° 30.01' E	608	**OFOS**	profile end
PS101/089-1a	2016-09-18 T09:21	86° 42.17' N	061° 12.14' E	214	**MAPR**	profile start
PS101/089-1a	2016-09-18 T14:52	86° 44.04' N	061° 29.87' E	574	**MAPR**	profile end
PS101/090-1	2016-09-18 T16:54	86° 42.50' N	061° 25.87' E	684	LOKI	profile start
PS101/090-1	2016-09-18 T17:16	86° 42.53' N	061° 28.09' E	674	LOKI	profile end
PS101/091-1	2016-09-18 T18:08	86° 42.62' N	061° 33.19' E	676	MN	on ground/ max depth
PS101/092-1	2016-09-18 T19:45	86° 42.61' N	061° 19.56' E	663	**BC**	on ground/ max depth
PS101/092-1a	2016-09-18 T19:45	86° 42.61' N	061° 19.56' E	663	**MTL**	profile start
PS101/092-1a	2016-09-18 T19:47	86° 42.61' N	061° 19.70' E	643	**MTL**	profile end
PS101/093-1	2016-09-18 T20:34	86° 42.54' N	061° 19.80' E	622	**BC**	on ground/ max depth
PS101/093-1a	2016-09-18 T20:34	86° 42.54' N	061° 19.80' E	622	**MTL**	profile start
PS101/093-1a	2016-09-18 T20:36	86° 42.54' N	061° 19.90' E	656	**MTL**	profile end
PS101/094-1	2016-09-18 T21:23	86° 42.54' N	061° 20.40' E	699	**BC**	on ground/ max depth
PS101/094-1a	2016-09-18 T21:23	86° 42.54' N	061° 20.40' E	699	**MTL**	profile start
PS101/094-1a	2016-09-18 T21:25	86° 42.54' N	061° 20.49' E	645	**MTL**	profile end
PS101/095-1	2016-09-18 T22:36	86° 46.03' N	061° 29.04' E	1130	HS_PS	profile start
PS101/095-1	2016-09-19 T02:37	86° 46.67' N	060° 44.86' E	2179	HS_PS	profile end
PS101/096-1	2016-09-19 T04:00	86° 48.84' N	061° 38.83' E	1059	ICE	on ground/ max depth
PS101/097-1	2016-09-19 T05:29	86° 49.21' N	061° 43.63' E	875	**CTD/ RO**	on ground/ max depth

Station	Date Time	Position Lat	Position Lon	Depth [m]	Gear	Action
PS101/097-1a	2016-09-19 T05:10	86° 49.13' N	061° 42.63' E	20	**MAPR**	profile start
PS101/097-1a	2016-09-19 T07:45	86° 49.66' N	061° 50.54' E	21	**MAPR**	profile end
PS101/097-1b	2016-09-19 T05:10	86° 49.13' N	061° 42.63' E	20	**MAPR**	profile start
PS101/097-1b	2016-09-19 T07:40	86° 49.65' N	061° 50.34' E	23	**MAPR**	profile end
PS101/097-2	2016-09-19 T05:58	86° 49.33' N	061° 45.30' E	795	**CTD/ RO**	on ground/ max depth
PS101/097-3	2016-09-19 T06:14	86° 49.39' N	061° 46.21' E	796	**CTD/ RO**	on ground/ max depth
PS101/097-4	2016-09-19 T06:27	86° 49.43' N	061° 46.93' E	803	**CTD/ RO**	on ground/ max depth
PS101/097-5	2016-09-19 T06:43	86° 49.49' N	061° 47.81' E	830	**CTD/ RO**	on ground/ max depth
PS101/097-6	2016-09-19 T06:58	86° 49.54' N	061° 48.51' E	828	**CTD/ RO**	on ground/ max depth
PS101/097-7	2016-09-19 T07:16	86° 49.59' N	061° 49.37' E	859	**CTD/ RO**	on ground/ max depth
PS101/098-1	2016-09-19 T10:25	86° 49.79' N	061° 53.24' E	1024	**MUC**	on ground/ max depth
PS101/099-1	2016-09-19 T11:34	86° 49.74' N	061° 52.03' E	908	MN	on ground/ max depth
PS101/100-1	2016-09-19 T14:32	86° 49.39' N	061° 57.84' E	988	**OFOS**	profile start
PS101/100-1	2016-09-19 T17:24	86° 47.93' N	061° 52.11' E	722	**OFOS**	profile end
PS101/100-1a	2016-09-19 T13:08	86° 49.62' N	062° 04.50' E	20	**MAPR**	profile start
PS101/100-1a	2016-09-19 T17:37	86° 47.73' N	061° 50.39' E	120	**MAPR**	profile end
PS101/100-1b	2016-09-19 T13:48	86° 49.56' N	062° 03.17' E	1272	**MTL**	profile start
PS101/100-1b	2016-09-19 T17:24	86° 47.93' N	061° 52.11' E	722	**MTL**	profile end
PS101/101-1	2016-09-19 T19:40	86° 42.29' N	061° 18.36' E	635	**MUC**	on ground/ max depth
PS101/102-1	2016-09-19 T20:35	86° 42.68' N	061° 19.35' E	645	**MUC**	on ground/ max depth
PS101/103-1	2016-09-19 T21:26	86° 42.56' N	061° 18.78' E	633	**MUC**	on ground/ max depth
PS101/104-1	2016-09-19 T22:13	86° 42.59' N	061° 18.62' E	634	**MUC**	on ground/ max depth
PS101/105-1	2016-09-19 T23:00	86° 42.62' N	061° 18.11' E	521	**GC**	on ground/ max depth
PS101/105-1a	2016-09-19 T23:00	86° 42.62' N	061° 18.11' E	521	**MTL**	profile start
PS101/105-1a	2016-09-19 T23:02	86° 42.61' N	061° 18.00' E	624	**MTL**	profile end
PS101/106-1	2016-09-19 T23:40	86° 42.59' N	061° 18.55' E	647	**GC**	on ground/ max depth

Station	Date Time	Position Lat	Position Lon	Depth [m]	Gear	Action
PS101/106-1a	2016-09-19 T23:40	86° 42.59' N	061° 18.55' E	647	**MTL**	profile start
PS101/106-1a	2016-09-19 T23:42	86° 42.61' N	061° 20.05' E	645	**MTL**	profile end
PS101/107-1	2016-09-20 T01:11	86° 41.52' N	060° 44.67' E	1035	HF	profile start
PS101/107-1	2016-09-20 T05:03	86° 40.29' N	060° 24.44' E	1589	**HF**	profile end
PS101/108-1	2016-09-20 T08:55	86° 43.78' N	061° 09.84' E	1267	MN	on ground/ max depth
PS101/109-1	2016-09-20 T11:35	86° 42.49' N	061° 08.27' E	551	**CTD/ RO**	on ground/ max depth
PS101/109-1a	2016-09-20 T11:24	86° 42.54' N	061° 08.51' E	21	**MAPR**	profile start
PS101/109-1a	2016-09-20 T11:45	86° 42.39' N	061° 07.95' E	39	**MAPR**	profile end
PS101/110-1	2016-09-20 T14:17	86° 41.30' N	061° 03.94' E	1059	ROV	profile start
PS101/110-1	2016-09-20 T15:57	86° 40.56' N	061° 03.01' E	1503	ROV	profile end
PS101/111-1	2016-09-20 T16:39	86° 40.31' N	061° 02.68' E	1460	HS_PS	profile start
PS101/111-1	2016-09-20 T20:37	86° 59.92' N	058° 20.25' E	4860	HS_PS	profile end
PS101/112-1	2016-09-20 T22:46	86° 59.58' N	058° 09.35' E	4851	CTD/ RO	on ground/ max depth
PS101/112-1a	2016-09-20 T21:01	86° 59.97' N	058° 10.25' E	4774	ISP	profile start
PS101/112-1a	2016-09-21 T04:16	86° 58.72' N	058° 16.21' E	4690	ISP	profile end
PS101/112-1b	2016-09-20 T21:05	86° 59.96' N	058° 10.12' E	4776	ISP	profile start
PS101/112-1b	2016-09-21 T04:12	86° 58.74' N	058° 16.02' E	4700	ISP	profile end
PS101/112-1c	2016-09-20 T21:22	86° 59.92' N	058° 09.83' E	4789	ISP	profile start
PS101/112-1c	2016-09-21 T03:54	86° 58.79' N	058° 15.44' E	4712	ISP	profile end
PS101/112-1d	2016-09-20 T21:42	86° 59.86' N	058° 09.65' E	4794	ISP	profile start
PS101/112-1d	2016-09-21 T03:32	86° 58.84' N	058° 14.99' E	4732	ISP	profile end
PS101/112-1e	2016-09-20 T21:45	86° 59.84' N	058° 09.62' E	4815	ISP	profile start
PS101/112-1e	2016-09-21 T03:30	86° 58.85' N	058° 14.93' E	4732	ISP	profile end
PS101/112-1f	2016-09-20 T22:04	86° 59.75' N	058° 09.59' E	4840	ISP	profile start
PS101/112-1f	2016-09-21 T03:06	86° 58.92' N	058° 14.39' E	4756	ISP	profile end
PS101/112-1g	2016-09-20 T22:06	86° 59.74' N	058° 09.60' E	4842	ISP	profile start

Station	Date Time	Position Lat	Position Lon	Depth [m]	Gear	Action
PS101/112-1g	2016-09-21 T03:04	86° 58.92' N	058° 14.35' E	4754	ISP	profile end
PS101/112-1i	2016-09-20 T21:06	86° 59.95' N	058° 10.09' E	4775	MAPR	profile start
PS101/112-1i	2016-09-21 T04:12	86° 58.74' N	058° 16.02' E	4700	MAPR	profile end
PS101/112-2	2016-09-21 T02:22	86° 59.04' N	058° 13.24' E	4758	CTD/ RO	on ground/ max depth
PS101/113-1	2016-09-21 T05:34	87° 00.99' N	058° 15.79' E	4724	**MOR**	on ground/ max depth
PS101/114-1	2016-09-21 T10:24	86° 59.53' N	057° 44.33' E	4751	ICE	on ground/ max depth
PS101/115-1	2016-09-21 T10:25	86° 59.53' N	057° 44.40' E	4748	CTD/ RO	on ground/ max depth
PS101/116-1	2016-09-21 T11:00	86° 59.56' N	057° 47.08' E	4762	LOKI	profile start
PS101/116-1	2016-09-21 T12:06	86° 59.60' N	057° 52.71' E	4802	LOKI	profile end
PS101/117-1	2016-09-21 T14:36	86° 59.59' N	058° 05.53' E	4848	MN	on ground/ max depth
PS101/118-1	2016-09-21 T21:25	86° 58.86' N	058° 18.14' E	4684	**MUC**	on ground/ max depth
PS101/119-1	2016-09-22 T01:57	86° 52.11' N	058° 02.67' E	3701	**HF**	profile start
PS101/119-1	2016-09-22 T04:30	86° 51.96' N	058° 29.50' E	3738	**HF**	profile end
PS101/120-1	2016-09-22 T08:36	86° 51.93' N	061° 19.55' E	967	**OFOS**	profile start
PS101/120-1	2016-09-22 T13:47	86° 51.13' N	062° 00.19' E	2117	OFOS	profile end
PS101/120-1a	2016-09-22 T07:58	86° 51.92' N	061° 15.40' E	21	**MAPR**	profile start
PS101/120-1a	2016-09-22 T13:45	86° 51.26' N	062° 02.88' E	2113	**MAPR**	profile end
PS101/121-1	2016-09-22 T16:46	86° 43.22' N	061° 20.65' E	749	ROV	profile start
PS101/121-1	2016-09-22 T16:58	86° 43.16' N	061° 21.17' E	699	ROV	profile end
PS101/122-1	2016-09-22 T17:18	86° 42.66' N	061° 34.67' E	728	ROV	profile start
PS101/122-1	2016-09-22 T17:30	86° 42.59' N	061° 35.48' E	744	ROV	profile end
PS101/123-1	2016-09-22 T18:18	86° 43.83' N	061° 36.95' E	651	MUC	on ground/ max depth
PS101/124-1	2016-09-22 T19:14	86° 43.81' N	061° 37.26' E	663	**MUC**	on ground/ max depth
PS101/125-1	2016-09-22 T20:14	86° 43.77' N	061° 36.76' E	664	**MUC**	on ground/ max depth
PS101/125-1a	2016-09-22 T20:14	86° 43.77' N	061° 36.76' E	664	**MTL**	profile start
PS101/125-1a	2016-09-22 T20:16	86° 43.77' N	061° 36.82' E	640	**MTL**	profile end

Station	Date Time	Position Lat	Position Lon	Depth [m]	Gear	Action
PS101/126-1	2016-09-22 T22:20	86° 44.15' N	061° 51.44' E	675	**CTD/ RO**	on ground/ max depth
PS101/126-1a	2016-09-22 T21:51	86° 44.20' N	061° 51.43' E	37	**ISP**	profile start
PS101/126-1a	2016-09-23 T02:43	86° 44.06' N	061° 56.26' E	730	ISP	profile end
PS101/126-1b	2016-09-22 T21:58	86° 44.18' N	061° 51.36' E	26	**MAPR**	profile start
PS101/126-1b	2016-09-23 T02:39	86° 44.05' N	061° 56.48' E	21	**MAPR**	profile end
PS101/126-1c	2016-09-22 T21:54	86° 44.20' N	061° 51.46' E	41	**ISP**	profile start
PS101/126-1c	2016-09-23 T02:41	86° 44.07' N	061° 56.24' E	731	ISP	profile end
PS101/126-1d	2016-09-22 T21:57	86° 44.19' N	061° 51.37' E	32	**ISP**	profile start
PS101/126-1d	2016-09-23 T02:39	86° 44.05' N	061° 56.48' E	21	**ISP**	profile end
PS101/126-1e	2016-09-22 T21:59	86° 44.18' N	061° 51.34' E	41	**ISP**	profile start
PS101/126-1e	2016-09-23 T02:38	86° 44.05' N	061° 56.49' E	54	**ISP**	profile end
PS101/126-1f	2016-09-22 T22:09	86° 44.17' N	061° 51.36' E	394	**ISP**	profile start
PS101/126-1f	2016-09-23 T02:23	86° 44.06' N	061° 56.13' E	386	**ISP**	profile end
PS101/126-1g	2016-09-22 T22:09	86° 44.17' N	061° 51.36' E	394	**ISP**	profile start
PS101/126-1g	2016-09-23 T02:21	86° 44.06' N	061° 56.06' E	395	**ISP**	profile end
PS101/126-1h	2016-09-22 T22:12	86° 44.16' N	061° 51.43' E	405	**ISP**	profile start
PS101/126-1h	2016-09-23 T02:20	86° 44.06' N	061° 56.05' E	405	**ISP**	profile end
PS101/126-2	2016-09-23 T02:08	86° 44.05' N	061° 55.72' E	707	**CTD/ RO**	on ground/ max depth
PS101/127-1	2016-09-23 T02:58	86° 43.86' N	061° 53.88' E	801	HS_PS	profile start
PS101/127-1	2016-09-23 T05:12	86° 42.06' N	062° 09.94' E	1552	HS_PS	profile end
PS101/128-1	2016-09-23 T07:00	86° 42.52' N	061° 11.19' E	607	ICE	on ground/ max depth
PS101/129-1	2016-09-23 T10:51	86° 42.87' N	061° 27.49' E	646	AUV	profile start
PS101/129-1	2016-09-23 T16:08	86° 41.25' N	061° 36.48' E	1191	AUV	profile end
PS101/130-1	2016-09-23 T17:06	86° 40.83' N	061° 34.10' E	1416	HS_PS	profile start
PS101/130-1	2016-09-23 T23:06	86° 57.23' N	054° 25.39' E	3669	HS_PS	profile end
PS101/131-1	2016-09-24 T00:48	86° 56.86' N	054° 32.69' E	3571	**CTD/ RO**	on ground/ max depth

Station	Date Time	Position Lat	Position Lon	Depth [m]	Gear	Action
PS101/131-1a	2016-09-23 T23:37	86° 57.11' N	054° 28.16' E	21	**MAPR**	profile start
PS101/131-1a	2016-09-24 T06:49	86° 54.99' N	055° 31.67' E	20	**MAPR**	profile end
PS101/131-1b	2016-09-23 T23:40	86° 57.09' N	054° 28.43' E	22	**MAPR**	profile start
PS101/131-1b	2016-09-24 T06:45	86° 55.02' N	055° 31.18' E	61	**MAPR**	profile end
PS101/131-1c	2016-09-23 T23:41	86° 57.09' N	054° 28.56' E	20	**MAPR**	profile start
PS101/131-1c	2016-09-24 T06:42	86° 55.03' N	055° 30.68' E	21	**MAPR**	profile end
PS101/131-1d	2016-09-23 T23:44	86° 57.07' N	054° 28.82' E	22	**MAPR**	profile start
PS101/131-1d	2016-09-24 T06:40	86° 55.05' N	055° 30.18' E	21	**MAPR**	profile end
PS101/131-1e	2016-09-23 T23:44	86° 57.07' N	054° 28.82' E	22	**MAPR**	profile start
PS101/131-1e	2016-09-24 T06:40	86° 55.05' N	055° 30.18' E	21	**MAPR**	profile end
PS101/131-2	2016-09-24 T01:43	86° 56.51' N	054° 37.88' E	3055	**CTD/ RO**	on ground/ max depth
PS101/131-3	2016-09-24 T02:24	86° 56.32' N	054° 42.01' E	2978	**CTD/ RO**	on ground/ max depth
PS101/131-4	2016-09-24 T03:04	86° 56.15' N	054° 47.13' E	2976	**CTD/ RO**	on ground/ max depth
PS101/131-5	2016-09-24 T03:44	86° 55.97' N	054° 53.22' E	2989	**CTD/ RO**	on ground/ max depth
PS101/131-6	2016-09-24 T04:05	86° 55.84' N	054° 58.12' E	1997	**CTD/ RO**	on ground/ max depth
PS101/131-7	2016-09-24 T04:27	86° 55.78' N	055° 01.33' E	2998	**CTD/ RO**	on ground/ max depth
PS101/131-8	2016-09-24 T05:12	86° 55.59' N	055° 07.27' E	4137	**CTD/ RO**	on ground/ max depth
PS101/132-1	2016-09-24 T07:42	86° 57.44' N	055° 36.45' E	3304	ICE	on ground/ max depth
PS101/133-1	2016-09-24 T09:36	86° 56.82' N	055° 43.38' E	3187	**CTD/ RO**	on ground/ max depth
PS101/134-1	2016-09-24 T12:39	86° 55.51' N	055° 56.97' E	4022	**OFOS**	profile start
PS101/134-1	2016-09-24 T13:52	86° 55.20' N	055° 55.64' E	4137	**OFOS**	profile end
PS101/134-1a	2016-09-24 T11:26	86° 55.03' N	056° 00.19' E	59	**MAPR**	profile start
PS101/134-1a	2016-09-24 T15:04	86° 54.43' N	055° 54.15' E	192	**MAPR**	profile end
PS101/134-1b	2016-09-24 T12:39	86° 55.51' N	055° 56.97' E	4022	**MTL**	profile start
PS101/134-1b	2016-09-24 T13:52	86° 55.20' N	055° 55.64' E	4137	**MTL**	profile end
PS101/135-1	2016-09-24 T18:09	86° 58.61' N	055° 32.72' E	3718	**OFOS**	profile start

Station	Date Time	Position Lat	Position Lon	Depth [m]	Gear	Action
PS101/135-1	2016-09-24 T22:17	86° 57.23' N	055° 49.63' E	2967	**OFOS**	profile end
PS101/135-1a	2016-09-24 T16:34	86° 59.48' N	055° 38.63' E	55	**MAPR**	profile start
PS101/135-1a	2016-09-24 T23:05	86° 57.42' N	055° 54.07' E	120	**MAPR**	profile end
PS101/135-1b	2016-09-24 T18:08	86° 58.61' N	055° 32.72' E	3708	**MTL**	profile start
PS101/135-1b	2016-09-24 T22:17	86° 57.23' N	055° 49.63' E	2967	**MTL**	profile end
PS101/136-1	2016-09-24 T23:32	86° 57.44' N	055° 54.54' E	3167	LOKI	profile start
PS101/136-1	2016-09-25 T00:36	86° 57.42' N	055° 53.52' E	3155	LOKI	profile end
PS101/137-1	2016-09-25 T04:23	86° 58.26' N	056° 53.47' E	4074	**CTD/ RO**	on ground/ max depth
PS101/137-1a	2016-09-25 T03:04	86° 58.09' N	056° 55.38' E	20	**MAPR**	profile start
PS101/137-1a	2016-09-25 T05:53	86° 58.78' N	056° 52.66' E	20	**MAPR**	profile end
PS101/137-1b	2016-09-25 T03:05	86° 58.09' N	056° 55.38' E	39	**MAPR**	profile start
PS101/137-1b	2016-09-25 T05:52	86° 58.77' N	056° 52.58' E	49	**MAPR**	profile end
PS101/137-1c	2016-09-25 T03:08	86° 58.09' N	056° 55.15' E	20	**MAPR**	profile start
PS101/137-1c	2016-09-25 T05:49	86° 58.76' N	056° 52.61' E	80	**MAPR**	profile end
PS101/137-1d	2016-09-25 T03:09	86° 58.09' N	056° 55.08' E	22	**MAPR**	profile start
PS101/137-1d	2016-09-25 T05:48	86° 58.75' N	056° 52.59' E	23	**MAPR**	profile end
PS101/138-1	2016-09-25 T10:18	86° 57.25' N	056° 15.29' E	3320	**CTD/ RO**	on ground/ max depth
PS101/138-1a	2016-09-25 T09:08	86° 57.10' N	056° 10.26' E	21	**MAPR**	profile start
PS101/138-1a	2016-09-25 T11:25	86° 57.41' N	056° 24.70' E	21	**MAPR**	profile end
PS101/138-1b	2016-09-25 T09:09	86° 57.10' N	056° 10.31' E	22	**MAPR**	profile start
PS101/138-1b	2016-09-25 T11:25	86° 57.41' N	056° 24.70' E	21	**MAPR**	profile end
PS101/138-1c	2016-09-25 T09:11	86° 57.10' N	056° 10.61' E	21	**MAPR**	profile start
PS101/138-1c	2016-09-25 T11:24	86° 57.41' N	056° 24.59' E	20	**MAPR**	profile end
PS101/138-1d	2016-09-25 T09:13	86° 57.10' N	056° 10.80' E	21	**MAPR**	profile start
PS101/138-1d	2016-09-25 T11:21	86° 57.41' N	056° 24.32' E	22	**MAPR**	profile end
PS101/138-1e	2016-09-25 T09:13	86° 57.10' N	056° 10.80' E	21	**MAPR**	profile start

Station	Date Time	Position Lat	Position Lon	Depth [m]	Gear	Action
PS101/138-1e	2016-09-25 T11:21	86° 57.41' N	056° 24.32' E	22	**MAPR**	profile end
PS101/139-1	2016-09-25 T14:06	86° 57.04' N	055° 33.29' E	3223	**CTD/ RO**	on ground/ max depth
PS101/139-1a	2016-09-25 T12:58	86° 56.95' N	055° 29.66' E	57	**MAPR**	profile start
PS101/139-1a	2016-09-25 T17:19	86° 57.80' N	055° 52.73' E	64	**MAPR**	profile end
PS101/139-1b	2016-09-25 T13:00	86° 56.96' N	055° 29.83' E	84	**MAPR**	profile start
PS101/139-1b	2016-09-25 T17:17	86° 57.80' N	055° 52.64' E	97	**MAPR**	profile end
PS101/139-1c	2016-09-25 T13:02	86° 56.96' N	055° 29.95' E	104	**MAPR**	profile start
PS101/139-1c	2016-09-25 T17:15	86° 57.80' N	055° 52.37' E	21	**MAPR**	profile end
PS101/139-1d	2016-09-25 T13:03	86° 56.96' N	055° 30.00' E	21	**MAPR**	profile start
PS101/139-1d	2016-09-25 T17:15	86° 57.80' N	055° 52.37' E	21	**MAPR**	profile end
PS101/139-1e	2016-09-25 T12:52	86° 56.93' N	055° 29.33' E	3466	MAPR	profile start
PS101/139-1e	2016-09-25 T17:17	86° 57.80' N	055° 52.64' E	97	**MAPR**	profile end
PS101/139-2	2016-09-25 T14:49	86° 57.16' N	055° 36.05' E	3089	**CTD/ RO**	on ground/ max depth
PS101/139-3	2016-09-25 T15:27	86° 57.30' N	055° 38.47' E	3112	**CTD/ RO**	on ground/ max depth
PS101/139-4	2016-09-25 T16:03	86° 57.46' N	055° 41.03' E	3163	**CTD/ RO**	on ground/ max depth
PS101/140-1	2016-09-25 T19:39	86° 57.50' N	055° 42.91' E	3169	**TVMUC**	on ground/ max depth
PS101/140-1a	2016-09-25 T18:02	86° 57.45' N	055° 28.89' E	54	**MAPR**	profile start
PS101/140-1a	2016-09-25 T20:16	86° 57.49' N	055° 49.56' E	1271	**MAPR**	profile end
PS101/141-1	2016-09-25 T22:50	86° 56.36' N	055° 52.53' E	3493	MN	on ground/ max depth
PS101/142-1	2016-09-26 T04:12	86° 50.51' N	058° 12.61' E	3429	ICE	on ground/ max depth
PS101/143-1	2016-09-26 T06:20	86° 50.29' N	058° 14.29' E	3480	**BC**	on ground/ max depth
PS101/144-1	2016-09-26 T08:34	86° 49.81' N	058° 16.67' E	3628	BC	on ground/ max depth
PS101/145-1	2016-09-26 T10:55	86° 49.36' N	058° 16.47' E	3600	**BC**	on ground/ max depth
PS101/146-1	2016-09-26 T13:14	86° 49.14' N	058° 13.77' E	3393	**BC**	on ground/ max depth
PS101/147-1	2016-09-26 T15:53	86° 49.29' N	058° 18.31' E	3586	**BC**	on ground/ max depth
PS101/148-1	2016-09-26 T19:00	86° 52.02' N	058° 32.76' E	3792	**GC**	on ground/ max depth

Station	Date Time	Position Lat	Position Lon	Depth [m]	Gear	Action
PS101/148-1a	2016-09-26 T19:00	86° 52.02' N	058° 32.76' E	3792	**MTL**	on ground/ max depth
PS101/149-1	2016-09-27 T00:10	86° 47.73' N	061° 50.69' E	751	**CTD/ RO**	on ground/ max depth
PS101/149-1a	2016-09-26 T23:38	86° 47.72' N	061° 52.64' E	46	**ISP**	profile start
PS101/149-1a	2016-09-27 T04:07	86° 48.41' N	061° 55.88' E	773	ISP	profile end
PS101/149-1b	2016-09-26 T23:40	86° 47.71' N	061° 52.62' E	35	**ISP**	profile start
PS101/149-1b	2016-09-27 T04:05	86° 48.42' N	061° 56.03' E	11	**ISP**	profile end
PS101/149-1c	2016-09-26 T23:43	86° 47.71' N	061° 52.50' E	43	**ISP**	profile start
PS101/149-1c	2016-09-27 T04:03	86° 48.41' N	061° 55.89' E	12	**ISP**	profile end
PS101/149-1d	2016-09-26 T23:46	86° 47.71' N	061° 52.27' E	37	**ISP**	profile start
PS101/149-1d	2016-09-27 T04:01	86° 48.40' N	061° 55.71' E	24	**ISP**	profile end
PS101/149-1e	2016-09-26 T23:53	86° 47.71' N	061° 51.54' E	297	**ISP**	profile start
PS101/149-1e	2016-09-27 T03:48	86° 48.35' N	061° 54.59' E	298	**ISP**	profile end
PS101/149-1f	2016-09-26 T23:57	86° 47.72' N	061° 51.02' E	312	**ISP**	profile start
PS101/149-1f	2016-09-27 T03:47	86° 48.35' N	061° 54.50' E	307	**ISP**	profile end
PS101/149-1g	2016-09-26 T23:59	86° 47.72' N	061° 50.96' E	317	**ISP**	profile start
PS101/149-1g	2016-09-27 T03:46	86° 48.34' N	061° 54.38' E	316	**ISP**	profile end
PS101/150-1	2016-09-27 T06:24	86° 43.36' N	061° 34.92' E	631	ROV	profile start
PS101/150-1	2016-09-27 T14:34	86° 43.78' N	061° 41.11' E	674	ROV	profile end
PS101/151-1	2016-09-27 T19:06	86° 49.76' N	061° 47.07' E	854	**TVMUC**	on ground/ max depth
PS101/152-1	2016-09-27 T20:06	86° 49.38' N	061° 40.16' E	892	**TVMUC**	on ground/ max depth
PS101/153-1	2016-09-27 T21:09	86° 49.56' N	061° 51.16' E	868	**MUC**	on ground/ max depth
PS101/154-1	2016-09-27 T22:05	86° 49.54' N	061° 50.32' E	795	**BC**	on ground/ max depth
PS101/155-1	2016-09-27 T23:13	86° 49.35' N	061° 43.69' E	796	**BC**	on ground/ max depth
PS101/156-1	2016-09-27 T23:59	86° 49.22' N	061° 37.46' E	683	**BC**	on ground/ max depth
PS101/157-1	2016-09-28 T00:30	86° 49.27' N	061° 43.35' E	871	HS_PS	profile start
PS101/157-1	2016-09-28 T04:12	86° 55.67' N	056° 17.41' E	3957	HS_PS	profile end

Station	Date Time	Position Lat	Position Lon	Depth [m]	Gear	Action
PS101/158-1	2016-09-28 T07:50	86° 57.51' N	055° 32.58' E	3321	**OFOS**	profile start
PS101/158-1	2016-09-28 T13:30	86° 57.56' N	055° 51.12' E	3016	**OFOS**	profile end
PS101/158-1a	2016-09-28 T06:47	86° 57.82' N	055° 35.15' E	20	**MAPR**	profile start
PS101/158-1a	2016-09-28 T14:28	86° 57.51' N	055° 44.08' E	135	**MAPR**	profile end
PS101/158-1b	2016-09-28 T07:50	86° 57.51' N	055° 32.58' E	3321	**MTL**	profile start
PS101/158-1b	2016-09-28 T13:30	86° 57.56' N	055° 51.12' E	3016	**MTL**	profile end
PS101/159-1	2016-09-28 T17:41	86° 57.53' N	056° 00.64' E	3222	**CTD/ RO**	on ground/ max depth
PS101/159-1a	2016-09-28 T16:36	86° 57.73' N	056° 03.54' E	39	**MAPR**	profile start
PS101/159-1a	2016-09-28 T21:50	86° 56.11' N	055° 37.46' E	45	**MAPR**	profile end
PS101/159-1b	2016-09-28 T16:38	86° 57.73' N	056° 03.41' E	60	**MAPR**	profile start
PS101/159-1b	2016-09-28 T21:48	86° 56.11' N	055° 37.55' E	65	**MAPR**	profile end
PS101/159-1c	2016-09-28 T16:42	86° 57.71' N	056° 03.09' E	21	**MAPR**	profile start
PS101/159-1c	2016-09-28 T21:46	86° 56.12' N	055° 37.80' E	81	**MAPR**	profile end
PS101/159-1d	2016-09-28 T16:42	86° 57.71' N	056° 03.09' E	21	**MAPR**	profile start
PS101/159-1d	2016-09-28 T21:44	86° 56.13' N	055° 38.01' E	22	**MAPR**	profile end
PS101/159-1e	2016-09-28 T16:43	86° 57.71' N	056° 03.08' E	20	**MAPR**	profile start
PS101/159-1e	2016-09-28 T21:44	86° 56.13' N	055° 38.01' E	22	**MAPR**	profile end
PS101/159-1f	2016-09-28 T16:41	86° 57.72' N	056° 03.16' E	100	**MAPR**	profile start
PS101/159-1f	2016-09-28 T21:45	86° 56.12' N	055° 37.91' E	99	**MAPR**	profile end
PS101/159-2	2016-09-28 T18:17	86° 57.36' N	055° 58.29' E	3088	**CTD/ RO**	on ground/ max depth
PS101/159-3	2016-09-28 T18:56	86° 57.15' N	055° 55.80' E	3088	**CTD/ RO**	on ground/ max depth
PS101/159-4	2016-09-28 T19:31	86° 56.95' N	055° 53.26' E	3093	**CTD/ RO**	on ground/ max depth
PS101/159-5	2016-09-28 T20:09	86° 56.74' N	055° 50.22' E	3249	**CTD/ RO**	on ground/ max depth
PS101/159-6	2016-09-28 T20:44	86° 56.54' N	055° 47.01' E	3111	**CTD/ RO**	on ground/ max depth
PS101/160-1	2016-09-29 T00:17	86° 57.70' N	055° 40.01' E	3270	**GC**	on ground/ max depth
PS101/160-1a	2016-09-29 T00:17	86° 57.70' N	055° 40.01' E	3270	**MTL**	on ground/ max depth

Station	Date Time	Position Lat	Position Lon	Depth [m]	Gear	Action
PS101/161-1	2016-09-29 T02:51	86° 57.70' N	055° 46.87' E	2949	**GC**	on ground/ max depth
PS101/161-1a	2016-09-29 T02:51	86° 57.70' N	055° 46.87' E	2949	**MTL**	on ground/ max depth
PS101/162-1	2016-09-29 T04:50	86° 57.46' N	056° 00.51' E	3229	ICE	on ground/ max depth
PS101/163-1	2016-09-29 T08:25	86° 56.50' N	056° 00.79' E	3456	CTD/ RO	on ground/ max depth
PS101/164-1	2016-09-29 T08:55	86° 56.34' N	056° 00.64' E	3517	LOKI	profile start
PS101/164-1	2016-09-29 T10:01	86° 56.01' N	056° 00.24' E	3666	LOKI	profile end
PS101/165-1	2016-09-29 T12:21	86° 55.52' N	055° 58.20' E	4038	MN	on ground/ max depth
PS101/166-1	2016-09-29 T17:48	86° 57.86' N	055° 47.01' E	3030	**TVMUC**	on ground/ max depth
PS101/167-1	2016-09-29 T21:21	86° 57.49' N	055° 41.48' E	3171	**TVMUC**	on ground/ max depth
PS101/168-1	2016-09-30 T18:47	86° 44.27' N	061° 55.99' E	691	ROV	profile start
PS101/168-1	2016-09-30 T18:48	86° 44.27' N	061° 55.99' E	690	ROV	profile end
PS101/169-1	2016-09-30 T20:26	86° 45.67' N	061° 51.86' E	878	**OFOS**	profile start
PS101/169-1	2016-10-01 T00:42	86° 48.32' N	061° 47.41' E	838	**OFOS**	profile end
PS101/169-1a	2016-09-30 T20:06	86° 45.66' N	061° 51.75' E	62	**MAPR**	profile start
PS101/169-1a	2016-10-01 T00:58	86° 48.35' N	061° 46.90' E	64	**MAPR**	profile end
PS101/169-1b	2016-09-30 T20:25	86° 45.67' N	061° 51.86' E	878	**MTL**	profile start
PS101/169-1b	2016-10-01 T00:42	86° 48.32' N	061° 47.41' E	838	**MTL**	profile end
PS101/170-1	2016-10-01 T02:16	86° 48.88' N	061° 47.41' E	539	**CTD/ RO**	on ground/ max depth
PS101/171-1	2016-10-01 T06:12	86° 51.86' N	061° 39.65' E	868	ICE	on ground/ max depth
PS101/172-1	2016-10-01 T06:53	86° 51.93' N	061° 35.28' E	622	**CTD/ RO**	on ground/ max depth
PS101/172-1a	2016-10-01 T06:23	86° 51.89' N	061° 38.50' E	857	ISP	profile start
PS101/172-1a	2016-10-01 T10:32	86° 52.56' N	061° 09.60' E	1708	ISP	profile end
PS101/172-1b	2016-10-01 T06:25	86° 51.88' N	061° 37.90' E	40	**ISP**	profile start
PS101/172-1b	2016-10-01 T10:30	86° 52.54' N	061° 09.74' E	43	**ISP**	profile end
PS101/172-1c	2016-10-01 T06:27	86° 51.88' N	061° 37.85' E	30	**ISP**	profile start
PS101/172-1c	2016-10-01 T10:28	86° 52.54' N	061° 09.76' E	36	**ISP**	profile end

Station	Date Time	Position Lat	Position Lon	Depth [m]	Gear	Action
PS101/172-1d	2016-10-01 T06:31	86° 51.89' N	061° 37.38' E	39	**ISP**	profile start
PS101/172-1d	2016-10-01 T10:26	86° 52.53' N	061° 10.04' E	45	**ISP**	profile end
PS101/172-1e	2016-10-01 T06:40	86° 51.91' N	061° 36.49' E	286	**ISP**	profile start
PS101/172-1e	2016-10-01 T10:17	86° 52.50' N	061° 11.13' E	285	**ISP**	profile end
PS101/172-1f	2016-10-01 T06:43	86° 51.91' N	061° 36.19' E	295	**ISP**	profile start
PS101/172-1f	2016-10-01 T10:15	86° 52.49' N	061° 11.49' E	299	**ISP**	profile end
PS101/172-1g	2016-10-01 T06:45	86° 51.92' N	061° 35.96' E	306	**ISP**	profile start
PS101/172-1g	2016-10-01 T10:13	86° 52.49' N	061° 11.61' E	310	**ISP**	profile end
PS101/173-1	2016-10-01 T10:54	86° 52.45' N	061° 08.31' E	1841	**LOKI**	profile start
PS101/173-1	2016-10-01 T12:07	86° 52.86' N	060° 59.35' E	1993	LOKI	profile end
PS101/174-1	2016-10-01 T15:08	86° 53.48' N	060° 44.92' E	2455	ADCP	profile start
PS101/174-1	2016-10-02 T13:00	87° 05.83' N	061° 37.75' E	3442	ADCP	profile end
PS101/175-1	2016-10-02 T14:19	87° 06.26' N	061° 36.73' E	949	**CTD/ RO**	on ground/ max depth
PS101/175-1a	2016-10-02 T13:14	87° 05.89' N	061° 37.44' E	21	**MAPR**	profile start
PS101/175-1a	2016-10-02 T15:39	87° 02.16' N	058° 40.98' E	34	**MAPR**	profile end
PS101/176-1	2016-10-02 T13:24	87° 05.97' N	061° 37.35' E	3428	ICE	on ground/ max depth
PS101/177-1	2016-10-03 T02:57	86° 57.16' N	055° 41.06' E	3079	**CTD/ RO**	on ground/ max depth
PS101/177-1a	2016-10-03 T02:13	86° 56.98' N	055° 40.96' E	943	**MAPR**	profile start
PS101/177-1a	2016-10-03 T06:46	86° 58.43' N	055° 38.81' E	22	**MAPR**	profile end
PS101/177-1b	2016-10-03 T02:13	86° 56.98' N	055° 40.96' E	943	**MAPR**	profile start
PS101/177-1b	2016-10-03 T06:45	86° 58.43' N	055° 38.81' E	70	**MAPR**	profile end
PS101/177-1c	2016-10-03 T02:13	86° 56.98' N	055° 40.96' E	943	**MAPR**	profile start
PS101/177-1c	2016-10-03 T06:44	86° 58.42' N	055° 38.86' E	86	**MAPR**	profile end
PS101/177-1d	2016-10-03 T02:13	86° 56.98' N	055° 40.96' E	943	**MAPR**	profile start
PS101/177-1d	2016-10-03 T06:41	86° 58.41' N	055° 38.96' E	21	**MAPR**	profile end
PS101/177-1e	2016-10-03 T02:13	86° 56.98' N	055° 40.96' E	943	**MAPR**	profile start

Station	Date Time	Position Lat	Position Lon	Depth [m]	Gear	Action
PS101/177-1e	2016-10-03 T06:41	86° 58.41' N	055° 38.96' E	21	**MAPR**	profile end
PS101/177-2	2016-10-03 T03:38	86° 57.37' N	055° 40.93' E	3174	**CTD/ RO**	on ground/ max depth
PS101/177-3	2016-10-03 T04:18	86° 57.56' N	055° 40.63' E	3146	**CTD/ RO**	on ground/ max depth
PS101/177-4	2016-10-03 T04:53	86° 57.75' N	055° 40.31' E	3020	**CTD/ RO**	on ground/ max depth
PS101/177-5	2016-10-03 T05:21	86° 57.89' N	055° 40.22' E	3008	**CTD/ RO**	on ground/ max depth
PS101/177-6	2016-10-03 T05:44	86° 58.02' N	055° 40.06' E	2857	**CTD/ RO**	on ground/ max depth
PS101/178-1	2016-10-03 T07:27	86° 58.66' N	055° 38.62' E	3794	AUV	profile start
PS101/178-1	2016-10-03 T07:28	86° 58.66' N	055° 38.60' E	3793	AUV	profile end
PS101/179-1	2016-10-03 T10:20	86° 56.83' N	055° 47.14' E	3235	**OFOS**	profile start
PS101/179-1	2016-10-03 T12:27	86° 57.69' N	055° 42.77' E	3254	**OFOS**	profile end
PS101/179-1a	2016-10-03 T09:24	86° 56.54' N	055° 47.18' E	114	**MAPR**	profile start
PS101/179-1a	2016-10-03 T13:27	86° 58.07' N	055° 41.96' E	67	**MAPR**	profile end
PS101/179-1b	2016-10-03 T10:19	86° 56.82' N	055° 47.09' E	3216	**MTL**	profile start
PS101/179-1b	2016-10-03 T12:27	86° 57.69' N	055° 42.77' E	3254	**MTL**	profile end
PS101/180-1	2016-10-03 T15:53	86° 57.56' N	055° 43.19' E	3156	**GC**	on ground/ max depth
PS101/180-1a	2016-10-03 T15:53	86° 57.56' N	055° 43.19' E	3156	**MTL**	on ground/ max depth
PS101/181-1	2016-10-03 T19:02	86° 57.00' N	055° 44.69' E	3037	**CTD/ RO**	on ground/ max depth
PS101/181-1a	2016-10-03 T17:49	86° 56.61' N	055° 46.95' E	12	**ISP**	profile start
PS101/181-1a	2016-10-03 T22:25	86° 58.78' N	055° 40.76' E	3821	ISP	profile end
PS101/181-1b	2016-10-03 T17:59	86° 56.69' N	055° 46.57' E	20	**MAPR**	profile start
PS101/181-1b	2016-10-03 T22:20	86° 58.77' N	055° 40.65' E	21	**MAPR**	profile end
PS101/181-1c	2016-10-03 T17:52	86° 56.64' N	055° 46.83' E	12	**ISP**	profile start
PS101/181-1c	2016-10-03 T22:23	86° 58.79' N	055° 40.55' E	40	**ISP**	profile end
PS101/181-1d	2016-10-03 T18:03	86° 56.72' N	055° 46.42' E	61	**MAPR**	profile start
PS101/181-1d	2016-10-03 T22:18	86° 58.75' N	055° 40.62' E	49	**MAPR**	profile end
PS101/181-1e	2016-10-03 T17:55	86° 56.65' N	055° 46.74' E	53	**ISP**	profile start

Station	Date Time	Position Lat	Position Lon	Depth [m]	Gear	Action
PS101/181-1e	2016-10-03 T22:19	86° 58.76' N	055° 40.64' E	23	**ISP**	profile end
PS101/181-1f	2016-10-03 T18:03	86° 56.72' N	055° 46.42' E	61	**MAPR**	profile start
PS101/181-1f	2016-10-03 T22:15	86° 58.72' N	055° 40.68' E	54	**MAPR**	profile end
PS101/181-1g	2016-10-03 T17:58	86° 56.68' N	055° 46.61' E	40	**ISP**	profile start
PS101/181-1g	2016-10-03 T22:18	86° 58.75' N	055° 40.62' E	49	**ISP**	profile end
PS101/181-1h	2016-10-03 T18:04	86° 56.72' N	055° 46.37' E	21	**MAPR**	profile start
PS101/181-1h	2016-10-03 T22:13	86° 58.71' N	055° 40.72' E	20	**MAPR**	profile end
PS101/181-1i	2016-10-03 T18:01	86° 56.70' N	055° 46.51' E	59	**ISP**	profile start
PS101/181-1i	2016-10-03 T22:15	86° 58.72' N	055° 40.68' E	54	**ISP**	profile end
PS101/181-1j	2016-10-03 T18:10	86° 56.77' N	055° 46.14' E	22	**MAPR**	profile start
PS101/181-1j	2016-10-03 T22:06	86° 58.64' N	055° 40.58' E	20	**MAPR**	profile end
PS101/181-1k	2016-10-03 T18:03	86° 56.72' N	055° 46.42' E	61	**ISP**	profile start
PS101/181-1k	2016-10-03 T22:14	86° 58.71' N	055° 40.71' E	68	**ISP**	profile end
PS101/181-1l	2016-10-03 T18:09	86° 56.76' N	055° 46.18' E	249	**ISP**	profile start
PS101/181-1l	2016-10-03 T22:07	86° 58.65' N	055° 40.58' E	249	**ISP**	profile end
PS101/181-2	2016-10-03 T21:03	86° 57.91' N	055° 41.10' E	3466	**CTD/ RO**	on ground/ max depth
PS101/182-1	2016-10-03 T22:49	86° 58.98' N	055° 40.98' E	3853	LOKI	profile start
PS101/182-1	2016-10-04 T00:01	86° 59.53' N	055° 42.21' E	3894	LOKI	profile end
PS101/183-1	2016-10-04 T02:31	87° 00.43' N	055° 47.65' E	4476	MN	on ground/ max depth
PS101/184-1	2016-10-04 T07:00	86° 57.72' N	055° 43.14' E	3300	ICE	profile start
PS101/184-1	2016-10-04 T07:32	86° 57.85' N	055° 44.27' E	3427	ICE	profile end
PS101/185-1	2016-10-04 T11:36	86° 57.45' N	055° 40.92' E	3190	**OFOS**	profile start
PS101/185-1	2016-10-04 T13:09	86° 57.58' N	055° 53.38' E	3131	**OFOS**	profile end
PS101/185-1a	2016-10-04 T10:37	86° 57.27' N	055° 34.64' E	21	**MAPR**	profile start
PS101/185-1a	2016-10-04 T14:01	86° 57.44' N	056° 03.05' E	123	**MAPR**	profile end
PS101/185-1b	2016-10-04 T11:36	86° 57.45' N	055° 40.92' E	3190	**MTL**	profile start

Station	Date Time	Position Lat	Position Lon	Depth [m]	Gear	Action
PS101/185-1b	2016-10-04 T13:09	86° 57.58' N	055° 53.38' E	3131	**MTL**	profile end
PS101/186-1	2016-10-04 T17:21	86° 57.66' N	055° 41.20' E	3254	DRG_C	profile start
PS101/186-1	2016-10-04 T17:42	86° 57.50' N	055° 45.02' E	3172	DRG_C	profile end
PS101/187-1	2016-10-04 T22:16	86° 57.61' N	055° 44.62' E	3199	**TVMUC**	on ground/ max depth
PS101/187-1a	2016-10-04 T20:43	86° 57.09' N	055° 39.70' E	53	**MAPR**	profile start
PS101/187-1a	2016-10-04 T22:59	86° 58.06' N	055° 49.21' E	1433	**MAPR**	profile end
PS101/187-1b	2016-10-04 T22:16	86° 57.61' N	055° 44.62' E	3199	**MTL**	profile start
PS101/187-1b	2016-10-04 T22:18	86° 57.61' N	055° 44.58' E	3199	**MTL**	profile end
PS101/187-1c	2016-10-04 T22:16	86° 57.61' N	055° 44.62' E	3199	**MTL**	on ground/ max depth
PS101/187-1d	2016-10-04 T22:16	86° 57.61' N	055° 44.62' E	3199	**MTL**	on ground/ max depth
PS101/188-1	2016-10-05 T03:13	86° 57.81' N	055° 52.05' E	2998	**CTD/ RO**	on ground/ max depth
PS101/188-1a	2016-10-05 T00:31	86° 56.52' N	055° 36.26' E	28	**ISP**	profile start
PS101/188-1a	2016-10-05 T04:32	86° 58.65' N	056° 07.25' E	3982	ISP	profile end
PS101/188-1b	2016-10-05 T00:38	86° 56.58' N	055° 36.95' E	43	**MAPR**	profile start
PS101/188-1b	2016-10-05 T04:26	86° 58.62' N	056° 06.25' E	51	**MAPR**	profile end
PS101/188-1c	2016-10-05 T00:34	86° 56.54' N	055° 36.60' E	40	**ISP**	profile start
PS101/188-1c	2016-10-05 T04:29	86° 58.64' N	056° 06.55' E	5	**ISP**	profile end
PS101/188-1d	2016-10-05 T00:44	86° 56.64' N	055° 37.68' E	66	**MAPR**	profile start
PS101/188-1d	2016-10-05 T04:23	86° 58.59' N	056° 05.60' E	47	**MAPR**	profile end
PS101/188-1e	2016-10-05 T00:38	86° 56.58' N	055° 36.95' E	43	**ISP**	profile start
PS101/188-1e	2016-10-05 T04:26	86° 58.62' N	056° 06.25' E	51	**ISP**	profile end
PS101/188-1f	2016-10-05 T00:46	86° 56.66' N	055° 37.89' E	77	**MAPR**	profile start
PS101/188-1f	2016-10-05 T04:20	86° 58.57' N	056° 05.34' E	68	**MAPR**	profile end
PS101/188-1g	2016-10-05 T00:38	86° 56.58' N	055° 36.95' E	43	**ISP**	profile start
PS101/188-1g	2016-10-05 T04:23	86° 58.59' N	056° 05.60' E	47	**ISP**	profile end
PS101/188-1h	2016-10-05 T00:47	86° 56.67' N	055° 37.98' E	21	**MAPR**	profile start

Station	Date Time	Position Lat	Position Lon	Depth [m]	Gear	Action
PS101/188-1h	2016-10-05 T04:18	86° 58.57' N	056° 05.24' E	20	**MAPR**	profile end
PS101/188-1i	2016-10-05 T00:44	86° 56.64' N	055° 37.68' E	66	**ISP**	profile start
PS101/188-1i	2016-10-05 T04:20	86° 58.57' N	056° 05.34' E	68	**ISP**	profile end
PS101/188-1j	2016-10-05 T00:54	86° 56.73' N	055° 38.62' E	24	**MAPR**	profile start
PS101/188-1j	2016-10-05 T04:10	86° 58.30' N	056° 00.32' E	22	**MAPR**	profile end
PS101/188-1k	2016-10-05 T00:46	86° 56.66' N	055° 37.89' E	77	**ISP**	profile start
PS101/188-1k	2016-10-05 T04:19	86° 58.57' N	056° 05.30' E	74	**ISP**	profile end
PS101/188-1l	2016-10-05 T00:52	86° 56.71' N	055° 38.48' E	263	**ISP**	profile start
PS101/188-1l	2016-10-05 T04:11	86° 58.30' N	056° 00.32' E	390	**ISP**	profile end
PS101/189-1	2016-10-05 T15:57	86° 46.65' N	061° 38.71' E	1219	**HF**	on ground/ max depth
PS101/189-2	2016-10-05 T17:25	86° 46.21' N	061° 37.57' E	1157	**HF**	profile start
PS101/189-2	2016-10-05 T17:45	86° 46.47' N	061° 40.84' E	1152	**HF**	profile end
PS101/189-3	2016-10-05 T19:24	86° 46.28' N	061° 36.83' E	1161	**HF**	profile start
PS101/189-3	2016-10-05 T21:25	86° 46.19' N	061° 39.97' E	1150	**HF**	profile end
PS101/190-1	2016-10-05 T23:01	86° 46.27' N	061° 30.63' E	1156	**BC**	on ground/ max depth
PS101/190-1a	2016-10-05 T22:35	86° 46.41' N	061° 32.46' E	50	**MAPR**	profile start
PS101/190-1a	2016-10-05 T23:19	86° 46.08' N	061° 27.97' E	119	**MAPR**	profile end
PS101/191-1	2016-10-06 T02:21	86° 44.29' N	061° 31.24' E	602	ROV	profile start
PS101/191-1	2016-10-06 T02:35	86° 44.25' N	061° 29.53' E	643	ROV	profile end
PS101/192-1	2016-10-06 T03:05	86° 44.21' N	061° 26.91' E	493	**CTD/ RO**	on ground/ max depth
PS101/193-1	2016-10-06 T07:03	86° 44.30' N	061° 24.68' E	1000	DRG_C	profile start
PS101/193-1	2016-10-06 T07:27	86° 44.26' N	061° 29.77' E	645	DRG_C	profile end
PS101/194-1	2016-10-06 T14:35	86° 51.22' N	061° 34.87' E	732	**TVMUC**	on ground/ max depth
PS101/194-1a	2016-10-06 T14:19	86° 51.22' N	061° 34.24' E	27	**MAPR**	profile start
PS101/194-1a	2016-10-06 T14:54	86° 51.23' N	061° 36.04' E	149	**MAPR**	profile end
PS101/194-1b	2016-10-06 T14:35	86° 51.22' N	061° 34.87' E	732	**MTL**	on ground/ max depth

Station	Date Time	Position Lat	Position Lon	Depth [m]	Gear	Action
PS101/195-1	2016-10-06 T16:40	86° 51.88' N	061° 34.61' E	638	**TVMUC**	on ground/ max depth
PS101/195-1a	2016-10-06 T16:22	86° 51.86' N	061° 33.10' E	22	**MAPR**	profile start
PS101/195-1a	2016-10-06 T16:50	86° 51.90' N	061° 35.96' E	181	**MAPR**	profile end
PS101/195-1b	2016-10-06 T16:40	86° 51.88' N	061° 34.61' E	638	**MTL**	on ground/ max depth
PS101/196-1	2016-10-06 T17:36	86° 51.59' N	061° 37.09' E	655	**TVMUC**	on ground/ max depth
PS101/196-1a	2016-10-06 T17:21	86° 51.59' N	061° 35.57' E	93	**MAPR**	profile start
PS101/196-1a	2016-10-06 T17:52	86° 51.61' N	061° 39.22' E	141	**MAPR**	profile end
PS101/196-1b	2016-10-06 T17:36	86° 51.59' N	061° 37.09' E	655	**MTL**	on ground/ max depth
PS101/197-1	2016-10-06 T18:34	86° 51.37' N	061° 34.72' E	648	**BC**	on ground/ max depth
PS101/198-1	2016-10-06 T19:38	86° 51.50' N	061° 32.81' E	679	**BC**	on ground/ max depth
PS101/199-1	2016-10-06 T20:31	86° 51.76' N	061° 36.76' E	760	**BC**	on ground/ max depth
PS101/200-1	2016-10-06 T21:12	86° 51.49' N	061° 35.76' E	684	**BC**	on ground/ max depth
PS101/201-1	2016-10-06 T22:46	86° 51.40' N	061° 30.05' E	766	MN	on ground/ max depth
PS101/202-1	2016-10-06 T23:56	86° 51.45' N	061° 28.95' E	724	**CTD/ RO**	on ground/ max depth
PS101/203-1	2016-10-07 T02:30	86° 53.40' N	061° 37.10' E	2011	DRG_C	profile start
PS101/203-1	2016-10-07 T02:56	86° 53.36' N	061° 28.75' E	1970	DRG_C	profile end
PS101/204-1	2016-10-07 T04:27	86° 54.29' N	061° 27.88' E	2845	ICE	on ground/ max depth
PS101/205-1	2016-10-07 T07:21	86° 49.53' N	061° 59.54' E	1132	**TVMUC**	on ground/ max depth
PS101/205-1a	2016-10-07 T06:56	86° 49.38' N	061° 57.21' E	21	**MAPR**	profile start
PS101/205-1a	2016-10-07 T07:43	86° 49.86' N	062° 03.94' E	150	**MAPR**	profile end
PS101/205-1b	2016-10-07 T07:21	86° 49.53' N	061° 59.54' E	1132	**MTL**	on ground/ max depth
PS101/206-1	2016-10-07 T09:21	86° 49.46' N	061° 57.99' E	1011	**BC**	on ground/ max depth
PS101/207-1	2016-10-07 T11:20	86° 46.36' N	061° 35.80' E	1055	**BC**	on ground/ max depth
PS101/208-1	2016-10-07 T12:27	86° 46.99' N	061° 39.73' E	1121	**BC**	on ground/ max depth
PS101/209-1	2016-10-07 T13:27	86° 47.49' N	061° 43.81' E	889	**BC**	on ground/ max depth
PS101/210-1	2016-10-07 T15:15	86° 45.50' N	061° 43.39' E	1014	**TVMUC**	on ground/ max depth

Station	Date Time	Position Lat	Position Lon	Depth [m]	Gear	Action
PS101/210-1a	2016-10-07 T14:57	86° 45.35' N	061° 42.32' E	391	**MAPR**	profile start
PS101/210-1a	2016-10-07 T15:35	86° 45.83' N	061° 45.17' E	168	**MAPR**	profile end
PS101/210-1b	2016-10-07 T15:15	86° 45.50' N	061° 43.39' E	1014	**MTL**	on ground/ max depth
PS101/211-1	2016-10-07 T17:09	86° 45.59' N	061° 47.85' E	927	**TVMUC**	on ground/ max depth
PS101/211-1a	2016-10-07 T16:27	86° 45.18' N	061° 45.23' E	62	**MAPR**	profile start
PS101/211-1a	2016-10-07 T17:27	86° 45.89' N	061° 49.60' E	150	**MAPR**	profile end
PS101/211-1b	2016-10-07 T17:09	86° 45.59' N	061° 47.85' E	927	**MTL**	on ground/ max depth
PS101/212-1	2016-10-07 T18:36	86° 45.87' N	061° 45.54' E	936	**TVMUC**	on ground/ max depth
PS101/212-1a	2016-10-07 T18:05	86° 45.63' N	061° 43.53' E	45	**MAPR**	profile start
PS101/212-1a	2016-10-07 T18:53	86° 46.08' N	061° 47.20' E	279	**MAPR**	profile end
PS101/212-1b	2016-10-07 T18:36	86° 45.87' N	061° 45.54' E	936	**MTL**	on ground/ max depth
PS101/213-1	2016-10-07 T19:30	86° 46.40' N	061° 49.85' E	543	**CTD/ RO**	on ground/ max depth
PS101/214-1	2016-10-07 T20:08	86° 46.70' N	061° 52.69' E	1039	LOKI	profile start
PS101/214-1	2016-10-07 T21:11	86° 47.11' N	061° 55.36' E	841	LOKI	profile end
PS101/215-1	2016-10-08 T01:01	86° 40.53' N	060° 22.67' E	1674	MN	on ground/ max depth
PS101/216-1	2016-10-08 T05:34	86° 42.68' N	060° 50.56' E		ROV	profile start
PS101/216-1	2016-10-08 T10:03	86° 41.31' N	060° 53.18' E		ROV	profile end
PS101/217-1	2016-10-08 T13:48	86° 40.03' N	060° 17.01' E	1686	**BC**	on ground/ max depth
PS101/218-1	2016-10-08 T16:29	86° 40.62' N	059° 56.70' E	1829	**TVMUC**	on ground/ max depth
PS101/218-1a	2016-10-08 T15:57	86° 40.82' N	059° 57.37' E	184	**MAPR**	profile start
PS101/218-1a	2016-10-08 T17:25	86° 40.06' N	059° 55.27' E	20	**MAPR**	profile end
PS101/218-1b	2016-10-08 T16:29	86° 40.62' N	059° 56.70' E	1829	**MTL**	on ground/ max depth
PS101/219-1	2016-10-08 T18:15	86° 39.64' N	059° 55.33' E	2005	**TVMUC**	on ground/ max depth
PS101/219-1a	2016-10-08 T18:00	86° 39.74' N	059° 55.25' E	1393	**MAPR**	profile start
PS101/219-1a	2016-10-08 T18:54	86° 39.14' N	059° 55.73' E	199	**MAPR**	profile end
PS101/219-1b	2016-10-08 T18:15	86° 39.64' N	059° 55.33' E	2005	**MTL**	on ground/ max depth

Station	Date Time	Position Lat	Position Lon	Depth [m]	Gear	Action
PS101/220-1	2016-10-08 T19:58	86° 38.60' N	059° 56.86' E	2016	**TVMUC**	on ground/ max depth
PS101/220-1a	2016-10-08 T19:13	86° 38.94' N	059° 56.08' E	25	**MAPR**	profile start
PS101/220-1a	2016-10-08 T20:38	86° 38.04' N	059° 57.73' E	137	**MAPR**	profile end
PS101/220-1b	2016-10-08 T19:58	86° 38.60' N	059° 56.86' E	2016	**MTL**	on ground/ max depth
PS101/221-1	2016-10-08 T23:49	86° 38.50' N	060° 05.39' E	25	**BC**	on ground/ max depth
PS101/222-1	2016-10-09 T01:25	86° 37.41' N	060° 02.83' E	1194	**BC**	on ground/ max depth
PS101/223-1	2016-10-09 T02:54	86° 37.05' N	060° 00.14' E	1696	LOKI	on ground/ max depth
PS101/224-1	2016-10-09 T05:14	86° 36.45' N	059° 57.71' E	1619	**CTD/ RO**	on ground/ max depth
PS101/225-1	2016-10-09 T16:45	86° 57.67' N	055° 39.19' E	3298	**OFOS**	profile start
PS101/225-1	2016-10-09 T22:06	86° 57.63' N	055° 43.37' E	3222	**OFOS**	profile end
PS101/225-1a	2016-10-09 T15:15	86° 57.69' N	055° 36.35' E	413	**MAPR**	profile start
PS101/225-1a	2016-10-09 T23:04	86° 57.69' N	055° 42.32' E	89	**MAPR**	profile end
PS101/225-1b	2016-10-09 T16:27	86° 57.72' N	055° 38.01' E	3051	**MTL**	profile start
PS101/225-1b	2016-10-09 T22:06	86° 57.63' N	055° 43.37' E	3222	**MTL**	profile end
PS101/226-1	2016-10-10 T02:13	86° 57.48' N	055° 42.78' E	3142	**CTD/ RO**	on ground/ max depth
PS101/226-1a	2016-10-09 T23:55	86° 57.44' N	055° 46.79' E	21	**MAPR**	profile start
PS101/226-1a	2016-10-10 T03:27	86° 58.30' N	055° 35.33' E	20	**MAPR**	profile end
PS101/226-1b	2016-10-09 T23:58	86° 57.45' N	055° 46.62' E	21	**MAPR**	profile start
PS101/226-1b	2016-10-10 T03:24	86° 58.27' N	055° 35.50' E	23	**MAPR**	profile end
PS101/227-1	2016-10-10 T12:20	86° 57.78' N	055° 42.36' E	3421	**TVMUC**	on ground/ max depth
PS101/227-1a	2016-10-10 T08:24	86° 56.21' N	055° 41.86' E	53	**MAPR**	profile start
PS101/227-1a	2016-10-10 T13:11	86° 58.52' N	055° 41.60' E	670	**MAPR**	profile end
PS101/227-1b	2016-10-10 T12:20	86° 57.78' N	055° 42.36' E	3421	**MTL**	profile start
PS101/227-1b	2016-10-10 T12:22	86° 57.79' N	055° 42.44' E	3346	**MTL**	profile end
PS101/228-1	2016-10-10 T12:55	86° 58.42' N	055° 43.15' E	3837	ICE	on ground/ max depth
PS101/229-1	2016-10-10 T17:54	86° 56.96' N	055° 48.75' E	3079	**OFOS**	profile start

Station	Date Time	Position Lat	Position Lon	Depth [m]	Gear	Action
PS101/229-1	2016-10-10 T19:54	86° 57.79' N	055° 39.42' E	3415	**OFOS**	profile end
PS101/229-1a	2016-10-10 T16:51	86° 56.47' N	055° 51.12' E	20	**MAPR**	profile start
PS101/229-1a	2016-10-10 T20:46	86° 58.32' N	055° 35.75' E	99	**MAPR**	profile end
PS101/229-1b	2016-10-10 T17:54	86° 56.96' N	055° 48.75' E	3079	**MTL**	profile start
PS101/229-1b	2016-10-10 T19:54	86° 57.79' N	055° 39.42' E	3415	**MTL**	profile end
PS101/230-1	2016-10-10 T23:45	86° 56.71' N	055° 40.36' E	3443	**ISP**	on ground/ max depth
PS101/230-1a	2016-10-10 T22:34	86° 56.38' N	055° 46.08' E	151	**MAPR**	profile start
PS101/230-1a	2016-10-11 T01:38	86° 57.67' N	055° 23.81' E	20	**MAPR**	profile end
PS101/230-1b	2016-10-10 T22:34	86° 56.38' N	055° 46.08' E	151	**MAPR**	profile start
PS101/230-1b	2016-10-11 T01:35	86° 57.66' N	055° 24.05' E	20	**MAPR**	profile end
PS101/230-1c	2016-10-10 T22:34	86° 56.38' N	055° 46.08' E	151	**MAPR**	profile start
PS101/230-1c	2016-10-11 T01:35	86° 57.66' N	055° 24.05' E	20	**MAPR**	profile end
PS101/230-1d	2016-10-10 T22:34	86° 56.38' N	055° 46.08' E	151	**MAPR**	profile start
PS101/230-1d	2016-10-11 T00:46	86° 57.10' N	055° 33.81' E	2491	**MAPR**	profile end
PS101/231-1	2016-10-11 T04:38	86° 57.43' N	055° 51.83' E	2573	**CTD/ RO**	on ground/ max depth
PS101/232-1	2016-10-11 T07:32	86° 57.00' N	055° 49.07' E	3061	**OFOS**	profile start
PS101/232-1	2016-10-11 T09:40	86° 57.46' N	055° 38.18' E	3173	**OFOS**	profile end
PS101/232-1a	2016-10-11 T06:42	86° 56.82' N	055° 52.41' E	21	**MAPR**	profile start
PS101/232-1a	2016-10-11 T10:27	86° 57.59' N	055° 31.05' E	71	**MAPR**	profile end
PS101/232-1b	2016-10-11 T07:32	86° 57.00' N	055° 49.07' E	3061	**MTL**	profile start
PS101/232-1b	2016-10-11 T09:40	86° 57.46' N	055° 38.18' E	3173	**MTL**	profile end
PS101/233-1	2016-10-13 T04:43	85° 07.81' N	022° 57.02' E	4362	XCTD	on ground/ max depth
PS101/234-1	2016-10-13 T10:44	84° 43.36' N	019° 53.52' E	4019	XCTD	on ground/ max depth
PS101/235-1	2016-10-13 T16:32	84° 28.45' N	016° 05.65' E	4016	XCTD	on ground/ max depth
PS101/236-1	2016-10-14 T00:00	83° 57.58' N	015° 59.96' E	4029	XCTD	on ground/ max depth
PS101/237-1	2016-10-14 T06:38	83° 26.80' N	014° 06.97' E	3865	XCTD	on ground/ max depth

Station	Date Time	Position Lat	Position Lon	Depth [m]	Gear	Action
PS101/238-1	2016-10-14 T18:00	82° 54.43' N	012° 29.93' E	2879	ICE	on ground/ max depth
PS101/239-1	2016-10-15 T07:16	82° 53.11' N	013° 01.97' E	501	**CTD/ RO**	on ground/ max depth
PS101/240-1	2016-10-15 T09:28	82° 52.81' N	013° 08.06' E	3068	**CTD/ RO**	on ground/ max depth
PS101/241-1	2016-10-16 T10:47	80° 42.91' N	014° 21.54' E	405	**OFOS**	profile start
PS101/241-1	2016-10-16 T12:24	80° 42.33' N	014° 14.49' E	208	**OFOS**	profile end
PS101/241-1a	2016-10-16 T10:46	80° 42.92' N	014° 21.60' E	406	**MTL**	profile start
PS101/241-1a	2016-10-16 T12:24	80° 42.33' N	014° 14.49' E	208	**MTL**	profile end
PS101/242-1	2016-10-17 T00:05	79° 27.09' N	007° 30.93' E	855	**MUC**	on ground/ max depth

A.5 SCIENTIFIC APPENDIX

A.5.1 Geology Appendix

Tab. A.5.1.1: Hard rock and sediment samples retrieved during PS101

Station	Gear	Sample	Comment
PS101/0064-1	BC	Hard rocks	One angular shaped clast, black, ~1.5x0.7x1 cm, presumably a metamorphite
PS101/0092-1	BC	Hard rocks	Several small volcanic rocks, presumably basaltic
PS101/0093-1	BC	Hard rocks	One large clast (PS101/093-R1), ~20x15x15 cm, volcanic w/ many phenocrysts, presumably olivine tholeiite; Several small volcanic rocks as in PS101/0092-1; One soft beige clast, ~5x3x3 cm, reminding of pumice
PS101/0094-1	BC	Hard rocks	One angular shaped clast, black, ~2x2x1 cm, presumably basaltic
PS101/0101-1	MUC	Hard rocks	One angular shaped clast, black, ~1x0.5x0.5 cm, presumably basaltic
PS101/0102-1	MUC	Hard rocks	Three angular shaped clasts, brown-black, up to ~2x1x1 cm, presumably basaltic
PS101/0103-1	MUC	Hard rocks	One angular shaped clast, black, ~2x1x1 cm, presumably basaltic
PS101/0105-1	GC	Gravity core	No recovery
PS101/0106-1	GC	Gravity core	Poor recovery w/o preservation of stratigraphy; Yellowish-brown sediment w/ volcanic fragments; Sponge-needles; Benthic organisms; Several small clasts, black, presumably basaltic
PS101/0118-1	MUC	Hard rocks	One elongated clast w/ flow structure, consisting of fresh and variably altered glass
PS101/0125-1	MUC	Hard rocks	Two angular shaped clasts, black, one ~2x1.5x1 cm in size, the other ~3x3x1.5 cm, presumably basaltic
PS101/0140-1	TVMUC	Sediment core	Sediment core, ~25 cm long
PS101/0141-1	MN	Sediments	Sediments consisting of mud and fresh to variably altered glass shards
PS101/0148-1	GC	Gravity core	Sediment core, ~3.15 m long, for core description see below
PS101/0151-1	TVMUC	Hard rocks	Four angular shaped clasts, black, up to ~2x2x1 cm, presumably basaltic
PS101/0152-1	TVMUC	Hard rocks	One large clast, ~5x5x4 cm, volcanic w/ phenocrysts of olivine, plagioclase and pyroxene, presumably basaltic

Station	Gear	Sample	Comment
PS101/0154-1	BC	Hard rocks	Several angular shaped clasts, black, up to ~5x5x4 cm, presumably basaltic; One clast of grey mudstone, ~5x3x2 cm; One large phenocryst of plagioclase, ~3x2x2 cm
PS101/0155-1	BC	Hard rocks	Several angular shaped clasts, up to ~3x2x1 cm, presumably basaltic
PS101/0160-1	GC	Gravity core	No recovery except for one glass shard
PS101/0161-1	GC	Gravity core	No recovery
PS101/0167-1	TVMUC	Sediments	Precipitates from top of core, consisting of orange spherules
PS101/0180-1	GC	Sediments	3 m long steel pipe; Recovery of a hydrothermally altered rock clast of ~5x5x4 cm, several smaller clasts, and hydrothermal sediments
PS101/0186-1	DRG_C	Hard rocks	Pieces of pillow basalt, partly glassy, rather fresh
PS101/0187-1	TVMUC	Hard rocks	One angular shaped clast, brown, ~4x3x3 cm, presumably basaltic
PS101/0190-1	BC	Hard rocks	Several angular shaped clasts, up to ~6x4x4 cm, presumably basaltic
PS101/0193-1	DRG_C	Hard rocks	Pieces of basalt w/ vesicles (PS101/193-R1); Basalt w/o vesicles (PS101/193-R2); Basalt w/ large phenocrysts (PS101/193-R3); Altered basalt w/ large phenocrysts (PS101/193-R4); Breccia w/ volcanic fragments (PS101/193-R5)
PS101/0194-1	TVMUC	Hard rocks	One angular shaped clast, ~2x2x1 cm, basaltic glass; One weathered brown clast, ~2x2x1 cm, presumably altered basalt; One grey clast, ~2x2x1 cm, presumably basaltic
PS101/0203-1	DRG_C	Hard rocks	Pieces of layered doleritic to gabbroic rock w/ large phenocrysts in a finer groundmass and epidote veins (PS101/203-R1); Doleritic to gabbroic rock as PS101/203-R1 but w/o layering (PS101/203-R4); Doleritic to gabbroic rock w/o large phenocrysts (PS101/203-R5); Serpentinised mantle rock w/ talc (PS101/203-R2); Hydrothermally altered rock w/ sulfide and possibly sulfate precipitates (PS101/203-R3)
PS101/0210-1	TVMUC	Hard rocks	Five angular shaped clasts, up to 5x3x3 cm, presumably basaltic

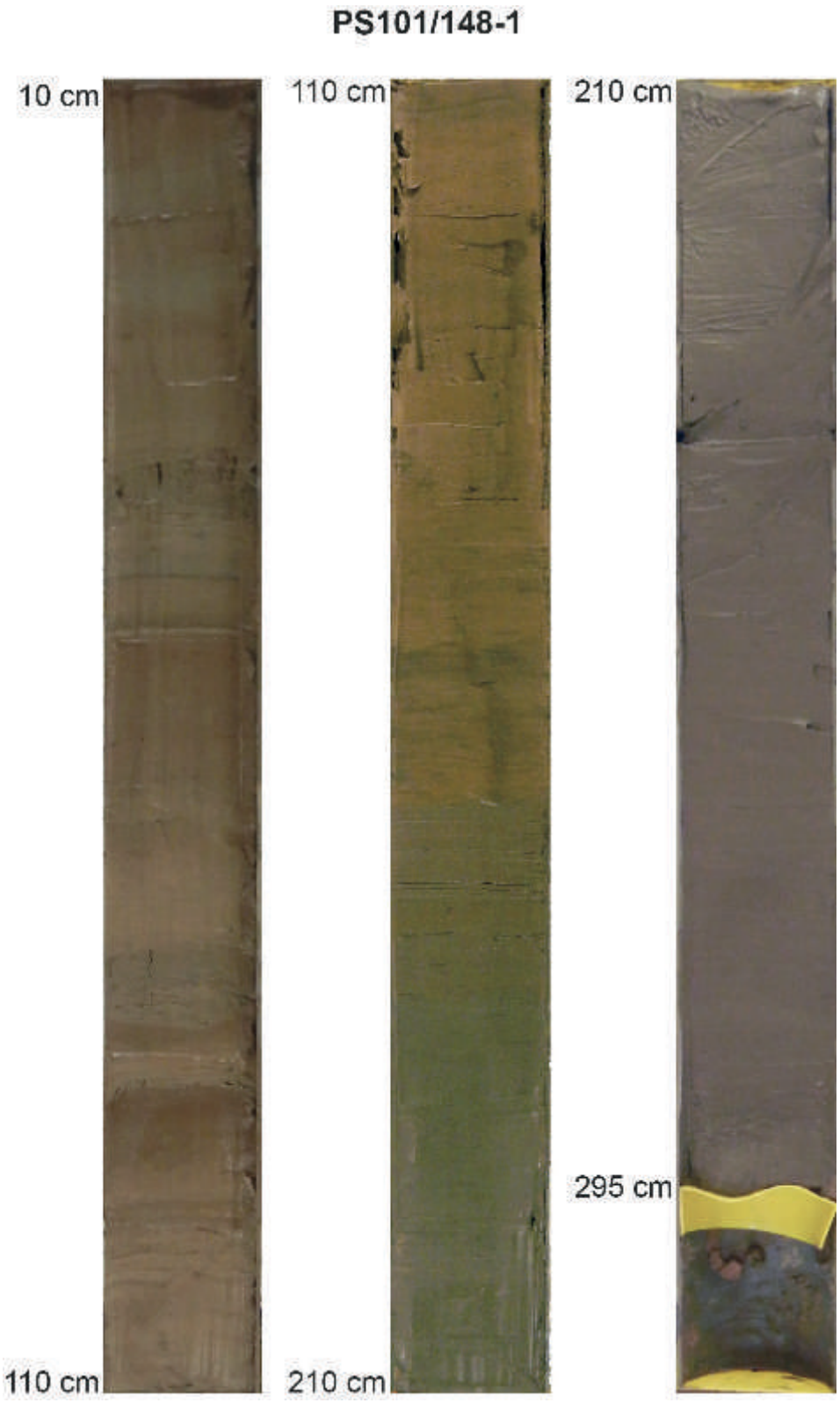

Fig. A.5.1.1: Photographs of gravity core PS101/148-1

Fig. A.5.1.2: Core description of gravity core PS101/148-1

A.5.2 Oceanography Appendix

A.5.2.1 In-situ pump casts

Tab. A.5.2.1: Summary of *in-situ* pump casts

	Pump#1	**Pump#2**	**Pump#3**	**Pump#4**	**Pump#5**	**Pump#6**	**Pump#7**
	Fred	Sebastian	Hulda	Jimmy	Frauke	Ginger	Frankie
	PS101/0055; 14.09.16, 23:30 UTC; pump time 180 min						
Operation depth	3870	3860	3070m	3060	3050	2070	2060
Volume (l)	190	470	588	274	1.5*	256	417
Filter type	PC	PES	PC	PC	PES	PC	PES
	PS101/0112; 19.09.16, 23:15 UTC; pump time 180 min						
Operation depth	4841	4831	4051	3051	3041	2051	2041
Volume(l)	0**	0**	9*	205	137	165	0**
Filter type	PC	PES	PC	PC	PES	PC	PES
	PS101/0126; 22.09.16, 23:00 UTC; pump time 180 min						
Operation depth	676	666	656	646	296	286	276
Volume (l)	195	513	1543**	1668*	57	151	657
Filter type	PC	PES	PC	PC	PC	PC	PC
	PS101/0149, 27.09.16, 00:30 UTC; pump time 180min						
Operation depth	750	740	730	720	470	460	450
Volume (l)	175	360	0	223	60	164	646
Filter type	PC	PC	PC	PC	PC	PC	PC
	PS101/0172, 01.10.16, 07:00 UTC; pump time 180 min						
Operation depth	598	588	578	568	318	308	298
Volume (l)	199	62	999	187	61	154	166
Filter type	PC	PC	PC	PC	PC	PC	PC
	PS101/0181, 03.10.16, 19:15 UTC, in plume pump time 90 min						
Operation depth	2665	2655	2645	2635	2625	2425	2615
Volume (l)	207	557	415	119	65	136	225

Filter type	PC	PES	PC	PC	PES	PC	PES
	PS101/0188, 5.10.16, 01:30:00 UTC; in plume, pump time 90 min						
Operation depth	2665	2655	2645	2635	2625	2425	2615
Volume (l)	331	268	388	196	73	150	230
Filter type	PC	PES	PC	PC	PES	PC	PES
	PS101/0230, weight on ground, 10.10.16, 23:30 UTC; pump time 60 min						
Operation depth	3390	3389	3380	3379	3370	3360	3369
Volume (l)	91	173	328	49	96	152	495
Filter type	PC	PES	PC	PC	PES	PC	PES

*sudden pressure release, ** too high pumping rates likely due to leaking filters

Table A.5.2.2: Details of water sample analyses carried out for each sample during PS101

Station number: 9																												
Bottle #	Depth (m)	Nuts	TA/DIC	H2/CH4 6ml	H2	S	He	3H	SF6/CFC	Microbiome	Metall	DNA	FISH	CO2	POC/PON	POP	PNSi	CHL	Bacteri	microscopy	HPLC	POC/PON stable isotope	RNA Fungi	microbial activity	CH4	13C-CH4
1	209	x																								
2	199	x																						xxx	x	
3	189	x																							x	
4	179	x																								
5	159	x																								
6	149	x				xx																				
7	140	x																								
8	129	x																							x	
9	119	x																								
10	109	x																								
11	99	x																								
12	89	x																								
13	79	x				xx																				
16	69	x																							x	
17	59	x																								
18	49	x																								
19	39	x																								
20	29	x																								
21	19	x																								
22	9	x																							x	
23	1	x																							x	
24																										

Station number: 44																													
Bott	Depth	Nuts	TA/DIC	H2/CH4 extr.	H2	S	He	3H	SF6/CFC	Microbiome	Metal	DNA	FISH	O2	POC/PON	POP	Plastic	CM	Sediment	microscopy	HPLC	POC/PON stable isotopes	RNA Fungi	microbial activity	CH4	13C-CH4
1	3975										x																
2	3975											x	xxx	xxx													
3	3975										x																
4	3975										x																
5	3975										x																
6	3975										x																
7	3975	x					x	x	x																xx	
8	3975										x													xxx	x	
9	2989																									
10	2989	x												xxx											xx	
11	2989											x	xxx											xxx		
12	2989																								x	
13	2890	x				xx	xx	x	xx																	
16	2000	x					x	x	x																xx	
17	2000											x	xxx											xxx		
18	2000					xx								xxxx												
19	1000	x					x	x	x					xxx											x	
20	1000																									
21	220	x					x	x	x					xxx											x	
22	220	x																								
23	50	x					x	x						xxx											xx	
24	10	x					x	x	x					xxx											xx	

Station number: 55																														
Bott	Depth	Nuts	TA/DIC	H2/CH4 extr.	H2	S	He	3H	SF6/CFC	Microbiome	Metall	DNA	FISH	O2	POC/PON	POP	Plastik	CHN	Seston	microscopy	HPLC	POC/PON stable isotopes	RNA Fungi	microbial activity	CH4	13C-CH4
1	3852						x		x	x																		
2	3852											x	xxx											xxx			
3	3852											x			x	x	x		x								
4	3852	x	x								x			xxx	x	x	x		x						x		
5	3852														x	x	x		x								
6	2998										x	x	xxx											xxx			
7	2999	x	x				x	x	x					xxx											x		
8	2999					xx																					
9	2500														x	x	x		x								
10	2500	x	x								x														x		
11	2500														x	x	x		x								
12	2487					xx																					
13	2001	x	x				x	x	x					xxx											x		
16	2001										x	x	xxx											xxx			
17	1489	x	x				x	x																	x		
18	1489										x				x	x	x		x								
19	1489														x	x	x		x								
20	1000	x	x											xxx											x		
21	500								x						x	x											
22	500	x	x				x	x			x														xx		
23	250	x	x												x	x									xx		
24	250										x				x	x											

Station number: 58																										
Bott	Depth	Nuts	TA/DIC	H2/CH4 expt.	H2	S	He	3H	SF6/CFC	Microbiome	Metal	DNA	FISH	O2	POC/PON	POP	PbSi	Chl	Seston	microscopy	HPLC	POC;PON stable isotope	RNA Fungi	microbial activity	CH4	13C-CH4
1	500														x	x	x		x							
2	500	x													x	x	x		x							
3	249														x	x	x		x							
4	249	x													x	x	x		x							
5	204													xxx												
6	97	x	x																							
7	97														x	x	x	x	x	x						
8	97														x	x	x	x	x							
9	97						x	x	x																	
10	74														x	x	x	x	x	x						
11	74														x	x	x	x	x							
12	74	x	x																							
13	49														x	x	x	x	x	x						
16	49	x	x											xxx												
17	49														x	x	x	x	x							
18	25														x	x	x	x	x	x						
19	25														x	x	x	x	x							
20	10	x	x											xxx												
21	10						xx	x	xx																	
22	10														x	x	x	x	x	x						
23	10														x	x	x	x	x							
24	1	x	x																							

Station number: 88																												
Bott	Depth	Nuts	TA/DIC	H2/CH4 extr.	H2	S	He	3H	SF6/CFC	Membrane	Metal	DNA	FISH	O2	POC/PON	POP	Phos	Chl	Sediment	microscopy	HPLC	POC/PON stable isotopes	RNA Fungi	microbial activity	CH4	13C-CH4
1	628				x					x															x	
2	592																								xx	
3	550				x		x		x																x	
4	500																								x	
5	449				x		x		x																x	
6	400																								x	
7	300				x		xx		xx																x	
8	249																									
9	199				x		x		x																x	
10	149																								x	
11	50				x																				x	
12	514																									
13	650				x																				x	
16	599				x																				x	
17	550																								x	
18	499				x																				x	
19	450																								x	
20	400				x																				x	
21	300																								x	
22	199				x																				x	
23	149																								x	
24	53				x																				x	

Station number: 97																												
Bott	Depth	Nuts	TA/DIC	H2/CH4 6sct	H2	S	He	3H	SF6/CFC	Membrane	Metal	DNA	FISH	O2	POC/PON	POP	Pistil	Chl	Season	microscopy	HPLC	POC/PON stable isotope	RNA Fungi	microbial activity xxx	CH4	13C-CH4
1	863																								x	
2	850																								x	
3	799						x	x	x																x	
4	750																								x	
5	692																								x	
6	650																								x	
7	598						x	x																	x	
8	549																								x	
9	500																								x	
10	853																									
11	853																									
12	853																									
13	853																									
16	853				x							x	xxx													
17	600											x														
18	600				x							x	xxx											xxx		
19	500																								x	
20	400				x							x	xxx												x	
21	300																								x	
22	200				x							x	xxx												x	
23	100																								x	
24	51				x							x	xxx												x	

Station number: 109																												
Bott	Depth	Nuts	TA/DIC	H2/CH4 extr.	H2	S	He	3H	SF6/CFC	Microbiome	Metal	DNA	FISH	O2	POC/PON	POP	Pfas	CM	Sediment	microscopy	HPLC	POC/PON stable isotopes	RNA Fungi	microbial activity	CH4	13C-CH4
1	11																									
2	11																									
3	11																									
4	11																									
5	11																									
6	10																									
7	10																									
8	10																									
9	10																									
10	10																									
11	10																									
12	10																									
13	10																									
16	10																									
17	10																									
18	10																									
19	10																									
20	10																									
21	10																									
22	10																									
23	10																									
24	10																									

Station number: 112																										
Bott	Depth	Nuts	TA/DIC	H2/CH4 expt.	H2	S	He	3H	SF6/CFC	Microbiome	Metal	DNA	FISH	O2	POC/PON	POP	PbSi	Chl	Seston	microscopy	HPLC	POC/PON stable isotope	RNA Fungi	microbial activity	CH4	13C-CH4
1	4729	x	x				x		x	x															x	
2	4729											x	xxx	xxx										xxx		
3	4729														x	x	x		x							
4	4729														x	x	x		x							
5	4729														x	x	x		x							
6	3479	x	x				x																		x	
7	2988	x	x											xxx											x	
8	2988											x	xxx											xxx		
9	2499														x	x	x		x							
10	2499														x	x	x		x							
11	2499	x	x				x	x																	x	
12	2499														x	x	x		x							
13	2000	x	x				x		xx					xxx											x	
16	2000											x	xxx											xxx		
17	1500														x	x	x		x							
18	1500														x	x	x		x							
19	1500	x	x				x		x																x	
20	1500														x	x	x		x							
21	999	x	x											xxx											x	
22	494														x	x	x		x							
23	494														x	x	x		x							
24	494														x	x	x		x							

Station number: 115																														
Bott	Depth	Nuts	TA/DIC	H2/CH4 extr.	H2	S	He	3H	SF6/CFC	Membrane	Metal	DNA	FISH	O2	POC/PON	POP	Pistil	Chl	Sediment	microscopy	HPLC	POC/PON stable isotopes	RNA Fungi	microbial activity	CH4	13C-CH4
1	501	x	x				x		x																		
2	249														x	x	x	x	x	x							
3	249														x	x	x	x	x								
4	249														x	x	x	x	x								
5	249	x	x																								
6	200													xxx													
7	100	x	x				x		x																		
8	100														x	x	x	x	x	x							
9	100														x	x	x	x	x								
10	75	x																									
11	75														x	x	x	x	x	x							
12	75														x	x	x	x	x								
13	50	x	x											xxx													
16	50														x	x	x	x	x	x							
17	50														x	x	x	x	x								
18	25														x	x	x	x	x	x							
19	25	x	x				xx	x	x																		
20	25														x	x	x	x	x								
21	10														x	x	x	x	x	x							
22	10														x	x	x	x	x								
23	10	x												xxx													
24	1	x	x																								

Station number: 126																														
Bott	Depth	Nuts	TA/DIC	H2/CH4 6spt	H2	S	He	3H	SF6/CFC	Membrane	Metal	DNA	FISH	CO2	POC/PON	POP	Phos	Chl	Sediment	microscopy	HPLC	POC/PON stable isotope	RNA Fungi	microbial activity	CH4	13C-CH4
1	715											x	xxx														
2	715													xxx										xxx			
3	715	x											xxx														
4	601											x		xxx													
5	601	x																									
6	550	x																									
7	500	x																									
8	450	x																									
9	394											x	xxx														
10	394	x												xxx													
11	350	x																									
12	300	x																									
13	250	x																									
16	200											x	xxx														
17	200	x												xxx													
18	150	x																									
19	97	x																									
20	50	x																									
21	12	x										x	xxx														
22	12													xxx													
23	12																										
24	12	x																									

Station number: 131																												
Bott	Depth	Nuts	TA/DIC	H2/CH4 exp.	H2	S	He	3H	SF6/CFC	Membrane	Metal	DNA	FISH	O2	POC/PON	POP	Phos	Chl	Season	microscopy	HPLC	POC/PON stable isotope	RNA Fungi	microbial activity	CH4	13C-CH4
1	3583	x													x	x	x	x		x					x	
2	4002					xx																		xx		
3	3002					xx																		xxx		
4	2799	x																							x	
5	2599	x					x																		x	
6	2497	x					x																		xx	
7	2302	x																							x	
8	99	x													x	x	x	x		x						
9	99														x	x	x	x								
10	99														x	x	x	x								
11	74	x													x	x	x	x		x						
12	74														x	x	x	x								
13	74														x	x	x	x								
16	49	x													x	x	x	x		x						
17	49														x	x	x	x								
18	49														x	x	x	x								
19	27	x													x	x	x	x		x						
20	27														x	x	x	x								
21	27														x	x	x	x								
22	7	x													x	x	x	x		x						
23	7														x	x	x	x								
24	7														x	x	x	x								

Station number: 133																														
Bott	Depth	Nuts	TA/DIC	H2/CH4 extr.	H2	S	He	3H	SF6/CFC	Microbiome	Metal	DNA	FISH	O2	POC/PON	POP	Phos	Chl	Sediment	microscopy	HPLC	POC/PON stable isotope	RNA Fungi	microbial activity	CH4	13C-CH4
1	2500	x					x																		xx	
2	2500										x															
3	3204	x								x																
4	3204																									
5	3204																									
6	2902											x	xxx													
7	2902	x																								
8	2902										x														xx	
9	2507						x																			
10	2507	x									x														xx	
11	2507											x	xxx													
12	2507																									
13	2507																									
16	2286	x									x														xx	
17	1962											x	xxx													
18	1962	x																								
19	1013	x																								
20	1011																									
21	1010																									
22	1009																									
23	1007																									
24	1004																									

Station number: 137																												
Bott	Depth	Nuts	TA/DIC	H2/CH4 extr.	H2	S	He	3H	SF6/CFC	Microbiome	Metal	DNA	FISH	O2	POC/PON	POP	Pfatt	Chl	Sediment	microscopy	HPLC	POC/PON stable isotope	RNA Fungi	microbial activity	CH4	13C-CH4
1	4074				xx																				x	
2	4074																									
3	3800																								x	
4	3800																									
5	3500				xx																				x	
6	3500																									
7	2803				xx																				x	
8	2803																									
9	2600				xx																				x	
10	2600																									
11	2499																								x	
12	2499																									
13	2398				xx																				x	
16	2398																									
17																										
18																										
19																										
20																										
21																										
22																										
23																										
24																										

Station number: 138																										
Bott	Depth	Nuts	TA/DIC	H2/CH4 expt.	H2	S	He	3H	SF6/CFC	Microbiome	Metal	DNA	FISH	O2	POC/PON	POP	PbSi	Chl	Seston	microscopy	HPLC	POC/PON stable isotope	RNA Fungi	microbial activity	CH4	13C-CH4
1	3330																								x	
2	3000																								x	
3	2800																								x	
4	2600																								x	
5	2500																								x	
6	2399																								x	
7																										
8																										
9																										
10																										
11																										
12																										
13																										
16																										
17																										
18																										
19																										
20																										
21																										
22																										
23																										
24																										

Station number: 139																												
Bott	Depth	Nuts	T&DIC	H2/CH4 extr.	H2	S	He	3H	SF6/CFC	Membrane	Metal	DNA	FISH	O2	POC/PON	POP	Pigs	Chl	Sediment	microscopy	HPLC	POC/PON stable isotope	RNA Fungi	microbial activity	CH4	13C-CH4
1	3222				xx							x	xxx											xxx		
2	3051	x			xx						x														xx	xx
3	3051											x	xxx											xxx		
4	2687	x									x															
5	2687				xx																					
6	2687																									
7	2687						x		x																	
8	2531	x									x														xx	xx
9	2531						xx		x																	
10	2531				xx																					
11	2531											x	xxx											xxx		
12	2300	x																							x	xx
13	2300											x	xxx											xxx		
16	2791	x									x														xx	
17	2791						x		x																	
18	2700	x									x														xx	xx
19	2700				xx		x																			
20	2646	x		x	xx		x				x														xx	xx
21	2000	x			xx							x	xxx													xx
22	1500																							xxx		
23	982	x																							x	xx
24	500	x																							xx	

Station number: 149																										
Bott	Depth	Nuts	TA/DIC	H2/CH4 expt.	H2	S	He	3H	SF6/CFC	Microbiome	Metal	DNA	FISH	O2	POC/PON	POP	PbSi	Chl	Seston	microscopy	HPLC	POC/PON stable isotope	RNA Fungi	microbial activity	CH4	13C-CH4
1	751											x	xxx											xxx		
2	751	x												xxx												
3	600											x	xxx													
4	600	x												xxx												
5	401											x	xxx													
6	401	x												xxx												
7	200											x	xxx													
8	200	x												xxx												
9	101																									
10	101														x	x	x	x		x						
11	98	x													x	x	x	x								
12	76														x	x	x	x		x						
13	76	x													x	x	x	x								
16	51														x	x	x	x		x						
17	51	x													x	x	x	x								
18	26														x	x	x	x		x						
19	26	x													x	x	x	x								
20	11														x	x	x	x		x		x				
21	11														x	x	x	x				x				
22	11	x													x	x	x	x				x				
23	2											x	xxx													
24	2	x												xxx												

Station number: 159																												
Bott	Depth	Nuts	TA/DIC	H2/CH4 extr.	H2	S	He	3H	SF6/CFC	Membrane	Metal	DNA	FISH	O2	POC/PON	POP	Phos	Chl	Sediment	microscopy	HPLC	POC/PON stable isotope	RNA Fungi	microbial activity	CH4	13C-CH4
1	2617				xx																			xxx		
2	2797										x	x	xxx											xxx		
3	2797	x			xx		x	x	x					xxx											xx	xx
4	2778										x	x	xxx													
5	2778	x			xx		x							xxx											xx	xx
6	2560										x	x	xxx													
7	2560	x			xx		x	x	x					xxx										x	xx
8	2298										x	x	xxx											xxx		
9	2299	x			xx		x							xxx										xx	xx
10	2608			x																						
11	2608	x			xx		x							xxx										xx	xx
12	2608										x	x	xxx													
13	2829	x			xx		x																	xx	xx
16	2830										x															
17	2953	x			xx		x							xxx										xx	xx
18	2953										x	x	xxx											xxx		
19	2508	x			xx		xx																	xx		
20	2508										x															
21	3093	x			xx		x							xxx										xx		
22	3093										x	x	xxx											xxx		
23	1500											x	xxx											xxx		
24	1500	x												xxx												

Station number: 163																												
Bott	Depth	Nuts	TA/DIC	H2/CH4 6sct	H2	S	He	3H	SF6/CFC	Membrane	Metal	DNA	FISH	O2	POC/PON	POP	Plastic	Chl	Sediment	microscopy	HPLC	POC/PON stable isotopes	RNA Fungi	microbial activity	CH4	13C-CH4
1	501																									
2	501																									
3	400																									
4	400																									
5	200																									
6	200																									
7	100														x	x	x	x		x						
8	100														x	x	x	x								
9	100																									
10	74														x	x	x	x		x						
11	74														x	x	x	x								
12	50														x	x	x	x		x						
13	50														x	x	x	x								
16	50																									
17	24														x	x	x	x		x						
18	24														x	x	x	x								
19	6														x	x	x	x		x		x				
20	6														x	x	x	x				x				
21	6														x	x	x	x				x				
22	5																									
23	5																									
24	1																									

Station number: 170																												
Bott	Depth	Nuts	TA/DIC	H2/CH4 extr.	H2	S	He	3H	SF6/CFC	Microbiome	Metal	DNA	FISH	O2	POC/PON	POP	Plastic	Chl	Sediment	microscopy	HPLC	POC/PON stable isotopes	RNA Fungi	microbial activity	CH4	13C-CH4
1	551									x																
2	551																									
3	551																									
4	551																									
5	551																									
6	551																									
7	551																									
8	551																									
9	551																									
10	551																									
11	551	x																								
12	500	x																								
13	401	x																								
16	300	x																								
17	249	x																								
18	149	x																								
19	101	x																								
20	74	x																								
21	50	x																								
22	26	x																								
23	10	x																								
24	1	x																								

Station number: 172																										
Bott	Depth	Nuts	TA/DIC	H2/CH4 expt.	H2	S	He	3H	SF6/CFC	Microbiome	Metal	DNA	FISH	O2	POC/PON	POP	PbSi	Chl	Seston	microscopy	HPLC	POC/PON stable isotope	RNA Fungi	microbial activity	CH4	13C-CH4
1	619	x																								
2	619									x																
3	619											x	xxx											xxx		
4	619													xxx												
5	604											x	xxx													
6	604													xxx												
7	604	x																								
8	391													xxx												
9	391											x	xxx													
10	391	x																								
11	200											x	xxx													
12	200	x												xxx												
13	100																									
16	100	x																								
17	75	x																								
18	50	x																								
19	23	x																								
20	10	x																								
21	10																									
22	1	x												xxx												
23	1											x	xxx													
24	1																									

Station number: 175																													
Bott	Depth	Nuts	TA/DIC	H2/CH4 extr.	H2	S	He	3H	SF6/CFC	Methane	Metal	DNA	FISH	CO2	POC/PON	POP	Plastic	CHL	Sediment	microscopy	HPLC	POC/PON stable isotope	RNA Fungi	microbial activity	CH4	13C-CH4
1	3342	x					x																				
2	3342											x		xxx										xxx		
3	2999					xx						x		xxx												
4	2999											x		xxx										xxx		
5	2500	x		x			x																			
6	2500																									
7	2000					xx																				
8	2000											x		xxx										xxx		
9	1490	x					x																			
10	1000											x		xxx												
11	1000	x																								
12	500	x					x																			
13	200											x		xxx												
14	100														x	x	x	x		x						
15	100														x	x	x	x								
16	69														x	x	x	x		x						
17	69	x																								
18	69														x	x	x	x								
19	50														x	x	x	x		x						
20	50											x		xxx												
21	50														x	x	x	x								
22	25														x	x	x	x		x						
23	25														x	x	x	x								
24	1	x																								

Station number: 177																										
Bott	Depth	Nuts	TA/DIC	H2/CH4 expt.	H2	δ	He	3H	SF6/CFC	Microbiome	Metal	DNA	FISH	O2	POC/PON	POP	PbSi	Chl	Seston	microscopy	HPLC	POC/PON stable isotope	RNA Fungi	microbial activity	CH4	13C-CH4
1	3079	x			xx		x																		xx	xx
2	3079											x	x	xxx										xxx		
3	2621	x			xx		x																		xx	xx
4	2621										x	x	x	xxx												
5	2587	x			xx		x																		xx	xx
6	2587										x															
7	2573	x			xx		x																		xx	xx
8	2573										x															
9	2670	x			xx		x																		xx	xx
10	2670										x															
11	2821	x			xx		x																		xx	xx
12	2821											x	x	xxx										xxx		
13	2595				xx																					
14	2595											x	x	xxx										xxx		
15	2595	x		x	xx		x																	xxx	xx	xx
16	2350											x	x	xxx										xxx		
17	2350	x			xx		x																		xx	xx
18	2594										x															
19	2594	x			xx		x																		xx	
20	2726										x															
21	2726	x			xx		x																		xx	
22	2714										x															
23	2714	x			xx		x																		xx	
24	2530	x					x				x														xx	

Station number: 181																										
Bott	Depth	Nuts	TA/DIC	H2/CH4 expt.	H2	S	He	3H	SF6/CFC	Microbiome	Metal	DNA	FISH	O2	POC/PON	POP	PbSi	Chl	Seston	microscopy	HPLC	POC/PON stable isotope	RNA Fungi	microbial activity	CH4	13C-CH4
1	2676						x																			
2	2676						x				x															
3	2676											x	x													
4	2675						x				x															
5	2675			x			xx																			
6	2675						x				x															
7	2675						x																			
8	2674										x															
9	3474	x	x																							
10	2500	x	x			xx																				
11	1001	x	x			xx																				
12	500	x	x																							
13	249	x	x																							
14	100	x	x																							
15	75		x																							
16	75														x	x	x	x		x						
17	75														x	x	x	x								
18	50	x													x	x	x	x		x						
19	50														x	x	x	x								
20	25														x	x	x	x		x						
21	25														x	x	x	x								
22	25	x	x																							
23	10	x	x				x																			
24	1	x	x																							

Station number: 188																										
Bott	Depth	Nuts	TA/DIC	H2/CH4 expt.	H2	S	He	3H	SF6/CFC	Microbiome	Metal	DNA	FISH	O2	POC/PON	POP	PbSi	Chl	Seston	microscopy	HPLC	POC/PON stable isotope	RNA Fungi	microbial activity	CH4	13C-CH4
1	2673	x			xx		x																		x	
2	2670						x																		xx	xx
3	2669				xx		x																		xx	
4	2669						x																			
5	2669				xx																				x	xx
6	2669											x	x	xxx										xxx		
7	2669			x	xx																					
8	2669																									
9	2669	x			xx		x																		xx	xx
10	2669						x																		xx	xx
11	2670				xx		x																		xx	xx
12	2801	x																							xx	xx
13	3001	x			xx							x	x	xxx										xxx		
14	3001																									
15	2568				xx		x																			
16	2568																								xx	xx
17	2450	x			xx																				x	
18	2450											x	x	xxx										xxx		
19	2450				xx																					
20	1001	x																								
21	501	x			xx																					
22	100	x																								
23	51	x																								
24	1	x																								

Station number: 192																												
Bott	Depth	Nuts	TA/DIC	H2/CH4 extr.	H2	S	He	3H	SF6/CFC	Microbiome	Metal	DNA	FISH	O2	POC/PON	POP	Plastic	Chl	Sediment	microscopy	HPLC	POC/PON stable isotope	RNA Fungi	microbial activity	CH4	13C-CH4
1	500	x																								
2	450	x																								
3	400	x																								
4	350	x																								
5	300	x																								
6	250	x																								
7	200	x																								
8	175	x																								
9	150	x																								
10	125	x																								
11	100	x													x	x	x	x		x						
12	100														x	x	x	x								
13	75	x													x	x	x	x		x						
14	75														x	x	x	x								
15	50	x													x	x	x	x		x						
16	50														x	x	x	x								
17	50														x	x	x	x								
18	25	x													x	x	x	x		x						
19	25														x	x	x	x								
20	25														x	x	x	x								
21	10	x													x	x	x	x		x		x				
22	10														x	x	x	x				x				
23	10														x	x	x	x				x				
24	1	x																								

Station number: 202																												
Bott	Depth	Nuts	TA/DIC	H2/CH4 6sct	H2	S	He	3H	SF6/CFC	Membrane	Metal	DNA	FISH	O2	POC/PON	POP	Plastic	Chl	Sediment	microscopy	HPLC	POC/PON stable isotope	RNA Fungi	microbial activity	CH4	13C-CH4
1	150																										
2	150																										
3	150																										
4	150																										
5	150																										
6	150																										
7	150																										
8	150																										
9	150																										
10	150																										
11	150																										
12	150																										
13	150																										
14	100														x	x	x	x		x		x				
15	100														x	x	x	x				x	x			
16	75														x	x	x	x		x		x				
17	75														x	x	x	x								
18	50														x	x	x	x		x						
19	50														x	x	x	x								
20	26														x	x	x	x		x						
21	26														x	x	x	x								
22	11														x	x	x	x		x						
23	11														x	x	x	x								
24	11														x	x	x	x								

Station number: 213																												
Bott	Depth	Nuts	TA/DIC	H2/CH4 extr.	H2	S	He	3H	SF6/CFC	Microbiome	Metal	DNA	FISH	O2	POC/PON	POP	Plastic	Chl	Sediment	microscopy	HPLC	POC/PON stable isotope	RNA Fungi	microbial activity	CH4	13C-CH4
1	501	x																								
2	450	x																								
3	400	x																								
4	350	x																								
5	300	x																								
6	275	x																								
7	250	x																								
8	225	x																								
9	200	x																								
10	175	x																								
11	150	x																								
12	125	x																								
13	100														x	x	x	x		x						
14	100	x													x	x	x	x								
15	74														x	x	x	x		x						
16	74														x	x	x	x								
17	50														x	x	x	x		x						
18	50	x													x	x	x	x								
19	25														x	x	x	x		x						
20	25	x													x	x	x	x								
21	9														x	x	x	x		x		x				
22	9														x	x	x	x				x				
23	9	x													x	x	x	x				x				
24	1	x																								

Station number: 224																												
Bott	Depth	Nuts	TA/DIC	H2/CH4 6sct.	H2	S	He	3H	SF6/CFC	Microbiome	Metal	DNA	FISH	O2	POC/PON	POP	Plastic	Chl	Sediment	microscopy	HPLC	POC/PON stable isotope	RNA Fungi	microbial activity	CH4	13C-CH4
1	1617	x																									
2	1500	x																									
3	1000	x																									
4	500	x																									
5	250	x																									
6	150	x																									
7	100	x													x	x	x	x									
8	100														x	x	x	x		x							
9	100														x	x	x	x									
10	75	x													x	x	x	x									
11	75														x	x	x	x		x							
12	75														x	x	x	x									
13	50	x													x	x	x	x									
14	50														x	x	x	x		x							
15	50														x	x	x	x									
16	25	x													x	x	x	x									
17	25														x	x	x	x		x							
18	25														x	x	x	x									
19	10	x													x	x	x	x									
20	10														x	x	x	x		x							
21	10														x	x	x	x									
22	10														x	x	x	x									
23	10														x	x	x	x									
24	1	x																									

Station number: 226																												
Bott	Depth	Nuts	TA/DIC	H2/CH4 exp.	H2	S	He	3H	SF6/CFC	Membrane	Metal	DNA	FISH	O2	POC/PON	POP	Phos	Chl	Sediment	microscopy	HPLC	POC/PON stable isotope	RNA Fungi	microbial activity	CH4	13C-CH4
1	2692				xx		x																		xx	xx
2	2692	x			xx						x															
3	3161	x									x													xxx		
4	2957	x		x	xx						x															
5	2957						x																		xx	xx
6	2799	x			xx						x															
7	2799						x		x																xx	xx
8	2750	x			xx						x															
9	2751						x																		x	xx
10	2701	x			xx						x															
11	2701						x													x					xx	xx
12	2650	x			xx						x															
13	2650						x													x					x	xx
14	2650				xx																			xxx		
15	2600						x		xx											x					xx	xx
16	2600	x			xx																					
17	2550						x																		xx	xx
18	2550	x			xx						x									x						
19	2500						x																		x	xx
20	2500	x			xx						x															
21	2450						x													x					x	x
22	2450	x			xx						x															
23	2400						x																		x	x
24	2400	x			xx						x															

Station number: 231																										
Bott	Depth	Nuts	TA/DIC	H2/CH4 expt.	H2	S	He	3H	SF6/CFC	Microbiome	[Metal]	DNA	FISH	O2	POC/PON	POP	PbSi	Chl	Sestion	microscopy	HPLC	POC/PON stable isotope	RNA Fungi	microbial activity	CH4	13C-CH4
1	2566																							x		
2	2566																							x		
3	2566																							x		
4	2566																							x		
5	2566																							x		
6	2566																							x		
7	2566																							x		
8	2566																							x		
9	2566																							x		
10	2566																							x		
11	2566																							x		
12	2566																							x		
13	2566																							x		
14	2566																							x		
15	2566																							x		
16	2566																							x		
17	2566																							x		
18	2566																							x		
19	2566																							x		
20	2566																							x		
21	2566																							x		
22	2566																							x		
23	2566																							x		
24	2566																							x		

Station number: 239																												
Bott	Depth	Nuts	TA/DIC	H2/CH4 extr.	H2	S	He	3H	SF6/CFC	Microbiome	Metal	DNA	FISH	O2	POC/PON	POP	Plastic	Chl	Sediment	microscopy	HPLC	POC/PON stable isotope	RNA Fungi	microbial activity	CH4	13C-CH4
1	501														x			x			x		x			
2	501														x			x		x	x		x			
3	501														x			x			x		x			
4	400																										
5	300																										
6	200																										
7	175																										
8	124																										
9	100														x			x			x					
10	100														x			x		x	x					
11	100														x			x			x					
12	75														x			x			x					
13	75														x			x		x	x					
14	75														x			x			x					
15	50														x			x			x		x			
16	50														x			x		x	x		x			
17	50														x			x			x		x			
18	25														x			x			x					
19	25														x			x		x	x					
20	25														x			x			x					
21	11														x			x			x		x			
22	11														x			x		x	x		x			
23	11														x			x			x		x			
24	1																										

Station number: 240																										
Bott	Depth	Nuts	TA/DIC	H2/CH4 exp.	H2	S	He	3H	SF6/CFC	Microbiome	Metal	DNA	FISH	O2	POC/PON	POP	PbSi	Chl	Seston	microscopy	HPLC	POC/PON stable isotope	RNA Fungi	microbial activity	CH4	13C-CH4
1	3068	x					x		x																	
2	2890																									
3	2890																									
4	2890	x																								
5	2890	x					x	x	x																	
6	2890	x				xx																				
7	2500	x																								
8	2000	x																								
9	2000	x					xx		x																	
10	2000					xx																				
11	1500						x		x																	
12	1000	x																								
13	800						x		x																	
14	200						x		x																	
15	10	x					x		x																	
16	10																									
17	10																									
18	10	x																								
19	10																									
20	10																									
21	10	x																								
22	10																									
23	10																									
24	10	x																								

PARAMETER	RESPONSIBLE TECHNICIAN / SCIENTIST
Nuts	L. Wischnewski
TA/DIC	L. Wischnewski
H2/CH4 Exp.	G. Wegener
H2	G. Wegener
S	M. Horn
He	M. Walter
3H	M. Walter
SF6/CFC	M. Walter

Microbiome	B. Slaby
Metal	A. Diehl
DNA	J. Bäger/J. Berz
FISH	J. Bäger/J. Berz
O2	J. Bäger/J. Berz
POC/PON	A. Stecher, PI E.-M. Noethig
POP	A. Stecher, PI E.-M. Noethig
PbSi	A. Stecher, PI E.-M. Noethig
Chl	A. Stecher, PI E.-M. Noethig
Seston	A. Stecher, PI E.-M. Noethig
Microscopy	A. Stecher, PI E.-M. Noethig
HPLC	A. Stecher, PI A. Bracher
POC/PON stable isotope	A. Stecher, PI A. Boetius
RNA Fungi	A. Stecher, PI E. Kilias
Microb. Activity	M. Molari
CH4	J. McDermott
13C-CH4	K. Hand

A.5.3 HROV Appendix

Tab. A.5.3.1: Details of transponders used in HROV deployments

	Frequencies		Command Codes				
Name	Rx [kHz]	Tx [kHz]	Enable	Disable	Release	s/n	Type
A	9	8	A	B	D	76591	Benthos TR-6001 17"
B	9	10.5	A	B	E	68284	Benthos TR-6001 17"
C	9	11	A	B	F	66871	Benthos TR-6001 17"

Deployments

Name	Station	Latitude	Longitude	Time [UTC]	Indicated Depth [m]	Water Depth [m]	Notes
A	PS101/122-1	66 42.656' N	061 34.694' E	2016-09-22 17:18:36	650	736	Weak, intermittent replies
B	PS101/121-1	66 43.221' N	061 20.709' E	2016-09-22 16:47:05	621	741	Robust replies
C	PS101/191-1	66 44.286' N	061 31.178' E	2016-10-06 02:21:07	510	601	Robust replies

Locations, times and water depths correspond to the location of the ship and the water depth measured by the ship at the time of release. Indicated depth was derived from ranging to each transponder during its descent. Descent times were approximately 5 minutes. No attempt was made to refine the locations of transponders once on the seafloor. Fast descents of ~60 m/min, shallow water, and weak currents suggest the release location and seafloor location are within O(10 m) of one another.

Transponders are enabled and expected to function for approximately 2 years. Ultimately the galvanized cables used as anchor lines will corrode, fail, and release the transponders.

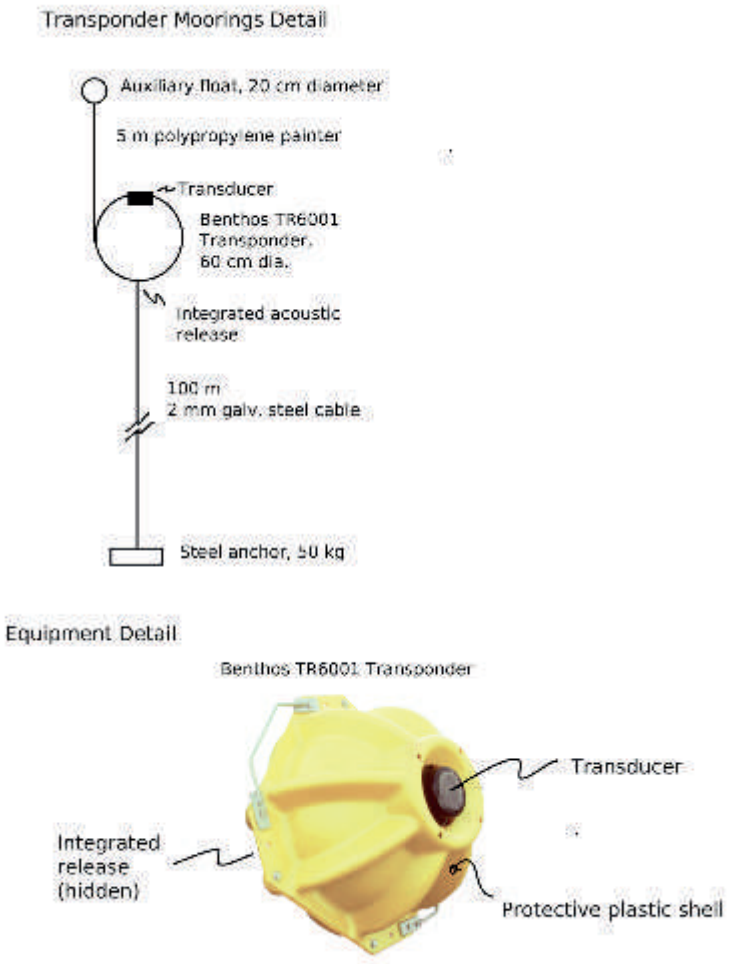

Fig. A.5.3.1: Transponder mooring schematic

A.5.4 Fram Appendix

Tab. A.5.4.1: Buoy deployments during PS10

Name	Buoy type	IMEI No.	Station	Date/Time(UTC)	Means	Comments
2016M1	ITBOB	300025060103020	PS101/0176-1	02.10.16 14:50	Mummy Chair	
2016M2	ITBOB	300025060205330	PS101/0114-1	21.09.16 22:30	Gangway	
2016T21	Thermistor IMB	300234061267820	PS101/0114-1	21.09.16 22:30	Gangway	
2016T35	Thermistor IMB	300234062429060	PS101/Heli-8	06.10.16 10:00	Helicopter	
2016T43	Thermistor IMB	300234062991690	PS101/084-1	17.09.16 18:58	Mummy Chair	
2016T44	Thermistor IMB	300234062421080	PS101/0057-1	15.09.16 20:00	Gangway	
2016S36	Snow Buoy	300234062788480	PS101/0057-1	15.09.16 20:00	Gangway	
2016S44	Snow Buoy	300234064010010	PS101/Heli-9	06.10.16 10:00	Helicopter	
2016S45	Snow Buoy	300234064011000	PS101/0114-1	21.09.16 22:30	Gangway	
2016S46	Snow Buoy	300234064015020	PS101/084-1	17.09.16 18:58	Mummy Chair	
2016S50	Snow Buoy	300234063227960	PS101/0176-1	02.10.16 14:50	Mummy Chair	
2016P29	SVP + drogue	300234064501430	PS101/0001-1	09.09.16 21:08	Drop from ship	Deployment in open water
2016P30	SVP + drogue	300234064506690	PS101/0002-1	10.09.16 02:32	Drop from ship	Deployment in open water
2016P31	SVP + drogue	300234064507510	PS101/0005-1	10.09.16 17:57	Drop from ship	Deployment in open water
2016P32	SVP + drogue	300234064508370	PS101/0003-1	10.09.16 12:46	Drop from ship	Deployment in open water
2016P33	SVP	300234064508550	PS101/Heli-12	09.10.16 07:15	Helicopter	
2016P34	SVP	300234064501620	PS101/Heli-4	16.09.16 11:10	Helicopter	
2016P35	SVP	300234064506570	PS101/0204-1	07.10.16 04:30	Mummy Chair	
2016P36	SVP	300234064508490	PS101/0053-1	14.09.16 12:08	Mummy Chair	

Name	Buoy type	IMEI No.	Station	Date/Time(UTC)	Means	Comments
2016P37	GPS Tracker	300434061137870	PS101/0132-1	24.09.16 07:50	Mummy Chair	
2016P40	GPS Tracker	300434061139990	PS101/Heli-5	21.09.16 07:30	Helicopter	
2016P41	GPS Tracker	300434061224420	PS101/Heli-5	21.09.16 08:00	Helicopter	
2016P43	GPS Tracker	300434061222910	PS101/0162-1	29.09.16 13:00	Gangway	
2016P44	GPS Tracker	300434061228900	PS101/Heli-9	21.09.16 08:30	Helicopter	
2016P45	GPS Tracker	300434061234000	PS101/0096-1	19.09.16 12:00	Gangway	
2016P46	GPS Tracker	300434060175780	PS101/0142-1	26.09.16 13:00	Gangway	
2016P47	GPS Tracker	300434061223890	PS101/0238	15.10.16 05:00	Gangway	Super Buoy Station from PS94

Tab. A.5.4.2: Sea ice stations and acquired data sets during PS101. For details on buoy deployments see Table A.5.4.1

Date	Station	Means of ice access	Buoy	ROV	Transects	Aerial Photos
14.09.16	PS101/053-1	Mummy Chair	yes			
15.09.16	PS101/057-1	Gangway	yes	yes	yes	Yes
16.09.16	PS101/Heli-4	Helicopter	yes			
17.09.16	PS101/084-1	Mummy Chair	yes		yes	
19.09.16	PS101/096-1	Gangway	yes	yes	yes	
21.09.16	PS101/0114-1	Gangway	yes	yes	yes	
21.09.16	PS101/Heli-5	Helicopter	yes		yes	
23.09.16	PS101/0128-1	Gangway			yes	
24.09.16	PS101/0132-1	Mummy Chair	yes			
26.09.16	PS101/0142-1	Gangway	yes	yes	yes	yes
29.09.16	PS101/0162-1	Gangway	yes	yes	yes	yes
01.10.16	PS101/0171-1	Gangway		yes	yes	
02.10.16	PS101/0176-1	Mummy Chair	yes		yes	
04.10.16	PS101/0184-1	Mummy Chair			yes	
06.10.16	PS101/Heli-8	Helicopter	yes			
06.10.16	PS101/Heli-9	Helicopter	yes			
06.10.16	PS101/Heli-11	Helicopter			yes	
07.10.16	PS101/0204-1	Mummy Chair	yes			
09.10.16	PS101/Heli-12	Helicopter	yes		yes	
09.10.16	PS101/Heli-13	Helicopter			yes	
09.10.16	PS101/Heli-14	Helicopter			yes	
09.10.16	PS101/Heli-15	Helicopter				
15.10.16	PS101/0238-1	Mummy Chair	yes			

Tab. A.5.4.3. Sample information of every samples taken at a certain position. x indicates data availability

Date	LabelEvent	Chl	POC/N	HPLC	POC/PON isotopes	AutoFIM DNA	AutoFIM RNA	AutoFIM Chl	Nutrients
10.09.16	PS101/0002-2	x	x						
10.09.16	PS101/0002-3	x	x			x	x	x	
10.09.16	PS101/0005-2	x	x						
10.09.16	PS101/0005-3	x	x			x	x	x	
11.09.16	PS101/0005-4	x	x				x	x	
11.09.16	PS101/0006-2	x	x			x	x	x	
11.09.16	PS101/0009-2	x	x			x	x	x	
11.09.16	PS101/0011-2	x	x			x	x	x	
12.09.16	PS101/0021-3	x	x			x	x	x	
12.09.16	PS101/0035-2	x	x			x	x	x	
13.09.16	PS101/0043-2	x	x				x		
14.09.16	PS101/0051-2	x	x			x	x	x	
17.09.16	PS101/0077-2	x	x			x	x	x	x
20.09.16	PS101/0107-2	x	x			x	x	x	x
22.09.16	PS101/0120-2	x	x			x	x	x	x
23.09.16	PS101/0128-2	-	x						
25.09.16	PS101/0137-1	x	x			x	x	x	x
26.09.16	PS101/0145-2	x	x			x	x	x	
28.09.16	PS101/0158-2	x	x			x	x	x	x
30.09.16	PS101/0168-2	x	x			x	x	x	x
03.10.16	PS101/0178-2	x	x			x	x	x	x
10.10.16	PS101/0226-2	x	x			x	x	x	x
12.10.16	PS101/0232-2	x	x			x	x	x	x
13.10.16	PS101/0233-2	x	x			x	x	x	x
13.10.16	PS101/0235-2	x	x	x		x	x	x	x
14.10.16	PS101/0237-2	x	x	x		x	x	x	x
15.10.16	PS101/0240-2	x	x	x		x	x	x	x
16.10.16	PS101/0240-3	x	x	x		x	x	x	x
16.10.16	PS101/0241-2	x	x	-	x	x	x	x	x

Date	LabelEvent	Chl	POC/N	HPLC	POC/PON isotopes	AutoFIM DNA	AutoFIM RNA	AutoFIM Chl	Nutrients
16.10.16	PS101/0241-2	x	x	x		x	x	x	x
17.10.16	PS101/0242-2	x	x	x		x	x	x	x
17.10.16	PS101/0242-3	x	x	x		x	x	x	x
17.10.16	PS101/0242-4	x	x	x		x	x	x	x
17.10.16	PS101/0242-5	x	x	x		x	x	x	x
17.10.16	PS101/0242-6	x	x	x		x	x	x	x
18.10.16	PS101/0242-7	x		x					x
18.10.16	PS101/0242-8	x		x					x
18.10.16	PS101/0242-9	x		x					x

Tab. A.5.4.4: Nutrients (Phosphate, Nitrate, Nitrite, Silicate, and Ammonia) samples during PS101

Station	Bottles																						
PS101/0009	1	2	3	4	5	6	7	8	9	10	11	12	13	16	17	18	19	20	21	22	23		
PS101/0044	1	7	10	13	16	19	21	23	24														
PS101/0055	4	7	10	13	17	20	22	23															
PS101/0058	2	4	6	12	16	20	24																
PS101/0112	1	6	7	11	13	19	21																
PS101/0115	1	5	7	10	13	19	23	24															
PS101/0126	3	5	6	7	8	10	11	12	13	17	18	19	20	21	24								
PS101/0131	1	4	5	6	7	8	11	16	19	22													
PS101/0133	1	3	7	10	16	18	19																
PS101/0139	2	4	8	12	16	18	20	21	23	24													
PS101/0149	2	4	6	8	11	13	17	19	22	24													
PS101/0159	3	5	7	9	11	13	17	19	21	24													
PS101/0170	11	12	13	16	17	18	19	20	21	22	23	24											
PS101/0172	1	7	10	12	16	17	18	19	20	22													
PS101/0175	1	5	9	11	12	17	24																
PS101/0177	1	3	5	7	9	11	15	17	19	21	23	24											
PS101/0181	9	10	11	12	13	14	15	18	22	23	24												
PS101/0188	1	9	12	13	17	20	21	22	23	24													
PS101/0192	1	2	3	4	5	6	7	8	9	10	11	15	18	21	24								
PS101/0213	1	2	3	4	5	6	7	8	9	10	11	12	14	16	18	20	23	24					
PS101/0224	1	2	3	4	5	6	7	10	13	16	19	24											
PS101/0226	2	3	4	6	8	10	12	16	18	20	22	24											
PS101/0239	1	4	5	6	7	8	9	12	15	18	21	24											

Tab. A.5.4.5: Expandable CTD (XCTD) stations during PS101

Sta. No. PS101/0	XCTD No.	XCTD s/n	Bottom Depth	XCTD depth
012-1	1	15062684	300	300
013-1	2	15062681	314	314
014-1	3	15062682	305	305
015-1	4	15062687	901	800
016-1	5	15062683	1638	1000
017-1	6	15062685	2442	1000
018-1	7	16037936	2830	1000
019-1	8	16037926	3104	1000
020-1	9	16037933	3234	1000
021-1	10	16037935	3284	380
021-2	11	16037932	3312	800
022-1	12	16037929	3388	650
023-1	13	16037934	3343	1000
024-1	14	16037931	3350	770
025-1	15	16037928	3315	1000
026-1	16	16037925	3354	950
027-1	17	16037927	3378	900
028-1	18	16037913	3431	800
029-1	19	16037916	3463	350
030-1	20	16037922	3464	350
031-1	21	16037919	3512	150
031-1	22	16037923	3514	150
032-1	23	16037920	3557	1000
033-1	24	16037921	3583	1000
034-1	25	16037914	3642	30
035-1	26	16037917	3694	850
036-1	27	16037915	3727	300
037-1	28	16037911	3790	1000
038-1	29	16037910	3795	350
039-1	30	16037907	3838	1000
040-1	31	16037912	3929	1000
041-1	32	16037905	3954	630
042-1	33	16037908	3968	1000
043-1	34	16037904	3996	1000
045-1	35	16037901	4005	1000
046-1	36	16037924	4007	1000
047-1	37	16037906	3993	1000
048-1	38	16037918	3984	400
049-1	39	16037903	3979	500
050-1	40	16037902	3968	1000
051-1	41	16037948	3952	300
052-1	42	16037942	3935	1000
054-1	43	16037945	3921	1000
070-1	44	16037938	3886	1100

Sta. No. PS101/0	XCTD No.	XCTD s/n	Bottom Depth	XCTD depth
071-1	45	16037941	3896	1100
072-1	46	16037937	3892	1000
073-1	47	16037944	3048	1000
074-1	48	16037947	3729	400
075-1	49	16037943	3552	1000
076-1	50	16037940	3884	120
077-1	51	16037939	3857	1000
078-1	52	16037946	2868	200
079-1	53	16048503	3317	1100
080-1	54	16048506	2427	1100
081-1	55	16048512	2548	1100
083-1	56	16048509	3873	850
085-1	57	16048511	2915	1000
086-1	58	16048508	1523	550
087-1	59	16048501	1457	850
233-1	60	16048502	4362	200
234-1	61	16048505	4019	1100
235-1	62	16048507	4016	1100
236-1	63	16048504	4029	1100
237-1	64	16048510	3865	1100

Tab. A.5.4.6: Sample information of every ice core taken at the different stations. x indicates data availability

Station PS101/	Core name	Length	DNA	CTD profile	Temp.	Salinity (complete melted core)
0128	DNA1	x	x	x		
	Temp/Sal1	x			x	x
	DNA2	x	x	x		
	Temp/Sal2	x			x	x
	DNA3	x	x	x		
	Temp/Sal3	x			x	x
	DNA4	x	x	x		
	Temp/Sal4	x			x	x
0142	DNA1	x	x	x		
	Temp/Sal1	x			x	x
	DNA2	x	x	x		
	Temp/Sal2	x			x	x
	DNA3	x	x	x		
	Temp/Sal3	x			x	x
	DNA4	x	x	x		
	Temp/Sal4	x			x	x
0162	DNA1	x	x	x		
	Temp/Sal1	x			x	x
	DNA2	x	x	x		
	Temp/Sal2	x			x	x
	DNA3	x	x	x		
	Temp/Sal3	x			x	x
	DNA4	x	x	x		
	Temp/Sal4	x			x	x
	DNA5	x	x	x		
	Temp/Sal5	x			x	x
0171	DNA1	x	x	x		
	Temp/Sal1	x			x	x
	DNA2	x	x	x		
	Temp/Sal2	x			x	x
	DNA3	x	x	x		
	Temp/Sal3	x			x	x
	DNA4	x	x	x		
	Temp/Sal4	x			x	x

Tab. A.5.4.7: Devices recovered from the Karasik Basin mooring and Nansen Basin moorings.

Mooring	Latitude Longitude	Water Depth	Instrument Type	Serial Number	Instrument Depth
Nansen	85° 17.520' N 60° 0.850' E	3870 m	ASL IPS5	51182	30
			RAS-500	13380-02	47
			SBE 37 ODO	13037	47
			ET861G	896	176
			ADCP	22388	176
			SBE 37 ODO	13012	178
			Sono Vault	1060	187
			Sediment trap	2004371	209
			ADCP	22389	216
			Seaguard	563	722
			SBE 37	12481	2168
			SBE 37	12479	3168
			Sediment trap	2004372	3723
			SBE 37	12477	3725
			Seaguard	522	3730
Karasik	87° 0.970' N 58° 15.520' E	4711 m	ASL IPS5	51184	65
			SBE 37 ODO	13491	72
			ET861G	835	126
			ADCP	23456	228
			SBE 37 ODO	13490	230
			Sediment tap	2009404	259
			ADCP	23549	266
			RCM7	8050	773
			SBE 37 ODO	13489	3259
			SBE 37 ODO	13488	3609
			Sediment trap	2012411	4564
			SBE 37 ODO	13487	4569
			RSM8	9391	4571

Die **Berichte zur Polar- und Meeresforschung** (ISSN 1866-3192) werden beginnend mit dem Band 569 (2008) als Open-Access-Publikation herausgegeben. Ein Verzeichnis aller Bände einschließlich der Druckausgaben (ISSN 1618-3193, Band 377-568, von 2000 bis 2008) sowie der früheren **Berichte zur Polarforschung** (ISSN 0176-5027, Band 1-376, von 1981 bis 2000) befindet sich im electronic Publication Information Center **(ePIC)** des Alfred-Wegener-Instituts, Helmholtz-Zentrum für Polar- und Meeresforschung (AWI); see http://epic.awi.de. Durch Auswahl “Reports on Polar- and Marine Research“ (via “browse”/”type”) wird eine Liste der Publikationen, sortiert nach Bandnummer, innerhalb der absteigenden chronologischen Reihenfolge der Jahrgänge mit Verweis auf das jeweilige pdf-Symbol zum Herunterladen angezeigt.

The **Reports on Polar and Marine Research** (ISSN 1866-3192) are available as open access publications since 2008. A table of all volumes including the printed issues (ISSN 1618-3193, Vol. 377-568, from 2000 until 2008), as well as the earlier **Reports on Polar Research** (ISSN 0176-5027, Vol. 1-376, from 1981 until 2000) is provided by the electronic Publication Information Center **(ePIC)** of the Alfred Wegener Institute, Helmholtz Centre for Polar and Marine Research (AWI); see URL http://epic.awi.de. To generate a list of all Reports, use the URL http://epic.awi.de and select “browse”/ ”type” to browse ”Reports on Polar and Marine Research”. A chronological list in declining order will be presented, and pdf-icons displayed for downloading.

Zuletzt erschienene Ausgaben:

Recently published issues:

706 (2017) The Expedition PS101 of the Research Vessel POLARSTERN to the Arctic Ocean in 2016, edited by Antje Boetius and Autun Purser

705 (2017) The Expedition PS100 of the Research Vessel POLARSTERN to the Fram Strait in 2016, edited by Torsten Kanzow

704 (2016) The Expeditions PS99.1 and PS99.2 of the Research Vessel POLARSTERN to the Fram Strait in 2016, edited by Thomas Soltwedel

703 (2016) The Expedition PS94 of the Research Vessel POLARSTERN to the central Arctic Ocean in 2015, edited by Ursula Schauer

702 (2016) The Expeditions PS95.1 and PS95.2 of the Research Vessel POLARSTERN to the Atlantic Ocean in 2015, edited by Rainer Knust and Karin Lochte

701 (2016) The Expedition PS97 of the Research Vessel POLARSTERN to the Drake Passage in 2016, edited by Frank Lamy

700 (2016) The Expedition PS96 of the Research Vessel POLARSTERN to the southern Weddell Sea in 2015/2016, edited by Michael Schröder

699 (2016) Die Tagebücher Alfred Wegeners zur Danmark-Expedition 1906/08, herausgegeben von Reinhard A. Krause

698 (2016) The Expedition SO246 of the Research Vessel SONNE to the Chatham Rise in 2016, edited by Karsten Gohl and Reinhard Werner

697 (2016) Studies of Polygons in Siberia and Svalbard**,** edited by Lutz Schirrmeister, Liudmila Pestryakova, Andrea Schneider and Sebastian Wetterich

696 (2016) The Expedition PS88 of the Research Vessel POLARSTERN to the Atlantic Ocean in 2014, edited by Rainer Knust and Frank Niessen

ALFRED-WEGENER-INSTITUT
HELMHOLTZ-ZENTRUM FÜR POLAR-
UND MEERESFORSCHUNG

BREMERHAVEN

Am Handelshafen 12
27570 Bremerhaven
Telefon 0471 4831-0
Telefax 0471 4831-1149
www.awi.de

HELMHOLTZ
GEMEINSCHAFT